



THE UNIVERSITY
of ADELAIDE

**Crack Front Shape Evolution in Structural Components
subjected to Fatigue Loading**

by

Behnam Zakavi

B.Eng (Mech.), M.Eng (Mech.), M.Eng (Adv.)

A thesis submitted for the degree of Doctor of Philosophy at the

School of Mechanical Engineering

The University of Adelaide

Australia

Submitted: November 2021

Abstract

Fatigue analysis is one of the most important and challenging aspects in the design and evaluation of engineering structures working under fluctuating mechanical or thermal loading. Although extensive research has been undertaken over the past two centuries to improve fatigue life prediction methods, there are still many issues and problems remaining, which warrant further study. One such issue is adequate modelling of the evolution of the shape of structural defects (cracks) in structural components subjected to fatigue loading.

Procedures and methods that are currently employed for fracture and fatigue failure forecasting are largely based on two-dimensional (2D) stress or strain field assumptions, which simplify the actual geometry of the structural components and defect shapes. As documented in many previous studies, these simplifications can lead to significant errors and to non-conservative predictions. There is also much experimental evidence indicating the significant influence of three-dimensional (3D) effects on fatigue crack growth, as well as on brittle fracture initiation. The 3D effects include, but are not limited to, the variation of stresses and stress intensity factors along the crack front, the presence of the 3D corner (vertex) singularities and the existence of coupled fracture modes, in addition to the classic fracture modes (modes I, II and III). In addition, there is the strong effect of the out-of-plane constraints on fatigue crack closure and crack growth rates in plate and shell components. Therefore, an account of more realistic (3D) shapes of structural defects and the 3D effects associated with these geometries is of a great importance in order to gain more confidence in fatigue life predictions, decrease the cost of inspections and maintenance, and allow structures to operate beyond design service life predictions. In addition, the implementation of 3D fatigue models can help to reduce various uncertainties and assumptions associated with the current 2D modelling.

Direct numerical simulations of 3D fracture and fatigue problems remain difficult. Therefore, this thesis aims to develop new, simplified, semi-analytical methods for the evaluation of front shapes of fatigue cracks and fatigue life in typical structural components, such as plates and round bars, which utilise more realistic geometries of structural defects. The thesis further elucidates the role of plasticity-induced crack closure and the 3D corner singularity on the crack front shape and its evolution.

It is expected that the new methods, which are developed in this thesis, may provide more accurate predictions of crack growth and fatigue life expectancy for typical structural components. This hypothesis is supported by extensive validation studies and comparisons against previous theoretical results and experimental data.

The main body of the thesis (Chapters 4 - 7) is presented in the form of a collection of published journal and conference articles authored by the candidate, who made a significant contribution to the conceptualisation, data analysis, calculations and drafting involved. A compilation of the candidate's publications relating to the main topic of the thesis but with less significant involvement is also provided in the Appendix. In addition, several Chapters (Chapters 1 - 3 and 8) are included to communicate the context, significance of this work and cohesive presentation, as well as to summarise the main outcomes of this thesis.

Declaration

I certify that this work contains no material which has been accepted for the award of any other degree or diploma in my name, in any university or other tertiary institution and, to the best of my knowledge and belief, contains no material previously published or written by another person, except where due reference has been made in the text. In addition, I certify that no part of this work will, in the future, be used in a submission in my name, for any other degree or diploma in any university or other tertiary institution without the prior approval of the University of Adelaide and, where applicable, any partner institution responsible for the joint award of this degree.

I give consent to this copy of my thesis, when deposited in the University Library, being made available for loan and photocopying, subject to the provisions of the Copyright Act 1968.

The author acknowledges that copyright of published works contained within this thesis resides with the copyright holder(s) of those works.

I also give permission for the digital version of my thesis to be made available on the web, via the University's digital research repository, the Library Search and also through web search engines, unless permission has been granted by the University to restrict access for a period of time.

Behnam Zakavi

24 / 11 / 2021

Date

Acknowledgements

Firstly, I would like to express my deepest gratitude and appreciation to my principal supervisor, Professor Andrei Kotousov, who has supported me throughout my candidature. I am extremely grateful for his guidance, encouragement, and our friendly chats at the end of our weekly meetings for more than 6 years. Without his dedication and wealth of knowledge, this work would not have been possible.

I truly appreciate the friendship, kindness, and technical support I received from my external supervisor, Professor Ricardo Branco throughout my academic research and in particular my stay at University of Coimbra, Portugal. I am also thankful to my supervisor, Dr Aditya Khanna, for his advice, suggestions, and direction on my research.

Finally, I want to extend my most gracious and special thanks to my loving wife, Golnoush Ahmadi Abhari, for her encouragement, patience, and constant support.

List of Publications

Journal Papers

1. **Zakavi, B.**, Kotousov, A., & Branco, R. (2021). An analytical-based approach for simulating fatigue crack growth in round bars, *International Journal of Fracture*, accepted: 8 June 2021.
<https://doi.org/10.1007/s10704-021-00558-3>
2. **Zakavi, B.**, Kotousov, A. & Branco, R. (2021). Does the front of fatigue crack intersect free surface at critical angle? *Theoretical and Applied Fracture Mechanics*, 114, 102985–.
<https://doi.org/10.1016/j.tafmec.2021.102985>
3. **Zakavi, B.**, Kotousov, A., & Branco, R. (2021). Overview of three-dimensional linear-elastic fracture mechanics. *International Journal of Fracture*.
<https://doi.org/10.1007/s10704-021-00528-9>.
4. **Zakavi, B.**, Kotousov, A., & Branco, R. (2021). The Evaluation of Front Shapes of Through-the-Thickness Fatigue Cracks. *Metals (Basel)*, 11(3), 403–.
<https://doi.org/10.3390/met11030403>.
5. Khanna, A., Kotousov, A., Yakubovich, S., & **Zakavi, B.** (2019). Asymptotic analysis of out-of-plane strain and displacement fields at angular corners. *International Journal of Solids and Structures*, 170, 111–122.
<https://doi.org/10.1016/j.ijsolstr.2019.04.024>.
6. **Zakavi, B.**, Kotousov, A., Khanna, A., & Branco, R. (2019). A new method for analysis of part-elliptical surface cracks in structures subjected to fatigue loading. *Theoretical and Applied Fracture Mechanics*, 103, 102258.
<https://doi.org/10.1016/j.tafmec.2019.102258>.
7. Kotousov, A., **Zakavi, B.**, Khanna, A., & Branco, R. (2018). On the analysis of structures with cracks of elliptical and part-elliptical shapes. *Theoretical and Applied Fracture Mechanics*, 98, 149–156.
<https://doi.org/10.1016/j.tafmec.2018.09.013>.

Conference Papers

1. **Zakavi B**, Kotousov A, Khanna A, Branco R. On the Simplified Modelling of Front Shapes of Fatigue Cracks, 11th International Conference on Structural Integrity and Failure (SIF-2018), 3 - 6 December 2018, Perth, Australia.
2. **Zakavi B**, Kotousov A, Khanna A, Branco R. On evaluation of fatigue crack front shapes. 9th Australasian Congress on Applied Mechanics (ACAM9), 27 - 29 November 2017, Sydney, Australia.

Table of Contents

Abstract.....	i
Declaration	iii
Acknowledgements	iv
List of Publications.....	1
Chapter 1 Introduction.....	5
1.1 Introduction.....	7
References.....	13
Chapter 2 Literature Review	14
2.1 Introduction.....	16
2.2 Part 1: Introduction to 3D Fracture Mechanics	17
2.3 Part 2: Introduction to Fatigue of Structures and Materials	35
2.3.1 Fatigue Phenomenon.....	35
2.3.2 Historical Overview.....	35
2.3.3 Fatigue Regimes	38
2.3.4 Fatigue Analysis	39
2.3.5 Stress-Life Methodology.....	40
2.3.6 Strain-Life Methodology.....	40
2.3.7 Hybrid Approaches.....	41
2.3.8 Fracture Mechanics Approach.....	42
2.3.9 Crack Front Shape Evolution Modelling	48
2.3.10 Numerical Procedures.....	48
2.3.11 Simplified Shape Modelling Approaches	49
2.3.12 Direct Shape Modelling Approaches.....	52
2.4 Conclusion	56
References.....	57
Chapter 3 Gaps, Objectives and Organisation of the Thesis.....	64
3.1 Research Gaps.....	66

3.2 Objectives	67
3.3 Organisation of the Thesis	67
Chapter 4 Investigation of the Effect of 3D Corner Singularity.....	71
Chapter 5 Development of Simplified Methods to Describe the Front Shapes of Through-the-thickness Fatigue Cracks	80
Chapter 6 Development of Simplified Methods to Describe the Front Shape Evaluation of Surface-breaking Fatigue Cracks.....	97
Chapter 7 Investigation of Plasticity Induced Crack Closure and 3D Effects on Front Shapes of Fatigue Cracks	116
Chapter 8 Conclusions and Future Work.....	145
8.1 Summary.....	147
8.2 Conclusions.....	148
8.3 Recommendations for Future Work.....	150
Appendix A Asymptotic Analysis of Out-of-plane Strain and Displacement Fields at Angular Corners.....	151

Chapter 1
Introduction

1.1 Introduction

The integrity, safety, and efficiency of operation of machines are largely affected by the presence of structural defects, which can lead to premature fatigue failures. In accordance with various estimates, from 60 to 90% of all structural failures are attributed to fatigue-related mechanisms. The direct cost of these structural failures can reach up to 4% of the Gross domestic product (GDP) or billions of dollars (Teixeira 2017). The dollars are important, but the cost of the many failures in human life and injury is infinitely more so.

A distinct feature of fatigue failures is that the peak design loads themselves are insufficient to cause immediate failure of a structural component weakening due to defects. However, these defects can grow under fluctuating loading, which is very common in many engineering applications. The growing defects can eventually reach critical shapes and sizes, causing premature failures, even under design loading conditions, during the design life span of the structural component. Therefore, it is very important to predict the rates of the propagation of defects accurately, as well as their critical shapes and sizes, notably those that cannot be sustained by the components under specified loading conditions. Fracture Mechanics addresses these challenges by developing methods and procedures for fracture and fatigue life assessments in the presence of crack-like defects.

Many of these methods and procedures are currently incorporated into industrial standards, codes, and guidelines. A brief overview of the main developments in the area of fatigue modelling is provided below. This overview will give an outline of the current state of the art in fatigue modelling, its challenges, the motivation behind this PhD project and the specific research gaps to be addressed in this thesis. A more comprehensive review of the research area will be presented in the next Section, which is devoted to a systematic literature review.

Fatigue was initially recognised as an important engineering problem in the beginning of the 19th century when railway and bridge engineers in Europe discovered that bridges and railroads were cracking when subjected to fluctuating (or cyclic) loading conditions. As the century progressed and the use of metallic materials significantly expanded with the increasing use of machines, more and more fatigue failures of structural components subjected to fluctuating loading conditions were encountered.

Today, fatigue has assumed an even greater importance for human society as a result of the ever-increasing use of advanced materials and the desire for higher strength, durability and performance from these materials, the increasing scale and complexity of machine and structures, and a greater reliance on these machine and structures in both the global economy and everyday life.

The stress and strain-based approaches were the earliest, but these are still the most common approaches for fatigue life assessments across many industries and engineering applications for High-Cycle Fatigue (HCF) and Low-Cycle Fatigue (LCF) regimes, respectively. Both approaches have a strong curve-fit ability and rely on several material constants, which must be determined from extensive, quite expensive and time-consuming fatigue tests. Therefore, a huge effort has been directed to link these constants to common material properties (e.g., yield stress, ductility, hardness, etc.), which can be obtained from simple, inexpensive and short uni-axial or indentation tests. However, this effort has had only partial success as many other factors can affect the fatigue life of structural components, e.g., the environment, surface finish and presence of stress concentrators.

An alternative approach to failure prediction is based on Continuum Damage Mechanics (CDM), which is a relatively new development in the mechanics of materials. The general concepts and fundamental aspects of this approach were described by Kachanov (1986). Chaboche and Lesne (1988) were the first to apply CDM to fatigue life predictions.

For the one-dimensional case, they postulated that the fatigue damage evolution per cycle is a function of the load and damage parameter, d , $0 \leq d \leq 1$, where $d = 0$ corresponds to the damage-free state and $d = 1$ to failure. Several linear and non-linear damage summation rules or principles were introduced to evaluate the failure conditions due to variable amplitudes of loading or in the presence of several damage mechanisms, e.g., fatigue and creep. The latter is considered to be the main advantage of CDMs.

All the above approaches have one common significant deficiency: there is no consistent definition of what the failure state is. It may be defined as, for example, when the first small detectable crack is found, or after a certain percentage decrease in stiffness, or as the actual complete fracture of the component. The differences in fatigue life predictions according to these fuzzy definitions of failure conditions may be small or appreciable. As mentioned above, failures are significantly affected by many controllable and uncontrollable factors, e.g., the quality of and procedure for material processing and manufacturing, geometry, stress states and the environment. The combined effect from all these factors can, and normally does, lead to a large scatter in fatigue life. This in turn dictates the utilisation of large safety factors in the design and evaluation of the safe life of structural components. Larger safety factors in design mean heavier, more expensive, and less efficient operation; meanwhile, larger safety factors in the safe life evaluation led to more frequent safety inspections and higher maintenance costs.

Many the above deficiencies of early approaches to fatigue life assessment have been eliminated using the fatigue crack propagation (FCP) approach. The first attempts at predicting the fatigue crack propagation length were based on Linear Elastic Fracture Mechanics (LEFM). The LEFM approach was first introduced by Paris et al. (1961), who equated the fatigue crack growth rate to the stress intensity factor range, which was considered the driving force of a propagating crack.

Later, researchers found that the crack growth rate curve as a function of the stress intensity factor range is not linear but normally has a sigmoidal shape for many structural metals and alloys, and is significantly influenced by the R-ratio, or the ratio of the minimum to maximum stress intensity factors during cyclic loading. To reduce the amount of fatigue testing, several empirical equations were suggested in the 1970s to extrapolate experimental fatigue data over different R-ratios. At the same time, the damage tolerance approach, as an alternative to the safe life approach, was developed and first applied in design procedures for aircraft structures, which require a high strength to weight ratio and reliability. The application of the damage tolerance approach, together with ultrasonic defect detection methods, enabled a significant decrease in safety factors, a reduction in manufacturing and maintenance costs, and made it possible to realise some advanced designs and engineering solutions.

However, the main challenge was (and remains) how to predict the fatigue life of a structure or component subject to a diverse (e.g., variable amplitude) loading history from limited materials data, which is very often available for the case of uniaxial cyclic loading at constant amplitude. Elber's discovery (1970) of fatigue (or plasticity-induced) crack closure, some 50 years ago, held out the prospect of addressing this challenge and delivering significant advances in this area.

A large amount of theoretical, computational, and experimental work has been carried since this discovery. Unfortunately, the initial expectations remain largely unsettled (de Matos & Nowell 2009). There are a number of reasons for this apparent lack of progress over the past five decades. These include: (1) the complexity of crack closure phenomena, which incorporate plasticity, roughness, and oxidation closure mechanisms; (2) difficulties with experimental measurements and significant inconsistencies in these measurements across different methods; (3) theoretical crack closure models are extremely computationally demanding and normally limited to two-dimensional (2D) geometries. The latter limitation represents another significant challenge in Fracture Mechanics and fatigue life assessments (Pook 2013) and it is the focus of the current thesis.

The three-dimensional (3D) effects are currently largely ignored despite the enormous amount of theoretical and experimental information that has been published over the past five decades. Contemporary stress analyses of cracks and fatigue life evaluations are based on the fundamental fracture mechanics concept of the stress intensity factor or effective stress intensity factor, as proposed by Wolf Elber in his thesis at UNSW Sydney in 1968.

In general, a stress intensity factor describes the linear elastic stress field in the vicinity of a crack tip, which has the inverse square root singular behaviour ($r^{-1/2}$). In actual 3D geometries, this is not the case in the vicinity of a corner point where a crack front intersects with a free surface. The singular behaviour at this corner point is different, and sometimes is called a vertex or 3D corner singularity, and is an important source of 3D effects. For example, it was demonstrated in a number of experimental and computational studies that the 3D corner singularity can influence the crack growth rates and shape of the crack front near free surface and fatigue life estimates.

Another important 3D effect is the out-of-plane stress distribution, which in the case of plate components with through-the-thickness cracks can be causally related to the plate thickness (Kotousov 2007). Contemporary Fracture Mechanics utilises two assumptions with respect to the out-of-plane or transverse conditions: plane stress or plane strain. The application of the plane strain assumption to fracture problems has a physical justification. When the plastic zone size is small in comparison with the specimen thickness, experiments indicate that it must be less than 2 percent of the plate thickness, then the fracture is dominated by plane strain conditions. There have been several 3D computational studies that have demonstrated that the plane stress conditions (or zero transverse stress) are never achieved near the crack tip, regardless of the plate thickness.

The effect of the out-of-plane stress on fatigue can be more profound, leading to significantly different crack growth rates in specimens of different thickness under the same applied stress cycle. The latter is often attributed to the change in the plasticity-induced crack closure with the change of the specimen thickness, which is larger for thin plates due to the reduction in the out-of-plane constraints.

The 3D corner singularity and out-of-plane constraint effects can lead to a very complex crack front evolution even for plane/plate problems with through-the-thickness cracks. The current fatigue evaluation procedures are largely based on simplified or idealised crack front shapes, e.g., a straight front for through-the-thickness cracks or part-elliptical for surface cracks, which may be not accurate enough to model the fatigue failure of actual structural components. Therefore, it is important to understand the situations when these idealised crack front shapes are appropriate and when these simplifications can lead to noticeable errors in evaluations of fatigue life expectancy. These two research questions motivated the current PhD project.

The overall aim of this thesis is to investigate theoretically, numerically, and experimentally the influence of the crack front shapes on the evaluation of the fatigue life of structural components. The ultimate goal of this research is to improve, or at least provide the limitations of, current fatigue life procedures by considering more realistic shapes of structural defects, which reflect the complex fatigue crack growth mechanisms.

References

- Chaboche, J., & Lesne, P. (1988). A Non-linear Continuous Fatigue Damage Model. *Fatigue & Fracture of Engineering Materials & Structures*, 11(1), 1-17.
- de Matos, P., & Nowell, D. (2009). Experimental and numerical investigation of thickness effects in plasticity-induced fatigue crack closure. *International Journal of Fatigue*, 31(11), 1795–1804.
- Elber, W. (1970). Fatigue crack closure under cyclic tension. *Engineering Fracture Mechanics*, 2(1), 37, in3, 45-44, in4,45.
- Kachanov, L. (1986). Introduction to continuum damage mechanics (1st ed. 1986.). Springer Netherlands.
- Kotousov, A. (2007). Fracture in plates of finite thickness. *International Journal of Solids and Structures*, 44(25), 8259–8273.
- Paris, P.C., Gomez, M.P. & Anderson, W.P. (1961). A rational analytical theory of fatigue. *The Trend of Engineering*, 13:9-14.
- Pook, L. (2013). A 50-year retrospective review of three-dimensional effects at cracks and sharp notches. *Fatigue & Fracture of Engineering Materials & Structures*, 36(8), 699–723.
- Teixeira, G. D. M. (2017). Fatigue of Metals: Failure and Success. Research and Development, Dassault Systemes Simulia, Sheffield, UK.

Chapter 2
Literature Review

2.1 Introduction

Given that Fracture Mechanics covers a wide range of theoretical, experimental, numerical, and practical developments, the focus of the current literature review is those specific aspects that are important for the current research. The present literature review consists of two parts: the first part is an introduction to three-dimensional (3D) Fracture Mechanics and the second part provides a general overview of fatigue phenomena, focusing on 3D effects associated with the evolution of crack front shapes during cyclic loading.

The first part was submitted and published as an invited review paper in the International Journal of Fracture. It offers an overview of three-dimensional linear-elastic fracture mechanics. A copy of the paper is provided below.

2.2 Part 1: Introduction to 3D Fracture Mechanics

An extensive investigation was conducted to provide a brief review of 3D Fracture Mechanics and the outcomes of the latest research in this area. The following research article is largely focused on linear-elastic materials.

Statement of Authorship

Title of Paper	Overview of three-dimensional linear-elastic fracture mechanics			
Publication Status	<input checked="" type="checkbox"/>	Published	<input type="checkbox"/>	Accepted for Publication
	<input type="checkbox"/>	Submitted for Publication	<input type="checkbox"/>	Unpublished and Unsubmitted work written in manuscript style
Publication Details	Zakavi, B., Kotousov, A., & Branco, R. (2021). Overview of three-dimensional linear-elastic fracture mechanics. International Journal of Fracture. https://doi.org/10.1007/s10704-021-00528-9			

Principal Author

Name of Principal Author	Behnam Zakavi		
Contribution to the Paper	Completed literature review, and wrote manuscript		
Overall percentage (%)	50		
Certification:	This paper reports on original research I conducted during the period of my Higher Degree by Research candidature and is not subject to any obligations or contractual agreements with a third party that would constrain its inclusion in this thesis. I am the primary author of this paper.		
Signature		Date	22 / 08 / 2021

Co-Author Contributions

By signing the Statement of Authorship, each author certifies that:

- i. the candidate's stated contribution to the publication is accurate (as detailed above);
- ii. permission is granted for the candidate to include the publication in the thesis; and
- iii. the sum of all co-author contributions is equal to 100% less the candidate's stated contribution.

Name of Co-Author	Prof. Andrei Kotousov		
Contribution to the Paper	Supervision, and provided major contribution on manuscript writing		
Signature		Date	24 / 08 / 2021

Name of Co-Author	Prof. Ricardo Branco		
Contribution to the Paper	Provided writing assistance, and participated in manuscript review and evaluation		
Signature		Date	23 / 08 / 2021

Name of Co-Author			
Contribution to the Paper			
Signature		Date	



Overview of three-dimensional linear-elastic fracture mechanics

Behnam Zakavi · Andrei Kotousov · Ricardo Branco

Received: 23 October 2020 / Accepted: 23 February 2021
© The Author(s), under exclusive licence to Springer Nature B.V. 2021

Abstract The aim of this contribution is to provide a brief overview of three-dimensional linear-elastic fracture mechanics (3D LEFM) as well as the latest advances in this area. The primary focus of this review is on the situations where the classical LEFM, which largely relies on plane stress or plane strain simplifications, provides peculiar or misleading results. As no exact analytical solutions are currently available for real cracks, which are inherently three-dimensional (3D), there are many controversial views in the literature and lack of understanding of the effects associated with 3D geometries. Fundamental results and general conclusions in 3D LEFM are largely based on dimensionless and energy considerations as well as on generalisations of outcomes of 3D numerical studies and application of asymptotic techniques. It is believed that 3D considerations alone cannot explain complex and diverse brittle fracture and fatigue phenomena, but these considerations can contribute into the further understanding of these phenomena.

Keywords Cracks · Plates · Fracture mechanics · Linear elasticity · 3D analysis · Finite element method

Abbreviations

a	Radius of cylindrical hole
A	Function of z -coordinate
b	Small number
$C_1 \dots C_4$	Constants
E	Young's modulus
h	Half plate thickness
F_i	Applied forces
F_S, F_A	Functions of angular position (ϑ, φ)
f_I, f_{II}, f_{III}	Functions
G	Energy release rate
G_I	Energy release rate in mode I
K_t	Stress concentration factor
K_c	Apparent fracture toughness
K_{IC}	Fracture toughness in mode I
K_I, K_{II}, K_{III}	Stress intensity factors in mode I, II and III, respectively
$K_I^\infty, K_{II}^\infty$	Remote stress intensity factors in mode I and II, respectively
K_S, K_A	Stress intensity factors of symmetric and antisymmetric vertex singularities, respectively
K_O	Stress intensity factor of the out-of-plane mode
K_{vertex}	Stress intensity factor of vertex singularity, $K_{\text{vertex}} = (K_S, K_A)$

B. Zakavi · A. Kotousov (✉)
School of Mechanical Engineering, The University of Adelaide, Adelaide, SA 5005, Australia
e-mail: andrei.kotousov@adelaide.edu.au

B. Zakavi
e-mail: behnam.zakavi@adelaide.edu.au

R. Branco
Department of Mechanical Engineering, CEMMPRE, University of Coimbra, Rua Luís Reis Santos, Pólo II, 3030-788 Coimbra, Portugal

J	J-integral
M	Maximum modulus of the prescribed edge tractions
n	Power exponent
R	Distance from the edge of hole or vertex point
r, ϕ	Polar coordinates
u_i	Displacement components, $i = (x, y, z)$
x, y, z	Coordinates
α	Positive constant
β_c	Critical angle
λ_S, λ_A	Strengths of symmetric and antisymmetric vertex singularities, respectively
$\lambda_{\text{vertex}}, \lambda_{\text{line}}$	Strengths of vertex and line singularities, respectively
σ or σ_{ij}	Stress components, $i = (x, y, z)$ and $j = (x, y, z)$
ε or ε_{ij}	Strain components
ξ	Minimum distance to the observation point from the edge of plate or free surface
η	Coordinate associated with crack front
λ, μ	Lame's constants
ν	Poisson's ratio
R, ϑ, φ	Angular coordinates of a point
β, θ	Angles which identify the local geometry of the vertex point

1 Introduction

Plane problems of linear elasticity are often treated with simplified 2D theories, which utilise plane stress or plane strain simplifications. However, stress analysis based on the classic plane theories of elasticity may occasionally lead to peculiar results due, in part, to the fact that these theories are approximate three-dimensional theories even when the plane stress or plane strain equations are solved exactly (Yang and Freund 1985). Subsequently, the aim of this paper is to provide a brief review of common situations and problems, which require 3D analysis (Maurizi and Berto 2020).

In the beginning, consider a classical example described in a textbook by (Broek 1974), which is related to the fatigue failure initiation due to a stress concentrator, i.e. a circular hole in a large plate subjected to uni-axial loading, as illustrated in Fig. 1a. Experimental evidence shows that for relatively thin

plates the crack originates either at the centre of the plate (Fig. 1b) or at the corner, where the hole meets the free surface of the plate (Fig. 1c). However, in relatively thick sections, cracks at holes are usually corner cracks instead of through cracks. Of course, cracks in general originate from small imperfections or discontinuities that may be present in the material. Such discontinuities may either be man-made or may be introduced in the material during the process of fabrication (Folias and Wang 1990). Thus, one possible explanation for this phenomenon is that such discontinuities are most likely to be present in the region where the hole meets the free surface of the plate. Another explanation could be that the stress levels may actually be higher near the surface on contrary to what is predicted by the 2D elasticity theories (Kotousov et al. 2019).

Figure 2 shows the stress concentration factor distribution across the thickness, $K_t(z/h)$, as derived by Folias and Wang (1990), based on a general 3D solution to Navier's equations, which was obtained using a double Fourier integral transform and the theory of integral equations. These results are also in an agreement with 3D FE studies conducted over the past two decades (e.g. Yang et al. 2008). Several conclusions can be drawn from these results. At relatively large hole diameter to thickness ratios (or a/h ratios) the 3D solution indeed converges to the classical plane stress result, $K_t = 3$, as first obtained by Kirsch more than two hundred years ago. When the radius of the hole, a , is larger than the plate thickness, $2h$, there is a certain difference between approximate 2D and exact 3D solutions. At high a/h values the maximum stress location is shifted closer to the free surface, or to $z/h = 1$ referring to Fig. 1. Therefore, the exact 3D solution alone is also able to explain the experimental observation regarding the crack initiation location. However, the difference with the 2D solution is small and within 5–7% for the in-plane stress components. It is interesting to note that 3D numerical studies indicate that the above estimates are also true for many other plane problems of linear elasticity, which have no stress singularities (Kotousov et al. 2010; Kotousov 2007). Therefore, 2D analytical solutions represent a good compromise for stress calculations in many practical situations. As a result, these solutions are widely utilised for design and stress analysis. Finally, it is of some academic and practical interest to examine the behaviour of 3D stress field near a circular edge, i.e. the points where the hole meets the free surface

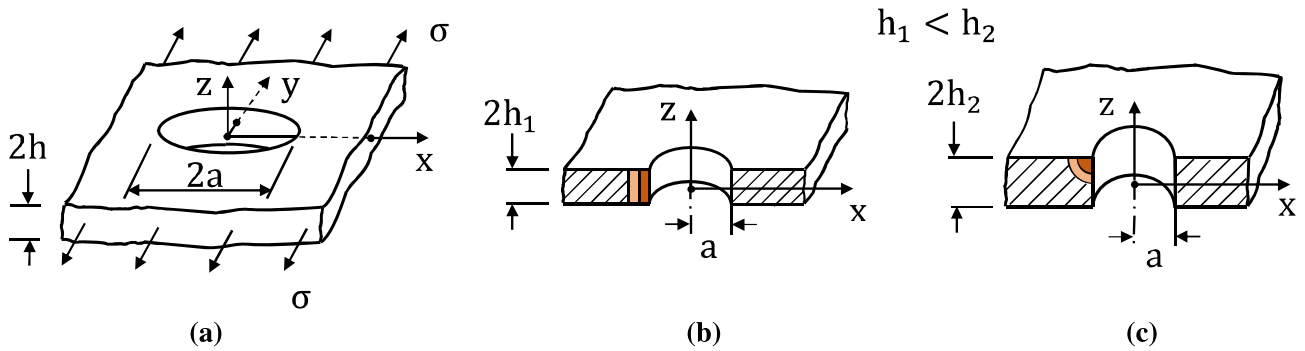


Fig. 1 a Plate with a circular hole under uni-axial loading. Fatigue failure initiation in b thin plate, and c thick plate, adopted from Broek (1974)

Fig. 2 Stress concentration factor, K_t , across the thickness for Poisson's ratio $\nu = 0.33$ and various a/h ratios (Folias and Wang 1990)

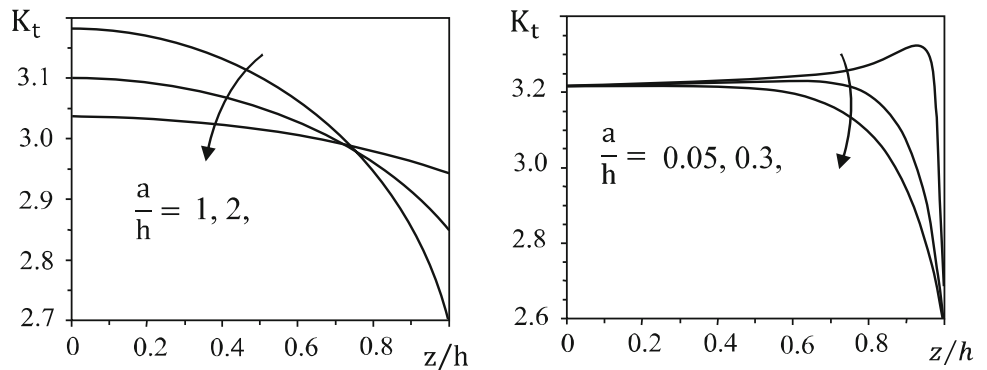
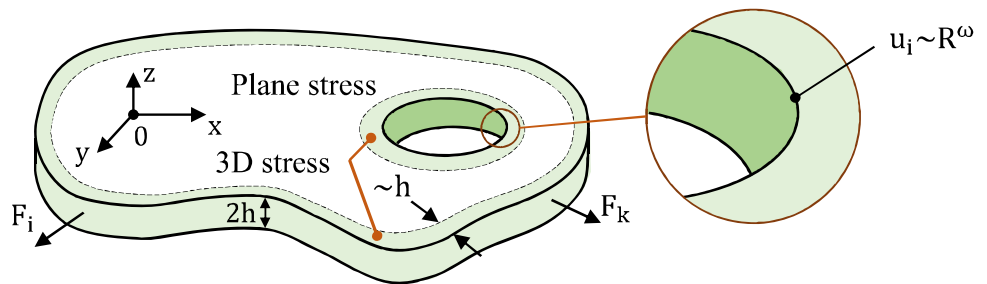


Fig. 3 Representation of the exact solution to plane problems of elasticity as a sum of an interior plane stress solution and 3D stress state near boundaries



of the plate. Without going into mathematical details, an asymptotic approach, which satisfies all boundary conditions and 3D equilibrium equations, leads to a characteristic equation with infinite number of complex roots. The first root of which is the same as that obtained by Williams solution for a 90° angular corner with free-free tractions, i.e. $\omega = 2.7396 \pm 1.1191i$ (Folias and Wang 1990). Therefore, the displacements near the edge are $u_i \sim R^\omega$ and stresses are limiting to zero at $R \rightarrow 0$, where R is the distance from the edge of the hole. This result is also in an agreement with careful 3D FE simulations, see for example, She and Guo (2007) and Yang et al. (2008), and it can be generalized for other plane geometries.

A different situation occurs for the out of plane (z) stress components. The plane assumptions of the 2D linear theory of elasticity provide a wide range for the normal stress: $\sigma_{zz} = 0$ (in the case of plane stress or for thin plates) and $\sigma_{zz} = \nu(\sigma_{xx} + \sigma_{yy})$ (in the case of plane strain or for thick plates). However, there is no generally accepted criterion for selecting the appropriate (plane stress or plane strain) assumption for a particular plate problem with prescribed boundary and loading conditions (Kotousov and Wang 2002). Moreover, the plate thickness may be irrelevant to the dominant stress state in a plate component. For example, the 3D stress state in an infinite plate with cylindrical hole (as well as without hole) subjected to remote hydro-

static pressure is identical to the plane stress solution, regardless of the plate thickness.

To address this uncertainty, [Gregory and Wan \(1988\)](#) formulated a general hypothesis regarding the decomposition of 3D and 2D stress states in plane problems of linear elasticity. In accordance with this hypothesis, the exact solution can be represented as a sum of an interior plane stress solution of the corresponding plane stress problem and decaying 3D layer solution, see [Fig. 3](#). The decaying behaviour of 3D solution is assumed to have a form :

$$\sigma \sim M \exp\left(-\alpha \frac{\xi}{h}\right), \quad (1)$$

where ξ is the minimum distance of the observation point from the edge of the plate, M is the maximum modulus of the prescribed edge tractions, and α is a positive constant independent of the half-plate thickness h .

While the interior two-dimensional solution is significant throughout the plate, the layer solution has only a localised effect in regions near the plate edges or applied loading. This resolution has not been proven rigorously yet, except for several special cases, however “(...) the asymptotic results of the sixties leave little doubt that such a resolution does exist” ([Gregory and Wan 1988](#)). In addition, numerical, analytical, and experimental studies largely confirm this hypothesis and indicate that the region of the 3D stress state is confined to approximately one-half of the plate thickness, or $\alpha \approx 1$ in [Eq. \(1\)](#). Many references to the present article can be listed here to support the above statements.

For many structural components, the plate thickness is normally much smaller than any in-plane characteristic dimension meaning that the region affected by the 3D stress state is usually very small in comparison with the overall volume of the structural component. However, failures, in particular fatigue failures, normally initiate from this region, which is associated with free boundaries, see [Figs. 1 and 2](#). Thus, 3D stress states can potentially influence the failure conditions as well as the fatigue life of structural components ([She et al. 2008](#); [Kotousov et al. 2010, 2013](#)), which motivates the reassessment of the validity of plane stress solutions to real 3D problems. This is particularly important for problems with singularities, e.g. problems with cracks, which are the focus of the current paper.

2 Singular stress states near crack front

Stress singularities obviously are not of the real world. Nonetheless, they are of a real fact of a stress analysis ([Sinclair 2004a](#)). Stress singularities can be associated with a sudden change of boundary conditions or applied loading (e.g. concentrated forces and moments) over vanishingly small areas or volumes, which is often termed as singular loads. This class of stress singularities is well investigated and the nature of their origin and asymptotic behaviour is presently well understood. For example, 2D and 3D analytical solutions for concentrated loads or edge dislocations are often utilised as Green’s functions in stress analysis or in integral equation approaches, which have wide applications in elasticity as well as in numerical methods.

Another class of singularities, which is the focus of the current paper, is generally not related to singular loads. Stress singularities from this class may occur due to abrupt changes of the geometry; singularities arising in fracture problems belong to this class. There were many papers and books in the past focusing on the 2D linear-elastic analysis of the singular stress states near the tip of a crack. [Sinclair \(2004a, b\)](#) presented the most comprehensive review of 2D singularities.

The classical 2D linear-elastic theories provide a power tool for analysis of various singular problems, and, in particular, crack problems. This tool is based on three main simplifications: (1) strains and displacements are small, (2) the stress-strain response is linear, i.e. implicitly adopting that the strains never exceed the limits of elasticity; and (3) the stress state near a crack tip follows to plane stress or plane strain assumptions. Nonetheless, the singular stress state near the crack tip is in violation of all three of these simplifications.

There were many attempts in the past to relax the above simplifications. It was demonstrated, for example, that the large strain analysis still demonstrates the persistence of singular behaviour, so the r^{-1} behaviour as $r \rightarrow 0$ of the crack-tip stress-strain product continues to be present. Several researchers have found that the stress singularities are not removed within the context of deformation theory of plasticity. For example, in accordance with Ramberg–Osgood model, the stress field near the crack tip behaves as $\sigma \sim r^{-1(n+1)}$ and $\sigma \cdot \varepsilon \sim r^{-1}$, where n is the strain hardening exponent and r is the distance from the crack tip.

The classical Linear-Elastic Fracture Mechanics (LEFM) naturally avoids two out of three simplifica-

tions in the treatment of singular problems by introducing an assumption regarding the smallness of the high stress/strain region associated with all sorts of nonlinearities. This theory propounds that the stress intensity factor dominates the stress state near the crack tip, and when the process zone is fully encapsulated by the K-dominance region, fracture initiates. The predictions of LEFM are expected to be valid as far as the underlining assumption is met (He et al. 2016b).

However, the contemporary Fracture Mechanics still largely relies on the third simplification regarding the state of stress near the crack front. This simplification, in particular, avoids the complexity of 3D stress analysis by reducing the problem dimensionality, which in turn, allows the application of the well-developed analytical methods of plane theory of linear elasticity. Many exact solutions were derived using these methods. These fundamental solutions and results form the foundation of the contemporary LEFM and are incorporated into many current life expectancy and integrity evaluation procedures. However, it is often acknowledged that these solutions may not be accurate or adequate for analysis of actual problems, which always have three dimensions (Pook 2010, 2013). In the following we will make an attempt to describe these situations as well as the main differences between exact 3D solutions and the corresponding 2D analytical results, and discuss what implications on fracture and fatigue these differences have.

Hartranft and Sih (1969) were the first who provided an approximate 3D solution near the straight front of a semi-infinite crack assuming plane strain conditions near the crack front. However, this solution has not been popular due to its complexity and lack of explicit representation. Leblond and Torlai (1992) attempted to derive 3D displacement and stress fields near straight and curved crack fronts adopting the plane strain assumption. Costabel et al. (2004) and Omer et al. (2004) obtained an explicit asymptotic solution near the front of a 3D crack. However, this solution disregards 3D stress states associated with vertex points, where there is a change of singular behaviour. There were many other attempts to obtain exact or approximate analytical 3D solutions for crack problems, e.g. Kotousov (2007), Omer and Yosibash (2005), Yosibash and Mittelman (2016), Kotousov et al. (2017), and Khanna et al. (2019) to name a few.

So far, numerous analytical attempts have had a limited success in deriving exact 3D or at least providing

3D asymptotic expansions of the stress and displacement fields. Therefore, the main results in 3D LEFM are largely based on generalisations of outcomes of numerical studies, which, however, have been conducted for specific geometries, material properties and boundary conditions, e.g. Hutař et al. (2009 and 2010), Branco et al. (2012), Maia et al. (2016) and Lopez-Crespo et al. (2018). Based on these numerical studies, as well as fundamental theoretical results for 2D geometries, the stress field near point, η , at the 3D crack front, see Fig. 4, is often represented as a sum of the stress states generated by the so-called line singularities, $K_{\text{line}} = (K_I, K_{II}, K_{III})$, and vertex (or 3D corner) singularities, $K_{\text{vertex}} = (K_S, K_A)$:

$$\sigma = \frac{K_I(\eta)}{\sqrt{r}}f_I + \frac{K_{II}(\eta)}{\sqrt{r}}f_{II} + \frac{K_{III}(\eta)}{\sqrt{r}}f_{III} + K_S F_S R^{-\lambda_S} + K_A F_A R^{-\lambda_A} \quad (2)$$

where $K_I(\eta)$, $K_{II}(\eta)$ and $K_{III}(\eta)$ are local stress intensity factors in mode I, I and III, respectively; f_I , f_{II} and f_{III} are associated functions of ϕ , see Shivakumar and Raju (1990), Heyder et al. (2005) and Kotousov et al. (2019). It is often hypothesised that the behaviour of line singularities on the planes perpendicular to the crack front can be described by the corresponding classical 2D asymptotic expansions. This assumption is often utilised to extract the local stress intensity factors from 3D numerical results and will be discussed later in this paper. K_S and K_A are stress intensities of symmetric and antisymmetric corner (vertex) singularities, respectively, F_S and F_A are functions of angular position (ϑ, φ), which are omitted in Fig. 4b for the sake of clarity; R is the distance from the corner point; λ_S and λ_A are strengths of symmetric and antisymmetric vertex singularities.

If the crack front has several vertex points, then Eq. (2) can be modified accordingly to include the contributions from singular states associated with these points. In particular, for surface cracks in plates, bars and shells, there are typically two vertex points associated with the intersection of two free surfaces by the crack front.

Figure 5 presents outcomes of numerical simulations for a linear elastic plate with a semi-infinite through-the-thickness crack loaded in mode I and II by a remote stress intensity factor, K_I^∞ and K_{II}^∞ , respectively. The crack front is assumed to be straight forming the right angles at the intersections with the free plate

Fig. 4 Representation of the stress field near the front of 3D crack

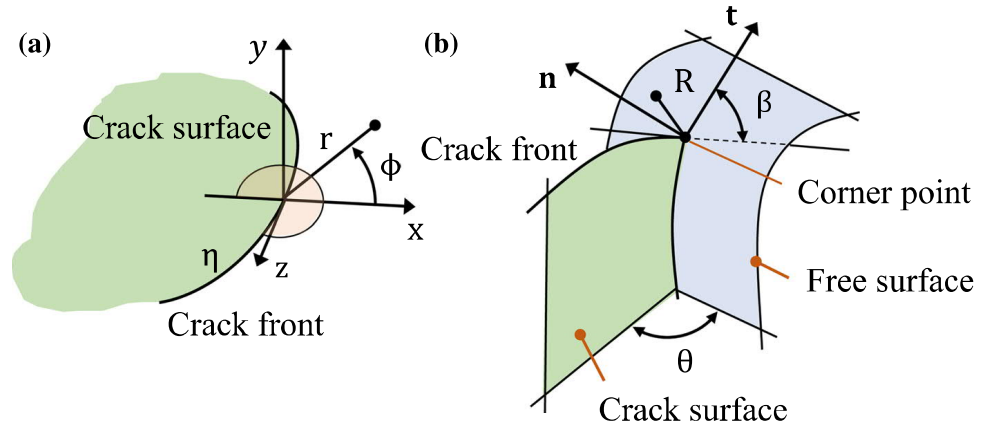


Fig. 5 Local stress intensity factors along a straight crack front. $K_{II}(z)$ is not significantly affected by Poisson's ratio, so only one result is shown ($\nu = 0.3$) for the sake of clarity

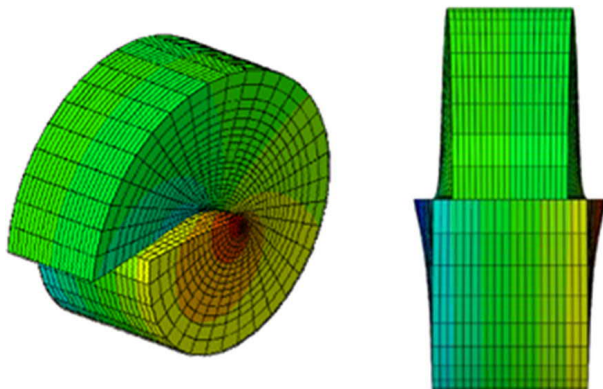
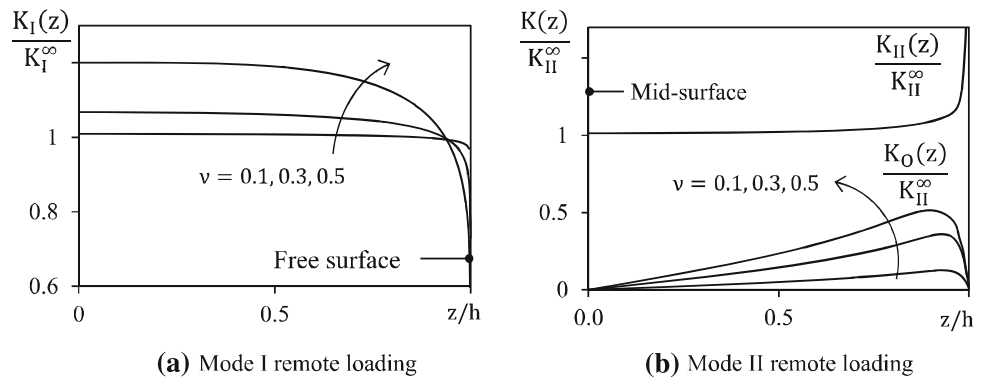


Fig. 6 Visualisation of the generation of the coupled fracture mode (mode O) due to Poisson's effect for a crack subjected to shear (mode II) loading

surfaces. Details of the finite element model as well as the applied boundary conditions can be found in many papers published over the past 20 years. It seems the first numerical study reporting results for this problem was conducted by Nakamura and Parks (Nakamura and Parks, Nakamura and Parks 1998 and Shivakumar and Raju (1990)).

From Fig. 5a, the variation of the local stress intensity factor, $K_I(z)$, increases with an increase of Poisson's ratio for mode I, and the variation of $K_{II}(z)$ with the change of Poisson's ratio is rather small and omitted in Fig. 5b. At $\nu = 0$, the stress intensity factor distributions for mode I converges to the 2D plane stress solution, where the stress intensity factor is constant along the crack front. The difference between the plane solution, $K_I(z) = K_I^\infty$, and the numerical 3D solution is small except near the free surfaces, or when $z/h = 1$. This behaviour needs a special consideration and will be discussed later in this paper.

Figures 5b and 6 also reveal a new fracture mode, the out-of-plane mode O, which is coupled with the applied fracture mode II (Kotousov et al. 2013). The existence and features of the coupled out-of-plane mode (mode O) in problems with cracks, and sharp and rounded notches have been discussed exhaustively in the literature (Camas et al. 2017; Maurizi and Berto 2020; Kotousov et al. 2013, 2019). A simple explanation of the mechanism behind the generation of this fracture mode can be as follow: mode II loading creates tensile and compressive stress states on two sides along the bi-sector line aligned with the crack, which leads to a

scissoring motion of the opposite sides due to the Poisson's effect, as illustrated in Fig. 6. This mechanism generates the new fracture mode, which has similar characteristics as the global fracture mode III. However, this is a different fracture mode, because it is the local mode decaying very rapidly from the distance from the crack front. It is confined to approximately half of the plate thickness in the radial direction, similar to other 3D stress states in plane problems of elasticity. In addition, $K_O(z)$ changes significantly along the crack front, zero at the mid-plane ($z/h = 0$) and free surfaces ($z/h = 1$) due to symmetry and free boundary conditions, respectively (Kotousov et al. 2010). It is also strongly dependent on Poisson's ratio, ν . Similar to mode I, at $\nu = 0$, the local stress intensity factor distribution, $K_{II}(z)$, converges to the corresponding 2D plane stress solution, $K_{II}(z) = K_{II}^\infty$, and mode O is vanishing, see Fig. 5b (Berto et al. 2012).

3 Effects of vertex singularity

The large difference between the 2D plane solution and 3D results near the free surfaces is generally attributed to the effect of vertex (3D corner) singularities, first described in the late 70th early 80th by Benthem and a number of other researchers (Benthem 1977, 1980). It was demonstrated that at the intersection (or vertex) of the crack front and a free surface, the square root singularity disappears, and at such a point, one has to deal with a different singular behaviour. The symmetric and anti-symmetric stress states associated with the corner singularities depend on the stress intensity value, K_S and K_A , respectively, the distance to the corner point, R , and the angular position (ϑ, φ), which are omitted in Fig. 4b for the sake of clarity. The strength of the corner singularity, λ_S or λ_A , is a complex function of the local geometry (β, θ) and Poisson's ratio, ν . The values of the stress intensities as well as the strength of singularities for different geometries and loading conditions can be obtained using various semi-analytical methods and direct numerical approaches, e.g. FEM or BFEM (Mittelstedt and Becker 2005; Luangarpa and Koguchi 2016; Doitrand et al. 2020).

The dependences of λ_S and λ_A from Poisson's ratio are given in Fig. 7a for the most commonly considered case of a plane through-the-thickness crack in linear-elastic plate $\beta = \theta = \pi/2$. These dependences have been obtained from fitting numerical results presented

in various papers (He et al. 2015). It can be noted that the strengths of the corner singularities at $\nu = 0$ are the same as the one for the line singularities (or 0.5). Another interesting observation is that Poisson's ratio affects the strength of the corner singularity for symmetric and antisymmetric loading in an opposite way. In the case of symmetric mode, a higher Poisson's ratio leads to lower values of λ_S , and the tendency is opposite for λ_A characterising the antisymmetric mode.

The influence of corner singularities on brittle fracture and fatigue behaviour is currently not well understood (Pook 2013; Branco et al. 2013). Several researchers suggested in the past that the presence of the corner singularity may lead to a deviation of the fatigue crack front from the orthogonal direction near the free surface, or $\beta >$ or $<$ than $\pi/2$, as illustrated in Fig. 7b. This phenomenon is normally observed in fatigue tests for various materials. However, the deviation from a straight shape can also be associated with fatigue crack closure mechanisms and loss of the out-of-plane constraints near the free surfaces (de Matos and Nowell 2008).

Based on energy considerations, several researchers suggested the stress singularity matching concept. In accordance with this concept, the front edge of a fatigue crack under fatigue intersects the free surface at a certain critical angle, β_c , to ensure the same singular behaviour along the whole length of the crack front. This critical angle, β_c , depending on Poisson's ratio, was obtained numerically, and verified in several latest studies, as shown in Fig. 7b (Pook 2013; He et al. 2014). The numerical results are rather accurate, and can be described by the following equations:

$$\beta_c = \tan^{-1} \left(\frac{\nu - 2}{\nu} \right), \tag{3}$$

for symmetric mode (S), and

$$\beta_c = \tan^{-1} \left(\frac{1 - \nu}{\nu} \right), \tag{4}$$

for antisymmetric mode (A).

Past experimental examinations of this hypothesis often led to opposite conclusions. This is likely due to the existence of at least two different mechanisms affecting the fatigue crack front shape: plasticity-induced crack closure and dominance of the vertex singularity stress state near the free surface. For example, for fatigue crack growth in brittle specimens of rectangular and trapezoidal shapes made of PMMA with a measured Poisson's ratio of 0.365, the results were found

Fig. 7 **a** Strength of corner singularity dependence from Poisson's ratio for $\beta = \theta = \pi/2$; **b** The critical angle, β_c , as a function of Poisson's ratio.

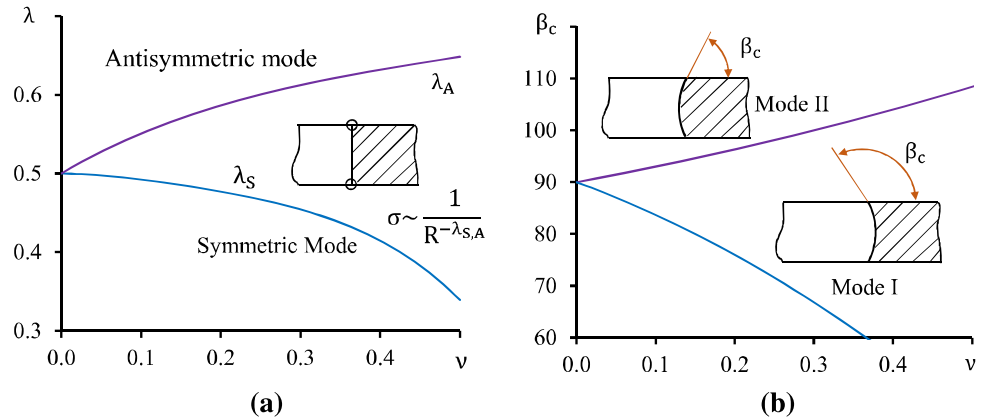


Fig. 8 Specimens with trapezoidal cross sections (**a** and **b**) and additional lengthwise notch (**c**) (Heyder and Kuhn 2006)

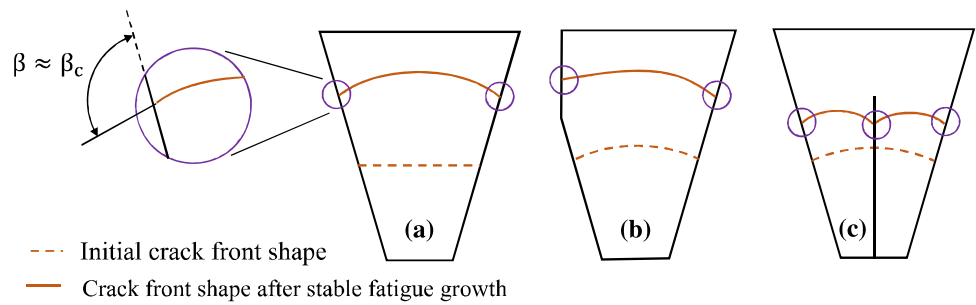
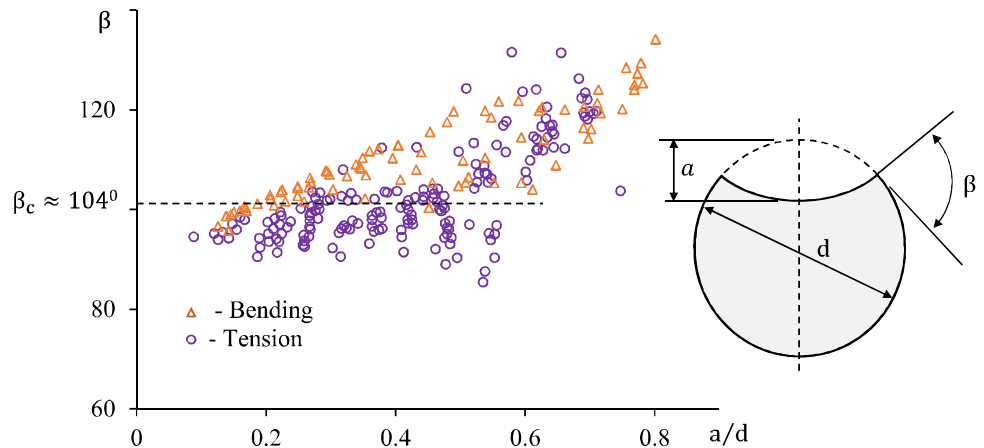


Fig. 9 Intersection angles for surface-breaking cracks in round bars subjected to tension and bending (Lebahn et al. 2013)



to be consistent with the stress singularity-matching concept, see Fig. 8 (Heyder and Kuhn 2006). In all cases the angle at which the crack intersects the free surface was around 104° , which is close to the theoretical prediction, see Fig. 7b. Moreover, the crack front shape changed with the change of the global geometry (Fig. 8b, c) during fatigue cycling and the shape evolved to keep the intersection angle roughly the same.

Another set of experimental data (Fig. 9) reported by the same research group, for surface-breaking cracks performed on round bars with a diameter of 20 mm made of 34CrNiMo6 high strength steel, does not generally support the stress singularity matching concept

(Lebahn et al. 2013). The reason, in this case, could be the relatively large size of plasticity region compared to the region controlled by the 3D corner singularity, which negates its influence on the evolution of the crack front shapes during cycling loading. In this case, the shape of fatigue crack is governed by the effective stress intensity factor, K_{eff} , which is influenced by the loss of the out-of-plane constraints near the free surfaces.

To meet LEFM requirements in these tests, as well as in many similar experimental studies, the plastic zone size must be small compared to the ligament. In particular, these requirements demanded that the plastic zone size, r_p , should be less than 0.5 mm (Lebahn et al. 2013).

However, this plastic zone size is certainly too large to avoid the influence of plasticity on the stress field associated with the 3D vertex singularity (often referred to as boundary layer), which is normally dominated within five–ten percent of the ligament length, or in this case $\approx d/10$, or approximately 1–2 mm. This size has been estimated based on several numerical studies (Branco et al. 2012; Hutař et al. 2009; He et al. 2016a; Camas et al. 2017). Thus, both regions have approximately the same characteristic length, and the intersection angle is the result of a complex interaction between competing mechanisms associated with 3D vertex singularity effect, plasticity and elasto-plastic constraints (Lopez-Crespo et al. 2018; Yu and Guo 2013; de Matos and Nowell 2008).

Attracting the similar arguments of the classical LEFM, the 3D vertex singularity dominates the stress state near the free surfaces: $r_p \ll r_{3D} \sim 0.05 \div 0.1 \times L$, where L is the length of the ligament, e.g. $2h$ for through-the-thickness cracks with straight front. It can be hypothesised that when this condition is met, then the crack front will tend to intersect the free surface at the critical angle, as in the previous set of fatigue test results for PMMA. However, this hypothesis is yet to be validated with carefully planned experimental studies.

4 Displacements and stresses near vertex point

The displacement field near the crack front is a quite controversial topic in LEFM. The plane stress assumption leads to infinite normal out-of-plane strain component, and subsequently, to infinite out-of-plane surface displacements near the crack front, which have no physical meaning. Therefore, in many textbooks and research articles, the plane strain conditions are normally assumed near the crack front. These conditions imply zero out-of-plane strains and zero out-of-plane displacements at the crack tip. The same result (zero out-of-plane displacements and strains) follows from a 3D (approximate) solution, which utilises the shadow functions approach (Costabel et al. 2004; Omer et al. 2004; Omer and Yosibash 2005). In this solution, the displacement components near the straight front of a semi-infinite crack straight allow the following asymptotic expansion:

$$\begin{pmatrix} u_x \\ u_y \\ u_z \end{pmatrix} = A(z) r^{\frac{1}{2}} \begin{pmatrix} -\sin \frac{\phi}{2} + C_1 \sin \frac{3\phi}{2} \\ -C_1 \cos \frac{\phi}{2} + C_1 \cos \frac{3\phi}{2} \\ 0 \end{pmatrix}$$

$$+ \frac{\partial A(z)}{\partial z} r^{\frac{3}{2}} \begin{pmatrix} 0 \\ 0 \\ C_2 \sin \frac{\phi}{2} \end{pmatrix} + \frac{\partial^2 A(z)}{\partial z^2} r^{\frac{5}{2}} \begin{pmatrix} C_3 \sin \frac{\phi}{2} + C_4 \sin \frac{3\phi}{2} \\ \frac{C_1}{6} \cos \frac{\phi}{2} - \frac{C_1}{6} \cos \frac{3\phi}{2} \\ 0 \end{pmatrix} \quad (5)$$

where constants $C_1 \dots C_4$:

$$C_1 = \frac{3\lambda + 7\mu}{\lambda + 5\mu}, C_2 = \frac{2(\lambda + \mu)}{\lambda + 5\mu}, C_3 = \frac{-3\lambda + \mu}{6(\lambda + 5\mu)},$$

$$C_4 = \frac{(3\lambda + 7\mu)^2}{6(\lambda + 5\mu)(7\lambda + 11\mu)} \quad (6)$$

are functions of Lamé's constants, λ and μ . However, as it can be seen from the expansion, this approach ignores the presence and effect of vertex singularities.

On contrary, the first-order plate (or Kane and Mindlin) theory, which takes into account the out-of-plane shear stress components and also disregards the effect of vertex singularities, predicts some finite displacements near the crack front (Kotousov 2007). The latest numerical studies (He et al. 2016a) supported by experimental investigations (He and Kotousov 2016) on thick brittle plates made of PMMA indicate that the transverse displacements at the crack tip for mode I are finite (as expected). At the free surface ($z = \pm h$), the out-of-plane displacement for a semi-infinite crack loaded in mode I by stress intensity factor, K_I^∞ , can be approximated by the following equation, the form of which follows from dimensionless considerations:

$$u_z(r, \phi, \pm h) \approx -\frac{1.34 \cdot \nu \cdot K_I^\infty \sqrt{h}}{E} \quad (7)$$

meaning that neither plane stress nor plane strain assumptions is valid near the crack front, even for a very thin plate. Figure 10 summarises the outcomes of predictions of the out-of-plane surface displacements from plane stress solution, first-order plate (Kane and Mindlin) theory, 3D FE simulations, and experimental studies.

Behaviour of stress intensity factors near the vertex points is another controversial topic, which has no generally accepted understanding among researchers (Leblond and Torlai 1992). For example, Hutař et al. (2009) and (2010) concluded from a FE analysis of middle tension specimens that the strength of the line singularity is different from 0.5 (or square root singularity) and decreases near the free surfaces. Many other numerical simulations for surface cracks show

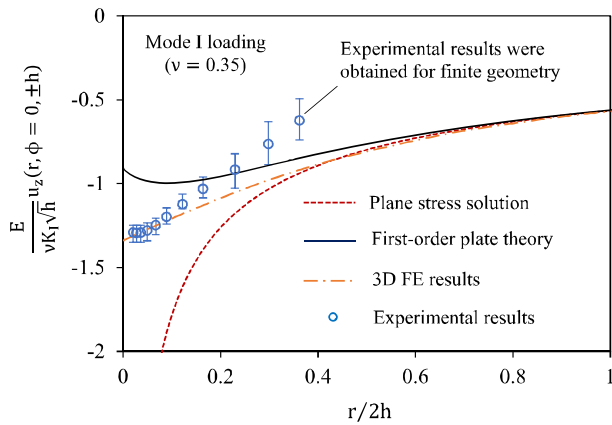


Fig. 10 A comparison between the theoretical predictions, FE simulations and experimental results (He and Kotousov 2016; He et al. 2016a, b; Khanna et al. 2019)

some finite values of the local stress intensity factors at the surface points arguing that the evaluation of the stress intensity factors at these points is inaccurate and affected by vertex singularities. The behaviour of the local stress intensity factor, $K(z)$, may also be affected by the different techniques, which are used to process numerical results (Camas et al. 2012).

The most common computational techniques are based on the stress field ahead of the crack front, displacements behind the crack front and J-integral, which implicitly assume the validity of the classical 2D asymptotic solutions in 3D problems. The corresponding formulae for the evaluation of stress intensity factors in mode I are summarised in Eqs. (8, 9, 10).

$$K_I = \sqrt{2\pi r} \sigma_y (\phi = 0) \tag{8}$$

$$K_I = \frac{\mu}{(\kappa + 1)} \sqrt{\frac{2\pi}{r}} u_y (\phi = \pi) \tag{9}$$

$$K_I = \sqrt{\frac{E}{1-\nu^2}} J \tag{10}$$

The outcomes of the evaluation of the local stress intensity factor behaviour for a through-the-thickness crack in accordance to Eqs. (8)–(10) are summarised in Fig. 11 for a Poisson’s ratio equal to 0.3. All approaches provide essentially the same dependences of $K(z)$ in the interior part of the crack front, but very different dependences near the free surfaces or vertex points. These results, in particular, indicate that despite many numerical studies in the past for homogeneous, anisotropic and composite materials, the evaluation of the line stress intensity factor behaviour near the vertex points still represents a significant challenge. For practical purposes of fatigue life evaluation of struc-

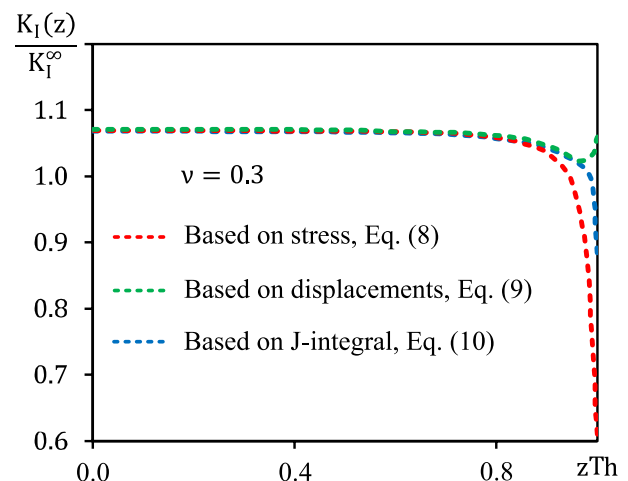


Fig. 11 Local stress intensity factor variations (de Matos and Nowell 2008)

tures with surface defects, some authors recommend ignoring values near the vertex points and rather utilise extrapolation techniques to evaluate the values of stress intensity factor values near free surfaces (Heyder et al. 2005; Shin and Cai 2004).

Instead of numerical simulations, analytical asymptotic approaches can shed some light on the above-formulated problem and clarify the behaviour of stress intensity factors near vertex points. As first shown by Benthem (1977, 1980), the behaviour of the stress intensity factor, K_I , in the area affected by the 3D corner singularity can be described as follows:

$$K_I(s) \sim s^{-\lambda_s+0.5} \tag{11}$$

where s is the curvilinear abscissa of the crack front with its origin at the end point on the free surface. A similar result was obtained by Leguillon and Sanchez-Palencia (1999) attracting the matched asymptotic expansion method. In particular, the following expression of the energy release rate was derived for points on the crack front located near the free surface:

$$G_I(s) \sim s^{-2\lambda_s+1}, \tag{12}$$

which agrees with Eq. (11).

Further, attracting dimensionless considerations, the variation of the stress intensity factor near the corner points can be written as:

for mode I

$$K_I(s) \sim K_I^\infty \times \xi^{-\lambda_s+0.5} \tag{13}$$

for mode II

$$K_{II}(s) \sim K_{II}^\infty \times \xi^{-\lambda_A+0.5} \tag{14}$$

where ξ is just the distance from the vertex point, or $\xi = 1 - z/h$. These dependencies were verified with careful FE studies (He et al. 2016a).

The differences between the strengths of the 3D corner and line singularities are positive for mode I and negative for mode II, see Fig. 5a. Therefore, the dimensionless considerations predict opposite tendencies of the stress intensity factor variations at corner point for these two fracture modes as it can also be observed from many FE simulations in the past. Thus, for a crack with a straight front subjected to mode II, the stress intensity factor, K_{II} , is unbounded near the free surface, or $z \rightarrow h$, which essentially means an immediate local (near free surfaces) failure. These conclusions are in general agreement with general tendencies of many published numerical results, see Fig. 5a, b.

In addition, FE simulations of composite joints reveal similar dependences near the vertex points at the bi-material interfaces. For example, from extensive 3D FE simulations, Luangarpa and Koguchi (2016) found that near the vertex point the line singularity has the following behaviour

$$K \sim s^{-\lambda_{\text{vertex}} + \lambda_{\text{line}}} + b \tag{15}$$

where b is a small number from 0.007 to 0.05. If one assumes that this small constant, b , is primary associated with numerical errors (indeed the numerical results have scatter of the same order) then Eq. (11) is consistent with the asymptotic results of Eqs. (8) and (9) for homogeneous materials.

Based on dimensionless considerations, the following dependences for the intensities of corner singularities can be derived in the case of a semi-infinite (or large) through-the-thickness crack loaded in mode I and II, respectively:

$$K^S \sim K_I^\infty h^{-\lambda_S + 0.5} \tag{16}$$

and

$$K^A \sim K_{II}^\infty h^{-\lambda_A + 0.5} \tag{17}$$

Indeed, the plate thickness and remote stress intensity factors are the only parameters of the problem (at fixed Poisson's ratio). These dependencies are also valid for arbitrary but similar crack front shapes, which are scaled in the same way as the plate thickness. Eqs (16) and (17) represent a new scaling law in Fracture Mechanics. Other 3D scaling laws have also been suggested based on dimensionless considerations and investigated numerically for sharp notches (Carpinteri et al. 2008; Kotousov et al. 2010; Berto et al. 2013).

5 2D and 3D brittle fracture criteria

LEFM is considered to be one of the most developed engineering disciplines with well-defined limitations and well justified criterion of fracture initiation. The classical brittle fracture criterion states that crack is unstable when

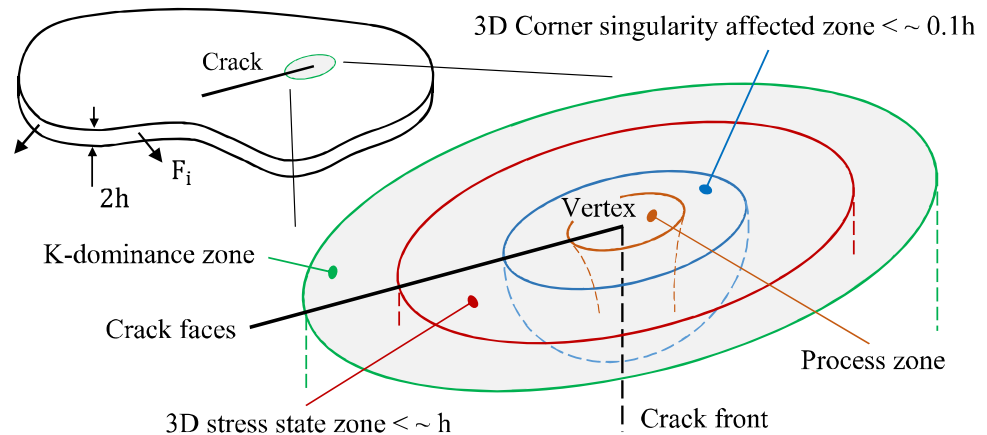
$$K_I = K_c \tag{18}$$

It is generally accepted that this criterion is valid when the stress intensity factor dominates the stress state near the crack tip, and when the K-dominance region is much larger than the process zone. K_c is the critical stress intensity factor and, in general case, it may depend on the plate thickness.

3D analysis indicates that along with K-dominance and process zones near the crack tip, which e.g. can be associated with plastic deformations, there are two other characteristic zones: the zones controlled by the 3D vertex singularity and the 3D stress state, see Fig. 12. The first zone is confined within $R < 0.1h$ half-spherical region with the centre in the vertex point and is fully encapsulated by the second zone (see Fig. 12), which is confined within $r < h$ cylindrical region with the axis aligned with the crack front (Rosakis and Ravi-Chandar 1986). The above estimates of the spread of both zones are based on numerical simulations conducted, however, for specific geometries only. The characteristic dimensions of these zones for other crack geometries, e.g. surface cracks in round bars, are currently unknown, and may be different to the above estimates.

The classical brittle fracture criterion can be readily adopted to incorporate the effect of these 3D zones as follows. The classical brittle fracture criterion is applicable to describe brittle fracture initiation if the K-dominance zone is much larger than both the process and 3D stress state zones. How much larger? It is difficult to answer this question. Past numerical studies indicate that the 3D stress state is confined to a half plate thickness in the plane directions, see Fig. 12. From past numerical simulations, the 3D stress states near the crack front are not affected by the boundaries if the size of the K-dominance zone is larger than $3-4h$ (or if the boundary conditions are applied at distances more than two plate thicknesses in plane directions). This condition, in general, aligns with the Saint-Venant's principle, which is common in stress analysis. Many standard fracture specimens, however, do not comply with this

Fig. 12 3D LEFM fracture criterion



condition; therefore, the distribution of the local stress intensity factors may be different for different test samples. This difference in turn can cause local and global fracture initiation under different values of the applied stress intensity factors, specifically for thick specimens made of a very brittle material.

What about experimental evidences? To assess the validity of the classical fracture criterion, Eq. (15), Sinclair and Chambers (1987) reviewed the open literature; drawing on data furnished in papers, technical publications, proceedings of conferences related to fracture mechanics, and technical reports. A number of strict restrictions were implemented to select the relevant and meaningful results. These restrictions and inclusion procedure can be found in the original paper of Sinclair and Chambers (1987). A few thousand of various fracture test results were reviewed and analysed within the LEFM two-dimensional framework. The main conclusion which can be made from this study is that the brittle fracture results generally follow tendencies predicted by LEFM, but these predictions are unsatisfactory. These authors concluded that “Therefore, there is reason to be concerned about basic fracture mechanics” and classical 2D LEFM criterion. Many recent experimental studies agree with this conclusion, which was formulated more than 30 years ago, see also Fig. 13 ahead.

If the K-dominance zone is much larger than both the process and 3D stress state zones, the 3D computational results for the local stress intensity factor, see Fig. 5a, generally support the classical LEFM criterion for mode I, i.e. $K_I = K_{IC}$, as the variation of $K_I(z)$ is relatively small; and fracture is expected to initiate in the interior section of the crack front. However, the same is not obvious for fracture mode II. The

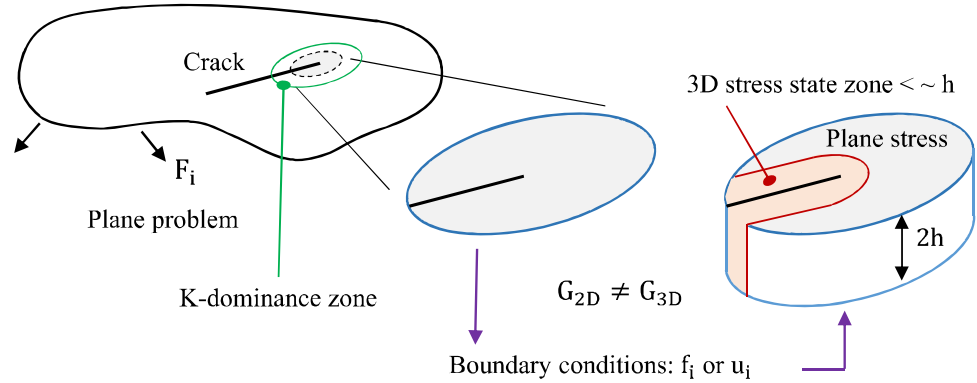
global $K_{II}(z)$ and the coupled $K_{IO}(z)$ stress intensity factors change significantly along the crack front (or plate thickness) and exceed considerably the applied stress intensity factor, K_{II}^∞ , specifically near the free surfaces. The latter can cause initiation of a local fracture near the free surfaces, which can lead to either global fracture, or remain local and change the crack front shape near free surfaces.

Fracture initiation under mixed mode conditions (e.g. I+II or I+III) is beyond the scope of the current review. It remains one of the most intriguing puzzles in LEFM despite it has been widely studied over the past decades (Pham 2016). The crack growth under such loading combinations is not planar anymore. For example, under combined mode I + III, the crack tends to rotate around the direction of propagation in order to reduce mode III and reach a pure mode I situation. This leads to a fragmentation of the initial crack into multiple daughter cracks (also called facets) and forms a very distinct fracture surface appearance. The latest developments in this area include careful experimental studies, investigations of T-stress and high-order terms on brittle failure initiation (e.g. Aliha and Ayatollahi 2011; Gardezabal et al. 2014; Yosibash and Mittelman 2016; Aliha et al. 2017; Qian et al. 2018) as well as numerical studies attempting to predict crack initiation and growth under such loading combinations.

6 Asymptotic expansion

Based on the energy balance equation (or J-integral or energy release rate) and an assumption that the classical (2D) asymptotic expansion is valid near and far from the crack front (in the case of 3D problem formulation) a link between the remotely applied stress intensity fac-

Fig. 13 Correspondence of 2D and 3D problems in linear elasticity



tors, K_I^∞ and K_{II}^∞ , and the local stress intensity factors, $K_I(z)$, $K_{II}(z)$ and $K_O(z)$, can be derived:

$$K_I^\infty = \left(\frac{1-\nu^2}{2h} \int_{-h}^h K_I^2(z) dz \right)^{\frac{1}{2}} \tag{19}$$

$$K_{II}^\infty = \left(\frac{1-\nu^2}{2h} \int_{-h}^h K_{II}^2(z) dz + \frac{1+\nu}{2h} \int_{-h}^h K_O^2(z) dz \right)^{\frac{1}{2}} \tag{20}$$

These relationships are sometimes utilised to verify the quality and accuracy of 3D numerical simulations (Nakamura and Parks 1998, 1989). However, these equations may be incorrect because, generally speaking, the classical (2D) asymptotic expansion is not valid for the corresponding 3D problem far from the crack front but still in K-dominance zone. The 2D asymptotic expansion, in particular, is not valid in the zone adjacent to the crack faces, as illustrated in Fig. 13 and explained earlier. This difference in 2D and 3D stress distributions far from the crack tip can lead to the inequality of the left and right parts of Eqs. (19) and (20).

One can even make an imaginary experiment: consider a 2D crack problem for which $K_I^\infty = K_{II}^\infty = 0$, or when the leading terms of the asymptotic expansion are zero and some higher order terms of the asymptotic expansion are not zero. If the corresponding boundary conditions far from the crack front apply to the corresponding 3D problem, this may lead to a surprising result: non-zero local stress intensity factors or non-zero energy release rates. This is because it would be impossible in the case of the 3D geometry to ensure that both the tractions and displacements in the 3D stress state zone are identical to the corresponding 2D plane stress solution, see Fig. 13 for illustration. This imaginary experiment was simulated in a careful 3D FE

study, which focused on the effect of the higher-order terms of asymptotic expansion on the 3D stress states near crack front (Berto et al. 2011). As expected, the application of the boundary conditions corresponding to non-singular terms of the classical asymptotic expansion produces non-zero values for the local stress intensity factors, specifically for even terms of the asymptotic expansion. The impact of these considerations on practical problems is unclear and needs further investigation. Therefore, one should be careful with the application of 2D results to real 3D problems even in the integral form like Eqs. (19) and (20), specifically when the values of the 2D stress intensity factors are near zero.

7 Conclusion

This article attempted to provide a brief overview of 3D LEFM. The main objective of this paper was to discuss the situations when the classical 2D stress analysis, which is usually based on plane stress and plane strain simplifications, leads to incorrect results or general conclusions. Another objective was to highlight some directions for future research in 3D LEFM, which can contribute into the understanding of brittle fracture and fatigue phenomena.

The 3D problems are much more difficult to analyse than their 2D counterparts, therefore in many cases stress analysis is limited to 2D. There are currently no exact solutions available for 3D crack geometries. Therefore, many fundamental results and general conclusions in 3D LEFM are largely based on dimensionless and energy considerations as well as on the application of complex asymptotic techniques and generalisations of outcomes of 3D numerical studies. However, the generalisation of numerical results, which seems

to be the most common and simple approach, without proper validation procedures and understanding can lead to misleading and incorrect results. This partially explains the existence of so many controversial views on the fundamental issues of 3D LEFM in the current literature.

In this article it was demonstrated, in particular, that the fundamentals of the contemporary LEFM, such as the linear elastic fracture criterion and the near crack tip asymptotic expansions for stress and displacement fields, may be not valid in the 3D formulation and may lead to peculiar results. Many other issues, such as the effects of vertex singularities and the plate thickness are still to be addressed in future analytical, numerical and experimental studies. Finally, it is believed that the 3D considerations alone cannot explain all brittle fracture or fatigue phenomena, but these considerations can contribute into the understanding of these phenomena.

Acknowledgements This research was sponsored by FEDER funds through the program COMPETE (Programa Operacional Factores de Competitividade) and by national funds through FCT (Fundação para a Ciência e a Tecnologia) under the project UIDB/00285/202.

References

- Aliha MRM, Ayatollahi MR (2011) Mixed mode I/II brittle fracture evaluation of marble using SCB specimen. *Procedia Eng* 10:311–318. <https://doi.org/10.1016/j.proeng.2011.04.054>
- Aliha MRM, Berto F, Bahmani A, Gallo P (2017) Mixed mode I/II fracture investigation of Perspex based on the averaged strain energy density criterion. *Phys Mesomech* 20:149–156. <https://doi.org/10.1134/S1029959917020059>
- Benthem JP (1977) State of stress at the vertex of a quarter-infinite crack in a half-space. *Int J Solids Struct* 13(5):479–492. [https://doi.org/10.1016/0020-7683\(77\)90042-7](https://doi.org/10.1016/0020-7683(77)90042-7)
- Benthem JP (1980) The quarter-infinite crack in a half space; alternative and additional solutions. *Int J Solids Struct* 16(2):119–130. [https://doi.org/10.1016/0020-7683\(80\)90029-3](https://doi.org/10.1016/0020-7683(80)90029-3)
- Berto F, Lazzarin P, Kotousov A (2011) On the presence of the out-of-plane singular mode induced by plane loading with $K_{II} = K_I = 0$. *Int J Fract* 167(1):119–126. <https://doi.org/10.1007/s10704-010-9530-5>
- Berto F, Lazzarin P, Kotousov A, Pook LP (2012) Induced out-of-plane mode at the tip of blunt lateral notches and holes under in-plane shear loading. *Fatigue Fract Eng Mater Struct* 35(6):538–555. <https://doi.org/10.1111/j.1460-2695.2011.01647.x>
- Berto F, Kotousov A, Lazzarin P, Pook LP (2013) On scale effect in plates weakened by Rounded V-Notches and subjected to in-plane shear loading. *Int J Fract* 180(1):111–118. <https://doi.org/10.1007/s10704-012-9796-x>
- Branco R, Antunes FV, Costa JD (2013) Extent of the surface region in notched Middle Cracked Tension specimens. *Key Eng Mater* 560:107–127. <https://doi.org/10.4028/www.scientific.net/KEM.560.107>
- Branco R, Antunes FV, Ricardo LCH, Costa JD (2012) Extent of surface regions near corner points of notched cracked bodies subjected to mode-I loading. *Finite Elem Anal Des* 50:147–160. <https://doi.org/10.1016/j.finel.2011.09.006>
- Broek D (1974) Elementary engineering fracture mechanics. In: Chapter. 14: Plates with holes, 4th edn. Groningen: Noordhoff, pp 361–370
- Camas D, Garcia-Manrique J, Gonzalez-Herrera A (2012) Crack front curvature: influence and effects on the crack tip fields in bi-dimensional specimens. *Int J Fatigue* 44:41–50. <https://doi.org/10.1016/j.ijfatigue.2012.05.012>
- Camas D, Lopez-Crespo P, Gonzalez-Herrera A, Moreno B (2017) Numerical and experimental study of the plastic zone in cracked specimens. *Eng Fract Mech* 185:20–32. <https://doi.org/10.1016/j.engfracmech.2017.02.016>
- Carpinteri A, Cornetti P, Pugno N, Sapora A, Taylor D (2008) A finite fracture mechanics approach to structures with sharp V-notches. *Eng Fract Mech* 75(7):1736–1752. <https://doi.org/10.1016/j.engfracmech.2007.04.010>
- Costabel M, Dauge M, Yosibash Z (2004) A quasi-dual function method for extracting edge stress intensity functions. *SIAM J Math Anal* 35(5):1177–1202. <https://doi.org/10.1137/S0036141002404863>
- de Matos PFP, Nowell D (2008) The influence of the Poisson's ratio and corner point singularities in three-dimensional plasticity-induced fatigue crack closure: A numerical study. *Int J Fatigue* 30(10):1930–1943. <https://doi.org/10.1016/j.ijfatigue.2008.01.009>
- Doitrand A, Leguillon D, Martin E (2020) Computation of generalized stress intensity factors of 3D singularities. *Int J Solids Struct* 190:271–280. <https://doi.org/10.1016/j.ijsolstr.2019.11.019>
- Folias ES, Wang JJ (1990) On the three-dimensional stress field around a circular hole in a plate of arbitrary thickness. *Comput Mech* 6(5):379–391. <https://doi.org/10.1007/BF00350419>
- Gardezabal D, He Z, Kotousov A (2014) On influence of non-singular stress states on brittle fracture. *Int J Fract* 185:201–208. <https://doi.org/10.1007/s10704-013-9903-7>
- Gregory RD, Wan FYM (1988) The interior solution for linear problems of elastic plates. *J Appl Mech* 55(3):551–559. <https://doi.org/10.1115/1.3125829>
- Hartranft R, Sih G (1969) The use of eigenfunction expansions in the general solution of three-dimensional crack problems. *Indiana Univ Math J* 55(3):551–559. <https://doi.org/10.1512/iumj.1970.19.19012>
- He Z, Kotousov A (2016) On evaluation of stress intensity factor from in-plane and transverse surface displacements. *Exp Mech* 56(8):1385(9). <https://doi.org/10.1007/s11340-016-0176-8>
- He Z, Kotousov A, Branco R (2014) A simplified method for the evaluation of fatigue crack front shapes under mode I loading. *Int J Fract* 188(2):203–211. <https://doi.org/10.1007/s10704-014-9955-3>
- He Z, Kotousov A, Berto F (2015) Effect of vertex singularities on stress intensities near plate free surfaces. *Fatigue Fract*

- Eng Mater Struct 38(7):860–869. <https://doi.org/10.1111/ffe.12294>
- He Z, Kotousov A, Berto F, Branco R (2016a) A brief review of recent three-dimensional studies of brittle fracture. *Phys Mesomech* 19:6–20. <https://doi.org/10.1134/S1029959916010021>
- He Z, Kotousov A, Fanciulli A, Berto F, Nguyen G (2016b) On the evaluation of stress intensity factor from displacement field affected by 3D corner singularity. *Int J Solids Struct* 78–79:131–137. <https://doi.org/10.1016/j.ijsolstr.2015.09.007>
- Heyder M, Kolk K, Kuhn G (2005) Numerical and experimental investigations of the influence of corner singularities on 3D fatigue crack propagation. *Eng Fract Mech* 72(13):2095–2105. <https://doi.org/10.1016/j.engfracmech.2005.01.006>
- Heyder M, Kuhn G (2006) 3D fatigue crack propagation: experimental studies. *Int J Fatigue* 28(5):627–634. <https://doi.org/10.1016/j.ijfatigue.2005.06.052>
- Hutař P, Náhlík L, Knésl Z (2009) Quantification of the influence of vertex singularities on fatigue crack behavior. *Comput Mater Sci* 45(3):653–657. <https://doi.org/10.1016/j.commatsci.2008.08.009>
- Hutař P, Náhlík L, Knésl Z (2010) The effect of a free surface on fatigue crack behaviour. *Int J Fatigue* 32(8):1265–1269. <https://doi.org/10.1016/j.ijfatigue.2010.01.009>
- Qian G, Cao Y, Niffenegger M, Chao YJ, Wu W (2018) Comparison of constraint analyses with global and local approaches under uniaxial and biaxial loadings. *Eur J Mech* 69:135–146
- Khanna A, Kotousov A, Yakubovich S, Zakavi B (2019) Asymptotic analysis of out-of-plane strain and displacement fields at angular corners. *Int J Solids Struct* 170:111–122. <https://doi.org/10.1016/j.ijsolstr.2019.04.024>
- Kotousov A (2007) Fracture in plates of finite thickness. *Int J Solids Struct* 44(25):8259–8273. <https://doi.org/10.1016/j.ijsolstr.2007.06.011>
- Kotousov A (2010) Effect of plate thickness on stress state at sharp notches and the strength paradox of thick plates. *Int J Solids Struct* 47(14):1916–1923. <https://doi.org/10.1016/j.ijsolstr.2010.03.029>
- Kotousov A, Wang CH (2002) Three-dimensional stress constraint in an elastic plate with a notch. *Int J Solids Struct* 39(16):4311–4326. [https://doi.org/10.1016/S0020-7683\(02\)00340-2](https://doi.org/10.1016/S0020-7683(02)00340-2)
- Kotousov A, Lazzarin P, Berto F, Harding S (2010) Effect of the thickness on elastic deformation and quasi-brittle fracture of plate components. *Eng Fract Mech* 77(11):1665–1681. <https://doi.org/10.1016/j.engfracmech.2010.04.008>
- Kotousov A, Lazzarin P, Berto F, Pook LP (2013) Three-dimensional stress states at crack tip induced by shear and anti-plane loading. *Eng Fract Mech* 108:65–74. <https://doi.org/10.1016/j.engfracmech.2013.04.010>
- Kotousov A, Bun S, Khanna A (2017) A new analytical method for the evaluation of transverse displacements and stresses in plane problems of elasticity. *Int J Solids Struct* 118–119:89–96. <https://doi.org/10.1016/j.ijsolstr.2017.04.020>
- Kotousov A, Khanna A, Branco R, De Jesus AMP, Correia JAF (2019) Review of current progress in 3D linear elastic fracture mechanics. *Struct Integr* 7:125–131. https://doi.org/10.1007/978-3-030-13980-3_16
- Lebahn J, Heyer H, Sander M (2013) Numerical stress intensity factor calculation in flawed round bars validated by crack propagation tests. *Eng Fract Mech* 108:37–49. <https://doi.org/10.1016/j.engfracmech.2013.04.013>
- Leblond JB, Torlai O (1992) The stress field near the front of an arbitrarily shaped crack in a three-dimensional elastic body. *J Elast* 29(2):97–131. <https://doi.org/10.1007/BF00044514>
- Leguillon D, Sanchez-Palencia E (1999) On 3D cracks intersecting a free surface in laminated composites. *Int J Fract* 99(1):25–40. <https://doi.org/10.1023/a:1018366720722>
- Lopez-Crespo P, Camas D, Antunes FV, Yates JR (2018) A study of the evolution of crack tip plasticity along a crack front. *Theor Appl Fract Mech* 98:59–66. <https://doi.org/10.1016/j.tafmec.2018.09.012>
- Luangarpa C, Koguchi H (2016) Analysis of singular stresses at a vertex and along a singular line in three-dimensional bonded joints using a conservative integral. *Eur J Mech A* 60:208–216. <https://doi.org/10.1016/j.euromechsol.2016.08.002>
- Maccagno TM, Knott JF (1989) The fracture behaviour of PMMA in mixed modes I and II. *Eng Fract Mech* 34(1):65–86. [https://doi.org/10.1016/0013-7944\(89\)90243-9](https://doi.org/10.1016/0013-7944(89)90243-9)
- Maia R, Branco R, Antunes FV, Oliveira MC, Kotousov A (2016) Three-dimensional computational analysis of stress state transition in through-cracked plates. *Math Comput Sci* 10(3):343–352. <https://doi.org/10.1007/s11786-016-0267-z>
- Maurizi M, Berto F (2020) 3D effects on fracture mechanics. *Procedia Struct. Integr* 25:268–281. <https://doi.org/10.1016/j.prostr.2020.04.032>
- Mittelstedt C, Becker W (2005) Semi-analytical computation of 3D stress singularities in linear elasticity. *Commun Numer Methods Eng* 21(5):247–257. <https://doi.org/10.1002/cnm.742>
- Nakamura T, Parks DM (1998) Three-dimensional stress field near the crack front of a thin elastic plate. *J Appl Mech* 55(4):805–813. <https://doi.org/10.1115/1.3173725>
- Nakamura T, Parks DM (1989) Antisymmetrical 3-D stress field near the crack front of a thin elastic plate. *Int J Solids Struct* 25(12):1411–1426. [https://doi.org/10.1016/0020-7683\(89\)90109-1](https://doi.org/10.1016/0020-7683(89)90109-1)
- Omer N, Yosibash Z (2005) On the path independency of the point-wise J integral in three-dimensions. *Int J Fract* 136(1):1–36. <https://doi.org/10.1007/s10704-005-3934-7>
- Omer N, Yosibash Z, Costabel M, Dauge M (2004) Edge flux intensity functions in polyhedral domains and their extraction by a quasidual function method. *Int J Fract* 129(2):97–130. <https://doi.org/10.1023/B:FRAC.0000045717.60837.75>
- Pham KH (2016) Ravi-Chandar K (2016) On the growth of cracks under mixed-mode I+III loading. *Int J Fract* 199:105–134. <https://doi.org/10.1007/s10704-016-0098-6>
- Pook LP (2010) Five decades of crack path research. *Eng Fract Mech* 77(11):1619–1630. <https://doi.org/10.1016/j.engfracmech.2010.04.010>
- Pook LP (2013) A 50-year retrospective review of three-dimensional effects at cracks and sharp notches. *Fatigue Fract Eng Mater Struct* 36(8):699–723. <https://doi.org/10.1111/ffe.12074>
- Rosakis AJ, Ravi-Chandar K (1986) On crack-tip stress state: An experimental evaluation of three-dimensional effects. *Int J Solids Struct*. [https://doi.org/10.1016/0020-7683\(86\)90002-8](https://doi.org/10.1016/0020-7683(86)90002-8)

- She C, Guo W (2007) Three-dimensional stress concentrations at elliptic holes in elastic isotropic plates subjected to tensile stress. *Int J Fatigue*. <https://doi.org/10.1016/j.ijfatigue.2006.03.012>
- She C, Zhao J, Guo W (2008) Three-dimensional stress fields near notches and cracks. *Int J Fract* 22(2):121–134. <https://doi.org/10.1007/s10704-008-9247-x>
- Shin CS, Cai CQ (2004) Experimental and finite element analyses on stress intensity factors of an elliptical surface crack in a circular shaft under tension and bending. *Int J Fract* 129(3):239–264. <https://doi.org/10.1023/B:FRAC.0000047784.23236.7d>
- Shivakumar KN, Raju IS (1990) Treatment of singularities in cracked bodies. *Int J Fract* 45(3):159–178. <https://doi.org/10.1007/BF00693347>
- Sinclair GB, Chambers AE (1987) Strength size effects and fracture mechanics: what does the physical evidence say? *Eng Fract Mech* 26(2):279–310. [https://doi.org/10.1016/0013-7944\(87\)90204-9](https://doi.org/10.1016/0013-7944(87)90204-9)
- Sinclair GB (2004) Stress singularities in classical elasticity - I: removal, interpretation, and analysis. *Appl Mech Rev* 57(4):251–298. <https://doi.org/10.1115/1.1762503>
- Sinclair GB (2004) Stress singularities in classical elasticity - II: asymptotic identification. *Appl Mech Rev* 57(5):385–439. <https://doi.org/10.1115/1.1767846>
- Yang W, Freund LB (1985) Transverse shear effects for through-cracks in an elastic plate. *Int J Solids Struct* 21(9):977–994. [https://doi.org/10.1016/0020-7683\(85\)90111-8](https://doi.org/10.1016/0020-7683(85)90111-8)
- Yang Z, Cho C, Kim CB, Beom HG (2008) The effect of biaxial load on stress and strain concentrations in a finite thickness elastic plate containing a circular hole. *Int J Numer Methods Eng* 75(1):103–126. <https://doi.org/10.1002/nme.2249>
- Yosibash Z, Mittelman B (2016) A 3-D failure initiation criterion from a sharp V-notch edge in elastic brittle structures. *Eur J Mech A* 60:70–94. <https://doi.org/10.1016/j.euromechsol.2016.06.003>
- Yu P, Guo W (2013) An equivalent thickness conception for evaluation of corner and surface fatigue crack closure. *Eng Fract Mech* 99:202–213. <https://doi.org/10.1016/j.engfracmech.2012.12.013>

Publisher's Note Springer Nature remains neutral with regard to jurisdictional claims in published maps and institutional affiliations.

2.3 Part 2: Introduction to Fatigue of Structures and Materials

2.3.1 Fatigue Phenomenon

Fatigue crack propagation is a complex phenomenon, which can be affected by several interacting factors. Fatigue crack propagation can be associated with cyclic plasticity, sliding or physical contact (fretting and rolling contact), environmental damage (corrosion fatigue), or elevated temperatures (creep fatigue) in mechanical components and structures (Milne et al. 2011). Therefore, there are many theoretical and experimental approaches, as well as predictive models, to analyse the fatigue phenomena. The scope of the current work is restricted to the crack growth associated with fatigue loading.

The current view on fatigue failure, shared by many researchers, is that it is a cumulative process consisting of three main stages: crack initiation, propagation, and final fracture of a component. During cyclic loading, localised, irreversible, plastic deformations may occur at sites with a high stress concentration, e.g., those associated with grain apexes or surface grains. These irreversible plastic deformations induce permanent damage to the material, leading to the development of micro-cracks. As the material experiences an increasing number of loading cycles, the length of the micro-cracks increases, and cracks can coalesce, progress or arrest. After a certain number of cycles, the dominant crack is formed, and when the dominant crack length reaches its critical size, the component fails by rupture (Lee et al. 2005).

2.3.2 Historical Overview

Fatigue phenomena have been studied for more than 170 years. The first studies were undertaken in the 19th century during the industrial revolution in Europe when some heavy-duty locomotives and boilers failed under cyclic loading conditions. It was William Albert who in 1837 first published an article on fatigue that established a correlation between the magnitude of the cyclic load and the durability of the structural component.

Two years later, in 1839, Jean Victor Poncelet, the designer of cast iron axles for mill wheels, officially used the term ‘fatigue’ for the first time in his works published at that time (Bhat 2011). Fatigue was recognised well over a hundred and fifty years ago; however, systematic research in this area started around the 1850s when August Wöhler conducted his classic cyclic load tests, which led to the development of the so-called S-N curves or S-N diagrams for various materials and conditions (Etube 2001). He is often named as the founder of design procedures against fatigue failures. In the period between 1858 and 1870, Wöhler published several papers on the fatigue strength of railway axles, as well as the outcomes of fatigue tests of small-scale specimens made of steel, iron and copper. From these tests he obtained the basic fatigue properties, which were further utilised to predict fatigue failures and guide the design of structures subject to cyclic loading (Zenner & Hinkelmann 2019).

A fundamental step in the understanding of fatigue phenomena at the micro-level was made at the beginning of the 20th century by Ewing and Humfrey (1903) who carried out the first microscopic investigation of fatigue failure in specimens made of iron, which failed due to cyclic bending. In particular, they observed the localised cyclic slips in surface grains and the formations of pronounced surface marks on failure surfaces. These microscopic observations demonstrated that crack initiation can be associated with the localised slip generating extrusions and intrusions on free surfaces; and that fatigue crack propagation is a process of a crack advance during each fatigue cycle.

In the middle of the 20th century, Peterson (1950) and Timoshenko (1954) provided comprehensive reviews of early studies in the area of fatigue and design against fatigue. Peterson considered fatigue as a material phenomenon from an historic perspective, highlighting the significance of the concept of the endurance limit introduced by Wöhler. He regarded this endurance limit as a material property, which can be used in the design of engineering structures and machines. Timoshenko emphasised the significance of stress concentrations around notches and recognised the necessity for theoretical analysis of stress distributions near the stress risers or stress concentrators (Schijve 2003).

The next key development in fatigue was associated with a revolutionary idea proposed by Paris and Erdogan in the early 1960s. They suggested that the range of the stress intensity factor is the driving force, and it fully describes the rate at which fatigue cracks grow during cyclic loading (Paris & Erdogan 1963). This idea was very fruitful and led to the development of many methods for assessing the acceptability of manufacturing or in-service defects, as well as fatigue life expectancy in the presence of crack-like defects. However, it was quickly realised that many other factors in addition to the stress intensity factor range influence the rate of propagation of fatigue cracks. These factors (e.g., the R-ratio or overload/underload ratio) were introduced as parameters into several empirical models aiming to improve fatigue life predictions.

Significant research effort has been directed to the study of the fatigue crack closure phenomenon, first introduced by Elber, to explain the experimentally observed features of fatigue crack growth in aluminum alloys (Elber 1970). He argued that a load cycle is only effective in driving the fatigue growth of a crack if the crack is fully open. Since his pioneering study in the 1970s, the number of scientific studies on this topic has grown progressively. In particular, it was later found that there are many different sources for crack closure, not just the plasticity-induced crack closure observed by Elber (Suresh & Ritchie 1984). The roughness of crack surfaces (roughness-induced crack closure) and oxides due to corrosion processes (oxide-induced crack closure) can also produce crack closure and influence the rates of fatigue crack growth (Rodrigues & Antunes 2009).

Plasticity-induced fatigue crack closure is a complex extrinsic mechanism, which has a shielding effect due to the change in deformation behaviour near the crack tip. Elber's discovery of fatigue crack closure, nearly 50 years ago, was a promising development with the prospect of significant advances in fatigue life predictions of structural components (Khanna & Kotousov 2020). A large amount of experimental, analytical, and computational work has been conducted since this discovery (de Matos & Nowell 2009). Unfortunately, the initial expectations have largely faded in the face of unprecedented difficulties in theoretical modelling.

The early two-dimensional crack closure models, which were based on the classic Dugdale or yield-strip model, were incorporated into several fatigue life-prediction codes, such as FASTRAN and NASGRO. These codes demonstrated encouraging results, specifically in predicting the R-ratio effect in the case of constant amplitude loading. The safety factors and conservative assumptions were used to address the inherent uncertainties associated with service loads. However, blind predictions of fatigue crack growth under variable loading conditions are usually disappointing (Khanna & Kotousov 2020). This is because real cracks are inherently three-dimensional (Kotousov et al. 2013) and the three-dimensional aspects of the problem, e.g., the plate thickness, have a significant effect on the crack closure mechanism (Roychowdhury & Bodds 2003). Further details about the plasticity-induced fatigue crack closure mechanism and the developed methods can be found in the following sections.

2.3.3 Fatigue Regimes

Three distinct regimes of fatigue behaviour are normally identified in the S-N diagrams for structural materials: Low Cycle Fatigue (LCF), High Cycle Fatigue (HCF) and Ultra High Cycle Fatigue (UHCF). The total fatigue life, N_T , can be decomposed into the following stages (McDowell & Dunne 2010):

$$N_T = N_F + N_{MS} + N_{PS} + N_L \quad (2.1)$$

where N_F is the number of cycles required to form a crack, and N_{MS} , N_{PS} and N_L represent the number of cycles to propagate a crack through the microstructurally small, physically small and long crack growth regions, respectively. The fraction of N_F in the total fatigue life is normally very small in an LCF regime, but it may comprise a significant fraction of N_T in HCF (up to 10^7 cycles) and fully dominates the total fatigue life in UHCF (up to 10^9 cycles and beyond). Various studies indicate that N_F can range generally from 10% to 50% of the total fatigue life in HCF, depending on the material, its microstructure, and the presence of pre-existing defects (Mughrabi 2013).

The discrepancies between various studies may be partially attributed to the differences in the definition of N_F , which, according to some researchers, should incorporate crack growth through several strong microstructural barriers (e.g., grain boundaries) in metals and alloys. There are also other decompositions of the total fatigue life to be found in the literature, e.g., Schijve (1967) and Miller (1987).

With the progress in technological development, the required fatigue life for many components may well exceed 10^8 load cycles. Nowadays, Very High Cycle Fatigue (VHCF) constitutes one of the main design challenges for several applications in aircraft, automobile, railway, and other industries. Some examples of such components are gas turbine disks, car engine cylinder heads and blocks, ball bearings, high frequency drilling machines, diesel engines of ships and high-speed trains (Kazymyrovych 2009). Nonetheless, the VHCF regime is beyond the scope of the current PhD project, which is limited to the HCF regime.

HCF is a type of fatigue caused by small elastic strains under a high number of load cycles (typically $> 10^4$ cycles) before failure occurs. The fatigue damage comes from a combination of mean and alternating stresses. The mean stress is usually due to the residual stress, the assembly load, or non-uniform temperature distribution. The alternating stress can be a mechanical or thermal stress at any frequency.

2.3.4 Fatigue Analysis

Contemporary fatigue analysis usually utilises one of three main methodologies, which are based on 1) the stress-life, 2) the strain-life, and 3) Fracture Mechanics approaches. In addition, Continuum Damage Mechanics (CDM) is the fourth main methodology, which applies to problems involving multiple damage mechanisms of different natures, e.g., creep, fatigue, and corrosion. However, CDM is not very popular in fatigue analysis, as the predictive capabilities of CDM-based models are generally lower than for their competitors. The current Section will briefly overview two first approaches and will specifically focus on the Fracture Mechanics approach as the most advanced and most accurate for fatigue life predictions.

2.3.5 Stress-Life Methodology

Fatigue failures can occur at stresses well below the monotonic loading levels that cause static failure. Since the pioneering systematic studies of August Wohler in 1890, it has become customary to represent fatigue data using the so-called S-N diagrams, where the stress amplitude is plotted versus the number of cycles to failure. The stress-based approach was the earliest, but it is still the most common approach for fatigue life evolutions across several industries. In this approach, the number of cycles to failure, N , in an HCF regime is related to the applied stress range or stress amplitude, S , as a power function, called Basquin's law (Basquin 1910):

$$S = C \times N^m \quad (2.2)$$

where C and m are material constants, found from fitting this equation to the experimental data. However, the life predictions with this approach have a large scatter. As discussed above, this scatter is due to many factors affecting fatigue life, which are not explicitly included in Basquin's law, e.g., the stress concentration and surface roughness. Many similar simple equations have been suggested over the past hundred years for different materials and loading conditions (Kim & Zhang 2001). These equations may be more accurate for any given specified conditions or materials and may partially reduce the large scatter (Kim et al. 2001) that is common for this methodology.

2.3.6 Strain-Life Methodology

Special attention should be paid to fatigue assessment of geometrical discontinuities in the fatigue design, as most engineering components experience variable amplitude loadings during operation. Examples of structural discontinuities are joints, welds, and junctions between components of different diameters or thicknesses. In these cases, any strong stress concentrations present in the component may result in crack initiation and local cyclic plastic deformation. The strain-life approach is commonly used in situations where local plasticity may occur.

The strain-life methodology assumes that the material at the notch root behaves in the same way as a smooth laboratory (un-notched) sample, for which fatigue resistance can be tested at various loadings. At the relatively high stresses where plastic deformation can occur, the Coffin–Manson fatigue design approach has been widely applied in the past to undertake fatigue assessments in Low Cycle Fatigue regimes (LCF); the correlation between the plastic strain amplitude and the fatigue life is expressed by:

$$\frac{\Delta\varepsilon_p}{2} = \varepsilon_f \times (2N_f)^c \quad (2.3)$$

where $\Delta\varepsilon_p$ is the plastic strain range, ε_f is the fatigue ductility coefficient and c is the fatigue ductility exponent (Dewa et al. 2017). Similar to S-N diagrams (equations), the Coffin–Manson equation currently has many modifications, which may provide better accuracy of the theoretical predictions (Wang et al. 2016).

2.3.7 Hybrid Approaches

Numerous hybrid approaches have been suggested, largely based on experimental data and concepts of merging equations for LCF and HCF regimes. For example, a hybrid method was proposed by Szala and Ligaj (2016) for calculations of fatigue life for C45 steel under multi-stage loads. The proposed hybrid method consists of an assumption that the overall fatigue properties of steel in the range of low cycle fatigue are defined by the Manson-Coffin equation, whereas in the HCF regime, the cyclic properties of this steel are described by the standard S-N diagram. In general, hybrid approaches can provide an adequate evaluation of fatigue life in the case of combined (LCH + HCF) loading; however, the accuracy and applicability of such predictions may be quite limited (Goedel et al. 2018).

2.3.8 Fracture Mechanics Approach

As an alternative to the Stress-life, Strain-life and Hybrid methods, the Fracture Mechanics approach was developed in the 1970s and is now widely applied to evaluate the remaining strength of structural components with defects in many industries and advanced applications. This approach tracks the propagation of structural defects, mainly cracks, and can predict the remaining life of structural components more accurately, avoiding both scatter and excessive conservatism. Below, a brief introduction to the Mechanics of Cracks is presented. It is not intended to cover all aspects of this approach.

Fatigue cracks usually start from the surface of a component, where fatigue damage begins on crystallographic slip planes. Free surfaces after cyclic loading normally exhibit some additional roughness, which is formed by intrusions and extrusions along the slip planes, as illustrated in Figure 1. Stage I is characterised by a rapid decrease in the crack growth rate, which is accompanied by a decrease in the cyclic plastic zone size. Behaviour in this stage is dependent on the microstructural features.

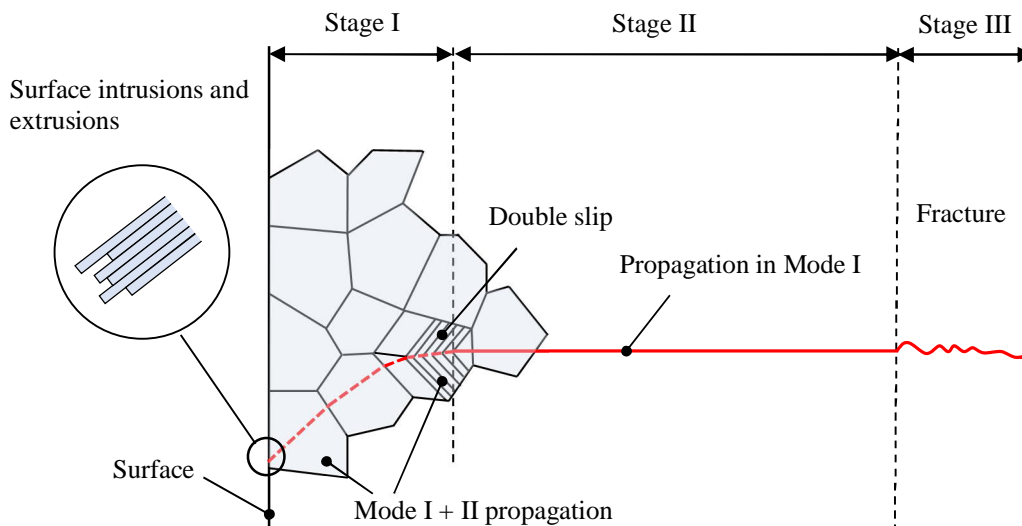


Figure 1. A schematic representation of crack formation and growth in polycrystalline metals, adopted from Cui (2002).

Previous studies have demonstrated that at least five major factors should be considered when attempting to establish the relationship between microstructure and fatigue crack propagation. These include the strain distribution, slip length and plastic zone size, crack path and crack extension forces, morphology, and properties of constituents in multiphase alloys and the environment (Cui 2002). After a transient region (Stage II), crack growth continues in a direction normal to the applied stress, or predominantly in mode I. The rate of crack propagation in Stage II increases rapidly until final fracture. This region corresponds to the onset of unstable and rapid crack growth and is characterized by either the material's fracture toughness or, in the case of ductile materials, by plastic instability. The environment has little effect in this region and deformation mechanisms are similar to those characteristics of monotonic loading (Etube 2000).

Microstructurally short and long cracks should be distinguished for fatigue analysis. Experimental studies of crack propagation for various materials and loading conditions (10 μm to 1 mm) have shown that small cracks grow much faster than would be predicted from the large crack data. (Newman et al. 1999). Typical fatigue growth behaviours for small and large cracks are shown in Figure 2.

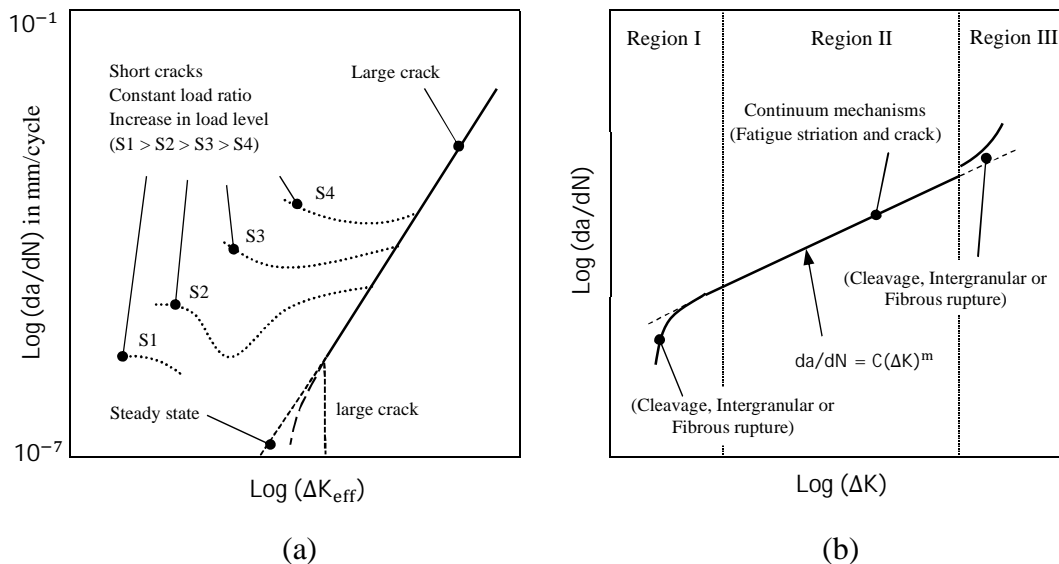


Figure 2: (a) Typical fatigue-crack-growth behaviour for small and large cracks, reproduced from Zerbst et al. (2016); (b) Schematic fatigue crack growth curve for large cracks.

Small cracks can also propagate below the long crack threshold stress intensity range (Chowdhury & Sehitoglu 2016). Short-crack growth behaviour might be explained by the concept of nonlinear or elastic–plastic Fracture Mechanics. However, the abnormal behaviour of small cracks is beyond the scope of the current thesis, which is focused on prediction of long cracks or cracks larger than 0.5 mm. It has been found that the fatigue crack growth models can be broadly classified into three main categories: (a) linear elastic, (b) geometrical, and (c) plastic accumulation models (Chowdhury & Sehitoglu 2016).

Linear Elastic Models

Linear elastic-based models have been widely used for analysis of the microstructure-insensitive stable propagation of a stage II crack in brittle and moderately ductile materials, provided the region of plastic deformation is small in comparison with all other geometry sizes (showing negligible or non-existent plasticity). This condition is called the Small-Scale Yielding (SSY) condition and the stress intensity factor governs the local plastic stresses. In this case, the plastic zone is in the order of a few percent compared with the characteristic dimensions of the crack, such as the component's thickness. Under these conditions, the growth rate depends only on the continuum parameters, such as the stress range far away from the crack, the crack length, and load ratio.

The first and most important empirical relationship of Stage II crack extension was proposed by Paris and his colleagues in the early 1960s (Paris and Erdogan 1963). It was observed experimentally that the linear region accounts for a significant portion of the overall lifetime, especially for specimens or structures with pre-existing cracks or sharp notches. They demonstrated that crack growth can be described as a function of the stress intensity factor caused by a remote load or residual stresses.

$$\frac{da}{dN} = C \times K^m \quad (2.4)$$

Parameters a and N are the crack length and the number of load cycles. The constant values of C and m are experimentally determined values for the different materials.

Later, the stress intensity factor K was replaced with the stress intensity factor range, ΔK . ASTM international standard (E647-13 2013) provides the method for the determination of fatigue crack growth rates from near-threshold to maximum stress intensity factor (K_{\max}) controlled instability.

Paris' law limitations have been well documented in the literature. For example, it is demonstrated that the proposed empirical crack growth rate law only models stable fatigue crack propagation behaviour (propagation regime II) and is also unable to account for the effects of the stress ratio in the crack growth rate. Many alternative fatigue crack propagation relationships have been proposed to overcome the limitations of Paris' law and also to deal with variable amplitude loading (Correia et al 2014). Nevertheless, Paris' law continues to be used frequently to model fatigue crack growth under constant amplitude loading due to its attractive simplicity. Numerous improvements have also been suggested by the industrial standards, with the intention of being able to model the full spectrum of fatigue crack growth. As an example, a two-stage power law relationship is recommended by BS7910 *Guide on methods for assessing the acceptability of flaws in metallic structures* to reduce the conservatism associated with crack growth near the fatigue threshold.

The fatigue design curves are normally given by simplified equations and are plotted in the design and safety standards for the welded and un-welded structures. There are a number of design and safety standards available in different industries and applications. In the most industrial standards, the front of the existing or postulated crack for different structural components is modelled by an idealised geometry such as straight, semi-elliptical or circular crack. The crack growth idealisation means that a flaw or crack with a complex shape is modelled with the conservative dimensions, so that the idealised crack geometry is severe, and the estimated design life is less than the actual design life. In addition, the variations of stress intensity factors across the crack front, coupled modes, and 3D corner (vertex) singularity effect are all currently ignored in industrial standards.

Geometrical Models

The geometrical models were developed based on the ΔK -dependent Paris law. One specific objective of these models is to consider the component's geometry, including thickness, crack shape, and stress concentrators. The geometrical model-based approaches were motivated by consideration of crack tip plasticity effects ahead of, behind and along 'wings' extending either side of the crack front, i.e., planes of shear. For example, Suresh and Ritchie (1982) presented a geometric model for the simulation of plasticity-induced fatigue crack closure by fracture surface roughness. This model specifically addressed the contribution from both Mode I and Mode II crack tip displacements in addition to considering the nature of the fracture surface morphology.

Plastic Accumulation Models

The third group of fracture mechanics-based fatigue crack growth models are dedicated to the investigation and simulation of the plastic zone and plastic wake for both small and large-scale yielding conditions. The purpose of the plastic accumulation-based predictions is to consider the plasticity in expressing the growth rate, da/dN . In these models, most attempts to model crack closure usually involve greatly simplifying crack tip plasticity phenomena: for example, the use of the plasticity-induced crack closure concept for consideration of the part of the load cycle when the crack tip is fully open. The main assumption of this concept is that, when the crack is closed, the external load produces negligible fatigue damage ahead of the crack tip.

The crack closure concept is often attractive to explain many aspects of fatigue behaviour in cracked components. It is now commonly accepted that the contribution of the plasticity-induced crack closure (PICC) is the most important mechanism on the crack closure under small-scale yielding conditions (Pippan & Hohenwarter 2017). Therefore, understanding and development of plasticity-induced crack closure models is essential for accurate evaluation of fatigue crack propagation behaviour as a function of the loading condition.

Therefore, the Paris crack growth rate equation can be re-defined by the following relationship:

$$\frac{da}{dN} = C(\Delta K_{\text{eff}}, R)^m \quad (2.5)$$

where R is the load ratio ($\sigma_{\text{min}}/\sigma_{\text{max}}$).

The crack closure phenomenon is a direct consequence of the permanent tensile plastic deformations left in the wake of the propagating crack. Plasticity-induced crack closure is based on the idea that any residual plastically deformed material ahead of the crack tip will remain on the crack faces. This approach employs a modified linear elastic stress intensity factor range (an effective stress intensity range) as shown below:

$$\Delta K_{\text{eff}} = K_{\text{max}} - K_{\text{op}} \quad (2.6)$$

where K_{max} and K_{op} are the maximum and opening stress intensity factors.

Many models have been developed for calculation of the opening load stress intensity factor in the past, but very little work has been undertaken for modelling of crack closure in three-dimensional bodies. A relatively small number of efforts have considered three-dimensional centre-cracked plates, and even fewer have focused on the more complex surface flaws (Skinner & Daniewicz 2002). Since crack closure dominates in the wake of the crack tip, and for short cracks this wake is limited, it is expected that short cracks will be subjected to a smaller degree of crack closure than long cracks. Differences in the local crack tip environment, plasticity-grain boundary interaction and crack deflection for short and long cracks may also be major factors.

For long cracks, the cyclic stress range is small, and a threshold will occur, while for short cracks the cyclic stress range can be large enough to overcome the obstacles and thus the short crack stress intensity factor range will be lower than that of long cracks, or possibly even disappear (Bu & Stephe 1986).

The numerical simulation of plasticity-induced crack closure using, for example, the Finite Element (FE) method is very attractive; however, it has some inherent difficulties related to the mesh refinement and the crack growth scheme, which usually consists of releasing nodes ahead of the initial crack tip and the region at which crack is allowed to grow in the component. Therefore, most of the numerical simulations have been developed based on simplified models of plasticity-induced crack closure.

As an alternative to numerical simulations, application of an analytical model for calculation of the effective stress intensity factor, based on classic plasticity-induced crack closure, allows for a significant reduction in the complexity of the evaluation procedure (He et al. 2014). For example, Codrington and Kotousov (2009) developed a simplified 3D analytical model of the analysis of plasticity-induced closure cracks in plates of finite thickness.

2.3.9 Crack Front Shape Evolution Modelling

The experimental studies largely confirm that the classic crack tip solutions cannot accurately describe the stress states in the close vicinity of the crack tip for three-dimensional (3D) problems. Despite great progress being made over the past two decades, obtaining 3D solutions for fatigue crack propagation still represents a technical and research challenge in linear and non-linear formulations. The derivation of the exact analytical 3D solutions is difficult, and these are usually limited to very simple problems. Numerical techniques can be utilised in practical situations as an alternative to the analytical solutions.

2.3.10 Numerical Procedures

Several numerical methods have been developed to predict the fatigue crack front shape's evolution and its effect on the crack growth rates. Different formulations of Finite Element Analysis (FEA) have been successfully employed to characterise the 3D stress and displacement fields near the crack tips over the past decade.

These include direct numerical techniques as well as simplified procedures. The direct numerical procedures for fatigue phenomena can be broadly divided into five main steps: (1) develop a numerical model of the cracked body, including all relevant geometry characteristics. The model needs to represent the component geometry, materials, boundary conditions, applied loads and initial crack shape accurately; (2) calculation of the effective stress intensity factors along the crack front; (3) application of the crack growth model and calculation of the crack front advance, normally by using a Paris-type law (4) comparison of the results along the crack front (5) determination of a new crack front. The different successive simulations need to be carried out until a stabilised crack front shape (or final fracture) is attained. The new crack front shape can normally be determined using two developed approaches: namely, the two-degree of freedom and multiple-degree of freedom models.

The two-degree of freedom models are based on the fitting equations, tables, and diagrams, and are available in the literature for node propagation in particular crack front shapes (i.e., elliptical shapes). In these methods, only the displacement of the deepest interior point, or both the deepest interior and the surface intersection points, or a limited number of key crack front points need to be considered. On the other hand, the displacement of crack front nodes should be analysed separately in the multiple degree of freedom models. These models take into account the more realistic fatigue crack front shapes (i.e., irregular crack shapes) as well as the effects of plasticity-induced crack closure and 3D corner singularity on the front shape evolution during fatigue growth. Some representative examples for the two-degree of freedom and the multiple-degree of freedom models are given in the following section.

2.3.11 Simplified Shape Modelling Approaches

Past experimental studies have demonstrated that for many structures subjected to cyclic loading surfaces, cracks normally maintain an almond shape up to the final region (fracture) of propagation (Carpinteri & Vantadori 2008).

It has also been found that the front of almond-shaped fatigue cracks can be approximated quite accurately by an elliptical curve (Brighenti & Carpinteri 2013). This finding greatly simplifies the crack growth modelling by reducing the number of variables describing the crack front. This simplification also allows for advanced design optimisation through parametric and sensitivity studies of various structures with surface defects (Couroneau & Royer 1998).

Fatigue crack front shape evolution and fatigue life can be simplified by reasonably assuming the crack geometry using classic linear elastic Fracture Mechanics, or with more advanced two-dimensional (2D) or three-dimensional (3D) fatigue models incorporating the crack tip plasticity effects, out-of-plane constraint, plasticity, or roughness-induced closure phenomena, etc. Kassir and Sih (1966) were among the first researchers who examined the general characteristics of the three-dimensional stress field near a crack tip. Hartranft and Sih (1970) developed an approximate theory for the stress distribution in an infinite plate containing a through-the-thickness crack by application of quite sophisticated integral equations. This work has demonstrated that the 2D elastic solutions are not valid near the free surface. Further improvements in the predictions were obtained by using an asymptotic solution near the fatigue crack front (Yosibash and Shannon, 2014). In this approach, the presence of a 3D corner (vertex) singularity at the points where the crack front intersects the plate's free surfaces is ignored.

The displacement stress fields and the power of singularities near the intersection of the crack front and the free surfaces (the boundary layer region) were investigated by Shivakumar and Raju (1990). Their log-log regression analysis along the crack front showed that finite sized cracked bodies have two singular stress fields (cylindrical and vertex) near the free surface and the strain energy release rate is an appropriate parameter to measure the severity of the crack. De Matos and Nowell (2008) employed a comprehensive 3D finite element analysis to finite thickness plates with a central through-thickness crack to understand the effect of the 3D corner point singularity and elastic constant (i.e., Poisson's ratio) on the stress intensity factors and elastic stress fields near the crack front.

The elliptical surface cracks in round bars under cyclic axial and pure bending loads have previously been studied by means of the Paris law as a function of bar diameter (Shin & Cai 2004). The crack aspect ratios of the initial flaw are normally utilised to vary from 0 (a straight crack front) to 1 (a circular-arc crack front) under stable conditions. Carpinteri and his colleagues have conducted extensive numerical studies to establish a link between the applied cyclic tension or bending loading and crack shape evolution in a round bar using the simplified models (Carpinteri et al. 1992, 1993, 1995, 2013). It was found that the propagation path is independent of the stress range of the cyclic axial loading, and the aspect ratio of the surface crack, defined by the ratio of its semi-axes, can be changed during fatigue growth. It has also been argued that the intersection angle between the crack front and the external surface of the bar (the critical angle) is barely affected by the normalised loading eccentricity parameter, which is the loading distance to the centre of the bar, divided by the bar radius (Carpinteri & Vantadori 2009). Similar conclusions have been derived by Couroneau and Royer (1998) using a two-parameter numerical model. It was demonstrated that a few parameters, namely the initial crack aspect ratio, the exponent in Paris law and the type of loading, have an influence on the crack front evolution.

Toribio et al. (2011) employed an elastic 3D finite element analysis to cylindrical geometries with transverse surface cracks subjected to axial tensile loading to understand the effect of fatigue crack growth parameters on the stress intensity factors. In this work it was proved that materials with higher values of the Paris parameter, m , produce slightly greater dimensionless compliance and a better convergence between the results for straight or circular initial cracks. He et al. (2014) proposed an efficient numerical technique for the evaluation of fatigue crack front shapes and their effect on the steady-state fatigue crack growth rates in plate components. The proposed simplified procedure is based on several implicit and explicit assumptions and utilises the earlier-developed analytical model (Codrington & Kotousov 2009) for plasticity-induced crack closure in plates of finite thickness.

So far, the available simplified solutions to 3D crack problems are usually limited to very simple problems, such as through-the-thickness cracks in an infinite elastic plate or semi-elliptical surface cracks in round bars. In addition, the simulation of plasticity-induced crack closure using FEA has some inherent difficulties related to the mesh refinement or the crack growth scheme, which usually consists of releasing nodes ahead of the initial crack tip and the region in which the crack is allowed to grow. The numerical study can be performed at minimum load, maximum load or during the loading/unloading cycle. Therefore, the outcomes of such numerical simulations should be treated with caution.

2.3.12 Direct Shape Modelling Approaches

Many numerical investigations in the past have focused on the development and optimisation of the multiple degree of freedom models. These methods can be generalised for many geometries and boundary conditions, specifically, for which the other approaches may not work or be costly (e.g., experimental validations). The most popular methods for investigating fatigue crack growth using direct shape modelling approaches is the use of finite element simulations with empirical correction factors. The use of finite element analysis allows for engineering problems to be examined in greater detail than was previously possible.

The different formulations of finite element analysis have been applied successfully over the last decades for simulation of the front shape evolution at stable fatigue crack propagation. Smith and Cooper (1989) were the first to apply multiple degree of freedom models with no shape constraints for the analysis of fatigue crack growth problems. In these models, the crack front needs to be divided into several segments and the nodes are connected to each other using straight lines or curves. Since their pioneering study, the number of scientific publications has grown progressively. For example, Lin et al. (1998, 1999a, 1999b) have demonstrated that numerical simulations developed using multiple degree of freedom models predict about thirty percent more accurate fatigue life estimations for engineering components in comparison with the results of two degree of freedom methods.

Lin and his colleagues examined the fatigue crack growth and characteristics of a range of different surface defects in finite thickness plates under tension and bending loads.

Branco and his colleagues (2008a, 2012 and 2015) developed the three-dimensional automatic fatigue crack growth technique to predict crack shape evolution and the number of fatigue cycles in various practical geometries such as plates and round bars. The automatic fatigue crack growth technique has since been extended in many of the following works, with incorporation of the plasticity-induced crack closure effect during fatigue growth up to failure (Branco et al., 2008b and 2014). In these studies, it was demonstrated that the crack closure has a significant effect on the independent tunnelling parameter (crack depth over thickness). The developed modified three-dimensional automatic fatigue crack growth techniques were validated successfully via a separate experimental study.

The automatic fatigue crack growth techniques utilised in numerical simulation are shown in Figure 3. The procedure comprises five main steps: (1) the initial step is setting up a three-dimensional finite element model. This step includes the definition of the geometry, boundary conditions, loadings, initial crack shape, and material properties; (2) calculation of the displacement field in the crack front nodes; (3) calculation of the stress intensity factors along the crack front using point matching techniques (the stress extrapolation method, displacement extrapolation method, hybrid extrapolation method, etc.) or energy-based methods (J-integral method, domain integral approach, etc.); (4) determination of a new crack front with the application of crack advance schemes; (5) move the location of the corner and mid side nodes using a parametric curve depending on the crack front shape and corner node position (i.e., cubic spline function). This process continues until a specified crack advance or final fracture is achieved.

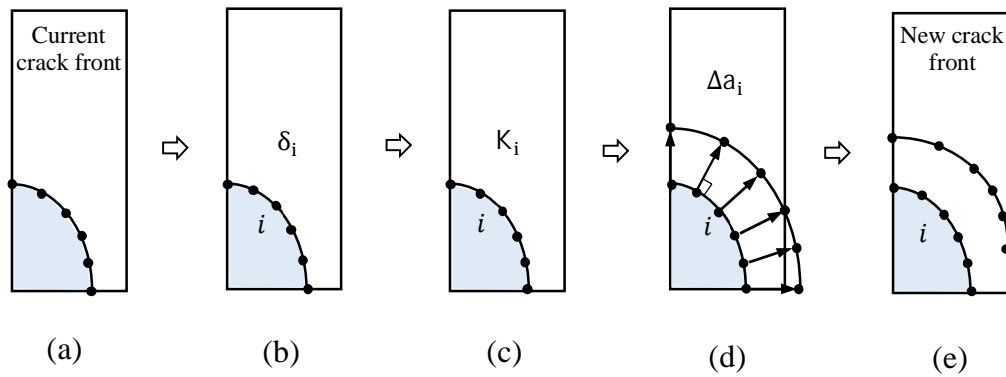


Figure 3: Schematic presentation of the 3D finite element automatic crack growth technique (a) crack front definition; (b) calculation of the displacement field of crack front nodes; (c) calculation of stress intensity factors at front nodes; (d) calculation of the advances of crack front nodes; (e) relocation of the corner and intermediate nodes of crack front (Branco et al. 2014)

Gardin and his collaborators have used two independent numerical models with increasing levels of complexity (parabolic and elliptical) for 3D numerical simulations of the plasticity-induced crack closure of through-thickness plane cracks (Gardin et al. 2016). Figure 4 illustrates the adopted scheme of the 3D adaptive re-meshing technique adopted by Gardin for prediction of crack front shapes. Sevcik et al. also developed an iterative technique for the estimation of a fatigue crack front shape based on linear elastic Fracture Mechanics using values of the stress singularity exponent. It is found from the careful numerical studies that the more significant influence of free surfaces on the stress singular behaviour is apparent in the case of thin-wall structures (Sevcik et al. 2012).

In general, traditional 3D FEMs are rather difficult to adopt for 3D crack propagation modelling, see Fig. 4. Moreover, these methods can be either mesh-dependent and require the incorporation of sophisticated re-mapping and re-meshing techniques.

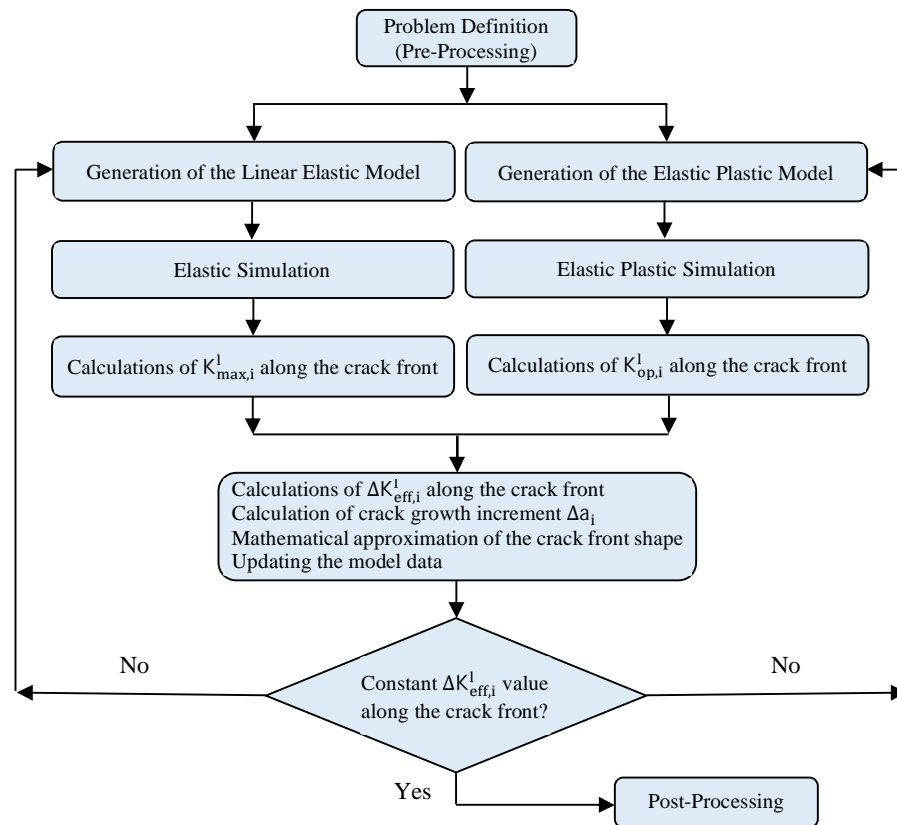


Figure 4: Prediction process for crack front shape estimation with re-meshing techniques (Gardin et al. 2016)

In order to eliminate the need to conduct frequent remeshings and reprojecting the solution on the updated mesh, Belytschko and Black (1999) presented a new mesh-independent method, which significantly reduced number of remeshing procedures during crack growth simulations. This method was further advanced (Moës et al. 1999) into a fully mesh-independent method without any need for re-meshing. The method has later become known as the eXtended Finite Element Method (X-FEM), and it has become widely popular for solving continuum mechanics problems containing discontinuities like cracks and material interfaces (Rege and Lemu 2017).

The X-FEM is now considered as a powerful numerical technique for obtaining approximate solutions of problems which involve singularities, discontinuities, localized deformations, and complex geometries.

In XFEM, the treatment of a discontinuous displacement field along the crack surface is accomplished by simply introducing additional discontinuous functions into the FE formulation. Furthermore, when XFEM is combined with level sets, the entire representation of the feature, such as the geometry and the displacement field of a crack, can be constructed in terms of nodal values at the nodes of the original mesh. An appealing feature of the XFEMs is that it can be applied to fracture problems with curved crack fronts in a straightforward manner without concern for element meshing details along the crack front (Ayhan 2011). However, control of the accuracy of numerical calculations remains the main drawback of XFEMs as well as other similar numerical methods, e.g., mesh-free methods.

2.4 Conclusion

An important advance in modern engineering analysis has been the introduction of techniques to evaluate the remaining life (fatigue assessment) of structures that have been in operation. These techniques are mostly based on Fracture Mechanics, and it is therefore important to acquire an understanding of Fracture Mechanics and its application in detail.

The overall conclusion is that the direct numerical approaches are able to describe the shape evaluation of fatigue cracks; however, the application of direct numerical approaches to particular problems is very difficult and may not work for specific conditions. The validation and convergence of the models are also major issues with direct numerical simulations. In addition, direct methods suffer from the many inconsistencies associated with the effects of the 3D corner (vertex) singularity, contact conditions as well as various material and geometry related non-linearities. Hence, it is more promising to investigate 3D fracture and fatigue problems using simplified analytical or semi-analytical approaches. The latter is the focus of the current thesis.

References

ASTM E2714-13 (2020), Standard Test Method for Creep-Fatigue Testing, ASTM International, West Conshohocken, PA.

Ayhan. (2011). Three-dimensional fracture analysis using tetrahedral enriched elements and fully unstructured mesh. *International Journal of Solids and Structures*, 48(3), 492–505.

Basquin, O.H., (1910). The exponential law of endurance tests, *American Society of Testing Materials Proceedings*, Vol. 10, 625-630.

Belytschko, T., & Black, T. (1999). Elastic crack growth in finite elements with minimal remeshing. *International Journal for Numerical Methods in Engineering*, 45(5), 601–620.

Belytschko, T., Gracie, R., & Ventura, G. (2009). A review of extended/generalized finite element methods for material modeling. *Modelling and Simulation in Materials Science and Engineering*, 17(4), 043001–.

Bhat, S., & Patibandla R. (2011). Metal fatigue and basic theoretical models: a review, IntechOpen. <https://doi.org/10.5772/28911>.

Branco, R., Antunes, F., & Costa, J. (2015). A review on 3D-FE adaptive remeshing techniques for crack growth modelling. *Engineering Fracture Mechanics*, 141, 170–195.

Branco, R., & Antunes, F. (2008a). Finite element modelling and analysis of crack shape evolution in mode-I fatigue Middle Cracked Tension specimens. *Engineering Fracture Mechanics*, 75(10), 3020–3037.

Branco, R., Antunes, F., & Costa, J. (2014). Lynx: A user-friendly computer application for simulating fatigue growth of planar cracks using FEM. *Computer Applications in Engineering Education*, 22(3), 529–540.

Branco, R., Antunes, F., Costa, J., Yang, F., & Kuang, Z. (2012). Determination of the Paris law constants in round bars from beach marks on fracture surfaces. *Engineering Fracture Mechanics*, 96, 96–106.

- Branco, R., Rodrigues, D., & Antunes, F. (2008b). Influence of through-thickness crack shape on plasticity induced crack closure. *Fatigue & Fracture of Engineering Materials & Structures*, 31(2), 209–220.
- Bu, R., & Stephens, R. (1986). Comparison of short and long fatigue crack growth in 7075-T6 aluminum. *Fatigue & Fracture of Engineering Materials & Structures*, 9(1), 35–48.
- Brighenti, R., & Carpinteri, A. (2013). Surface cracks in fatigued structural components: a review. *Fatigue & Fracture of Engineering Materials and Structures*, 36(12).
- Carpinteri, A. (1992). Elliptical-arc surface cracks in round bars. *Fatigue & Fracture of Engineering Materials & Structures*, 15(11), 1141–1153.
- Carpinteri, A. (1993). Shape change of surface cracks in round bars under cyclic axial loading. *International Journal of Fatigue*, 15(1), 21–26.
- Carpinteri, A., & Majorana, C. (1995). Fatigue growth of edge flaws in cylindrical bars. *Strength of Materials*, 27(1), 14–22.
- Carpinteri, A., & Vantadori, S. (2009). Sickle-shaped cracks in metallic round bars under cyclic eccentric axial loading. *International Journal of Fatigue*, 31(4), 759–765.
- Chowdhury, P., & Sehitoglu, H. (2016). Mechanisms of fatigue crack growth - a critical digest of theoretical developments: Fatigue Crack Growth Modelling. *Fatigue & Fracture of Engineering Materials & Structures*, 39(6), 652–674.
- Codrington, J., & Kotousov, A. (2009). A crack closure model of fatigue crack growth in plates of finite thickness under small-scale yielding conditions. *Mechanics of Materials*, 41(2), 165–173.
- Correia, J., de Jesus, A., & Fernández-Canteli, A. (2014). Modelling probabilistic fatigue crack propagation rates for a mild structural steel. *Frattura Ed Integrità Strutturale*, 9(31), 80–96.

- Couroneau, N., Royer, J. (1998). Simplified model for the fatigue growth analysis of surface cracks in round bars under mode I. *International Journal of Fatigue*, Vol.20(10), pp.711-718.
- Cui, W. (2002). A state-of-the-art review on fatigue life prediction methods for metal structures. *Journal of Marine Science and Technology*, 7(1), 43–56.
- de Matos, P., & Nowell, D. (2009). Experimental and numerical investigation of thickness effects in plasticity-induced fatigue crack closure. *International Journal of Fatigue*, 31(11), 1795–1804.
- Dewa, R., Kim, S., Kim, W., & Kim, E. (2017). Effect of Strain Range on the Low Cycle Fatigue in Alloy 617 at High Temperature. *Metals (Basel)*, 7(2), 54.
- Elber, W. (1970). Fatigue crack closure under cyclic tension. *Engineering Fracture Mechanics*, Vol. 2(1), 37.
- Etube, L.S. (2011). *Fatigue and Fracture Mechanics of Offshore Structures*. ISBN: 978-1-860-58312-4.
- Ewing, J., & Humfrey, J. (1903). The fracture of metals under repeated alternations of stress. *Proceedings of the Royal Society of London*, 71(467), 79–79.
- Gardin, C., Fiordalisi, S., Sarrazin-Baudoux, C., Gueguen, M., & Petit, J. (2016). Numerical prediction of crack front shape during fatigue propagation considering plasticity-induced crack closure. *International Journal of Fatigue*, 88, 68–77.
- Goedel, F., Mezzomo, G., & Chamberlain Pravia, Z. (2018). Fatigue lifespan of a fillet welded joint - Hybrid approach to obtain the S-N curve with a reduced number of tests. *Latin American Journal of Solids and Structures*, 15(10).
- Hartranft, R.J., Sih, G.C. (1970). An approximate three-dimensional theory of plates with application to crack problems. *International Journal of Engineering Science*, Vol. 8(8), pp.711-729.
- He, Z., Kotousov, A., & Branco, R. (2014). A simplified method for the evaluation of fatigue crack front shapes under mode I loading. *International Journal of Fracture*, 188(2), 203–211.

- Kassir, M., & Sih, G. (1966). Three-Dimensional Stress Distribution Around an Elliptical Crack Under Arbitrary Loadings. *Journal of Applied Mechanics*, 33(3), 601–611.
- Kazymyrovych, V. (2009). Very high cycle fatigue of engineering materials: A literature review. Karlstad, Sweden, 2009.
- Khanna, A., & Kotousov, A. (2020). The potential for structural simulation to augment full scale fatigue testing: A review. *Progress in Aerospace Sciences*, 121, 100641.
- Kim H. S. (2019). Prediction of S-N curves at various stress ratios for structural materials. *Procedia Structural Integrity*, 19 (2019) 472–481.
- Kim, H., & Zhang, J. (2001). Fatigue Damage and Life Prediction of Glass/Vinyl Ester Composites. *Journal of Reinforced Plastics and Composites*, 20(10), 834–848.
- Kotousov, A., Lazzarin, P., Berto, F., & Pook, L. (2013). Three-dimensional stress states at crack tip induced by shear and anti-plane loading. *Engineering Fracture Mechanics*, 108, 65–74.
- Kuna, M. (2013). Finite Elements in Fracture Mechanics: Theory - Numeric - Applications (Vol. 201). Springer Netherlands.
- Lee, Y. (2005). Fatigue testing and analysis theory and practice. Elsevier Butterworth-Heinemann.
- Lin, X., & Smith, R. (1998). Fatigue growth simulation for cracks in notched and unnotched round bars. *International Journal of Mechanical Sciences*, 40(5), 405–419.
- Lin, X., & Smith, R. (1999a). Finite element modelling of fatigue crack growth of surface cracked plates: Part I: The numerical technique. *Engineering Fracture Mechanics*, 63(5), 503–522.
- Lin, X., & Smith, R. (1999b). Shape evolution of surface cracks in fatigued round bars with a semicircular circumferential notch. *International Journal of Fatigue*, 21(9), 965–973.

- McDowell, D., & Dunne, F. (2010). Microstructure-sensitive computational modeling of fatigue crack formation. *International Journal of Fatigue*, 32(9), 1521–1542.
- Miller, R. (1987). Current status of thermal barrier coatings - An overview. *Surface & Coatings Technology*, 30(1), 1–11.
- Milne, I., Ritchie, R., & Karihaloo, B. (2011). *Comprehensive Structural Integrity*. Amsterdam; Boston: Elsevier/Pergamon.
- Moës, Dolbow, J., & Belytschko, T. (1999). A finite element method for crack growth without remeshing. *International Journal for Numerical Methods in Engineering*, 46(1), 131–150.
- Newman, J., Phillips, E., & Swain, M. (1999). Fatigue-life prediction methodology using small-crack theory. *International Journal of Fatigue*, 21(2), 109–119.
- Paris, P., & Erdogan, F. (1963). A critical analysis of crack propagation laws. *Journal of Basic Engineering*, vol. 85, no. 4, pp. 528-533.
- Peterson, R. E. (1950). Discussion of a century ago concerning the nature of fatigue, and review of some of the subsequent researches concerning the mechanism of fatigue, *ASTM Bulletin*, No. 164, 50–56.
- Pippan, R., & Hohenwarter, A. (2017). Fatigue crack closure: a review of the physical phenomena. *Fatigue & Fracture of Engineering Materials & Structures*, 40(4), 471–495.
- Rege, & Lemu, H. G. (2017). A review of fatigue crack propagation modelling techniques using FEM and XFEM. *IOP Conference Series. Materials Science and Engineering*, 276(1), 12027–.
- Rodrigues, D.M., Antunes F.V. (2009). Finite element simulation of plasticity induced crack closure with different material constitutive models. *Engineering Fracture Mechanics*, Vol. 76(9), 1215-1230.
- Roychowdhury, S., & Bodds, R. (2003). Three-dimensional effects on fatigue crack closure in the small-scale yielding regime - A finite element study. *Fatigue & Fracture of Engineering Materials & Structures*, 26(8).

Schijve J. (1967). Significance of fatigue cracks in micro-range and macro-range. Fatigue crack propagation. ASTM STP 415, pp. 415-459.

Schijve, J. (2003). Fatigue of Structures and Materials in the 20th Century and the State of the Art. *Materials Science*, 39(3), 307–333.

Sevcik, M., Hutar, P., Zouhar, M., & Nahlik, L. (2012). Numerical estimation of the fatigue crack front shape for a specimen with finite thickness. *International Journal of Fatigue*, 39, 75–80.

Shin, C., & Cai, C. (2004). Experimental and finite element analyses on stress intensity factors of an elliptical surface crack in a circular shaft under tension and bending. *International Journal of Fracture*, 129(3), 239–264.

Shivakumar, K., & Raju, I. (1990). Treatment of singularities in cracked bodies. *International Journal of Fracture*, 45(3), 159–178.

Skinner, J., & Daniewicz, S. (2002). Simulation of plasticity-induced fatigue crack closure in part-through cracked geometries using finite element analysis. *Engineering Fracture Mechanics*, 69(1), 1–11.

Smith, R., & Cooper, J. (1989). A finite element model for the shape development of irregular planar cracks. *International Journal of Pressure Vessels and Piping*, 36(4), 315–326.

Sornette, D., Magnin, T., & Brechet, Y. (1992). The Physical Origin of the Coffin-Manson Law in Low-Cycle Fatigue. *Europhysics Letters*, 20(5), 433–438.

Suresh, S. & Ritchie, R. (1982), A geometric model for fatigue crack closure induced by fracture surface roughness. *Metallurgical Transactions A*, 13, 1627–1631.

Suresh, S., Ritchie R.O. (1984). Propagation of short fatigue cracks. *International Metals Reviews*, Vol. 29(1), 445-475.

Szala, G., & Ligaj, B. (2016). Application of hybrid method in calculation of fatigue life for C45 steel (1045 steel) structural components. *International Journal of Fatigue*, 91, 39–49.

Timoshenko, S. (1954). Stress concentration in the history of strength of materials. The William M. Murray Lecture, Proc. SESA, 12, 1–12.

- Toribio, J., Matos, J., González, B., & Escuadra, J. (2011). Compliance evolution in round cracked bars under tensile fatigue. *Engineering Fracture Mechanics*, 78(18), 3243–3252.
- Wang, Y., & Susmel, L. (2016). The Modified Manson–Coffin Curve Method to estimate fatigue lifetime under complex constant and variable amplitude multiaxial fatigue loading. *International Journal of Fatigue*, 83, 135–149.
- Yosibash, Z., Shannon, S. (2014). Computing edge stress intensity functions (ESIFs) along circular 3-D edges. *Engineering Fracture Mechanic*, 117, 127–151.
- Zakavi, B., Kotousov, A., & Branco, R. (2021). Overview of three-dimensional linear-elastic fracture mechanics. *International Journal of Fracture*.
- Zenner, H., & Hinkelmann, K. (2019). August Wöhler – founder of fatigue strength research. *Steel Construction*, 12(2), 156–162.
- Zerbst, U., Madia, M., & Vormwald, M. (2017). Fatigue strength and fracture mechanics. *Procedia Structural Integrity*, 5, 745–752.

Chapter 3
Gaps, Objectives and Organisation of the Thesis

3.1 Research Gaps

Considerable amounts of research on the fatigue crack growth phenomenon have been conducted over the years. Despite the significant effort, there are still many issues that need to be investigated and addressed in order to improve theoretical predictions. In particular, it is not possible to accurately predict fatigue crack front shapes and their evolutions during cycling loading with the current methods for various structural components of practical interest. The influence of the idealised (or simplified) shapes utilised in the current standards and assessment procedures in terms of the accuracy of the existing fatigue life evaluation procedures is also unclear and has not been well investigated to date.

It was also found from the review of the relevant literature that application of the current numerical techniques for fatigue crack growth evaluation is highly complex and normally very demanding in terms of time and computational effort. Moreover, the numerical techniques suffer from many uncertainties and still frequently require calibration or validation against experimental results.

The current project aimed to address the issue of 3D modelling of fracture and fatigue problems through the development of new simplified methods, which incorporate more realistic 3D crack front shapes into fatigue and fracture analysis. The outcomes of the current 3D analysis of fatigue and fracture problems are compared with previous experimental studies for several materials and a range of load conditions and geometries. The developed methods have been found to be in good agreement with past experimental studies and agree well with the outcomes of numerical simulations.

3.2 Objectives

The overall objective of the present PhD research project is to understand and elucidate the role of 3D stress states in fracture and fatigue phenomena and consider the influence of more realistic 3D crack front shapes on fatigue lifetime evaluations.

The specific aims of this project are as follows:

- Investigate the effect of 3D corner singularity on stress and displacement fields, as well as on the fatigue crack front shape evolution near free surfaces.
- Develop and verify new simplified modelling methods for the front shape evaluation in typical structural components, e.g., plates and circular bars.
- Investigate and incorporate the plasticity induced crack closure effects into the simplified models and validate these models against past experimental studies.

3.3 Organisation of the Thesis

This thesis is presented in the form of a compendium of publications in high impact international journals. It is comprised of published articles, which represent the main outcomes of the research undertaken by the author, united by the same research objectives, as specified above. The articles, which form the main body of the thesis, are also united within a common framework, which is 3D Fracture Mechanics.

This thesis is organised into eight chapters. In the Introductory chapter, the overall significance of the research undertaken in the areas of fatigue and fracture is described. The historical development of the field and the main motivation of the current research are also provided. The second chapter is devoted to the literature review. The literature review was divided into two main parts: (1) Introduction to 3D Fracture Mechanics and (2) General overview of fatigue phenomena, focusing on 3D effects associated with the evolution of crack front shapes during cyclic loading. The provided literature review identified research gaps in the current knowledge and methods in relation to the role of the 3D stress states in deformation and failure phenomena. Chapter 3 covers the research gaps and objectives and provides the organisation of the thesis.

The specific investigations and developments undertaken in this study can be found in each of the research articles published or submitted for publication by the candidate in collaboration with his colleagues.

The outcomes of the thesis are described in separate articles representing four chapters of this thesis. One additional paper, which is relevant to the topic of the thesis and a limited contribution of the candidate, is also provided in the Appendix. The purpose of the following sections is to provide a brief description of Chapters 4 to 7.

Chapter 4: Understanding the influence of 3D corner singularity on crack front shapes near a free surface

The chapter is devoted to the investigation of the 3D corner (vertex) singularity's effects on the crack front shapes and the conditions that can affect the shape of the crack front near free surfaces. Contrary to the in-plane singularities, for which the strength is described by the inverse square root behaviour, the strength of the corner singularity also depends on Poisson's ratio, alongside the intersection angle between the crack front and the free surface.

Many experimental studies and test results have demonstrated that fatigue crack front shapes are not straight. There are at least two main phenomena responsible for this experimentally-observed phenomenon: plasticity and 3D corner singularity effects. The concept of the critical angle, which has been widely investigated experimentally in recent years, is tested against past experimental results for different geometries and loading conditions. It is demonstrated in this chapter that the critical angle is a valid hypothesis if the plastic (or process) zone is much smaller than the size of the region controlled by the 3D vertex singularity.

Chapter 5: Development of simplified methods to describe the front shapes of through-the-thickness fatigue cracks

Four different semi-analytical models for the evaluation of front shapes of fatigue cracks under quasi-steady state conditions are developed in this chapter. These simplified models are based on the Stress Singularity Matching concept, the use of first-order shear deformation theory, modelling effects of the out-of-plane and in-plane constraints on crack closure levels, and the iso-K criterion.

Chapter 6: Development of simplified methods to describe the front shape evaluation of surface-breaking fatigue cracks

The major outcome of this chapter is the development of a new analytical approach for the evaluation of fatigue growth of surface flaws to a wide range of practical situations. One of the desired outcomes of this part of the research was to develop a simplified approach capable of incorporating plasticity-induced crack closure into the developed tools. In this study, analytical equations were developed based on two characteristic points for distribution of the stress intensity factor along the front of elliptical or part-elliptical cracks. A very good agreement is observed between the present results and the experimental data. This agreement could be further improved by introducing the crack closure effects.

The second objective of this chapter was to develop an effective new method based on the compliance function (the ratio of displacement to applied force) for the evaluation of elliptical, semi-elliptical and part-elliptical cracks. A theoretical relationship is derived for the distribution of stress intensity factors along the fatigue crack fronts from energy considerations in the linear-elastic materials. The technique presented in this thesis is applicable to a wide range of practical geometries and loading conditions.

Chapter 7: Development of simplified analytical models to investigate the effects of plasticity-induced crack closure on the front shape evolution of fatigue cracks

A new, combined, semi-analytical method was developed to simulate the fatigue growth of surface cracks in round bars subjected to cyclic tension and/or bending. It is assumed that the crack has elliptical or part-elliptical shapes. The developed method is capable of incorporating plasticity-induced crack closure models. This procedure is based on the concept of equivalent thickness using the out-of-plane and in-plane constraints for evaluation of the plasticity-induced crack closure effect. It is demonstrated that fatigue crack growth is very sensitive to the initial crack length, the initial crack shape, the exponent of Paris law, the loading scenario, and plasticity-induced crack closure effects. Comparison with the experimental results demonstrated a good agreement.

The overall conclusions and suggestions for further work are provided in the last chapter. An Appendix is also included, which represents a compilation of the candidate's publications related to the main topic of the thesis.

Chapter 4

Investigation of the Effect of 3D Corner Singularity

Statement of Authorship

Title of Paper	Does the front of fatigue crack intersect free surface at critical angle?		
Publication Status	<input checked="" type="checkbox"/>	Published	<input type="checkbox"/> Accepted for Publication
	<input type="checkbox"/>	Submitted for Publication	<input type="checkbox"/> Unpublished and Unsubmitted work written in manuscript style
Publication Details	Zakavi, B., Kotousov, A., & Branco, R. (2021). Does the front of fatigue crack intersect free surface at critical angle? Theoretical and Applied Fracture Mechanics, 114, 102985–. https://doi.org/10.1016/j.tafmec.2021.102985		

Principal Author

Name of Principal Author	Behnam Zakavi		
Contribution to the Paper	Completed literature review, interpreted data and wrote manuscript		
Overall percentage (%)	50		
Certification:	This paper reports on original research I conducted during the period of my Higher Degree by Research candidature and is not subject to any obligations or contractual agreements with a third party that would constrain its inclusion in this thesis. I am the primary author of this paper.		
Signature		Date	22 / 08 / 2021

Co-Author Contributions

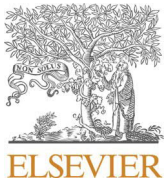
By signing the Statement of Authorship, each author certifies that:

- i. the candidate's stated contribution to the publication is accurate (as detailed above);
- ii. permission is granted for the candidate to include the publication in the thesis; and
- iii. the sum of all co-author contributions is equal to 100% less the candidate's stated contribution.

Name of Co-Author	Prof. Andrei Kotousov		
Contribution to the Paper	Supervised work development, participated in work discussions and co-wrote manuscript		
Signature		Date	24 / 08 / 2021

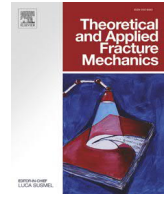
Name of Co-Author	Prof. Ricardo Branco		
Contribution to the Paper	Participated in manuscript review, assisted in data interpretation, and co-wrote manuscript		
Signature		Date	23 / 08 / 2021

Name of Co-Author			
Contribution to the Paper			
Signature		Date	



Contents lists available at ScienceDirect

Theoretical and Applied Fracture Mechanics

journal homepage: www.elsevier.com/locate/tafmec

Does the front of fatigue crack intersect free surface at critical angle?

ARTICLE INFO

Keywords

Fatigue
Crack front
Vertex singularity
3D fracture mechanics
Linear elasticity
Finite element analysis

ABSTRACT

More than forty years ago, several researchers suggested a hypothesis that the front of a fatigue crack must intersect the free surfaces at a certain (critical) angle to ensure the finite energy flux at the terminal (vertex) point (s). Since its formulation, this hypothesis was under scrutiny in many studies, which utilised various materials, cyclic loading conditions and different specimen geometries. The outcomes of these studies were very divisive: from overwhelming confirmation of this hypothesis to total abjuration. In this paper, we first discuss the conditions, which can affect the shape of the crack front near free surfaces. Further, we demonstrate that the critical angle hypothesis seems to be valid when the plastic (or process) zone is much smaller than the size of the region controlled by 3D vertex singularity. As demonstrated in a number of past numerical studies, this size is related to the crack and specimen geometry, e.g., to the crack front length. Past experimental studies also indicate that fatigue crack fronts tend to intersect the free surface at the critical angle at the steady-state growth rather than when the crack propagation leads to the changes or evolution of the crack front, e.g., during propagation of fatigue cracks in round bars.

1. Introduction

In the case of a linear elastic material, at the intersection (or vertex point) of the crack front and a free surface, the square root singularity disappears, and at such a point, one has to deal with a different singular behaviour. Using a semi-analytical method, this singular behaviour was first described by Benthem as well as a number of other researchers in the late 70th [1]. Afterwards, several techniques were developed to determine the stress states associated with vertex points, which can be classified into two categories: global and local approaches. The global approach consists in directly determining the stress singularity exponent from the resolution of a linear elastic problem containing vertex singularity, such as: semi-analytical, finite difference, singular integral equation and finite element methods [2–4].

In contrast, the local approach is based on the logarithmic regression of stress or displacement fields near the crack tip or of stress intensity factors in the boundary layer close to the free surface. Later several studies have been focused on the improvement of the numerical schemes in terms of convergence speed and accuracy. However, there are still some, typically small, discrepancies between different theoretical studies, which largely motivate further research and the development of new and more accurate computational methods. In this paper we consider fatigue cracks propagating in mode I (or symmetric fracture mode) when only one parameter characterises the local crack front shape geometry near the free surfaces. This parameter is angle β , or the angle at which the crack front intersects the free surface, as illustrated in Figs. 1 and 2.

The dependence of the strength of the vertex singularity, λ_v , from Poisson's ratio is given in Fig. 1a for the case when a through-the-thickness crack in a linear-elastic plate intersects the free surfaces at right angle, or $\beta = \pi/2$. This dependence represents an average result of several numerical studies [5]. It can be noted that the strengths of the

vertex singularities at $\nu = 0$, is the same as the one for the line singularities (or $\lambda_v = 1/2$) meaning that there is no mismatch in singular behavior in this special case.

It is also often postulated that the stress field near a vertex point can be represented as a superposition of line and vertex singularities, see Fig. 2. For example, under pure mode I (or symmetric) loading the stress state near surface can be described as:

$$\sigma = \frac{K_I(\eta)}{\sqrt{r}} f(\phi) + K_V R^{-\lambda_v} g(\vartheta, \theta) \quad (1)$$

where $K_I(\eta)$ is the local stress intensity factors in mode I; K_V is the stress intensity factor of the symmetric vertex singularity, which, however, has no commonly accepted definition in the literature. R , ϑ and θ are the spherical coordinates with the origin in the vertex point (the spherical coordinates are not shown in Fig. 2a for clarity reasons); r and ϕ are the local polar coordinates, see Fig. 2a; and η is the distance along the crack front with $\eta = 0$ corresponding to the terminal (vertex) point.

The dependence of K_I near the free surface, or at $\eta = 0$, is still the subject of some controversy in the literature. Most of the 3D finite element studies published in the past normally provide a final value of K_I at the vertex point, $\eta = 0$ or just ignore this region. As first shown by Benthem [1,6], the behaviour of the stress intensity factor, K_I , in the area affected by the 3D corner singularity can be described as follows:

$$K_I(\eta) \sim \eta^{-\lambda_v+1/2}. \quad (2)$$

A similar result was obtained by Leguillon and Sanchez-Palencia [7] attracting the matched asymptotic expansion method. In particular, the following asymptotic expression of the energy release rate, $G_I(\eta)$, was derived for points on the crack front located near the free surface:

$$G_I(\eta) \sim \eta^{-2\lambda_v+1} \quad (3)$$

<https://doi.org/10.1016/j.tafmec.2021.102985>

Received 3 March 2021; Received in revised form 29 March 2021; Accepted 30 March 2021

Available online 5 April 2021

0167-8442/© 2021 Elsevier Ltd. All rights reserved.

Nomenclature	
E	Young's modulus
$G_1(\eta)$	energy release rate in mode I
K_{app}	remote applied stress intensity factor
K_{max}	maximum stress intensity factor
K_I	stress intensity factor in Mode I
$K_I(\eta)$	local stress intensity factor in Mode I
K_V	stress intensity factor characterising the stress intensity of vertex singularity
2L	crack front length
R	radial distance in spherical coordinates
r	local radial distance
r_p	plastic zone size
(x, y)	rectangular coordinates
β_c	critical intersection angle
β_{exp}	experimental intersection angle
θ	polar angle in spherical coordinates
ϑ	azimuthal angle in spherical coordinates
σ	stress
σ_y	yield strength of material
λ_V	strength of corner singularity
ν	Poisson's ratio

which agrees with Eq. (2). These dependencies were also verified with careful FE studies (see, for instance, the paper by He et al. [8]). It means, in particular, that $\lim_{\eta \rightarrow 0} K_I(\eta) = 0$ at $\nu > 0$

Currently, many researchers agree that the presence of vertex singularity may lead to a deviation of the fatigue crack front from the orthogonal direction near the free surface, as illustrated in Fig. 1b. This phenomenon is often observed in fatigue tests. Based on an energy flux argument, Bazant and Estenssoro [9] and Pook [10] suggested that the front of a fatigue crack must intersect the free surface at a certain angle, β_c . This condition ensures the finite energy flux along the whole crack front including the vertex (terminal) point. The critical angle can be found from careful 3D numerical simulations, and its value can be rather accurately approximated by the following formula:

$$\beta_c = \tan^{-1} \left(\frac{\nu - 2}{\nu} \right) \quad (4)$$

where ν is the Poisson's ratio. The dependence of the critical angle upon the Poisson's ratio is also shown in Fig. 1b indicating that for common

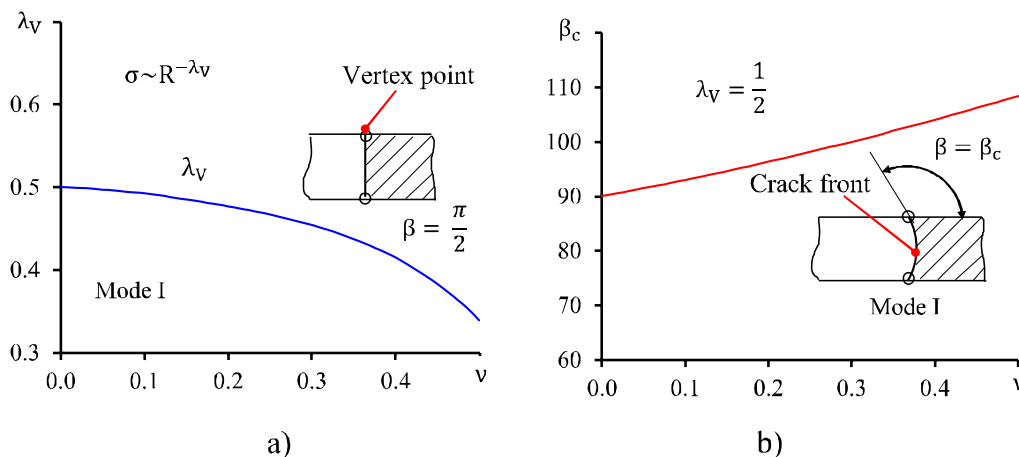


Fig. 1. (a) Strength of corner singularity dependence from Poisson's ratio for $\beta = \pi/2$; (b) The critical angle, β_c , as a function of Poisson's ratio.

materials with Poisson's ratio 0.3 the intersection angle has to be around 102° .

The concept of critical angle (β_c) was widely investigated experimentally in the past using various materials, geometries and cyclic loading conditions [10–23]. The outcomes of these studies were diverse and controversial (see, for example, Fig. 6 ahead). This controversy can be explained by the presence of another mechanism (or mechanisms), which can influence the shape of the fatigue crack near the free surfaces. The deviation from a straight shape can also be associated with fatigue crack closure phenomenon and loss of the out-of-plane constraints near the free surfaces or transition from a 3D stress state to plane stress [24]. Therefore, it is quite logical to postulate a necessary condition of validity of the critical angle hypothesis: it is valid when the stress state associated with the vertex singularity near the surface fully encapsulates the region associated with plasticity or process zone effects. In the first approximation, the characteristic dimension of the plasticity effects can be taken or calculated as the plane stress radius of the plastic (process) zone. Thus, we can expect that the intersection angle will follow the critical angle when the radius of the plastic zone is much smaller than the size of the region controlled by the 3D vertex singularity. Before proceeding with the experimental validation of this condition in Section 3, we will discuss the characteristic size of the region, which is dominated by the singular stress state associated with vertex points.

2. The region dominated by the vertex singularity

The only way to evaluate the region dominated by the vertex singularity for a particular geometry and loading conditions is to use numerical methods. Below we present some typical outcomes of a 3D Finite Element (FE) study for a through-the-thickness crack in a linear elastic infinite plate (as shown in Fig. 1a and 1b) loaded remotely by K_{app} , see Fig. 3. The meshes near the crack front for straight and curved crack fronts are shown Fig. 4. Due to symmetry, only one eighth of the models is simulated. The mesh typically has a non-uniform layer distribution through the thickness to better capture the stress gradients near the free surface. The similar mesh was utilised in many previous computational studies.

In particular, the results for the local stress intensity factor distribution, $K_I(\xi)$, generally confirm the theoretical tendency given by Eq. (2). These results also indicate that the region, which is controlled by the vertex singularity, is approximately five percent of the plate thickness or crack front length. This conclusion was also confirmed in many previous 3D FE studies for cracked plates and round bars including the first 3D study for a semi-infinite by Nakamura and Parks [25]. In the case of the curved crack front with the intersection angle $\beta = \beta_c$, the variation of K_I

is significantly lesser, indicating a much smaller influence of the vertex singularity on the variation of the line singularity (square root singularity) near the free surface, which is again consistent with Eq. (2). However, it is important to note that both results for straight and curved crack front shapes are influenced by numerical errors and have to be treated with caution, specifically near the free surface, i.e. at $1 - \xi = \eta \rightarrow 0$.

To the best knowledge of the authors, there were no dedicated numerical studies investigating the regions affected by vertex singularities for other geometries and types of cracks, e.g. as shown in Fig. 4a and b. However, there were many 3D finite element studies in the past devoted to the evaluation of the stress intensity factors for different geometries. Several authors recommended disregarding the variations of the stress intensity factor along the crack front near the surface, again, typically within five percent of the crack front length from the vertex point, as these variations are attributed to the effect of the stress state associated with the vertex singularity. Summarising the past numerical studies for different geometries and crack shapes, it can be concluded that the region affected by vertex singularity is roughly five percent of the crack front length for a wide range of geometries [8,14,20,25–27].

3. Evaluation of the critical angle hypothesis

Fig. 5 shows the intersection angle, β , for common geometries: a through-thickness crack in a plate (a), a surface crack in a plate (b), and a surface crack in a solid circular bar (c). It is important to note that the steady state (or self-similar) crack growth occurs only for the through-the-thickness crack. Fatigue crack growth for other geometries is associated with a continuous crack front evolution and transient effects.

The summary of experimental studies, which have been utilised for the present evaluation of the critical angle concept, is presented in Table 1. Further details can be found in the original references. The outcomes of the evaluation are shown in Fig. 6, where the ratios of the experimental intersection angle, β_{exp} , to the critical angle, β_c , are plotted against the ratios of the half crack front length, L , to plastic zone size, r_p , for various materials, loading conditions and specimen geometries. Squares in Fig. 6 correspond to the geometry shown in Fig. 5a (through-the-thickness cracks in plates), triangles correspond to Fig. 5b (surface cracks in plates) and circles correspond to Fig. 5c (surface cracks in round bars). The size of the plastic zone, which is adopted as a first approximation to characterise the plasticity effects near the free surface, is evaluated using the standard equation of Linear Elastic Fracture Mechanics (LEFM):

$$r_p = \frac{1}{2\pi} \left(\frac{K_{max}}{\sigma_Y} \right)^2 \quad (5)$$

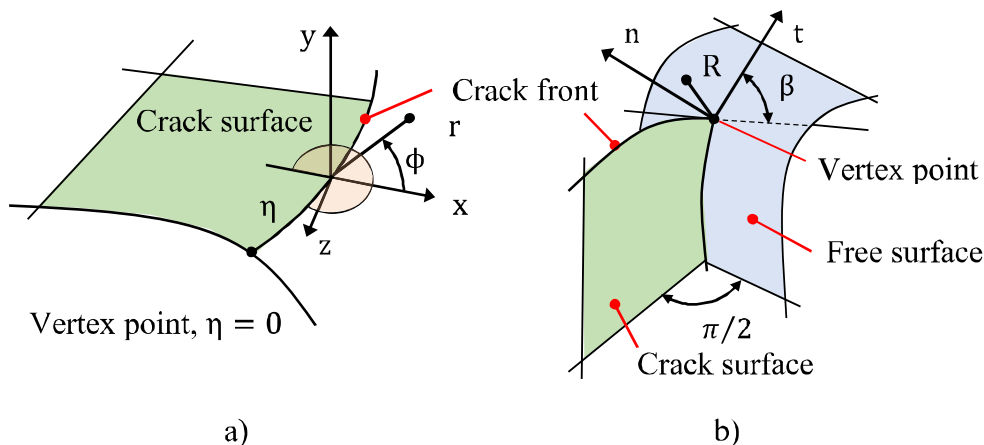


Fig. 2. Representation of the stress field near the front of crack.

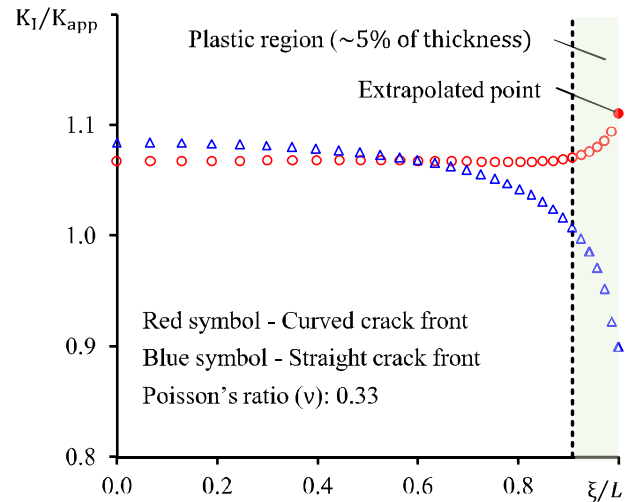


Fig. 3. Normalised stress intensity factor. In these figures, K_{app} is the remotely applied stress intensity factor in mode I, $\xi = 1 - \eta$, and L is the half plate thickness or the half crack front length.

where σ_Y is the yield strength, K_{max} is the maximum stress intensity factor in cyclic loading, and plane stress conditions are assumed near the free surface.

Results presented in Fig. 6, in particular, indicate that the through-the-thickness cracks, which propagate under steady-state conditions, better comply with the critical angle hypothesis. There is a clear trend that the discrepancies between the β_{exp} and β_c decrease with the increase of L/r_p . However, a similar trend is not clear for surface cracks propagating in round bars and plates. The propagation of surface cracks is generally not steady state but, instead, it is essentially a transient process as mentioned above. In other words, the shape of the crack as well as its size constantly changes (evolves) during fatigue growth. Thus, another factor, which influences the validity/applicability of the critical angle hypothesis, is the evolution of the crack geometry with crack propagation. Obviously, when the crack front evolution is relatively slow, then we can expect that the experimental results would comply with this hypothesis. However, there are currently not sufficient data to derive a quantitative condition for the rate of the crack front evolution, which could be qualified as slow or fast in order to verify this expected behaviour.

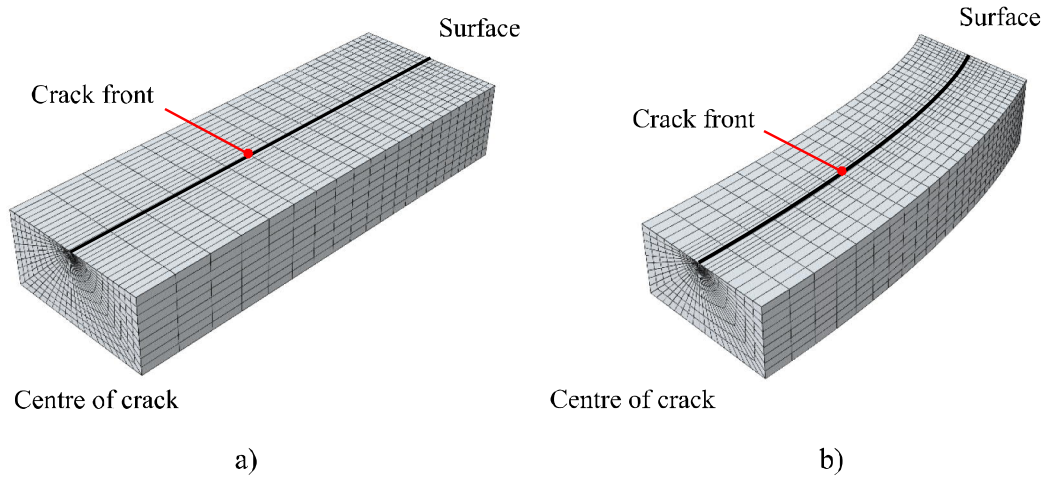


Fig. 4. Finite element mesh around a: (a) straight crack front, (b) curved crack front.

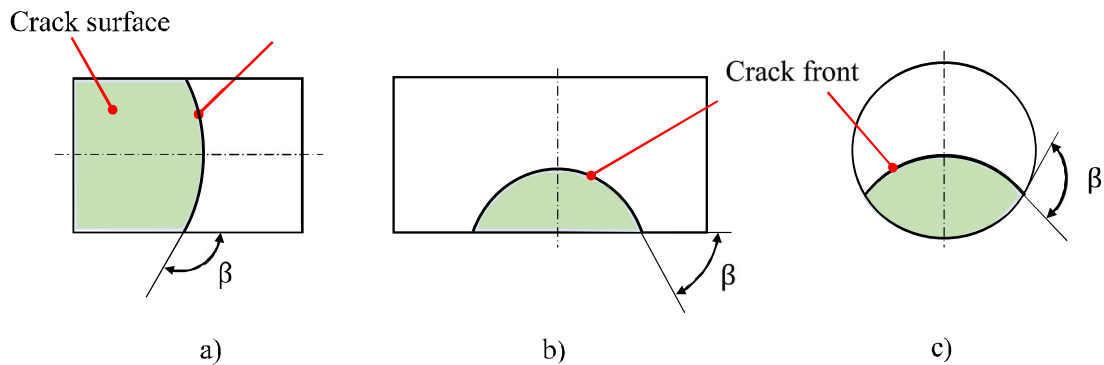


Fig. 5. Definition of crack front intersection angle, β : (a) through-the-thickness crack, (b) surface crack in a plate, (c) surface crack in a round bar.

Table 1
Summary of the experimental studies.

Reference research article	[12]	[12]	[15]	[16]	[17]	[18]	[19]	[20]	[21]	[22]	[23]
Theoretical intersecting angle (β_c)	103.6°	100.0°	101.2°	101.2°	102.6°	100.0°	102.0°	98.9°	101.2°	100.0°	100.8°
Experimental intersecting angle (β_{exp})	104.4°	100.3°	100.4°	112.0°	107.0°	96~120°	130.8°	121.0°	87~143°	64~105°	115.0°
Yield stress of material (MPa)	455	531	307	334	74	825	287	220	509	206	896
Poisson's ratio (ν)	0.39	0.30	0.33	0.33	0.37	0.30	0.35	0.27	0.33	0.30	0.32
Thickness or radius of specimen (mm)	20.0	20.0	3.0	6.35	40.0	10	6	10.0	9.6	12	6.35
Theoretical plastic zone size (mm)	0.40	0.29	0.14	0.37	0.01	0.1~0.2	0.20	0.50	0.1~0.15	0.1~0.3	1.02
Stress ratio (R)	0.1	0.1	0.25	0.05	-	0.1	0.1	0.1	0.1	0.1	0.05
Maximum applied load (kN ¹ / MPa√m ²)	25 ¹	25 ¹	7.5 ¹	16 ²	16 ²	3.7 ¹	2.0 ¹	12 ²	12~15 ²	25 ¹	4.9 ¹

4. Conclusion

In this work, we suggested a new condition, which has to be satisfied, for the intersection angle of a fatigue crack front to comply with the critical angle hypothesis, which was suggested more than forty years ago. From the analysis of the experimental results sourced from various studies published in the past, L/r_p (the ratio of the half crack front length to the plane plastic zone stress radius) has to be larger than 10^2 – 10^3 , as it can be seen from Fig. 6. Indeed, this condition complies with the LEFM, which is valid when the plastic zone size is much less than the characteristic size of the structure or the specimen. The ratio of this characteristic size to the radius of the plastic zone (as evaluated under plane stress conditions) has to be above 50. This ratio is typically utilised in many standards to justify the application of methods of LEFM; and it has been confirmed by a large number of fracture test results. The region

dominated by the vertex singularity, as discussed in Section 2, is approximately 20 times smaller than the half crack front length (which is roughly equal to the half plate thickness for through-the-thickness cracks). Therefore, the obtained threshold value of 10^3 can also be related to the same condition: r_p (size of the plastic zone) has to be approximately 50 times less than the region dominated by the vertex singularity ($\sim L/20$).

Another important finding of this experimental evaluation is a strong effect of the geometry and fatigue crack propagation conditions. It seems that the evolution of the crack front shape with the fatigue crack growth tend to deviate the intersection angle from the theoretical critical angle, see Fig. 6. As mentioned before, it is expected that the critical angle hypothesis is more appropriate for slow crack front changes or evolution. However, there are currently not many experimental and theoretical results to assess and confirm this expectancy. The further

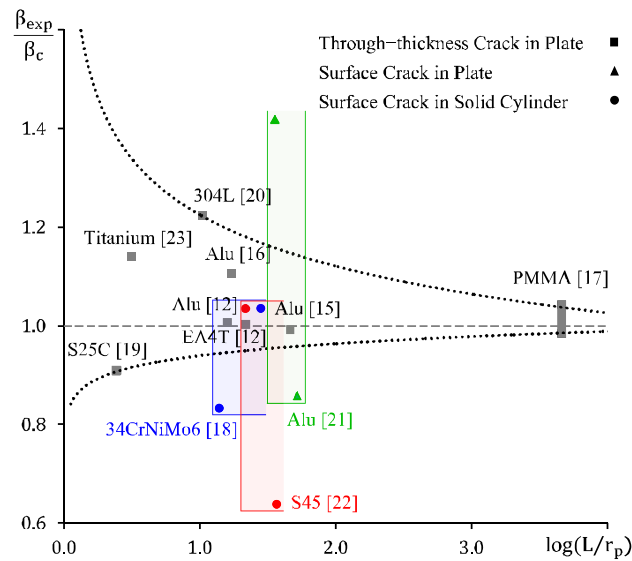


Fig. 6. The ratio of theoretical critical intersection angle, β_c , to the experimental intersection angle, β_{exp} , as a function of the ratio of the plastic zone size, r_p , to half crack front length, L .

research could address this issue by conducting systematic experimental and numerical studies, which may be directed on the measurement of the intersection angle, β , for relatively brittle materials and the evaluation of the vertex singularity and plasticity dominated regions, respectively. This would help to understand the role of the vertex singularity in fracture phenomena. Another interesting aspect is the effect of the vertex singularity on brittle fracture, which is expected to be much stronger for fracture modes II and III than for mode I. This singular effect can be significant for sharp notches, which was only theoretically demonstrated and described in [28,29].

Declaration of Competing Interest

The authors declare the following financial interests/personal relationships which may be considered as potential competing interests: Andrei Kotousov reports was provided by The University of Adelaide. Andrei Kotousov reports a relationship with The University of Adelaide.

Acknowledgment

This research is sponsored by FEDER funds through the program COMPETE – Programa Operacional Factores de Competitividade – and by national funds through FCT – Fundação para a Ciência e a Tecnologia –, under the project UIDB/00285/2020.

References

- J.P. Benthem, State of stress at the vertex of a quarter-infinite crack in a half-space, *Int. J. Solids Struct.* 13 (5) (1977) 479–492, [https://doi.org/10.1016/0020-7683\(77\)90042-7](https://doi.org/10.1016/0020-7683(77)90042-7).
- C. Mittelstedt, W. Becker, Semi-analytical computation of 3D stress singularities in linear elasticity, *Commun. Numer. Methods Eng.* 21 (5) (2005) 247–257, <https://doi.org/10.1002/cnm.742>.
- C. Luangarpa, H. Koguchi, Analysis of singular stresses at a vertex and along a singular line in three-dimensional bonded joints using a conservative integral, *Eur. J. Mech. A/Solids*. 60 (2016) 208–216, <https://doi.org/10.1016/j.euromechsol.2016.08.002>.
- D. Doitrand, E. Leguillon, Martin, Computation of generalized stress intensity factors of 3D singularities, *Int. J. Solids Struct.* 190 (2020) 271–280, <https://doi.org/10.1016/j.ijsolstr.2019.11.019>.
- Z. He, A. Kotousov, F. Berto, Effect of vertex singularities on stress intensities near plate free surfaces, *Fatigue Fract. Eng. Mater. Struct.* 38 (7) (2015) 860–869, <https://doi.org/10.1111/ffe.12294>.
- J.P. Benthem, The quarter-infinite crack in a half space; Alternative and additional solutions, *Int. J. Solids Struct.* 16 (2) (1980) 119–130, [https://doi.org/10.1016/0020-7683\(80\)90029-3](https://doi.org/10.1016/0020-7683(80)90029-3).
- D. Leguillon, E. Sanchez-Palencia, On 3D cracks intersecting a free surface in laminated composites, *Int. J. Fract.* 99 (1) (1999) 25–40, <https://doi.org/10.1023/a:1018366720722>.
- Z. He, A. Kotousov, A. Fanciulli, F. Berto, G. Nguyen, On the evaluation of stress intensity factor from displacement field affected by 3D corner singularity, *Int. J. Solids Struct.* 78–79 (2016) 131–137, <https://doi.org/10.1016/j.ijsolstr.2015.09.007>.
- Z.P. Bazant, L.F. Estenssoro, Surface singularity and crack propagation, *Int. J. Solids Struct.* 15 (1979) 405–426, [https://doi.org/10.1016/0020-7683\(79\)90062-3](https://doi.org/10.1016/0020-7683(79)90062-3).
- L.P. Pook, Some implications of corner point singularities, *Eng. Fract. Mech.* 48 (1994) 367–378, [https://doi.org/10.1016/0013-7944\(94\)90127-9](https://doi.org/10.1016/0013-7944(94)90127-9).
- M. Heyder, K. Kolk, G. Kuhn, Numerical and experimental investigations of the influence of corner singularities on 3D fatigue crack propagation, *Eng. Fract. Mech.* 72 (13) (2005) 2095–2105, <https://doi.org/10.1016/j.engfracmech.2005.01.006>.
- T. Oplt, P. Hutar, P. Pokorný, L. Náhlík, Z. Chlup, F. Berto, Effect of the free surface on the fatigue crack front curvature at high stress asymmetry, *Int. J. Fatigue* 118 (2019) 249–261, <https://doi.org/10.1016/j.ijfatigue.2018.08.026>.
- L.P. Pook, A 50-year retrospective review of three-dimensional effects at cracks and sharp notches, *Fatigue Fract. Eng. Mater. Struct.* 36 (8) (2013) 699–723, <https://doi.org/10.1111/ffe.12074>.
- P. Hutar, L. Náhlík, Z. Knésl, Quantification of the influence of vertex singularities on fatigue crack behavior, *Comput. Mater. Sci.* 45 (3) (2009) 653–657, <https://doi.org/10.1016/j.commatsci.2008.08.009>.
- R. Branco, F.V. Antunes, Finite element modelling and analysis of crack shape evolution in mode-I fatigue Middle Cracked Tension specimens, *Eng. Fract. Mech.* 75 (10) (2008) 3020–3037, <https://doi.org/10.1016/j.engfracmech.2007.12.012>.
- H. Hosseini-Toudeshky, G. Sadeghi, H.R. Daghyani, Experimental fatigue crack growth and crack-front shape analysis of asymmetric repaired aluminium panels

- with glass/epoxy composite patches, *Compos. Struct.* 71 (3) (2005) 401–406, <https://doi.org/10.1016/j.compstruct.2005.09.032>.
- [17] M. Heyder, G. Kuhn, 3D fatigue crack propagation: Experimental studies, *Int. J. Fatigue* 28 (5) (2006) 627–634, <https://doi.org/10.1016/j.ijfatigue.2005.06.052>.
- [18] J. Lebahn, H. Heyer, M. Sander, Numerical stress intensity factor calculation in flawed round bars validated by crack propagation tests, *Eng. Fract. Mech.* 108 (2013) 37–49, <https://doi.org/10.1016/j.engfracmech.2013.04.013>.
- [19] S. Ishihara, Y. Sugai, A.J. McEvily, On the distinction between plasticity-and roughness-induced fatigue crack closure, *Metall. Mater. Trans. A Phys. Metall. Mater. Sci.* 43 (9) (2012) 3086–3096, <https://doi.org/10.1007/s11661-012-1121-9>.
- [20] C. Gardin, S. Fiordalisi, C. Sarrazin-Baudoux, M. Gueguen, J. Petit, Numerical prediction of crack front shape during fatigue propagation considering plasticity-induced crack closure, *Int. J. Fatigue* 88 (2016) 68–77, <https://doi.org/10.1016/j.ijfatigue.2016.03.018>.
- [21] I.S. Putra, J. Schijve, Crack opening stress measurements of surface cracks in 7075-T6 Al alloy plate specimens through electron fractography, *Fatigue Fract. Eng. Mater. Struct.* 15 (4) (1992) 323–338, <https://doi.org/10.1111/j.1460-2695.1992.tb01274.x>.
- [22] R. Branco, F.V. Antunes, J.D. Costa, F.P. Yang, Z.B. Kuang, Determination of the Paris law constants in round bars from beach marks on fracture surfaces, *Eng. Fract. Mech.* 96 (2012) 96–106, <https://doi.org/10.1016/j.engfracmech.2012.07.009>.
- [23] Z.P. Bazant, L.F. Estenssoro, Surface singularity and crack propagation, *Int. J. Solids Struct.* 15 (5) (1979) 405–426, [https://doi.org/10.1016/0020-7683\(79\)90062-3](https://doi.org/10.1016/0020-7683(79)90062-3).
- [24] P.F.P. de Matos, D. Nowell, The influence of the Poisson's ratio and corner point singularities in three-dimensional plasticity-induced fatigue crack closure: a numerical study, *Int. J. Fatigue* 30 (10) (2008) 1930–1943, <https://doi.org/10.1016/j.ijfatigue.2008.01.009>.
- [25] T. Nakamura, D.M. Parks, Antisymmetrical 3-D stress field near the crack front of a thin elastic plate, *Int. J. Solids Struct.* 25 (12) (1989) 1411–1426, [https://doi.org/10.1016/0020-7683\(89\)90109-1](https://doi.org/10.1016/0020-7683(89)90109-1).
- [26] D. Camas, J. Garcia-Manrique, A. Gonzalez-Herrera, Numerical study of the thickness transition in bi-dimensional specimen cracks, *Int. J. Fatigue* 33 (7) (2011) 921–928, <https://doi.org/10.1016/j.ijfatigue.2011.02.006>.
- [27] R. Branco, F.V. Antunes, L.C.H. Ricardo, J.D. Costa, Extent of surface regions near corner points of notched cracked bodies subjected to mode-I loading, *Finite Elem. Anal. Des.* 50 (2012) 147–160, <https://doi.org/10.1016/j.finel.2011.09.006>.
- [28] A. Kotousov, P. Lazzarin, F. Berto, L.P. Pook, Three-dimensional stress states at crack tip induced by shear and anti-plane loading, *Eng. Fract. Mech.* 108 (2013) 65–74, <https://doi.org/10.1016/j.engfracmech.2013.04.010>.
- [29] A. Kotousov, Effect of plate thickness on stress state at sharp notches and the strength paradox of thick plates, *Int. J. Solids Struct.* 47 (14–15) (2010) 1916–1923, <https://doi.org/10.1016/j.ijsolstr.2010.03.029>.

Behnam Zakavi^{a,*}, Andrei Kotousov^{a,*}, Ricardo Branco^b

^a School of Mechanical Engineering, The University of Adelaide, Adelaide, SA 5005, Australia

^b Department of Mechanical Engineering, CEMMPRE, University of Coimbra, Rua Luís Reis Santos, Pólo II, 3030-788 Coimbra, Portugal

* Corresponding authors at: School of Mechanical Engineering, The University of Adelaide, Adelaide, SA 5005, Australia.

E-mail addresses: behnam.zakavi@adelaide.edu.au (B. Zakavi), andrei.kotousov@adelaide.edu.au (A. Kotousov).

Chapter 5

Development of Simplified Methods to Describe the Front Shapes of Through-the-thickness Fatigue Cracks

Statement of Authorship

Title of Paper	On evaluation of fatigue crack front shapes			
Publication Status	<input checked="" type="checkbox"/>	Published	<input type="checkbox"/>	Accepted for Publication
	<input type="checkbox"/>	Submitted for Publication	<input type="checkbox"/>	Unpublished and Unsubmitted work written in manuscript style
Publication Details	Zakavi, B., Kotousov, A., Khanna, A., & Branco, R. (2017). On evaluation of fatigue crack front shapes. 9th Australasian Congress on Applied Mechanics (ACAM9), 828–835.			

Principal Author

Name of Principal Author	Behnam Zakavi		
Contribution to the Paper	Created models, performed all analyses, interpreted data, and co-wrote manuscript		
Overall percentage (%)	50		
Certification:	This paper reports on original research I conducted during the period of my Higher Degree by Research candidature and is not subject to any obligations or contractual agreements with a third party that would constrain its inclusion in this thesis. I am the primary author of this paper.		
Signature		Date	22 / 08 / 2021

Co-Author Contributions

By signing the Statement of Authorship, each author certifies that:

- i. the candidate's stated contribution to the publication is accurate (as detailed above);
- ii. permission is granted for the candidate to include the publication in the thesis; and
- iii. the sum of all co-author contributions is equal to 100% less the candidate's stated contribution.

Name of Co-Author	Prof. Andrei Kotousov		
Contribution to the Paper	Performed analysis, interpreted data, reviewing the literature, and co-wrote manuscript		
Signature		Date	23 / 08 / 2021

Name of Co-Author	Dr. Aditya Khanna		
Contribution to the Paper	Assisted in data interpretation, and manuscript evaluation		
Signature		Date	24 / 08 / 2021

Name of Co-Author	Prof. Ricardo Branco		
Contribution to the Paper	Participated in manuscript review and evaluation, checked the derivation solutions		
Signature		Date	24 / 08 / 2021

On Evaluation of Fatigue Crack Front Shapes

B. Zakavi¹, A. Kotousov¹, A. Khanna¹ and R. Branco²

¹School of Mechanical Engineering
The University of Adelaide
Adelaide, SA 5005
AUSTRALIA

²Department of Mechanical Engineering
The University of Coimbra
3030-788 Coimbra
PORTUGAL

E-mail: behnam.zakavi@adelaide.edu.au

Abstract: *The front of through-the-thickness fatigue cracks in plates made of the various materials is often notably curved, specifically near the plate surfaces. However, for the sake of simplicity, the crack shape front and its evolution during crack propagation are normally disregarded in the current procedures of the fatigue crack growth evaluation. Our long term objective is to understand this phenomenon, develop modelling tools and incorporate more realistic crack front shapes into fatigue failure analysis. These modelling tools are expected to better predict failure and life-time of plate and shell components subjected to the cycling loading.*

In this study, the steady-state front shapes of the through-the-thickness cracks are investigated. When the size of the plastic zone is very small, the angle at which the crack front intersects the free surface is governed by the three-dimensional (3D) corner singularity or by a critical angle, which is a function of Poisson's ratio. The steady state conditions of fatigue crack propagation also require the uniform distribution of the local effective stress intensity factor range along the crack front. This parameter is evaluated numerically for different crack front shapes using 3D Finite Element Analysis (FEA). This paper presents the methodology, selected results of the numerical simulations, and a comparison between the obtained results and the outcomes of the experimental studies.

Keywords: *Numerical study, Crack front shape, Small scale yielding, Through-the-thickness cracks, Fatigue life estimation*

1. INTRODUCTION

Fatigue growth of cracks in plate components is often simplified with the plane geometry i.e. assuming that the crack front is straight and all points along the crack front are subjected to the same loading conditions. This assumption allows the evaluation of fatigue crack propagation with the classical linear elastic fracture mechanics or with more advanced two-dimensional (2D) fatigue models incorporating, the crack tip plasticity effects, out-of-plane constraint, plasticity or roughness induced closure phenomena, etc. The plane models (2D) are capable to accurately evaluate the fatigue life of structural components in many cases. However, recent studies provided numerous evidences that these fatigue models may lead to the inaccurate predictions when applied to the certain practical situations. For example, Bellett et al. [1] demonstrated that commonly used methods for notch fatigue assessment are not able to predict the behaviour of 3D stress concentration features in both welded joints and features machined from solid steel. Therefore, the further progress is necessary towards the development of more adequate fatigue life evaluation procedures. The three-dimensional modelling of the crack geometry can improve upon the prediction of plane models as the real fatigue cracks are inherently three-dimensional [2].

Many experimental studies and test results demonstrated that fatigue crack front shapes are not straight but curved [3,4]. There are at least two main phenomena responsible for the experimentally observed curvature of the front of fatigue cracks: the thickness effect and 3D corner singularity effect. In plate components of finite thickness, the stress state near the plate surfaces approaches plane stress,

whereas in regions away from the plate's free surfaces, the stress state is tri-axial. The variation of the out-of-plane (transverse) stresses leads to a variation in the constraint factor and the plasticity-induced crack closure values across the initially straight crack front. Therefore, the crack front shape normally evolves during fatigue crack propagation until it can (or cannot) reach a steady-state conditions. This condition corresponds to the uniform distribution of the fatigue crack driving force along the crack front. The local stress intensity factor is often considered regarded as the fatigue crack driving force in high cycle fatigue propagation.

The other phenomenon leading to the crack front curvature is the presence of the 3D corner (or vertex) singularity at the points where the crack front intersects the plate free surfaces. In 3D crack problems, the order of the singularity at the free surface depends on the Poisson's ratio and the intersection angle of the crack front with the free surface. Bazant and Estenssoro [5] argued from energy and other considerations that the front edge of a propagating crack must terminate at the free surface at an oblique, critical angle β_c , see Fig.1. The critical angle is a function of the Poisson's ratio ensuring inverse square root singularity ($r^{-1/2}$) at the corner points, same as the other points on the crack front. An analytical solution for the critical intersection angle is not available, although several numerical results can be found in the literature. The concept of critical angle was widely investigated experimentally in the recent years. It was demonstrated in several studies that when the plastic zone at the fatigue crack front is very small, the front edge intersects the free surface at the critical angle as predicted theoretically. For example, Heyder et. al. [6, 7] reported experimental measurements of the angle, at which the crack fronts break the free surface for the transparent specimens (PMMA) under four-point bending conditions. These measurements have shown that the crack front is shaped so as to ensure the same singular behaviour at the intersection of the crack front with the free surface and in the rest of the crack front for fatigue crack growth under pure fracture mode I.

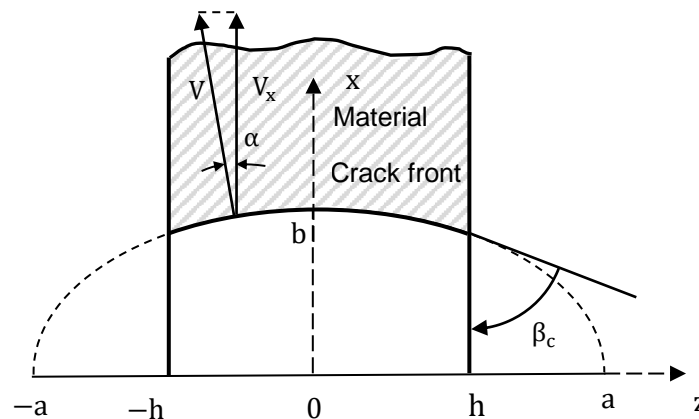


Figure 1. Elliptical-arc crack front shape for geometrical parameters crack propagation

Despite many experimental evidences supporting 3D considerations, only a limited number of 3D studies have been conducted on fatigue crack growth propagation. This is primarily because 3D simulations are far more complex, more time consuming and demand more powerful computing resources. The simulation of plasticity-induced crack closure using the FEA has some inherent difficulties related to the mesh refinement, crack growth scheme, which usually consists of releasing nodes ahead of the initial crack tip, and the stage at which crack is allowed to grow. The numerical study can be performed at minimum load, maximum load or during the loading/unloading cycle. Therefore, the outcomes of such numerical simulations should be treated with caution.

In this paper, we present a simplified procedure for the evaluation of the fatigue crack front shapes under steady-state growth when the plastic effects at the crack front are very small in comparison with the other dimensions, and in particular with the size of the region controlled by the 3D corner singularity. In this case, the angle at which the crack front intersects the free surface is very close to the critical angle in accordance with the previous experimental studies. The smallness of the plastic zone allows utilising the local elastic stress intensity factor range as the fatigue crack driving force. By considering a simple parametric family of the shapes of the crack front we select the one, which provides a more uniform driving force along the crack front. This is accomplished with the help of a series of careful 3D finite element simulations. In this paper, we present the selected outcomes of the FE simulations and provide a comparison between the obtained numerical results and the outcomes of experimental studies.

2. METHODOLOGY

In this section, we briefly outline the adopted methodology for the evaluation of the steady-state front in the through-the-thickness cracks. First, we approximate the shape of the crack front by a two-parameter elliptical curve, which can be described as:

$$x = b \sqrt{1 - \frac{z^2}{a^2}} \quad -h \leq z \leq h \quad (1)$$

where a and b are the major and minor axis of ellipse as shown in Fig. 1. As discussed in the Introduction, when the plasticity effects are small, the crack front tends to intersect the free plate surface at the critical angle, β_c . The critical angle is a function of Poisson's ratios and type of loadings. It is found that the critical intersection angle can be approximated by the following formula [8]:

$$\tan \beta_c = \frac{\nu - 2}{\nu} \quad (2)$$

The above empirical equation suggested by Pook is only valid for the brittle materials. When the size of the plastic zone is greater than 1% of the plate thickness (typically), the stress state near the vertex location is not controlled by the elastic singularity. In these cases, the plasticity effects become more important and together with the vertex singularity effect leads to the greater critical angles for elastic-plastic materials. To find b , we need to make sure that

$$\left. \frac{\partial x}{\partial z} \right|_{z=\pm h} = -\frac{bh}{a\sqrt{a^2 - h^2}} = \frac{\nu}{\nu - 2} \quad (3)$$

From the previous equation:

$$b = \frac{av}{(2 - \nu)} \sqrt{\frac{a^2}{h^2} - 1} \quad (4)$$

Substituting Eq. (4) into Eq. (1):

$$x(z) = \frac{av}{(2 - \nu)} \sqrt{\frac{a^2}{h^2} - 1} \times \sqrt{a^2 - z^2} \quad -h \leq z \leq h \quad (5)$$

This equation meets the condition that the crack front intersects with the free surface at the critical angle given by Eq. (2), and represents a parametric curve with one single parameter, a . Further, the Paris law is utilised to identify the steady state shapes. In accordance with the Paris law the speed of the crack growth, V , is given as:

$$V = C(\Delta K)^m \quad (6)$$

where ΔK is the stress intensity factor range of fatigue driving force, C and m are the material constants. The steady-state condition of the crack propagation requires that the projection of the crack growth speed along the crack propagation direction (which is x -direction, see Fig.1) to be constant for all points along the crack front, or

$$V_x(z) = V(z)\cos \alpha = \text{Constant} \quad (7)$$

This condition cannot be satisfied exactly with any multi-parametric equation describing the possible crack front shapes. However, the shape, which minimises the difference of the crack growth speed (7) along the crack front, can be considered as a first approximation of the actual fatigue crack front shape. The standard deviation approach can also be used to quantify this difference at different values of the parameter a in Eq. (5):

$$SD(V_x) = \frac{1}{2h} \int_{-h}^h (V_x^{\text{avg}} - V_x(z))^2 dz \quad (8)$$

where V_x^{avg} is the average speed of the crack front.

In other words, we determine the value of parameter a , which minimises the standard deviation of the crack growth rate along the crack front ($-h \leq z \leq h$), or $SD(V_x) \rightarrow \min$ to identify the realistic crack front shape. The local stress intensity factor range, ΔK , in Eq. (6) is evaluated numerically using the 3D finite element method. The modelling approach is briefly described in the next section.

3. 3D FINITE ELEMENT MODELLING APPROACH

The finite element geometry of a through-the-thickness crack in an elastic plate is shown in Fig. 2. By taking advantage of the symmetry conditions, only a one quarter of the crack problems is modelled. The crack front is normal to the free surface. The radial dimension of the FE model is taken approximately seven times larger than the plate thickness. In accordance with the previous studies, this is sufficient to accurately describe the 3D effects near the crack front [9].

The FE models corresponding to different values of the parameter, a , are meshed with 20 node hexahedral elements. The global and local meshes are shown in Fig. 2. A more dense mesh is applied near the crack front where the stress gradient is expected to be maximum. Further details of the modelling approach can be found in papers published by the present authors [10,11,12]. The numerical simulations were carried out using APDL scripts and ANSYS finite element software package, version 17.2.

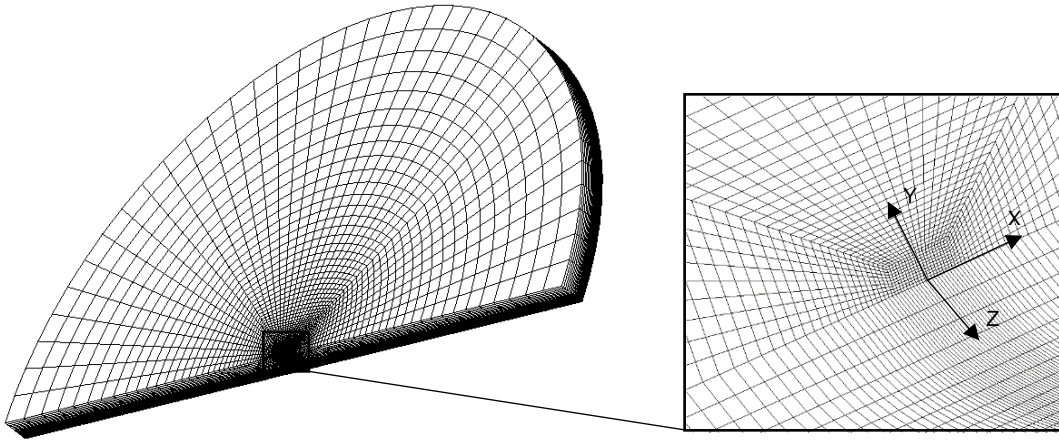


Figure 2. Finite element mesh around crack front

The opening mode is a major mode of the crack propagation and failure in components with the cracks. As such, Mode I fracture is the focus of our discussion and crack front estimation in the elastic materials. The displacement boundary conditions are applied on the plate edges corresponding to pure mode I. The plane-stress displacements far from the crack tip were calculated in accordance with the William's solution [13]:

$$u_x(r, \theta) = \left(\frac{r}{2\pi}\right)^{1/2} \frac{(1+\nu)}{E} [K_I^\infty f_x^I(\theta)] \quad (9)$$

$$u_y(r, \theta) = \left(\frac{r}{2\pi}\right)^{1/2} \frac{(1+\nu)}{E} [K_I^\infty f_y^I(\theta)] \quad (10)$$

where

$$f_x^I(\theta) = \cos\frac{\theta}{2} \left(k - 1 + 2 \sin^2\frac{\theta}{2}\right) \quad (11)$$

$$f_y^I(\theta) = \sin\frac{\theta}{2} \left(k + 1 + 2 \cos^2\frac{\theta}{2}\right) \quad (12)$$

Here r is the distance from the crack tip, θ is the angle measured from the symmetry line, and K_I^∞ is the remotely applied mode I stress intensity factor. k is Kolosov's constant for plane stress and plane strain conditions. The plane stress k value has been considered in the boundary conditions:

$$k = \frac{3-\nu}{1+\nu} \quad (13)$$

Bakker [14] showed that a cracked plate under plane stress undergoes a change to plane strain behaviour near the crack tip. He adds that the radial position where the plane stress to plane strain transition takes place strongly depends on the position in the thickness direction. The degree of plane strain is essentially zero at distances from the tip greater than five times of thickness, even in the middle plane of the plate [15].

4. SELECTED RESULTS

In this section, we show the influence of Poisson's ratio, ν , and Paris law exponent, m , on the crack front shapes at the condition of the steady-state propagation. It is clear that the constant C in the Paris law does not affect the calculations and the minimisation of the standard deviation (Eq. 8).

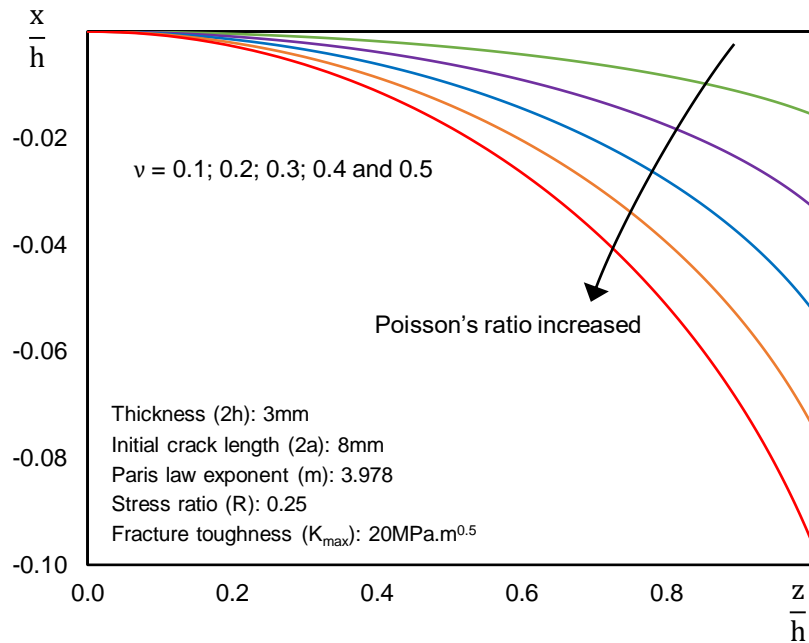


Figure 3. Effect of the Poisson's ratio on the crack front shapes

Fig. 3 shows the effect of Poisson's ratio on the crack front shapes. The shapes become more curved and deeper with the increase of Poisson's ratio as the critical angle, β_c , becomes larger at the greater Poisson's ratios, see Eq. (2). It is interesting to note that the 3D corner singularity effect is normally confined to a close vicinity of the vertex region, typically to the distance of several percent of the plate thickness, however, its effect on the crack front shapes is quite significant. This can be explained by the intersection angle governed by the 3D corner singularity, which significantly affects the shape. This is because the shape cannot be changed in an abrupt manner, so it follows this initial direction given by the critical angle.

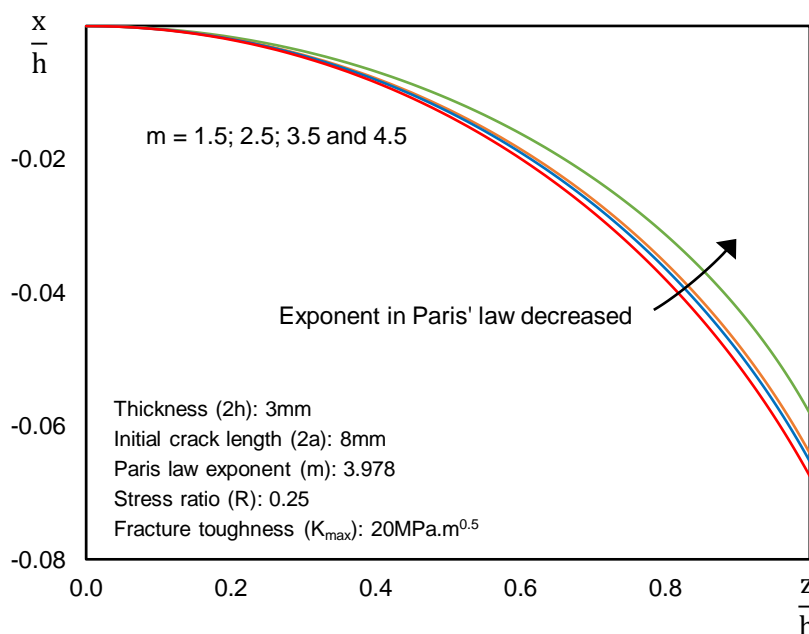


Figure 4. Crack front shapes corresponding to various values of fatigue constant m

Contrary to the strong effect of Poisson's ratio on the crack front shapes, it seems, the effect of the fatigue crack growth material constants, C and m is quite small. The whole range of possible fatigue exponent corresponding to structural materials was investigated with the proposed method for the particular geometry and loading conditions. However, these material constants are expected to have a large effect on the evolution of the front shape in the case of changing in the loading or boundary conditions.

5. COMPARISON AGAINST EXPERIMENTAL RESULTS

The proposed method for the evaluation of the steady-state crack front shapes was compared against an experimental study of Borrego, 2001 [16]. In this study, the centre-cracked panels with a thickness of 3mm were subjected to the constant fatigue loading. The panels were made of 6082-T6 aluminium alloy. The fatigue properties and parameters of fatigue loading are given in Table 1. The fatigue cracks were grown over a sufficiently large distance from the initial notch to ensure the quasi-steady state conditions of propagation (Fig 5).

Table 1. Material properties and cyclic loading conditions for an aluminium plate with a through-thickness crack under fracture opening mode [Borrego, 2001]

Poisson's ratio (ν)	Young's Modulus (E)	Load ratio (R)	Crack length (2a)	Exponent in Paris' law (m)	Material yield stress ($\bar{\sigma}_y$)
0.33	74GPa	0.25	8mm	3.456	307MPa



Figure 5. The experimental crack front shape with a through-the-thickness crack [16]

Fig. 6 shows a comparison of the experimental crack front shape and the one, which was obtained with the proposed method. It can be stated that the experimental results and theoretical predictions are in a good agreement.

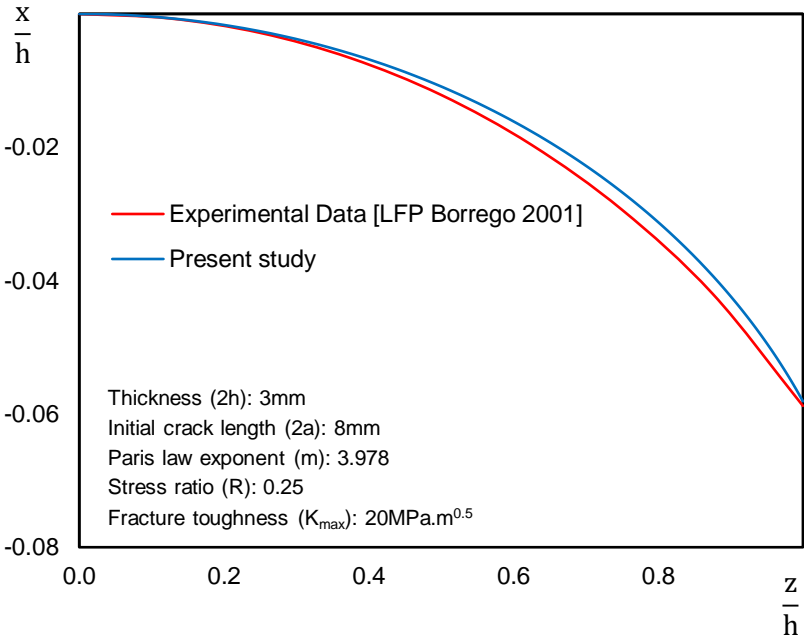


Figure 6. Comparison between the predicated and experimental crack front shape

Table 2 presents some intermediate results of numerical simulations, from which the realistic shape is selected. Parameter a is changed from 1 (this value corresponds to straight crack front) to 1.5, which results into the aspect ratio of the principle axis of the elliptical curve 0.34. A finite element model was developed for each parameter a , and the standard deviation of the crack growth rate along the crack front, $S(V_x)$, was evaluated in accordance with the procedure presented in Sections 2 and 3.

Table 2. Comparison between the maximum stress intensity factor and standard deviation of the average crack speed under Mode I loading ($m = 4.224$, $2h = 3\text{mm}$, $\nu = 0.33$, $R = 0.25$)

a/h	1.00	1.05	1.10	1.2	1.50
b/a	0.00	0.06	0.09	0.15	0.22
Tunnelling effect, P_t	0	0.023	0.029	0.035	0.042
$S(V_x)$	2.38E-05	2.87E-06	2.06E-07	1.06E-06	8.07E-06

From Table 2, it follows that $a/h = 1.10$ provides the minimum error, which corresponds to the steady state condition. In addition, the tunnelling effect, P_t , which is the ratio of the crack depth to the plate thickness, is also determined from the numerical simulations. This tunneling effect for the steady state shape is 0.03. The obtained tunnelling effect is in an agreement with the previous numerical studies, which were focused on the evaluation of this parameter [17,18].

The corresponding estimated life cycles without consideration of the crack closure effect for the different crack front shapes are summarised in Table 3. The plate thickness and crack length were set at 3mm and 23.52mm. The values of the maximum stress intensity factor analysed were $20\text{MPa}\sqrt{\text{m}}$ with zero minimum stress intensity factor ($K_{\text{min}} = 0$), which corresponds to $R = 0$.

Table 3. Comparison between the maximum estimated design life ($m = 3.456$, $C = 2.5054\text{E-}11$)

	Straight crack front	Present study
Max. Stress Intensity Factor at the Crack Front	21.282	21.002
Estimated Life Cycles	2.42E+07	2.53E+07

6. CONCLUSION

In this paper, a new method and the outcomes of the numerical simulations of the steady-state crack front shape are presented. The main conclusions, which can be drawn from these simulations, are:

- Poisson's ratio has a strong effect on the fatigue crack front shapes;
- The depth of crack front curvature increases with an increase in the Paris exponent. The effect of fatigue constants on the steady state shape of fatigue through-the-thickness crack was found to be small. However, these constants are expected to play a significant role in the evolution of the crack front shape until it reaches the steady-state (or quasi-steady-state) shape.

The comparison with experimental results is quite encouraging and demonstrates the validity of the underlying assumptions, which were utilised in the present study: (1) the crack front shape intersects the free plate surface at the critical angle, (2) the local stress intensity factor can be considered as the fatigue crack driving force, which leads to the formation of the crack front shape under high cycling loading. The above assumptions might not be correct in the case of sufficiently large plastic effects near the crack tip. In this case, the plasticity induced closure, which is significantly different along the crack front, will be the one of the most influential factors affecting the crack front shape. The future work can be directed on the incorporation the plasticity induced crack closure effects into the calculation of the fatigue driving force, and the more complex geometries and crack shapes.

7. ACKNOWLEDGMENTS

The Authors would like to appreciate Dr. Zhuang He from the school of Mechanical Engineering, The University of Adelaide who provided the technical support for this study.

8. REFERENCES

1. Bellett D, Taylor D, Marco S, Mazzeo E, Guillois J, Pircher T. The fatigue behaviour of three-dimensional stress concentrations. *International Journal of Fatigue*. 2005; Vol.27(3), pp.207-221.
2. Camas D, Garcia-Manrique J, Gonzalez-Herrera A. Crack front curvature: Influence and effects on the crack tip fields in bi-dimensional specimens. *International Journal of Fatigue*. 2012; Vol.44, pp.41-50.
3. Hosseini H, Sadeghi G, Daghyani HR. Experimental fatigue crack growth and crack-front shape analysis of asymmetric repaired aluminium panels with glass/epoxy composite patches. *Composite Structures*, 2005; Vol.71(3), pp.401-406.
4. Hutar P, Seitzl S, Garcia TE, Fernandez-Canteli A. Experimental and numerical analysis of in- and out- of plane constraint effects on fracture parameters: Aluminum alloy 2024. *Applied and Computational Mechanics*, 2013; Vol.7(1), pp.53-64.
5. Bazant ZP, Estenssoro LF. Surface singularity and crack propagation. *International Journal Solid Structure*. 1979; Vol.15:405-426.
6. Heyder M, Kolk K, Kuhn G. Numerical and experimental investigations of the influence of corner singularities on 3D fatigue crack propagation. *Engineering Fracture Mechanics*. 2005; Vol.72(13), pp.2095-2105.
7. Heyder M, Kuhn G. 3D fatigue crack propagation: Experimental studies. *International Journal of Fatigue*. 2006; Vol.28(5), pp.627-634.
8. Pook, LP. Some implications of corner point singularities. *Engineering Fracture Mechanics*. 1994; Vol.48(3), pp.367-378.
9. Nakamura T, Parks DM. Antisymmetrical 3-D stress field near the crack front of a thin elastic plate. *International Journal of Solids and Structures*. 1989; Vol. 25(12), pp.1411-1426.
10. Kotousov A, Lazzarin P, Berto F, Pook LP. Three-dimensional stress states at crack tip induced by shear and anti-plane loading. *Engineering Fracture Mechanics*, 2013; Vol. 108, pp.65-74.
11. Kotousov A. Fracture in plates of finite thickness. *International Journal of Solids and Structures*, 2007; Vol. 44(25), pp.8259-8273.
12. He Z, Kotousov A, Branco R. A simplified method for the evaluation of fatigue crack front shapes under mode I loading. *International Journal of Fracture*, 2014; Vol. 188(2), pp.203-211.
13. Williams ML. On the stress distribution at the base of a stationary crack. *Journal of Applied Mechanics*, 1957; Vol.24, pp.109-114.
14. Bakker A. Three Dimensional Constraint Effects on Stress Intensity Distributions in Plate Geometries with Through-thickness Cracks. *Fatigue & Fracture of Engineering Materials & Structures*,1992; Vol.15.11, pp.1051-1069.
15. Levy N, Marcal PV, Rice JR. Progress in three-dimensional elastic-plastic stress analysis for fracture mechanics. *Nuclear Engineering and Design*, 1971; Vol.17(1), pp.64-75.
16. Borrego LPF. Fatigue crack growth under variable amplitude load in an AlMgSi alloy. PhD thesis, Department of Mechanical, Engineering, University of Coimbra, 2001.
17. Branco R, Antunes FV. Finite element modelling and analysis of crack shape evolution in Mode-I fatigue Middle Cracked Tension specimens. *Engineering Fracture Mechanics*. 2008; Vol.75(10), pp.3020-3037.
18. Branco R, Rodrigues DM, Antunes FV. Influence of through-thickness crack shape on plasticity induced crack closure. *Fatigue & Fracture of Engineering Materials & Structures*, 2008, Vol.31(2), pp.209-220.
19. Nowell D, de Matos PFP. The influence of the Poisson's ratio and corner point singularities in three-dimensional plasticity-induced fatigue crack closure: A numerical study. *International Journal of Fatigue*, 2008; Vol. 30(10), pp.1930-1943.

Statement of Authorship

Title of Paper	On the Simplified Modelling of Front Shapes of Fatigue Cracks			
Publication Status	<input checked="" type="checkbox"/>	Published	<input type="checkbox"/>	Accepted for Publication
	<input type="checkbox"/>	Submitted for Publication	<input type="checkbox"/>	Unpublished and Unsubmitted work written in manuscript style
Publication Details	Zakavi B, Kotousov A, Khanna A, Branco R. On the Simplified Modelling of Front Shapes of Fatigue Cracks, 11th International Conference on Structural Integrity and Failure (SIF-2018), 3 - 6 December 2018, Perth, Australia.			

Principal Author

Name of Principal Author	Behnam Zakavi		
Contribution to the Paper	Created FE models, performed analyses, interpreted data, and co-wrote manuscript		
Overall percentage (%)	50		
Certification:	This paper reports on original research I conducted during the period of my Higher Degree by Research candidature and is not subject to any obligations or contractual agreements with a third party that would constrain its inclusion in this thesis. I am the primary author of this paper.		
Signature		Date	22 / 08 / 2021

Co-Author Contributions

By signing the Statement of Authorship, each author certifies that:

- i. the candidate's stated contribution to the publication is accurate (as detailed above);
- ii. permission is granted for the candidate to include the publication in the thesis; and
- iii. the sum of all co-author contributions is equal to 100% less the candidate's stated contribution.

Name of Co-Author	Prof. Andrei Kotousov		
Contribution to the Paper	Supervised development of work, and provided major contribution on manuscript writing		
Signature		Date	24 / 08 / 2021

Name of Co-Author	Dr. Aditya Khanna		
Contribution to the Paper	Participated in work discussions, manuscript review and evaluation		
Signature		Date	24 / 08 / 2021

Name of Co-Author	Prof. Ricardo Branco		
Contribution to the Paper	Checked the derivation solutions, participated in manuscript review and evaluation,		
Signature		Date	23 / 08 / 2021

On the Simplified Modelling of Front Shapes of Fatigue Cracks

B. Zakavi^{1, a*}, A. Kotousov^{1, b}, A. Khanna^{1, c} and R. Branco^{2, d}

¹ School of Mechanical Engineering, The University of Adelaide, Adelaide, SA 5005, Australia

² Department of Mechanical Engineering, University of Coimbra, 3030-788, Coimbra, Portugal

^a behnam.zakavi@adelaide.edu.au, ^b andrei.kotousov@adelaide.edu.au,

^c aditya.khanna@adelaide.edu.au, ^d ricardo.branco@dem.uc.pt

Keywords: Numerical analysis, Front shape, Crack closure, Plasticity, Steady-state conditions

Abstract. A direct three-dimensional (3D) finite element modelling of fatigue crack growth in structural components still represents a formidable task due to a complex singular behaviour of the stress field along the crack front as well as strong non-linearities associated with material plasticity and the change of contact conditions between crack faces during the loading cycle. The complexity of the 3D numerical modelling of fatigue crack growth largely motivates the development of simplified approaches. This paper describes several possible approaches for the evaluation of front shapes of fatigue cracks. These approaches are based on (1) the elimination of the corner singularity effect, (2) predictions based on the first-order plate theory, (3) the equivalent thickness concept, and (4) the Iso-K criterion. This paper briefly outlines these simplified approaches and presents some theoretical predictions for the case of through-the-thickness cracks propagating in plates under quasi-steady-state conditions. The theoretical predictions are also compared with experimental observations.

Introduction

The evaluation of fatigue failure of structural components is of permanent and primary interest for engineers. Hence, significant research effort has been directed towards the development of fatigue crack growth models over the past four decades. In particular, numerous early publications were dedicated to the study of the fatigue crack closure concept, which was first introduced by Elber [1] to explain the experimentally-observed features of fatigue crack growth in aluminum alloys. The number of publications grew rapidly since his pioneering study, reaching a maximum around 1970. It is now commonly accepted that the contributions of various mechanisms of crack closure, specifically the plasticity-induced closure, are significant, particularly at the near threshold fatigue crack growth, in retardation effects associated with overloads and acceleration of crack growth rates of physically short cracks [2]. In accordance with this approach, the crack growth and the shape evolution are governed by the effective stress intensity factor, ΔK_{eff} , which is defined as:

$$\Delta K_{\text{eff}} = K_{\text{max}} - K_{\text{op}} = U\Delta K = U(K_{\text{max}} - K_{\text{min}}) \quad (1)$$

where K_{max} and K_{min} are the maximum and minimum values respectively and U is the normalised load ratio parameter (or the normalised effective stress intensity factors) which is often used to describe the effects of loading and plate geometry on crack closure.

Prior to 1970, the plasticity and crack closure mechanisms were intensively investigated for two-dimensional (2D) geometries utilising both plane strain and plane stress simplifications. With advances in numerical modelling and the increase in computational power, it became possible to study more realistic three-dimensional (3D) geometries as well as investigate the various near crack front 3D effects. A number of finite element (FE) models have been developed in the past to evaluate the effective stress intensity factor, ΔK_{eff} , and normalised load ratio parameter, U , for various geometries and loading conditions. However, these methods are difficult to implement in fatigue analysis due to convergence and repeatability issues. One of the reasons behind the difficulties in modelling plasticity and contact nonlinearities is the complex 3D singular stress fields, specifically near the vertex (corner) points.

In 3D problems the order of the singularity at the intersection of the crack front with the free surface depends on the Poisson's ratio and intersection angle. From energy considerations, it follows that shape of the fatigue crack front must evolve to preserve the inverse square root singular behaviour along the entire crack front. Therefore the fatigue crack has to intersect the free surface at a critical angle, β_c , which is a function of Poisson's ratio, ν . Several experimental studies, specifically for quasi-brittle materials, have confirmed this prediction for mode I fatigue cracks. Other studies have indicated that the effect of 3D corner singularity might not be very significant in the presence of a sufficiently large crack front process zone. This is because the 3D corner singularity effect is a point effect and is quite localised. The experimental results for surface fatigue cracks in round bars show that the fatigue front preserves a semi-elliptical shape rather than the critical angle [3].

In this paper, we briefly outline four simplified approaches for the prediction of front shapes of fatigue cracks. We also describe the application of these approaches to through-the-thickness cracks as well as a comparison with experimental data.

Methods for Evaluating the Front Shapes of Fatigue Cracks

In this Section we briefly describe four simplified approaches for evaluating the front shapes of fatigue cracks propagating in plates under quasi-steady state conditions. These approaches are based on (1) the elimination of the corner singularity effect; (2) predictions based on the first-order plate theory; (3) incorporation of plasticity-induced fatigue crack closure effect using the equivalent thickness concept; and (4) the Iso-K concept.

1. Approach Based on the Elimination of Corner Singularity Effect

This approach is based on the so-called stress singularity matching. In accordance with this assumption, the evolution of the crack front occurs in a manner that all points over the crack front (including the corner points) have the same inverse square root singularity of the stress field. This assumption implies that the angle, β , is the same during the crack front evaluation and equal to the critical angle, $\beta = \beta_c$, (see Fig. 1) at the condition of the steady-state propagation [4]. The critical angle is a function of Poisson's ratio only; for example, for $\nu = 0.3$, $\beta_c \approx 100.40$. It is interesting to note that in accordance to the experimental study by Heyder et al. [5], in structures with flat free surfaces, such as beams of rectangular or trapezoidal cross-sections, the fatigue crack front appears to follow the stress singularity matching assumption; however, it is generally not supported by experimental observations for structures with curved surfaces such as round bars [6].

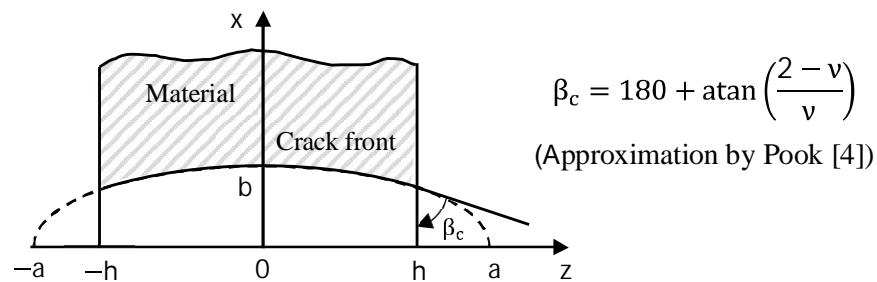


Fig. 1. Critical angle, β_c , in the case of a through-the-thickness crack propagating in a plate

An application of this approach to a steady state fatigue crack propagation requires the fulfilment of two conditions: (1) stress singularity matching (or $\beta = \beta_c$ at the intersection with the free boundary) and (2) the same value of the stress intensity factor along the crack front (Iso-K approach). The practical realisation of this approach can be based on a minimisation of the stress intensity factor variation along different front shapes, which can be described by a multi-parametric equation.

2. First-Order Plate Theory Predictions

Another approach for the front shape evaluation is based on first-order theory predictions. This simplified theory is a natural extension of the classical plane stress/plane strain theories. The first-order plate theory explicitly incorporates the plate thickness and the transverse stress components into the governing equations, which retain the simplicity of 2D models.

Based on this theory, and utilising Budiansky-Hutchinson crack closure model [7], Codrington and Kotousov [8] provided the following solution for the normalised load ratio, U , in the case of the small-scale plasticity:

$$U(R, \eta) = a(\eta) + b(\eta)R + c(\eta)R^2 \quad (2)$$

where R is the load ratio; a , b and c are fitting functions given by the following equations:

$$a(\eta) = 0.446 + 0.266 \cdot e^{-0.41\eta}; \quad b(\eta) = 0.373 + 0.354 \cdot e^{-0.235\eta}; \quad c(\eta) = 0.2 - 0.667 \cdot e^{-0.515\eta} \quad (3)$$

where $\eta = K_{\max}/(h\sqrt{\sigma_f})$ is a dimensionless parameter, K_{\max} is the maximum stress intensity factor, h is the half-plate thickness, and σ_f is the flow stress.

These equations correctly recover the limiting cases of very thin and very thick plates, i.e. when $\eta \rightarrow \infty$ or $\eta \rightarrow 0$, respectively. The details of the derivation of these equations can be found in the original paper [8]. The application of this solution to the evaluation of the front shape of through-the-thickness cracks can be found in He et al. [9], and will not be repeated here due to page restrictions.

3. Equivalent Thickness Concept

Several researches suggested a concept which simplifies the evaluation of the plastic constraint effect on the plasticity-induced crack closure [10,11]. For example, based on an extensive 3D elastoplastic FE analysis for through-the-thickness cracks, She et al. [12] proposed to define the equivalent thickness for arbitrary point, P , located on the crack front, see Fig. 2, as follows:

$$h_{eq} = h - z^2/h \quad (4)$$

where z is the distance from the mid-plane and h is still the half-thickness of the plate.

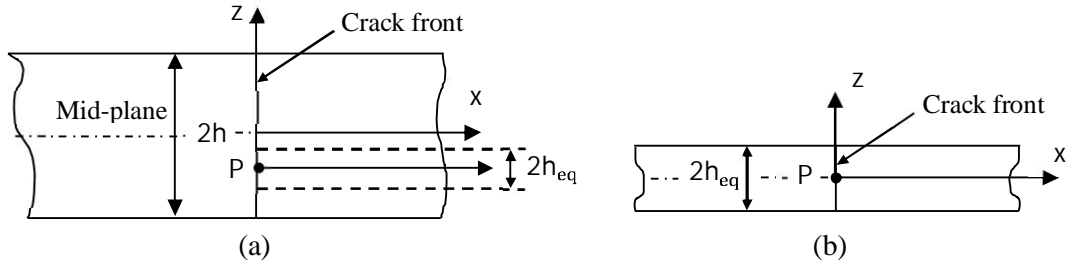


Fig. 2. Schematic illustration of the equivalent thickness method in the through-the-thickness cracks

The normalized load ratio is defined as:

$$U = \frac{\sqrt[3]{\kappa}}{1 - R} \quad (5)$$

where κ (see Eq. (6)) is a function of R and a global constraint factor, α_g .

$$\kappa = \frac{(1 - R^2)^2(1 + 10.34R^2)}{\left[1 + 1.67R^{1.61} + \frac{1}{0.15\pi^2\alpha_g}\right]^{4.6}} \quad (6)$$

The global constraint factor is a thickness (t) and Poisson's ratio (ν) dependence parameter:

$$\alpha_g = \frac{1 + t}{1 - 2\nu + t} \quad (7)$$

The normalized load ratio increases with an increase in the constraint factor at the constant applied stress ratio. In the last equation, t can be calculated from the following equation:

$$t = 0.2088 \sqrt{\frac{r_0}{h_{eq}}} + 1.5046 \frac{r_0}{h_{eq}} \quad (8)$$

with the plastic zone size, r_0 , as a function of flow stress, σ_f , defined as:

$$r_0 = \frac{\pi}{16} \left(\frac{K_{\max}}{\sigma_f}\right)^2 \quad (9)$$

The practical realisation of this approach is normally accomplished by a simple crack advance scheme, in which each point along the crack front moves in accordance with the effective stress intensity factor range, ΔK_{eff} , see Eq. (1), with U provided by relationships (5) – (9).

4. Iso-K approach

In accordance with the Iso-K approach, the steady state fatigue crack propagation requires the uniform distribution of the local stress intensity factor range along the crack front. The stress intensity factor range can be evaluated numerically using 3D linear-elastic FEA.

The practical realisation of this approach for a steady-state propagation of through-the-thickness cracks in plates can involve the evaluation of the stress intensity factor for two characteristic points: at the middle, $z = 0$ and at the surface, $z = h$ for a two-parametric set of equations representing the front shapes, e.g. elliptical shapes. Further, the higher value of the crack closure at the free surface may be incorporated into the theoretical predictions using various empirical equations for crack closure proposed in the past, e.g. the one suggested by Newman and Raju [13]. The steady-state crack growth requires the same fatigue crack growth rate, or

$$\frac{da}{dN} = C_S(\Delta K_S)^n = \frac{db}{dN} = C(\Delta K_M)^n \quad (10)$$

where ΔK_S and ΔK_M are the stress intensity factor ranges at the surface and the mid-thickness points of the crack front; C and n are Paris constants, which can be obtained experimentally for different materials. Newman and Raju proposed the following relationship between the Paris coefficients at the surface and deepest points for the plate components with a semi-circular crack under pure tension cyclic loading condition [13]:

$$C_S = 0.9^n C \quad (11)$$

In this study we also utilized a coefficient of 0.8 for both selected materials to get a better agreement with experimental data.

Comparison of Different Approaches

The proposed approaches for the evaluation of the steady-state crack front shapes were compared against experimental studies [5,14]. In these studies, the centre-cracked panels were made of 2024-T3 aluminum alloy and Polymethylmethacrylate (PMMA) with a thickness of 6.35mm and 40mm, respectively. The advantage of PMMA material is its transparency which enabled an in-situ evaluation of the crack front shape.

For the aluminum alloy specimens such an evaluation was done using benchmarking technique and post-mortem analysis of fracture surfaces. Both specimens were subjected to constant amplitude fatigue loading. The fatigue cracks were grown over a sufficiently large distance from the initial notch to ensure the quasi-steady state conditions of propagation.

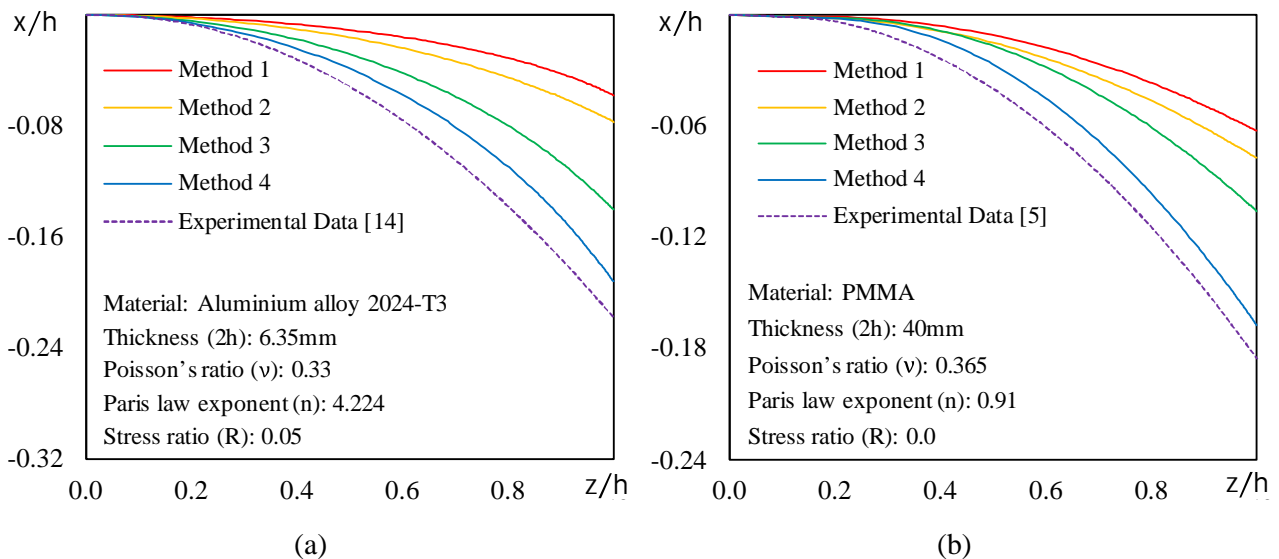


Fig. 3. Comparison between the predicted crack shapes and experimental data for the specimens made of a) 2024-T3 aluminium alloy, and b) Polymethyl methacrylate (PMMA)

As it follows from the analysis of Fig.3, the simplified approaches work a bit better for the quasi-brittle material (PMMA); and the Iso-K approach provides the best correlation with the experimental results. Unfortunately, none of the approaches is capable to accurately describe the front shape of fatigue cracks. This can be explained by the complexity of the crack closure phenomenon, which currently represents one of the major challenges in 3D Fracture Mechanics.

Conclusion

The capability of several simplified approaches for the evaluation of the shape of fatigue crack fronts has been studied using experimental results for a steady-state propagation of fatigue through-the-thickness cracks in different materials. It is demonstrated that none of the approaches is capable to accurately describe the shape of the fatigue cracks. An empirically introduced crack closure equation allows for a better matching of the theoretical and experimental predictions. The outcomes of this work and the comparison justify a need of further research in this area.

References

- [1] W. Elber, Fatigue crack closure under cyclic tension, *Eng. Fract. Mech.* Vol.2(1) (1970) 37-44.
- [2] A.K. Vasudeven, K. Sadananda, N. Louat, A review of crack closure, fatigue crack threshold and related phenomena, *Mater. Sci. Eng.* Vol.188(1) (1994) 1-22.
- [3] D. Nowell, P.F.P. de Matos, The influence of the Poisson's ratio and corner point singularities in three-dimensional plasticity-induced fatigue crack closure: A numerical study, *Int. J. Fatigue* Vol. 30(10) (2008) 1930-1943.
- [4] L.P. Pook, Some implications of corner point singularities, *Eng. Fract. Mech.* Vol.48(3) (1994) 367-378.
- [5] M. Heyder, G. Kuhn, 3D fatigue crack propagation: Experimental studies, *Int. J. Fract. Mech.* Vol.28(5) (2006) 627-634.
- [6] J. Lebahn, H. Heyer, M. Sander, Numerical stress intensity factor calculation in flawed round bars validated by crack propagation tests, *Eng. Fract. Mech.* Vol.108 (2013) 37-49.
- [7] B. Budiansky, J.W. Hutchinson, Analysis of closure in fatigue crack growth, *J. Appl. Mech* 45(2) (1978) 267-276.
- [8] J. Codrington, A. Kotousov, A crack closure model of fatigue crack growth in plates of finite thickness under small-scale yielding conditions, *Mech. of Mater.* Vol.41(2) (2009) 165-173.
- [9] Z. He, A. Kotousov, R. Branco, A simplified method for the evaluation of fatigue crack front shapes under mode I loading, *Int. J. Fract. Mech.* Vol.188(2) (2014) 203-211.
- [10] W. Guo, Three-dimensional analyses of plastic constraint for through-thickness cracked bodies, *Eng. Fract. Mech.* Vol.62(4-5) (1999) 383-407.
- [11] P. Yu, W. Guo, An equivalent thickness conception for evaluation of corner and surface fatigue crack closure, *Eng. Fract. Mech.* Vol.99 (2013) 202-212.
- [12] C. She, J. Zhao, W. Guo, Three-dimensional stress fields near notches and cracks, *Int. J. Fract.* Vol.151(2) (2008) 151-160.
- [13] J.C. Newman, I.S. Raju, An empirical stress-intensity factor equation for the surface crack, *Eng. Fract. Mech.* Vol.15(1) (1981) 185-192.
- [14] H. Hosseini-Toudeshky, B. Mohammadi, G. Sadeghi, H.R. Daghyani, Numerical and experimental fatigue crack growth analysis in mode-I for repaired aluminum panels using composite material, *Compos. P. A* Vol.38(4) (2007) 1141-1148.

Chapter 6

Development of Simplified Methods to Describe the Front Shape

Evaluation of Surface-breaking Fatigue Cracks

Statement of Authorship

Title of Paper	A new method for analysis of part-elliptical surface cracks in structures subjected to fatigue loading		
Publication Status	<input checked="" type="checkbox"/>	Published	<input type="checkbox"/> Accepted for Publication
	<input type="checkbox"/>	Submitted for Publication	<input type="checkbox"/> Unpublished and Unsubmitted work written in manuscript style
Publication Details	Zakavi, B., Kotousov, A., Khanna, A., & Branco, R. (2019). A new method for analysis of part-elliptical surface cracks in structures subjected to fatigue loading. Theoretical and Applied Fracture Mechanics, 103, 102258-. https://doi.org/10.1016/j.tafmec.2019.102258		

Principal Author

Name of Principal Author	Behnam Zakavi		
Contribution to the Paper	Performed analysis, interpreted data, literature review, and wrote manuscript		
Overall percentage (%)	50		
Certification:	This paper reports on original research I conducted during the period of my Higher Degree by Research candidature and is not subject to any obligations or contractual agreements with a third party that would constrain its inclusion in this thesis. I am the primary author of this paper.		
Signature		Date	22 / 08 / 2021

Co-Author Contributions

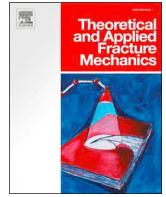
By signing the Statement of Authorship, each author certifies that:

- i. the candidate's stated contribution to the publication is accurate (as detailed above);
- ii. permission is granted for the candidate to include the publication in the thesis; and
- iii. the sum of all co-author contributions is equal to 100% less the candidate's stated contribution.

Name of Co-Author	Prof. Andrei Kotousov		
Contribution to the Paper	Supervised the development of theoretical models and co-wrote manuscript		
Signature		Date	24 / 08 / 2021

Name of Co-Author	Dr. Aditya Khanna		
Contribution to the Paper	Participated in manuscript review and evaluation		
Signature		Date	24 / 08 / 2021

Name of Co-Author	Prof. Ricardo Branco		
Contribution to the Paper	Participated in manuscript review and evaluation		
Signature		Date	23 / 08 / 2021



A new method for analysis of part-elliptical surface cracks in structures subjected to fatigue loading

Behnam Zakavi^{a,*}, Andrei Kotousov^a, Aditya Khanna^a, Ricardo Branco^b

^a School of Mechanical Engineering, The University of Adelaide, SA 5005, Australia

^b CEMMPRE, Department of Mechanical Engineering, University of Coimbra, Rua Luís Reis Santos, 3030-788 Coimbra, Portugal

ARTICLE INFO

Keywords:

Part-elliptical crack
Surface crack
Stress intensity factor
Crack closure
Crack advance scheme
Fatigue

ABSTRACT

This paper presents a new analytical method for the analysis of fatigue growth of surface cracks in various structural components. The method is based on a governing equation describing the front evolution of surface cracks of elliptical and part-elliptical shapes. This method avoids the need for various numerical schemes for the calculation of the incremental crack front advance, which were used in all previous studies. Plasticity-induced crack closure models can also be incorporated into the method or these models can be deduced from a correlation of experimental data and the method predictions. When the plastic constraint conditions change significantly along the crack front, the implementation of the plasticity induced crack closure models can significantly improve the accuracy of fatigue life predictions. The method is validated against previous theoretical and experimental studies.

1. Introduction

A great deal of attention over the past several decades was devoted to the analysis of surface crack growth in structural components subjected to cyclic loading. This attention is not surprising because fatigue failure in low and high cycle fatigue regimes is often initiated from a surface flaw induced by fabrication or developed during cyclic loading from a virtually free from defects surface [1]. For metals and metallic alloys there are several crack formation mechanisms, which may compete, and thereby often causing a significant scatter in fatigue life. These mechanisms have been comprehensively discussed in several recent review papers. It is generally agreed that in the absence of surface defects, the crack formation stage is largely associated with the accumulation of fatigue damage in the form of irreversible micro-plastic deformations within slip bands which normally form intrusions/extrusions at the surface grains or impinge on grain boundaries for non-surface grains [2].

One of the most important issues related to the analysis of surface cracks propagating under fatigue loading is the evolution of the crack front shape [3–5]. Past experimental studies have demonstrated that for many structures subjected to cyclic loading surface, cracks normally maintain a so-called “almond” shape up to the final stage of propagation (fracture) [4,5]. It was also found that the front of the “almond” shaped fatigue cracks can be quite accurately approximated by an

elliptical curve [5–7]. This finding greatly simplifies the crack growth modelling by reducing the number of variables describing the crack front. This simplification also allows for advanced design optimization, parametric and sensitivity studies of various structures with surface defects [8].

The aspect ratio of the part-elliptical geometry does not necessarily remain constant, and this ratio normally varies during fatigue crack propagation [4–7]. The evaluation of the crack shape changes is necessary for fatigue life calculations, and the theoretical prediction of these changes is a main focus of the current paper. It was also well documented in several experimental studies that the geometry of fatigue crack front can be affected by load cycles creating a large plastic zone or overloads, so the rate of crack propagation near the free surface is significantly smaller than for the rest of the crack front (or even ceases for some time in the case of the overload) [9]. These phenomena can lead to significant deviations from the elliptical shape, see Fig. 2b ahead, and these are beyond of the scope of the present work.

The quantitative analyses of the crack front shape evolution and fatigue crack growth of surface cracks require a relationship between of the stress intensity factor (SIF) along the crack front and the problem geometry and loading conditions [3–9]. The SIF solutions for 3D geometries are most commonly obtained by using the finite element (FE) method. However other general methods e.g. boundary integral equation and weight function, or experimental approaches including photo-

* Corresponding author.

E-mail address: behnam.zakavi@adelaide.edu.au (B. Zakavi).

<https://doi.org/10.1016/j.tafmec.2019.102258>

Received 21 November 2018; Received in revised form 28 May 2019; Accepted 28 May 2019

Available online 04 June 2019

0167-8442/ © 2019 Elsevier Ltd. All rights reserved.

Nomenclature			
A	deepest point of part-elliptical crack	K_{op}	opening stress intensity factor
a	length of semi-minor axis	ΔK_{eff}	effective stress intensity factor range
b	length of semi-major axis	m	Paris law exponent
C	Paris law constant	N	number of cycles
c	half focal distance	$ P_0 P_1 $	segment length
D	outer diameter	R	stress ratio
d	inner diameter	S	surface point
da	increment of semi-minor axis, a	t	plate thickness
db	increment of semi-major axis, b	U	normalised load ratio
ds	distance between two elliptical curves at some point	V	crack growth rate
E	Young's modulus	$\bar{V}(\eta)$	relative crack growth speed at point η
F	crack growth rate (per one cycle)	(x, y)	rectangular coordinates
F_I	geometry correction factor (stress intensity magnification factor)	(ξ, η)	elliptical coordinates
K_{max}	maximum stress intensity factor	(ξ_0, η_0)	initial shape of fatigue crack front in elliptical coordinates
K_{min}	maximum stress intensity factor	β	ratio of a to b
		δ	ratio of a to D for circular bars or a to t for plates
		η_S	elliptical coordinate of the surface (corner) point
		ν	Poisson's ratio

elasticity, compliance measurements and fatigue tests have also been utilised for deriving or validation of SIF solutions [10].

The early SIF solutions often demonstrated significant discrepancies between different computational studies [11,12]. This could be attributed to the insufficient computer power available for the analysis of 3D crack problems in the early modelling attempts [10]. With the advances in computer power and development of new numerical approaches, the scatter in various computational solutions has been decreased to just few percent [9,13,14]. However, the large discrepancies (of order 10–50 percent or even more) can be still found for crack front regions near the free surface, or in a so-called “boundary layer” [15]. This is because the square root stress singularity, which exists for the interior points, is replaced by the 3D corner singularity at the corner point where the crack front intersects the free surface. The influence of the 3D corner singular stress state causes many difficulties in extracting SIF near the corner points, specifically when the corner singularity is stronger than the inverse square root singularity for the rest of the crack front [16–18]. Previous researchers have adopted a pragmatic approach to deal with the effects of the 3D singular stress state at corner points on the SIF calculations. This approach is to exclude the boundary layer from calculations and extrapolate SIF results obtained for the interior regions over the crack front segments located in the boundary layer [9,13,14].

Another important issue related to fatigue life analysis is related to crack closure mechanisms (i.e. roughness, oxide and plasticity-induced crack closure) [19,20]. It was found that the effect of the oxide- and roughness-induced crack closure on the fatigue crack propagation may be significant near threshold fatigue regime, and normally insignificant in the mid-Paris fatigue regime. An appropriate theoretical description of oxide- and roughness-induced closure would require information on the growth of oxide layer or asperities, friction and surface properties, etc. However, most of these details required for the prediction are unknown. Therefore, the existing oxide- or roughness-induced crack closure models are largely empirical or oversimplified and are all based on many radical assumptions.

The roughness induced crack closure can be significant for the life evaluation for which the initial defects of order few micrometers. In particular, it is often argued that the roughness-induced crack closure mechanisms contributes to various small crack propagation phenomena: (i) an increased crack growth rate in comparison with long cracks at the same ΔK ; (ii) crack propagation below stress intensity factor threshold, which was established for long cracks; (iii) transition behavior from physically-small crack to long-crack propagation regime, which can be associated with a decrease of the crack growth rate; (iv) significant effect of the material microstructure on the crack growth rates. There are currently no predictive models for the oxide- and

roughness-induced crack closures as a function of ΔK , the stress ratio, R , the surface roughness or environment parameters) [20].

In contrast to the oxide and roughness-induced closure mechanisms, plasticity-induced crack closure doesn't (many) questionable assumptions and can be modelled using different approaches [21–32]. The factors affecting the plasticity-induced crack closure, and consequently the rate of crack propagation, include the elastic and plastic material properties, history of loading, crack and structure geometry. This closure mechanism is more profound for the mid-Paris fatigue regime, however, it can also effect on the propagation of physically small cracks due to (i) the change of constraint conditions; and (ii) different characteristics of the plasticity wake for short and large cracks at the same ΔK history. However, it is arguable that the plasticity-induced crack closure alone can explain the small crack propagation behavior.

Two-dimensional (2D) modelling of the plasticity-induced crack closure with the direct finite element simulations [28,29] and semi-analytical methods [20–22,32] has progressed significantly over the last twenty years. These simulations can replicate many experimentally observed metal fatigue effects such as mean stress effect, crack growth retardation due to overloads, etc. However, 3D crack closure analysis still represents a formidable task even for modern numerical approaches. Several 3D results from the direct numerical simulations of plastic deformations and crack closure have been recently reported for plane geometries, however, the convergence and accuracy of the numerical computations have not been independently verified or reproduced elsewhere [24–27]. A summary of state of the art of 3D fatigue crack simulations accounting for plasticity-induced crack closure is provided in [30,31].

The difficulties associated with 3D elasto-plastic FE analysis of fatigue cracks have motivated the development of simplified analytical methods, including the method presented in the current work, for the analyses of the crack shape evolution and fatigue life. The method presented herein is based on the commonly accepted assumption regarding the surface front crack geometry, which was introduced above, i.e. the fatigue crack front maintains a part-elliptical shape during its growth. It also utilises solutions for SIFs, which have been previously obtained and validated for a wide range of geometries, loading and boundary conditions. The developed analytical method has several advantages against the previous approaches, e.g. it does not require a discretisation of the fatigue crack path or the application of crack advance schemes, which make the results easily reproducible. In addition, it allows the analysis of the crack front shape evolution based on two arbitrary points along the crack front, thereby avoiding the potential errors associated with corner points and boundary layer.

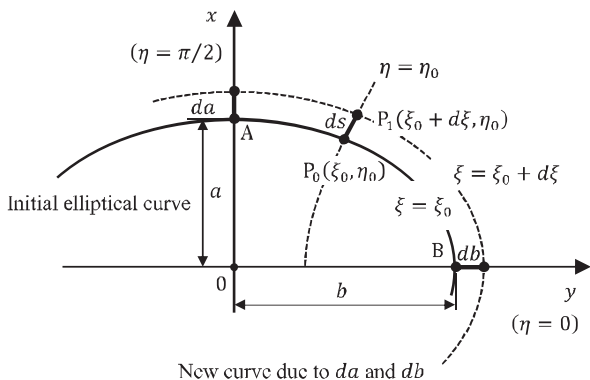


Fig. 1. Elliptical coordinates and crack front change.

2. Derivation of the governing equation

The goal of the derivations briefly described in this section is to link a small change of an elliptical shape, which is represented by incremental changes of the semi-axes, da and db, to the normal displacement, ds, at an arbitrary location, η, along the elliptical curve, see Fig. 1. This dependence will be used to obtain an inverse relationship between the increments at different points on the crack front and the incremental variation of the aspect ratio (a/b) of the elliptical curve representing the front of a surface fatigue crack [4–8,10]. Finally, these derivations will result into an ordinary differential equation governing the crack front shape evolution.

2.1. Governing equation

It is natural to introduce orthogonal elliptical coordinates (ξ, η), for the present problem, and these coordinates are related to the rectangular coordinates by the well-known equations:

$$x = c \sinh \xi \sin \eta \tag{1a}$$

$$y = c \cosh \xi \cos \eta \tag{1b}$$

In particular, the half-lengths of the semi-axes (a and b) of the initial elliptical curve is found by setting, ξ = ξ₀ and η = π/2 and 0, respectively, leading to

$$a = c \sinh \xi_0 \tag{2a}$$

$$b = c \cosh \xi_0 \tag{2b}$$

where the half-focal length is

$$c = \sqrt{b^2 - a^2}, \tag{3a}$$

and

$$\xi_0 = \operatorname{atanh} \left(\frac{a}{b} \right). \tag{3b}$$

Here and below, it is assumed that b ≥ a or β = a/b ≤ 1, in the opposite case the coordinates x and y can be swapped and renamed.

Any point P on the initial elliptical curve can be identified in terms of its rectangular coordinates (x, y) or elliptical coordinates (ξ, η), where -π < η < π. Consider now the change of the elliptical shape due to small increments of dc and dξ₀ leaving the x and y coordinate axes unchanged, then, from Eqs. (2):

$$da = dc \sinh \xi_0 + d\xi_0 c \cosh \xi_0 \tag{4a}$$

$$db = dc \cosh \xi_0 + d\xi_0 c \sinh \xi_0 \tag{4b}$$

The equation describing the new elliptical curve can be written using the same Eqs. (1a) and (1b) by replacing c and ξ₀ with c + dc and ξ₀ + dξ₀, respectively. From the last equations, the increments dc and dξ₀ can be written in terms of da and db as follows

$$dc = db \cosh \xi_0 - da \sinh \xi_0 \tag{5a}$$

$$d\xi_0 = \frac{da \cosh \xi_0 - db \sinh \xi_0}{c} \tag{5b}$$

Consider point P₀ with coordinates (ξ₀, η₀) on the initial elliptical curve, which represents the initial crack front shape. The distance between point P₀ and point P₁, which is located on the new elliptical curve, can be obtained from the intersection of the segment orthogonal to the original elliptic curve given by the parametric equation (ξ₀ + dξ, η₀) and the new elliptical curve due to increments of da and db. Using Eqs. (1), the rectangular coordinates of point P₁ (x_{P1} and y_{P1}) can be written in both elliptical coordinate systems associated with the initial and new elliptical curves as

$$x_{P1} = c \sinh(\xi_0 + d\xi) \sin \eta_0 = (c + dc) \sinh(\xi_0 + d\xi) \sin(\eta_0 + d\eta) \tag{6a}$$

$$y_{P1} = c \cosh(\xi_0 + d\xi) \cos \eta_0 = (c + dc) \cosh(\xi_0 + d\xi) \cos(\eta_0 + d\eta) \tag{6b}$$

Using Taylor expansion of hyperbolic and trigonometric functions and excluding variable dη, the increment dξ can be obtained as

$$d\xi = \frac{1}{c} \frac{\cosh \xi_0 \sin^2 \eta_0 da + \sinh \xi_0 \cos^2 \eta_0 db}{\cosh^2 \xi_0 \sin^2 \eta_0 + \sinh^2 \xi_0 \cos^2 \eta_0}. \tag{7}$$

From Eq. (1), the length of the segment |P₀P₁|, ds, see Fig. 1, is:

$$ds = c \sqrt{\cosh^2 \xi_0 \sin^2 \eta_0 + \sinh^2 \xi_0 \cos^2 \eta_0} d\xi. \tag{8}$$

Substituting dξ from Eqs. (7) into (8) yields

$$ds = \frac{\cosh \xi_0 \sin^2 \eta_0 da + \sinh \xi_0 \cos^2 \eta_0 db}{\sqrt{\cosh^2 \xi_0 \sin^2 \eta_0 + \sinh^2 \xi_0 \cos^2 \eta_0}}. \tag{9}$$

By introducing the aspect ratio of the ellipse β = a/b into Eq. (9), and after some algebraic manipulations, Eq. (9) can be represented in the following form:

$$ds = \frac{\tan^2 \eta_0 + \left(\frac{1}{\beta} - \frac{a}{\beta^2} \frac{d\beta}{da} \right) \tanh \xi_0}{\sqrt{\tan^2 \eta_0 + \tanh^2 \xi_0}} \cos \eta_0 da. \tag{10}$$

Therefore, the ratio of the normal distances between the initial and new curves at the deepest (η = π/2) and arbitrary (η = η₀) points is simply

$$\frac{ds}{da} = \frac{\tan^2 \eta_0 + \left(\frac{1}{\beta} - \frac{a}{\beta^2} \frac{d\beta}{da} \right) \tanh \xi_0}{\sqrt{\tan^2 \eta_0 + \tanh^2 \xi_0}} \cos \eta_0. \tag{11}$$

Taking into account Eq. (3b) or that tanh ξ₀ = β = a/b, finally, Eq. (11) can be re-written in a simple form as:

$$\frac{ds}{da} = \frac{\tan^2 \eta + \left(1 - \frac{a}{\beta} \frac{d\beta}{da} \right) \cos \eta}{\sqrt{\tan^2 \eta + \beta^2}}. \tag{12}$$

in which we omitted the lower index for variable η, so this equation applies for an arbitrary point on the elliptical curve. This relationship can be considered as an ordinary differential equation with respect to ds/da, which represents the relative speed of propagation of two points on the crack front, or dβ/da, in this case this differential equation describes the evolution of a part-elliptical shape.

To validate the derived equation, consider a limiting case of self-similar elliptical shape evolution, or when a/b = β is constant or dβ/da = 0. In this case Eq. (12) can be rewritten as

$$\frac{ds}{da} = \frac{\tan^2 \eta + 1}{\sqrt{\tan^2 \eta + \beta^2}} \cos \eta. \tag{13}$$

Through a simple analysis of Eq. (13), it can be demonstrated that, as expected, along x-direction (or η = π/2): ds/da = da/da = 1; and along y-direction (or η = 0): ds/da = db/da = β⁻¹. Other simple cases of shape evolutions, e.g. when the length of one of the semi-axes, a or b,

does not change can be considered in a similar manner. In the next section, the derived equations are applied to analyse the shape evolution of fatigue cracks.

2.2. Shape evolution of fatigue cracks

The analysis of the fatigue crack growth is normally based on various Paris-type equations, which can be written in the following general form [1,5]:

$$\frac{ds}{dN} = V = F(\Delta K, R) \quad (14)$$

where V or $F(\Delta K, R)$ is the crack growth rate or speed of the crack propagation due to a single cycle. The function F may incorporate several constants, which are usually obtained from fatigue tests. The relative speed at arbitrary point η , normalised by the speed, for example, at the deepest point of the crack front $\eta = \pi/2$ (point A, see Fig. 1), is given by:

$$\bar{V}(\eta) = \frac{F(\Delta K(\eta), R)}{F(\Delta K(A), R)} = \frac{\tan^2 \eta + \left(1 - \frac{a}{\beta} \frac{\partial \beta}{\partial a}\right)}{\sqrt{\tan^2 \eta + \beta^2}} \cos \eta \quad (15)$$

After a rearrangement, Eq. (15) can be written as an ordinary differential equation describing the shape evaluation equation of the front of a crack maintaining its semi-elliptical shape during fatigue growth:

$$\frac{\partial \beta}{\partial a} = \frac{\beta}{a} \left(1 + \tan^2 \eta - \frac{F(\Delta K(\eta), R) \sqrt{\tan^2 \eta + \beta^2}}{F(\Delta K(A), R) \cos \eta}\right) \quad (16)$$

In order to apply this governing equation, an appropriate SIF solution for two arbitrary points along the crack front is required. Most of the SIF solutions in the past have been typically obtained for the deepest and surface points i.e. where the crack front intersects the free surface. However, as mentioned in the Introduction, the evaluation of SIF near the free surface needs some care, and in some cases the SIF values near the free surface might be inaccurate. In the following section we will apply the governing equation, Eq. (16), to a number of geometries and derive the shape evolution equations specifically for these geometries.

2.3. Physical restrictions on the crack shape evolution

As the fatigue crack growth is an irreversible process, meaning that $ds \geq 0$ and $ds/da \geq 0$ from Eq. (12), it follows that

$$\tan^2 \eta + \left(1 - \frac{a}{\beta} \frac{d\beta}{da}\right) \geq 0 \quad (17)$$

After simplifications, the irreversibility of fatigue crack growth leads to the following equation:

$$\frac{d\beta}{da} \leq \frac{1}{b \cos^2 \eta} \quad (18)$$

For all points on the crack front $\eta \in (\eta_S - \pi/2)$, where $\eta = \pi/2$ corresponds to the deepest point on the crack front (point A) and $\eta = \eta_S$ corresponds to the surface point (point S). It is clear that if Eq. (18) is satisfied at the surface point (or $\eta = \eta_S$), then it will automatically be also satisfied for the rest of the crack front.

Experimental data may violate Eq. (18) as the approximation of the actual crack front shape by an elliptical curve inevitably leads to errors associated with the adopted fitting approach, which may be based e.g. on different points along the crack front, best fit or on the equivalent fractured area. Fig. 2 demonstrates the approximation of the actual crack fronts with semi-elliptical and part-elliptical curves. Fig. 2b also shows the significant deviations from the elliptical shape as a result of large plasticity-induced crack closure near the surface.

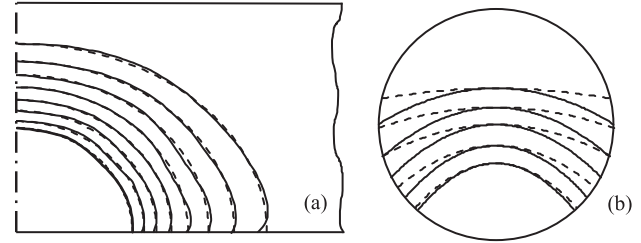


Fig. 2. Beach marks (solid lines) and semi- or part-elliptical fitting curves (dotted lines) for surface crack propagation in a plate and solid circular bar [33]. Deviation from the elliptical shape in b) is associated with the development of a large plastic zone and crack closure effects near the free surface [9].

3. Application of the governing equation to various structural components

3.1. Semi-elliptical and quarter-elliptical surface cracks

In the cases of semi-elliptical or quarter elliptical cracks propagating in wide plate components or in a long thick-walled cylinder, see Fig. 3, the independent variables in the governing equation can be normalised by the plate/wall thickness t , as

$$\frac{\partial \beta}{\partial \delta} = \frac{\beta}{\delta} \left(1 + \tan^2 \eta - \frac{F(\Delta K(\eta), R) \sqrt{\tan^2 \eta + \beta^2}}{F(\Delta K(A), R) \cos \eta}\right) \quad (19)$$

where $\delta = a/t$. For the shape evolution and fatigue crack growth analysis, this equation has to be supplemented by the initial conditions, i.e. the initial crack front shape $\delta = \delta_0$ and $\beta = \beta_0$ has to be specified. The direct integration of Eq. (19) is difficult and the integral has to be evaluated numerically.

The governing equation can also be rewritten in a finite difference form as

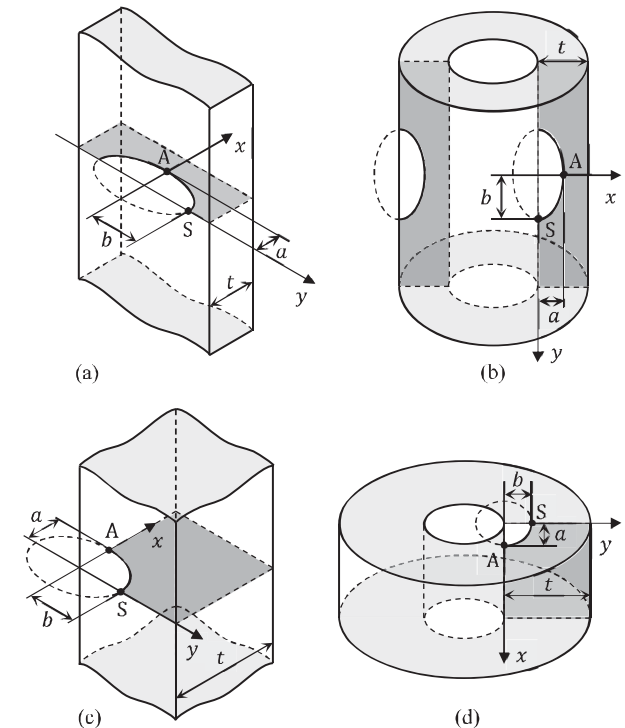


Fig. 3. Semi-elliptical crack in (a) flat plate, and (b) thick-walled cylinder, quarter-elliptical crack in (c) square bar, and (d) plate with hole.

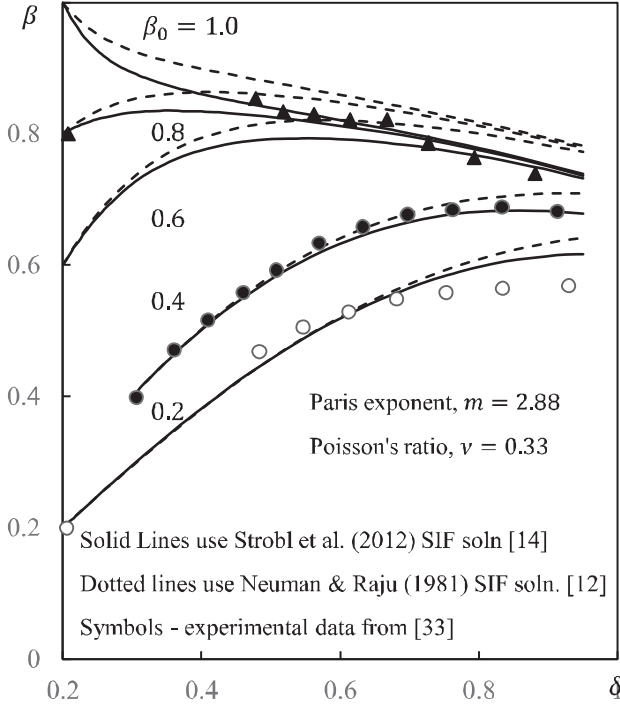


Fig 4. Comparison of analytical predictions based on different SIF solutions [12,14] with experimental results [33].

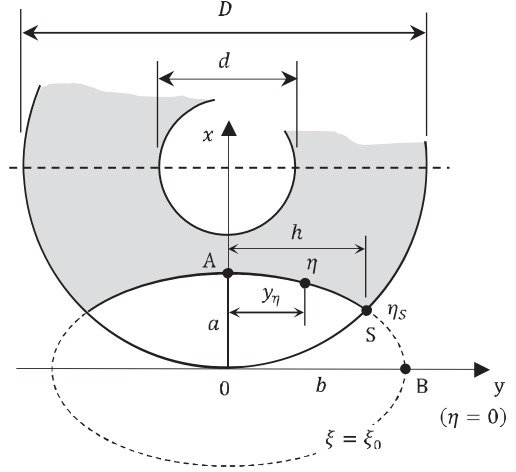


Fig. 5. Propagation of part elliptical crack in round bar.

Fig. 4 shows the theoretical predictions of fatigue crack shape evolution for semi-elliptical cracks in plates, see Fig. 2a (solid lines). The present results utilise SIF solutions of Neuman and Raju [12] and a recent extensive FE study of the corresponding crack geometries published by Strobl et al. [14]. It is seen that overall the latest SIF solution [14] provides a better correlation with experimental results of Putra and Schijve [33].

3.2. Part-elliptical surface crack in round solid and tubular bars

Similar to the previous cases, the analysis of fatigue crack growth of a part elliptical crack in round bars is also based on two characteristic points: the deepest point, A, with the coordinate $\eta = \pi/2$ and surface point, S identified by $\eta = \eta_s$. In contrast to the previous cases, the coordinate of point S, see Fig. 6, changes with the crack propagation. Our objective is to identify this point as a function of the crack and bar geometries. It is convenient to introduce a new dimensionless variable $\delta = a/D$, then the elliptical coordinates of the surface point (S_η) can be found as an intersection of the circle describing the bar shape and the elliptical curve describing the crack, which both can be written in the elliptical coordinates, or

$$\sinh^2 \xi \sin^2 \eta_s + \cosh^2 \xi \cos^2 \eta_s = \frac{\beta}{\delta \sqrt{1 - \beta^2}} \sinh \xi \sin \eta_s \quad (24)$$

from which the following relationship for two surface points, which are symmetric with respect to the x-axis, see Fig. 6, can be found:

$$\cos \eta_s = \pm \sqrt{1 - \left(\frac{\beta^2 - \sqrt{\beta^4 - 4\delta^2(\beta^2 - 1)}}{2\delta(\beta^2 - 1)} \right)^2} \quad (25)$$

The governing shape evolution equation can also be rewritten in dimensionless form similar to Eq. (19), in which $\delta = a/D$. The same finite difference scheme, Eq. (20) can be utilised for this case as well.

Similar to the considered case of semi-elliptical cracks, for fatigue life and shape evolution calculations, Eqs. (22) and (23) have to be supplemented with the initial conditions, i.e. $\delta = \delta_0$ and $\beta = \beta_0$ and a suitable SIF solution reflecting the actual loading conditions, e.g. pure tension, bending or mixed loading.

In general, two arbitrary points on the crack front can be utilised for the analysis of the crack front shape evolution if an appropriate SIF is available. One of such solutions represents SIF as a function of β , δ and κ , see Fig. 5. In the case of round bars, the SIF solutions can be

$$\beta_{n+1} = \frac{\beta_n}{\delta_n} \left(1 + \tan^2 \eta - \frac{F(\Delta K(\eta, \beta_n, \delta_n), R) \sqrt{\tan^2 \eta + \beta_n^2}}{F(\Delta K(A, \beta_n, \delta_n), R) \cos \eta} \right) \Delta \delta$$

$$\delta_{n+1} = \delta_n + \Delta \delta \quad (20)$$

so, the solution can be easily obtained from the recurrent relationships (20) and the step $\Delta \delta$ can be selected to achieve the desired accuracy of calculations. These relationships can be programmed accordingly using various computer-based programs.

In the case of quarter- and semi-elliptical cracks, the physical restriction on the shape evolution, Eq. (18) at $\eta = 0$ (surface point) leads to the following conditions:

$$\frac{d\beta}{da} \leq \frac{1}{b} \quad \text{or} \quad \frac{d\beta}{d\delta} \leq \frac{\beta}{\delta} \quad (21)$$

which have a simple meaning that the slope of $\beta(\delta)$ curve must be always less than the slope of the line passing through the origin (0, 0) and the point with coordinates (δ, β) . As mentioned above, the experimental data may not comply with Eq. (21) due to inevitable errors associated with the approximation of the actual crack front with elliptical shapes.

If the analysis of fatigue crack growth is based on two characteristic points: the deepest point A, and the surface point, then, the crack front shape evolution equation can be simplified as:

$$\frac{\partial \beta}{\partial \delta} = \frac{\beta}{\delta} \left(1 - \beta \frac{F(\Delta K(S), R)}{F(\Delta K(A), R)} \right) \quad (22)$$

It can be shown that in this case the last equation, Eq. (22) can be reduced to the following well-known relationships:

$$db = F(\Delta K(S), R) \times dn \quad \text{and} \quad da = F(\Delta K(A), R) \times dn \quad (23)$$

which are often applied to simulate the semi-elliptical fatigue crack growth (dn is an increment of fatigue cycles).

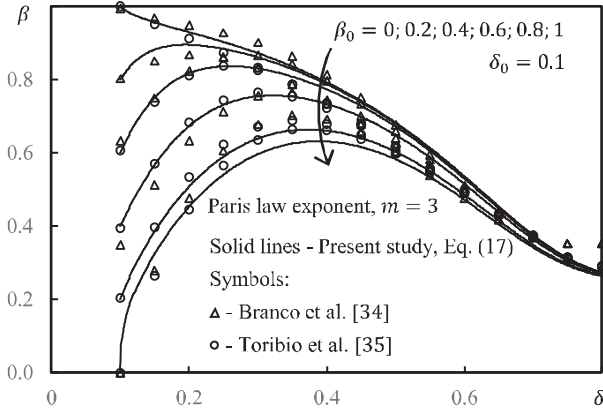


Fig. 6. Comparison between prediction of the present method and previous published data.

represented in the following form:

$$K_I = F_I(\beta, \delta, \kappa) \sigma \sqrt{\pi a} \quad (26)$$

where σ is a characteristic or nominal stress, a is the crack depth, and

$$\kappa = \frac{y_s/h}{\cos \eta_s} = \frac{\cos \eta}{\cos \eta_s} \quad (27)$$

where η_s is given by Eq. (25).

A comparison of the previous numerical studies and the current analytical results utilising Eqs. (19), (25) and (26) and the classical (Paris) crack growth law:

$$\frac{da}{dN} = C(\Delta K)^m \quad (28)$$

is given in Fig. 6 together with the previous studies [34,35], which utilised different crack advance schemes. A very good correlation can be observed between all studies.

4. Conclusion

In this work, a new method was developed for the evaluation of fatigue growth of surface flaws in various structural components. The analytical method avoids computational schemes to analyse the crack advance. It can be also easily modified to incorporate the plasticity-induced crack closure effects. The method was validated against the previous numerical results and experimental data. The comparison demonstrates an excellent agreement with the numerical simulations and reasonable agreement with experimental data. This agreement can be improved by introducing crack closure models, which might incorporate the geometry, material properties and loading conditions. For example, the plasticity-induced crack closure concept can be relatively easy incorporated into the developed method. In accordance with this concept, the stress intensity factor range, ΔK , is replaced by the effective stress intensity, ΔK_{eff} , to reflect the damage accumulation when crack tip is closed. The effective stress intensity factor range ΔK_{eff} is defined as [20]:

$$\Delta K_{\text{eff}} = U \Delta K = U(K_{\text{max}} - K_{\text{min}}) = K_{\text{max}} - K_{\text{op}} \quad (29)$$

where K_{max} and K_{min} are the maximum and minimum values of SIF during fatigue cycle, respectively, and U is the normalised load ratio parameter, which is often used to describe the effects of the loading and geometry on crack closure. With account of the crack closure phenomena, the governing shape evolution equation, Eq. (16) can be

rewritten as

$$\frac{\partial \beta}{\partial a} = \frac{\beta}{a} \left(1 + \tan^2 \eta - \left(\frac{U_r \Delta K_r}{U_A \Delta K_A} \right)^m \frac{\sqrt{\tan^2 \eta + \beta^2}}{\cos \eta} \right) \quad (30)$$

This equation can be utilised not to just incorporate the plasticity induced closure models into fatigue life calculations but also used to develop empirical models of the crack closure based on experimental results, or $\beta(\delta)$ dependences. By rearranging Eq. (30) the experimental ratio of U_r/U_A can be obtained, which then can be utilised for fatigue crack shape and life evaluations.

References

- [1] U. Zerbst, M. Madia, C. Klinger, D. Bettge, Y. Murakami, Defects as a root cause of fatigue failure of metallic components. Parts I-III, Eng. Fail. Anal. 97 (2019).
- [2] H. Mughrabi, Microstructural fatigue mechanisms: cyclic slip irreversibility, crack initiation, non-linear elastic damage analysis, Int. J. Fatigue 57 (2013) 2–8.
- [3] X.B. Lin, R.A. Smith, Shape growth simulation of surface cracks in tension fatigued round bars, Int. J. Fatigue 129 (1997) 239–264.
- [4] A. Carpinteri, S. Vantadori, Surface cracks in round bars under cyclic tension or bending, Key Eng. Mater. 378–379 (2008) 341–354.
- [5] R. Brighenti, A. Carpinteri, Surface cracks in fatigued structural components: a review, Fatigue Fract. Eng. Mater. Struct. 36 (4) (2013) 1209–1222.
- [6] J. Toribio, J.C. Matos, B. González, J. Escudra, Numerical modelling of crack shape evolution for surface flaws in round bars under tensile loading, Eng. Fail. Anal. 16 (2009) 618–630.
- [7] A. Carpinteri, Shape change of surface cracks in round bars under cyclic axial loading, Int. J. Fatigue 15 (1993) 21–26.
- [8] N. Couroneau, J. Royer, Simplified model for the fatigue growth analysis of surface cracks in round bars under mode I, Int. J. Fatigue 20 (1998) 711–718.
- [9] J. Lebahn, H. Heyer, M. Sander, Numerical stress intensity factor calculation in flawed round bars validated by crack propagation tests, Eng. Fract. Mech. 108 (2013) 37–49.
- [10] A. Kotousov, B. Zakavi, A. Khanna, R. Branco, On the analysis of structures with cracks of elliptical and part-elliptical shapes, Theor. Appl. Fract. Mech. 98 (2018) 149–156.
- [11] L.A. James, W.J. Mills, Review and synthesis of stress intensity factor solutions applicable to cracks in bolts, Eng. Fract. Mech. 30 (1988) 641–654.
- [12] J.C. Newman, I.S. Raju, An empirical stress-intensity factor equation for the surface crack, Eng. Fract. Mech. 151 (1981) 185–192.
- [13] C.S. Shin, C.Q. Cai, Experimental and finite element analyses on stress intensity factors of an elliptical surface crack in a circular shaft under tension and bending, Int. J. Fract. 129 (2004) 239–264.
- [14] S. Strobl, P. Supancic, T. Lubea, R. Danzer, Surface crack in tension or in bending – a reassessment of the Newman and Raju formula in respect to fracture toughness measurements in brittle materials, J. Eur. Ceram. Soc. 32 (2012) 1491–1501.
- [15] M. Sevcik, P. Hutar, M. Zouhar, L. Nahlik, Numerical estimation of the fatigue crack front shape for a specimen with finite thickness, Int. J. Fatigue 39 (2012) 75–80.
- [16] L.P. Pook, A 50-year retrospective review of three-dimensional effects at crack sand sharp notches, Fatigue Fract. Eng. Mater. Struct. 36 (2013) 699–723.
- [17] A. Kotousov, P. Lazzarin, F. Berto, L.P. Pook, Three-dimensional stress states at crack tip induced by shear and anti-plane loading, Eng. Fract. Mech. 108 (2013) 65–74.
- [18] A. Kotousov, Effect of plate thickness on stress state at sharp notches and the strength paradox of thick plates, Int. J. Solids Struct. 47 (14–15) (2010) 1916–1923.
- [19] W. Elber, Fatigue crack closure under cyclic tension, Eng. Fract. Mech. 2 (1970) 37–45.
- [20] R. Pippin, A. Hohenwarter, Fatigue crack closure: a review of the physical phenomena, Fatigue Fract. Eng. Mater. Struct. 40 (2017) 471–495.
- [21] F.V. Antunes, M.S.C. Ferreira, R. Branco, P. Prates, C. Gardin, C. Sarrazin-Baudoux, Fatigue crack growth versus plastic CTOD in the 304L stainless steel, Eng. Fract. Mech. 214 (2019) 487–503.
- [22] J.A.F.O. Correia, A.M.P. De Jesus, P.M.G.P. Moreira, P.J.S. Tavares, Crack closure effects on fatigue crack propagation rates: application of a proposed theoretical model, Adv. Mater. Sci. Eng. (2016) art. no. 3026745.
- [23] J.A.F.O. Correia, S. Blasón, A. Arcari, M. Calvente, N. Apetre, P.M.G.P. Moreira, A.M.P. De Jesus, A.F. Canteli, Modified CCS fatigue crack growth model for the AA2019-T851 based on plasticity-induced crack-closure, Theor. Appl. Fract. Mech., Part A 85 (2016) 26–36.
- [24] P. Lopez-Crespo, D. Camas, F.V. Antunes, J.R. Yates, A study of the evolution of crack tip plasticity along a crack front, Theor. Appl. Fract. Mech. 98 (2018) 59–66.
- [25] R. Branco, F.V. Antunes, L.C.H. Ricardo, J.D. Costa, Extent of surface regions near corner points of notched cracked bodies subjected to mode-I loading, Finite Elem. Anal. Des. 50 (2012) 147–160.
- [26] F.V. Antunes, D.M. Rodrigues, Numerical simulation of plasticity induced crack closure: identification and discussion of parameters, Eng. Fract. Mech. 75 (2008) 3101–3120.
- [27] C.Y. Hou, Simultaneous simulation of closure behavior and shape development of

- fatigue surface cracks, *Int. J. Fatigue* 30 (2008) 1036–1046.
- [28] J. Codrington, A. Kotousov, Crack growth retardation following the application of an overload cycle using a strip-yield model, *Eng. Fract. Mech.* 76 (2009) 1667–1682.
- [29] J. Codrington, A. Kotousov, A crack closure model of fatigue crack growth in plates of finite thickness under small-scale yielding conditions, *Mech. Mater.* 41 (2009) 165–173.
- [30] R. Branco, F.V. Antunes, J.D. Costa, A review on 3D-FE adaptive remeshing techniques for crack growth modelling, *Eng. Fract. Mech.* 141 (2015) 170–195.
- [31] D. Camas, J. García-Manrique, B. Moreno, A. Gonzalez-Herrera, Numerical modelling of three-dimensional fatigue crack closure: mesh refinement, *Int. J. Fatigue* 113 (2018) 193–203.
- [32] P. Yu, W. Guo, An equivalent thickness conception for prediction of surface fatigue crack growth life and shape evolution, *Eng. Fract. Mech.* 93 (2012) 65–74.
- [33] I.S. Putra, J.S. Schijve, Crack opening stress measurements of surface cracks in 7075-T6 aluminum alloy plate specimen through electron fractography, *Eng. Fract. Mech.* 15 (4) (1992) 323–338.
- [34] R. Branco, F.V. Antunes, J.D. Costa, F.P. Yang, Z.B. Kuang, Determination of the Paris law constants in round bars from beach marks on fracture surfaces, *Eng. Fract. Mech.* 96 (2012) 96–106.
- [35] J. Toribio, J.C. Matos, B. González, J. Escudra, Numerical modelling of cracking path in round bars subjected to cyclic tension and bending, *Int. J. Fatigue* 58 (2014) 20–27.

Statement of Authorship

Title of Paper	On the analysis of structures with cracks of elliptical and part-elliptical shapes		
Publication Status	<input checked="" type="checkbox"/>	Published	<input type="checkbox"/> Accepted for Publication
	<input type="checkbox"/>	Submitted for Publication	<input type="checkbox"/> Unpublished and Unsubmitted work written in manuscript style
Publication Details	Kotousov, A., Zakavi, B., Khanna, A., & Branco, R. (2018). On the analysis of structures with cracks of elliptical and part-elliptical shapes. Theoretical and Applied Fracture Mechanics, 98, 149–156. https://doi.org/10.1016/j.tafmec.2018.09.013		

Principal Author

Name of Principal Author	Prof. Andrei Kotousov	
Contribution to the Paper	Performed analysis, interpreted data, literature review, and wrote manuscript	
Overall percentage (%)	50	
Certification:	This paper reports on original research I conducted during the period of my Higher Degree by Research candidature and is not subject to any obligations or contractual agreements with a third party that would constrain its inclusion in this thesis. I am the primary author of this paper.	
Signature	Date	23 / 08 / 2021

Co-Author Contributions

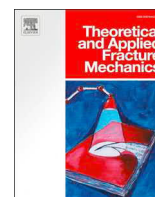
By signing the Statement of Authorship, each author certifies that:

- i. the candidate's stated contribution to the publication is accurate (as detailed above);
- ii. permission is granted for the candidate to include the publication in the thesis; and
- iii. the sum of all co-author contributions is equal to 100% less the candidate's stated contribution.

Name of Co-Author	Behnam Zakavi	
Contribution to the Paper	Performed analysis, participated in work discussions, and co-wrote manuscript	
Signature	Date	23 / 08 / 2021

Name of Co-Author	Dr. Aditya Khanna	
Contribution to the Paper	Provided writing assistance, and	
Signature	Date	24 / 08 / 2021

Name of Co-Author	Prof. Ricardo Branco	
Contribution to the Paper	Participated in manuscript review and evaluation, checked the derivation solutions	
Signature	Date	24 / 08 / 2021



On the analysis of structures with cracks of elliptical and part-elliptical shapes



Andrei Kotousov^{a,*}, Behnam Zakavi^a, Aditya Khanna^a, Ricardo Branco^b

^a School of Mechanical Engineering, The University of Adelaide, SA 5005, Australia

^b CEMMPRE, Department of Mechanical Engineering, University of Coimbra, Rua Luís Reis Santos, 3030-788 Coimbra, Portugal

ARTICLE INFO

Keywords:

Stress intensity factor
Elliptical crack
Part-elliptical crack
Round bar
Compliance

ABSTRACT

Stress intensity factors for cracks of elliptical or part-elliptical shapes in structural components, e.g. plates, bars and pressure vessels, are normally obtained using numerical methods. Due to the lack of exact benchmark solutions, the evaluation of the accuracy and quality of the numerical results and the corresponding fitting equations are largely based on the comparison against the outcomes of the previous numerical studies. In this work, a new relationship for the exact distribution of the stress intensity factor along the crack front is derived based on the divergence theorem for the compliance function. The application of the developed theoretical relationship is demonstrated towards the evaluation of the quality of previously obtained empirical equations for elliptical, semi-elliptical and part-elliptical cracks.

1. Introduction

Fatigue growth of surface or embedded cracks of elliptical or part-elliptical shapes in plates, bars, pipes and shells have received a great deal of attention over the past fifty years [1,2], due to at least two reasons: (1) these structural components have wide applications in many industries, and (2) surface cracks often maintain elliptical geometry during propagation. The latter is normally attested by post-mortem failure investigations as well as fatigue crack propagation tests [3].

Many investigators thought that a part-ellipse is a very good approximation to the surface crack profiles observed experimentally in many structures, e.g. bolts, wires, flanges of steel beams, turbine blades, stiffeners, pipes and shells. This important approximation, in particular, leads to a significant simplification of the fatigue crack growth analysis and residual life calculations as only two parameters describing this shape need to be identified [1].

It is well-known that the knowledge of the stress intensity factor (SIF) or K-solutions represents a basic requirement for fatigue crack growth calculations, which are prerequisites for efficient and safe operation of many structural components [1–23]. The SIF results can be obtained analytically, e.g. boundary integral equations, using either numerical methods, such as Finite Element (FE) [4] or meshless methods, weight function methods [5] or experimental techniques including photoelasticity, alternative current field measurement technique, compliance measurements and fatigue tests [6–9]. However, in

the case of elliptical or part-elliptical cracks, SIF (K-) solutions are commonly obtained by use of the FE method. Many such numerical solutions, represented in a form of fitting equations, tables and diagrams, are currently available in the literature for the deepest interior point or the both deepest interior and surface intersection points or for the whole crack front [3].

Some of the early SIF solutions have been summarised and compared by James and Mills [10]. This comparison demonstrated a significant difference between K-solutions developed for part-circular cracks in round bars as a result of a limited computer power and necessity to use a coarse mesh. With the continuous advance in the computer power and numerical approaches, the scatter in various computational results, at least, for interior crack front points has been decreased dramatically to a few percent [11]. However, there are still large discrepancies (of order 10–50 percent or even more) between various simulations of SIF for crack front regions near the free surface of the structure. This is because the square root singular behaviour for the stress field, which exists for the interior points, is replaced by the 3D corner singularity at the vertex point. This singular behaviour creates uncertainty leading to an ambiguity in the evaluation of SIF near the free surface [12,15].

The strength of the 3D corner singularity depends on the material Poisson's ratio, ν , and the angle, γ at which the crack front intersects the free surface. Therefore, K-solutions have to be also dependent upon the Poisson's ratio of the material. This effect is often disregarded in the

* Corresponding author.

E-mail address: Andrei.kotousov@adelaide.edu.au (A. Kotousov).

<https://doi.org/10.1016/j.tafmec.2018.09.013>

Received 28 May 2018; Received in revised form 14 September 2018; Accepted 24 September 2018

Available online 26 September 2018

0167-8442/ © 2018 Elsevier Ltd. All rights reserved.

Nomenclature

a	ellipse semi-axis along the x -axis	n_a, n_b	projections of the unit vector along the path
b	ellipse semi-axis along the y -axis	P	applied force
C	compliance	R	deviation from the theoretical value
$\Delta C(a, b)$	increment of compliance function in (a, b) coordinates	S	crack surface area
d	bar diameter	t	plate thickness
$E(k)$	complete elliptic integral of the second kind	v	displacement
E	Young's modulus	$ P_0 P_1 $	segment length
\bar{E}	effective Young's modulus	γ	crack surface intersection angle
G	strain energy release rate	γ_{cr}	critical angle
$g(l)$	energy release rate per unit length of the crack front	λ	aspect ratio (a/b)
K	stress intensity factor	ν	Poisson's ratio
$K(l)$	local stress intensity factor	ξ	angular elliptical coordinate
l	length coordinate along the crack front	(ξ, η)	elliptical coordinates
L	length of the crack front	(ξ_0, η_0)	initial crack front at elliptical coordinates
M_{ijk}	coefficient used to calculate the stress intensity factor	σ	uniform axial or bending stress
		Φ	function describing the angular variation of stress intensity factor

reference solutions, which are normally provided for $\nu = 0.3$ (mid-range). However, this dependence seems to not be very large and can be disregarded for many practical purposes [21].

One common assumption in fatigue crack growth modelling, which is partially supported by energy considerations, is based on the so-called stress singularity matching [24–26]. In accordance to this assumption, the evolution of the crack front occurs in a manner that all points over the crack front (including the corner points) have the same square root stress singularity. This assumption implies that the angle, γ , is the same during the crack front evaluation and equal to the critical angle, $\gamma = \gamma_{cr}$, the latter is a function of Poisson's ratio only. For example, for $\nu = 0.3$ the critical angle $\gamma_{cr} \approx 100.4^\circ$. It is interesting to note that in accordance to the experimental study by Heyder et al. [12], in structures with flat free surfaces, such as beams of rectangular or trapezoidal cross-sections, the fatigue crack front appears to follow the stress singularity matching assumption. However, it is generally not supported by experimental observations for structures with curved surfaces such as round bars [2].

As a result of the complex singular behaviour, there is currently no generally accepted technique to extract the value of the SIF near the surface where the stress and displacement fields are affected by the 3D corner (vertex) singularity. Some investigators utilise a polynomial regression function to fit the SIFs in the regression domain of the crack front, which excludes approximately 1/5th of the crack front segments adjacent to the free surfaces [2]. In other works, the investigators suggest using “a pragmatic stress intensity factor” for the surface points, which can be obtained by an extrapolation of a quadratic or higher order curve fitting to the values of SIF in the interior points [11].

Despite that the 3D corner singularity effect is quite localised, influencing the stress and displacement fields over, say, ten-twenty percent of the crack front [14], the discrepancies in the evaluation of SIF near the surface can also influence the accuracy of the SIF evaluations for the whole crack front. This is because the fitting equations, which are developed to facilitate the use of discrete numerical (FE) results, are usually derived using procedures which minimise the overall error, e.g. the least square regression procedure. The minimisation typically includes the near surface domains as well, where the FE results are not reliable. This can lead to discrepancies in the values of SIF for interior and near the free surface points across different computational results or fitting equations [11].

The dominance of the numerical methods in the analysis of elliptical and part-elliptical cracks in structures is largely attributed to many difficulties associated with the application of other methods, such as experimental or analytical, to the problem under consideration. For example, experimental fatigue crack growth data can be affected by the plasticity induced crack closure [13,27], which is largely unknown for

the elliptical and part-elliptical crack geometries. For instance, conflicting values for plasticity induced crack closure are often reported in different studies for part-elliptical cracks in round bars [11,13]. Therefore, the unknown effect of the crack closure does not allow to link directly the rate of the fatigue crack propagation, which can be found from fractography, to the SIF distribution along the crack front.

From the theoretical point of view, the only analytical solution was obtained for an elliptical crack fully embedded in an infinite elastic body [28]. This theoretical solution has been extensively utilised to develop empirical and fitting equations in the past, specifically to model the distribution of SIF along the crack front. However, crack problems in finite geometries of practical structures cannot be solved analytically. As a result, a common way to evaluate the accuracy and quality, as well as to validate numerical calculations is to compare new FE simulations with the previously obtained numerical results. However, the comparison between approximate solutions or fitting equations cannot provide a conclusive answer whether the new data or proposed fitting equation are more or less accurate than those which were published previously. This uncertainty motivates investigators for new numerical studies or, as in the current paper, a search for alternatives in the evaluation of the accuracy of the numerical or empirical SIF solutions.

In the current paper, a new theoretical relationship is derived for the exact distribution of the stress intensity factor along the front of elliptical or part-elliptical cracks. It is based on the divergence theorem for the compliance function, and, as such, utilises the most fundamental energy conservation principle. It was not a purpose of this work to apply this new relationship to analyse the near surface SIF distribution or propose new fitting equations, which would comply with the energy and compliance considerations. This will be a focus of further developments. Instead, the paper illustrates the application of this theoretical development to the derivation and assessment of the accuracy of empirical equations for semi-elliptical and part-elliptical cracks, which were suggested in the past [11,16–19,21]. It is also demonstrated that the exact analytical SIF solution for an elliptical crack in an infinite medium complies with the derived relationship, thus, providing a confidence in the presented analytical results.

2. The theoretical relationship for SIF distribution

The compliance, i.e. the inverse of stiffness, is defined for a linear-elastic body as the ratio of displacement, v , to applied force, P , i.e.

$$C = \frac{v}{P} \quad (1)$$

The strain energy release rate, G , can then be determined by

differentiating the compliance function versus the area of the crack surface, S ,

$$G = \frac{P^2}{2} \frac{dC}{dS} \tag{2}$$

An increment in the compliance associated with a crack advance, dS , can be found from the last equation as

$$dC = \frac{2}{P^2} G dS \tag{3}$$

If L is the crack front and l is the length coordinate along the crack front, see Fig. 1, then the energy release rate for the cracked body can be expressed as follows:

$$G = \int_L g(l) dl = \int_L \frac{K(l)^2}{\bar{E}} dl \tag{4}$$

where $g(l)$ is the strain energy density release rate (the energy release rate per unit length of the crack front), $K(l)$ is the local stress intensity factor (SIF) along the crack front, and \bar{E} is the effective Young's modulus, $\bar{E} = E/(1-\nu^2)$. Eq. (4) implies the plane strain conditions near the crack tip, which have been demonstrated to be true in many computational results [2].

In the case of mode I loading, for elliptical or part-elliptical cracks the strain energy density and the local SIF are also function of the crack shape, which can be specified by the lengths of the semi-axes, a and b , in other words, $g = g(a, b, \eta)$ and $K_I = K(a, b, \eta)$; η is the angular elliptical coordinate, as is shown in Fig. A1 provided in the Appendix A.

The crack surface increment due to the change of the length of semi-axes, da and db , as a function of coordinate, η , is, see Appendix A,

$$ds(\eta) = a \cos^2(\eta) db + b \sin^2(\eta) da \tag{5}$$

Then, the compliance Eq. (3) can be rewritten as follows:

$$dC(a, b) = \frac{2}{P^2} \left(\int_{\eta_0}^{\eta_1} \frac{K(a, b, \eta)^2}{\bar{E}} b \sin^2(\eta) d\eta \right) da + \frac{2}{P^2} \left(\int_{\eta_0}^{\eta_1} \frac{K(a, b, \eta)^2}{\bar{E}} a \cos^2(\eta) d\eta \right) db \tag{6}$$

where η_0 corresponds to the start point on the crack front ($l = 0$) and η_1 is the end point along the crack front ($l = L$), see Fig. 1.

Consider the compliance function in (a, b) coordinates or $C = C(a, b)$. At fixed geometry, loading and material properties, the increment of this function, $\Delta C(a, b)$, depends only on the initial (a_0, b_0) and final (a_1, b_1) points:

$$\int_{(a_0, b_0)}^{(a_1, b_1)} dC(a, b) = C(a_1, b_1) - C(a_0, b_0) \tag{7}$$

Eq. (7) can also be written using the compliance equation as

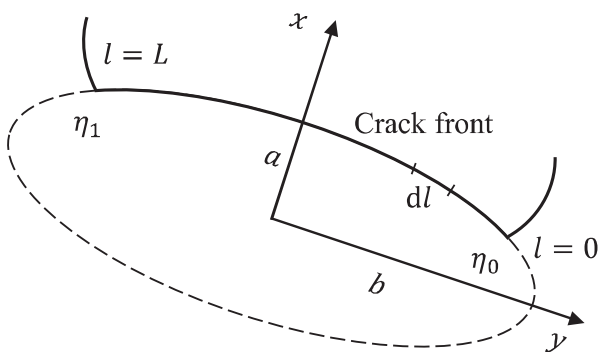


Fig. 1. Part-elliptical crack front.

$$\int_{(a_0, b_0)}^{(a_1, b_1)} dC(a, b) = \frac{2}{\bar{E}P^2} \int_{(a_0, b_0)}^{(a_1, b_1)} \left[\int_{\eta_0}^{\eta_1} K(a, b, \eta)^2 b \sin^2(\eta) d\eta \right] da + \left[\int_{\eta_0}^{\eta_1} K(a, b, \eta)^2 a \cos^2(\eta) d\eta \right] db \tag{8}$$

The last equation can be also represented in the vector form

$$\int_{(a_0, b_0)}^{(a_1, b_1)} dC(a, b) = \int_{(a_0, b_0)}^{(a_1, b_1)} \bar{F} d\bar{u} = \int_{(a_0, b_0)}^{(a_1, b_1)} (F_a n_a + F_b n_b) du \tag{9}$$

where n_a and n_b are projections of the unit vector along the path, see Fig. 2, and

$$F_a = \frac{2}{\bar{E}P^2} \int_{\eta_0}^{\eta_1} K(a, b, \eta)^2 b \sin^2(\eta) d\eta \tag{10}$$

$$F_b = \frac{2}{\bar{E}P^2} \int_{\eta_0}^{\eta_1} K(a, b, \eta)^2 a \cos^2(\eta) d\eta \tag{11}$$

For any (simple) closed curve with the same start and end points, $(a_0, b_0) = (a_1, b_1)$, Eq. (9) can be written using the divergence theorem as follows:

$$\int_{(a_0, b_0)}^{(a_1, b_1)} (F_a n_a + F_b n_b) du = \int_A \left(\frac{\partial F_a}{\partial b} - \frac{\partial F_b}{\partial a} \right) dA = C(a_1, b_1) - C(a_0, b_0) = 0 \tag{12}$$

which requires that the distribution of the stress intensity factor along the elliptical or part-elliptical crack front has to satisfy the following relationship:

$$\frac{\partial}{\partial b} \left(\frac{2}{\bar{E}P^2} \int_{\eta_0}^{\eta_1} K(a, b, \eta)^2 b \sin^2(\eta) d\eta \right) = \frac{\partial}{\partial a} \left(\frac{2}{\bar{E}P^2} \int_{\eta_0}^{\eta_1} K(a, b, \eta)^2 a \cos^2(\eta) d\eta \right) \tag{13}$$

Because it is assumed that the material properties (\bar{E}) and loading (P) do not change during the crack propagation, then Eq. (13) can be rewritten in a simplified form as

$$\frac{\partial}{\partial b} \int_{\eta_0}^{\eta_1} K(a, b, \eta)^2 b \sin^2(\eta) d\eta = \frac{\partial}{\partial a} \int_{\eta_0}^{\eta_1} K(a, b, \eta)^2 a \cos^2(\eta) d\eta \tag{14}$$

Thus, the exact distribution of the SIF along the crack front must satisfy Eq. (14). A simple method for the evaluation of the quality of an approximate solution for $K(a, b, \eta)$ can be based on the assessment of the discrepancies between the right and left part of Eq. (14). The method largely generalises an approach suggested by Fett [16] for quality

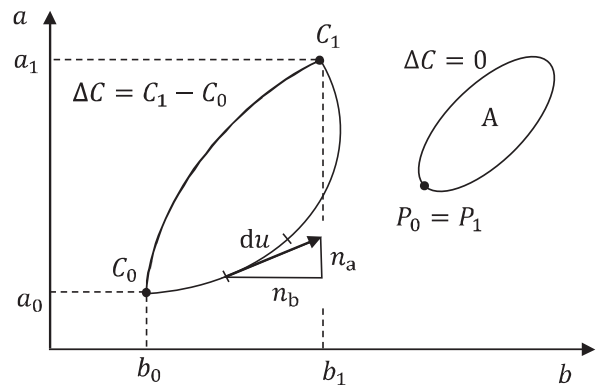


Fig. 2. Path-independence of compliance function in (a, b) coordinates.

evaluation of stress intensity factor solutions. This approach was suggested for a particular case of pure tensile loading. It is based on energy considerations that “the total energy must be independent of the special shape of crack increments” and, essentially, is equivalent to Eq. (8). This approach was successfully applied to evaluate alternative solutions for semi-elliptical cracks in finite plates using specifically selected integration paths characterised by (1) $a/b = \text{const.}$, (2) $a = \text{const.}$ and (3) $b = \text{const.}$ The proposed Eqs. (13) and (14) are more general, in particular, do not require selection of specific paths and can be applied to evaluate the quality of SIF solutions corresponding to specific combinations of parameters characterising the problem geometry, or for any combination of a and b . It can be easily generalised for many other geometries as well as boundary conditions, e.g. bending or torsion. In the following, a few examples illustrating the possible applications of Eq. (14) for analysis of approximate solutions are considered.

3. Examples

3.1. Elliptical crack subjected to tensile loading

In this case the exact solution for SIF is well-known and can be written in the following form [28]

$$K_I = K(a, b, \eta) = \frac{\sigma\sqrt{\pi a}}{E(k)}(\lambda^2\cos^2(\eta) + \sin^2(\eta))^{\frac{1}{4}} \tag{15}$$

with $E(k)$ is a complete elliptic integral of the second kind, which can be found as

$$E(k) = \int_0^{\frac{\pi}{2}} \sqrt{1-k^2\sin^2(\xi)} d\xi \tag{16}$$

where $k = \sqrt{1-\lambda^2}$ and $\lambda = a/b$.

The proof that Eq. (14) is satisfied exactly is quite cumbersome and involves tedious manipulations with elliptic functions. Instead, in the next section, Eq. (14) is verified with numerical calculations for $0 < \lambda < 1$, which will demonstrate that Eq. (14) is true for the exact distribution of SIF over the front of an elliptical crack, given by Eq. (15).

However, one case can be easily analysed analytically, specifically when $a/b = \lambda \rightarrow 0$ (straight crack). In this case $\partial K^2/\partial \lambda \rightarrow 0$, $E(k) = E(\sqrt{1-\lambda^2}) = 1$, and the SIF can be simplified as

$$K_I = K(a, b, \eta) = K(a, \eta) = \sigma\sqrt{\pi a} \sqrt{|\sin(\eta)|} \tag{17}$$

The compliance Eq. (14) can now be rewritten as

$$\frac{\partial}{\partial b} \int_0^{2\pi} ab |\sin(\eta)| \sin^2(\eta) d\eta = \frac{\partial}{\partial a} \int_0^{2\pi} a^2 |\sin(\eta)| \cos^2(\eta) d\eta \tag{18}$$

which is reduced to the following equality, which can be verified easily:

$$\int_0^{2\pi} |\sin(\eta)| \sin^2(\eta) d\eta = 2 \int_0^{2\pi} |\sin(\eta)| \cos^2(\eta) d\eta \tag{19}$$

as both left and right parts of Eq. (19) are equal to $8/3$.

3.2. Elliptical crack in finite plate

In this case, the following approximate solution has been suggested [17]:

$$K(a, \lambda, \eta) = \frac{\sigma\sqrt{\pi a}}{E(k)} \left(1 + \frac{0.05}{0.11 + \lambda^{3/2}} \left(\frac{a}{t}\right)^2 + \frac{0.29}{0.23 + \lambda^{3/2}} \left(\frac{a}{t}\right)^4 \right) f_{\phi} g \tag{20}$$

Utilising the similar angular distribution of SIFs along the crack front as in the exact solution (15):

$$f_{\phi} = (\lambda^2\cos^2(\eta) + \sin^2(\eta))^{\frac{1}{4}} \tag{21}$$

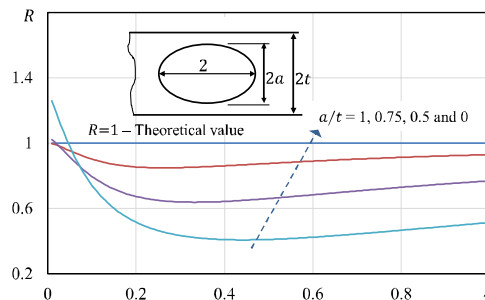


Fig. 3. Elliptical crack in a finite plate: Evaluation of the quality of approximate solution [17]

and

$$g = 1 - \left(\frac{a}{t}\right)^4 \frac{\cos\eta}{1 + 4\lambda} \tag{22}$$

As before, $E(k)$ is a complete elliptic integral of the second kind, and $k = \sqrt{1-\lambda^2}$ and $\lambda = a/b$.

Consider the theoretical relationship (14) and represent it as a ratio of the derivatives:

$$R = \frac{\partial F_a/\partial b}{\partial F_b/\partial a} \tag{23}$$

where

$$F_a = \int_0^{2\pi} K(a, \lambda, \eta)^2 b \sin^2(\eta) d\eta \tag{24a}$$

and

$$F_b = \int_0^{2\pi} K(a, \lambda, \eta)^2 a \cos^2(\eta) d\eta \tag{24b}$$

It can be demonstrated that $R = R(\lambda, a/t)$, so the dependence of R from the actual geometry sizes in Eq. (23) disappears. If this relationship is applied to an approximate solution, then the ratio $R \neq 1$, and the deviation from the theoretical value (unity) can serve as an indicator of the quality of this approximate solution. It is clear that at small values of the ratio a/t the approximation Eq. (20) converges to the analytical solution of Eq. (15), for which $R = 1$ (see Fig. 3) as is discussed in the previous Section 3.1. With an increase of the value of a/t , as expected, the deviation of R from the theoretical value given for the exact solution increases or the solution becomes less accurate.

3.3. Comparison of approximations for semi-elliptical surface crack in tension

Relationships (13) and (14) are not able to provide a quantitative assessment of how significant the error is. However, these relationships are capable to provide a comparison between different approximate solutions. Consider, for example, four approximate solutions developed over the past thirty years for the evaluation of SIF along the semi-elliptical crack [16–21]. Let us focus on the simplest case of a semi-infinite plate and when the crack is subjected to tensile stresses, σ . The approximate K -solutions will not be presented in this article as these solutions have been widely published and discussed in many articles, e.g. Fett [16] or Toribio et al. [3]. As is mentioned in the Introduction, the continuous advance in the computer power and numerical approaches normally leads to more accurate K -solutions, which can be observed from Fig. 4, i.e. the subsequent approximations deviate less from the theoretical value, $R = 1$.

The first numerical solution for the problem under consideration was obtained by Newman and Raju and summarised in [17]. The accuracy of the FE results was claimed to be within $\pm 3\%$ and the fitting

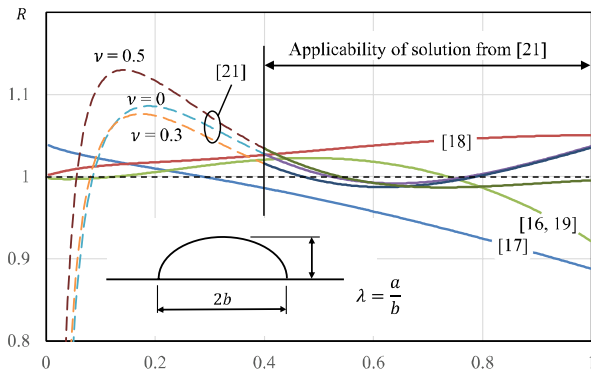


Fig. 4. Semi-elliptical crack in a semi-infinite finite plate: Evaluation of the quality of approximations.

function has maximum error of $\pm 5\%$. The motivation behind the development of a new solution for the same problem in [18], was a quite large deviation of Newman and Raju’s empirical equation from some FE studies, specifically for a semi-infinite plate geometry. Fett [16] utilised the results of Isida et al. [19], obtained by means of a modified body-force method, and suggested a more complicated equation (K-solution). One of the reasons for the revision of the previous results and development of a more sophisticated solution [21] was the dependence of K-solution upon the Poisson’s ratio as is discussed in the Introduction.

The latest solution [21] was specifically derived, in 2012, for aspect ratios above 0.4 ($\lambda > 0.4$). It can be seen from Fig. 4 that R ratios for this solution are the closest to the theoretical value (1) among all other approximate solutions. One can also observe that the first approximate solution to the problem [17] has the largest deviation of R from 1. Therefore, it is demonstrated that the suggested method largely replicates the conclusions of the previous studies regarding the FE progress and the accuracy of fitting equations, and it is capable to evaluate the quality of approximate solutions.

3.4. Part-elliptical crack in round bar

The theoretically derived Eqs. (13) or (14) can be also useful to identify deficiencies of suggested approximate solutions. Consider, for example, the case of part-elliptical cracks in round bars. The derivation of SIF solutions for this case was a subject of many papers [20]. It seems that the most comprehensive results have been provided by Shin and Cai [11]. The K-solution can be represented as

$$K(a, b, d, \eta) = \sigma \sqrt{\pi a} F_p \tag{25}$$

with

$$F_p = F_p \left(\frac{a}{b}, \frac{a}{d}, \frac{x}{h} \right) = \sum_{i=0}^2 \sum_{j=0}^7 \sum_{k=0}^2 M_{ijk} \left(\frac{a}{b} \right)^i \left(\frac{a}{d} \right)^j \left(\frac{x}{h} \right)^k \tag{26}$$

The coefficients M_{ijk} are presented in several papers and will not be repeated here, see e.g. [3,11]. The R ratios (Eq. (23)) for different values of $\lambda = a/b$ can be obtained by substituting Eqs. (25) and (26) into Eq. (23). These ratios have been plotted in Fig. 5.

It can be observed from Fig. 5 that the deviation of fitting Eqs. (25) and (26) from the theoretical value for the exact solution ($R = 1$) is consistent and reasonable up to $a/d \approx 0.9$, except at very small values of $\lambda = a/b$. This exception can be explained by the effect of the corner singularity, the strength of which is larger than the square root singularity, which prevails for the rest of the crack front.

This is because, at this combination of geometry parameters, (see Fig. 5) the angle, γ , at which the crack front intersects the free surface, is above the critical value, $\gamma_{cr} \approx 100.4^\circ$. As a result, a large portion of the crack front can be affected by 3D corner singularity leading to less accurate results. A similar effect was reported in Heyder et al. [12], who

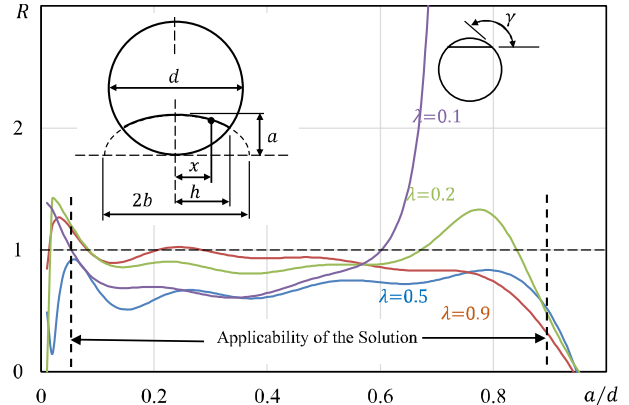


Fig. 5. Part-elliptical crack in round bar: Analysis of approximate solution [11].

concluded that the most accurate numerical results normally correspond to the case when γ is close to the critical value of 100.4° . This can also be observed from Fig. 5.

At small values of a/d the SIF solution has to be reduced to the solution for semi-infinite crack with the corresponding a/b ratio. Specifically, for $a/b = 0$, the angular distribution is described by a third order polynomial function:

$$F_p = F_p \left(\frac{a}{b} = 0, \frac{a}{d} = 0, \frac{x}{h} \right) = \sum_{k=0}^2 M_{00k} \left(\frac{x}{h} \right)^k \tag{27}$$

It is clear that Eq. (27) is not capable to describe a quite complicated behaviour of SIF along the crack front, see e.g. [21], which utilises a dozen of fitting constants to describe the angular dependence of SIF. This is also reflected by large deviations of R from its theoretical value for the exact solution at $a/d < 0.1$, see Fig. 5.

4. Development of approximate solutions

In this Section, it is demonstrated that the obtained theoretical equations can help to derive approximate K-solutions for different geometries and structures. The SIF approximate solutions for elliptical, semi-elliptical, quarter-elliptical (corner) cracks for various structures (such as plates, pressure vessels, rods, etc.) are often presented in the following form [16–21]

$$K(a, \lambda, \eta, g_n) = \sigma \frac{\sqrt{\pi a}}{E(k)} F(\lambda, g_n) \Phi(\lambda, \eta, g_n) \tag{28}$$

where $E(k)$ is a complete elliptic integral of the second kind, $\Phi(\lambda, \eta, g_n)$ is an empirical function of $\lambda = a/b$, η and some other dimensionless geometry parameters g_1, g_2, \dots, g_n .

Function $\Phi(\lambda, \eta, g_n)$ approximates the distribution of SIF along the crack front. $F(\lambda, g_n)$ is another empirical (fitting) function, which takes into account the effect of the final geometry of the problem described by the parameters g_n and a/b ratio on the values of SIF. In a limiting case this function could be just a number.

Substituting Eq. (28) into Eq. (14) gives

$$\frac{\partial}{\partial b} \left(\int_{\eta_0}^{\eta_1} b \left(\frac{\sqrt{a}}{E(k)} F(\lambda, g_n) \Phi(\lambda, \eta, g_n) \sin(\eta) \right)^2 d\eta \right) - \frac{\partial}{\partial a} \left(a \int_{\eta_0}^{\eta_1} \left(\frac{\sqrt{a}}{E(k)} F(\lambda, g_n) \Phi(\lambda, \eta, g_n) \cos(\eta) \right)^2 d\eta \right) = 0 \tag{29}$$

Let

$$A(\lambda, g_n) = \frac{1}{\lambda E(k)^2} \int_{\eta_0}^{\eta_1} (\Phi(\lambda, \eta, g_n) \sin(\eta))^2 d\eta \tag{30a}$$

$$B(\lambda, g_n) = \frac{1}{E(k)^2} \int_{\eta_0}^{\eta_1} (\Phi(\lambda, \eta, g_n) \cos(\eta))^2 d\eta \tag{30b}$$

Then the following partial differential equation can be written for function $F(\lambda, g_n)$

$$\frac{\partial}{\partial b} (a^2 F(\lambda, g_n)^2 A(\lambda, g_n)) - \frac{\partial}{\partial a} (a^2 F(\lambda, g_n)^2 B(\lambda, g_n)) = 0 \tag{31}$$

This equation can be solved numerically or analytically, using, for example, the method of characteristics. In other words, if the function describing the angular variation of SIF is selected, then the geometry correction function, $F(\lambda, g_n)$, can be obtained analytically rather than through the use of numerical calculations. Moreover, this function will agree with energy and compliance equations, and, potentially, minimize the error associated with FE simulations and fitting procedures.

Consider an example when there is the only one geometry parameter for the problem: $\lambda = a/b$ or $F(\lambda, g_n) = F(\lambda)$ and $f(\lambda, \eta, g_n) = f(\lambda, \eta)$. This is a typical case for infinite or semi-infinite geometries, which have no other characteristic dimensions. Taking into account that the derivatives can be rewritten as $\partial/\partial a = b^{-1} \partial/\partial \lambda$ and $\partial/\partial b = -\lambda b^{-1} \partial/\partial \lambda$, the partial differential Eq. (31) can be rewritten as

$$\lambda^2 \frac{\partial}{\partial \lambda} (F(\lambda)^2 A(\lambda)) + 2F(\lambda)^2 B(\lambda) + \lambda \frac{\partial}{\partial \lambda} (F(\lambda)^2 B(\lambda)) = 0 \tag{32}$$

leading to an ordinary differential equation for $F(\lambda)$:

$$\frac{\partial F(\lambda)}{\partial \lambda} (\lambda^2 A(\lambda) + \lambda B(\lambda)) + \frac{F(\lambda)}{2} \left(2B(\lambda) + \lambda^2 \frac{\partial A(\lambda)}{\partial \lambda} + \lambda \frac{\partial B(\lambda)}{\partial \lambda} \right) = 0 \tag{33}$$

This equation can be easily integrated by using standard techniques.

Consider, for example, a semi-elliptical crack in a semi-infinite plate as in Section 3.2. Newman and Raju approximate K-solution [17] can be written as

$$K(a, \lambda, \eta) = \sigma \frac{\sqrt{\pi a}}{E(k)} (1.13 - 0.09\lambda)(1 + 0.1(1 - \sin(\eta))^2) f_\phi(\eta) \tag{34}$$

Then the function describing the angular variation of SIF is

$$\Phi(\lambda, \eta) = (1 + 0.1(1 - \sin(\eta))^2) f_\phi(\eta) \tag{35}$$

where $f_\phi(\eta)$ is given by Eq. (21), and the corrective function is given by

$$F(\lambda) = 1.13 - 0.09\lambda \tag{36}$$

However, this function can be also found from Eq. (33). The solution of differential Eq. (33) is presented in Fig. 6 along with the suggested empirical function (36).

It can be noted a good correlation between the empirical fitting Eq. (36) and the dependence, which was derived from differential Eq. (33) almost for all values of λ . For small values of λ the difference is quite significant, which was also noted in [18]. This can indicate that the selected function $\Phi(\lambda, \eta)$, Eq. (35), is not appropriate for “flat semi-elliptical cracks”, when λ is close to 0. This conclusion is also confirmed

Appendix A. Elliptical Coordinates and Crack Advance Equation

The aim of the derivations provided in this Appendix A is to link the change of the shape of ellipse, which can be represented by the change of the length of semi-axes, da and db , to an increment of the area, ds , at different points, see Fig. A1. This equation is necessary to evaluate the change of the compliance.

It is natural to introduce elliptical coordinates, (ξ, η) , which are orthogonal and related to the rectangular coordinates by the well-known equations:

$$x = c \sinh(\xi) \sin(\eta) \tag{A1a}$$

$$y = c \cosh(\xi) \cos(\eta) \tag{A1b}$$

In particular, the length of semi-axes, a and b , can be found by setting, $\xi = \xi_0$ and $\eta = \pi/2$ and 0 , respectively, leading to

$$a = c \sinh(\xi_0) \tag{A2a}$$

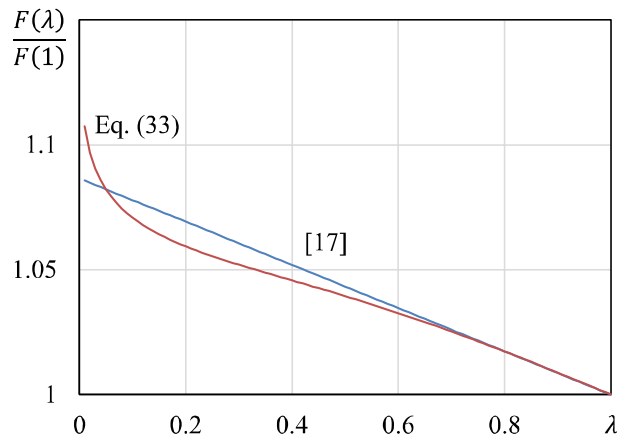


Fig. 6. Comparison of empirical equation and dependence developed theoretically.

in other papers, some of which suggested alternative and more complicated forms of function $\Phi(\lambda, \eta)$ [16,18,19 and 21].

5. Conclusion

In this paper, a theoretical relationship for the distribution of SIF along the front of elliptical or part-elliptical cracks was derived based on divergence theorem for compliance function. The exact solutions, which are largely unobtainable for the problems under consideration, have to comply with this relationship. The deviation from this theoretical relationship in the case of various approximate solutions can serve as a quality criterion of these approximations. It was demonstrated that the quality criterion adequately reflects the accuracy of various empirical solutions suggested in the past. It also can help to identify the deficiencies of various empirical equations, whose accuracy otherwise can only be evaluated from the comparison with the similar approximate or fitting equations derived using different analytical methods or different numerical approaches.

The theoretical relationship has also been rewritten in the form of a partial differential equation, see Eq. (31). The solution of this differential equation can provide an alternative form of the approximate solutions, which also complies with energy principles. From this perspective, this theoretical development will allow to significantly reduce the number of numerical simulations without compromising the accuracy of the final results.

The derived theoretical Eq. (14) can be easily generalised for other geometries and boundary conditions. Therefore, this development can provide an independent way of the assessment of the quality of approximate solutions in many situations, specifically, for which other approaches might not work or might be expensive (e.g. experimental validations).

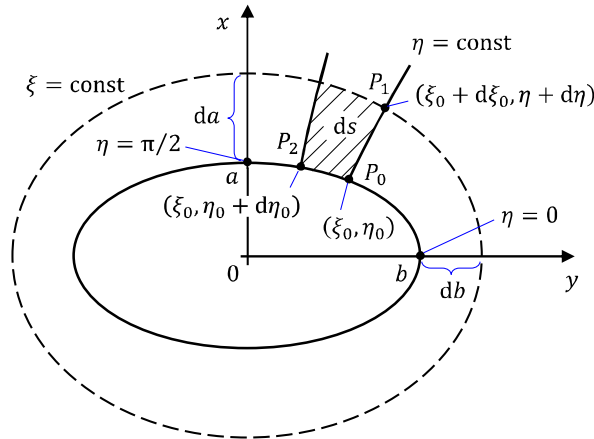


Fig. A1. Elliptical Coordinates.

$$b = c \cosh(\xi_0) \tag{A2b}$$

with

$$c = \sqrt{b^2 - a^2} \tag{A3a}$$

$$\xi_0 = \operatorname{atanh}\left(\frac{a}{b}\right) \tag{A3b}$$

Any point P on the ellipse can be written in terms of its coordinate (x_0, y_0) or in elliptical coordinates as (ξ_0, η) , where $0 < \eta < 2\pi$. Consider now a very small crack advance due to small increments in the length of semi-axes, da and db , then

$$da = dc \sinh(\xi_0) + d\xi_0 c \cosh(\xi_0) \tag{A4a}$$

$$db = dc \cosh(\xi_0) + d\xi_0 c \sinh(\xi_0) \tag{A4b}$$

The new crack front (ellipse) can be described by replacing c and ξ_0 in (A1) with $c + dc$ and $\xi_0 + d\xi_0$, respectively. The increments dc and $d\xi_0$ can be found from Eq. (A4):

$$dc = db \cosh(\xi_0) - da \sinh(\xi_0) \tag{A5a}$$

$$d\xi_0 = \frac{da \cosh(\xi_0) - db \sinh(\xi_0)}{c} \tag{A5b}$$

Consider point P_0 with coordinates (ξ_0, η_0) on the initial crack front, our next step is to find the coordinate of point P_1 , which belongs to the orthogonal segment given by $(\xi_0 + d\xi, \eta_0)$ and the new ellipse (crack front), or this point can be written as $(\xi_0 + d\xi_0, \eta_0 + d\eta)$. The coordinates for point P_1 are:

$$x_1 = c \sinh(\xi_0 + d\xi) \sin(\eta_0) = (c + dc) \sinh(\xi_0 + d\xi_0) \sin(\eta_0 + d\eta) \tag{A6a}$$

$$y_1 = c \cosh(\xi_0 + d\xi) \cos(\eta_0) = (c + dc) \cosh(\xi_0 + d\xi_0) \cos(\eta_0 + d\eta) \tag{A6b}$$

Using Taylor expansion of hyperbolic and trigonometric functions and removing variable $d\eta$, it can be found that that

$$d\xi = \frac{1}{c} \frac{\cosh(\xi_0) \sin^2(\eta) da + \sinh(\xi_0) \cos^2(\eta) db}{\cosh^2(\xi_0) \sin^2(\eta) + \sinh^2(\xi_0) \cos^2(\eta)} \tag{A7}$$

The length of the segment $|P_0P_1|$ is

$$|P_0P_1| = c \sqrt{\cosh^2(\xi_0) \sin^2(\eta_0) + \cosh^2(\xi_0) \cos^2(\eta_0)} d\xi \tag{A8}$$

The length of the segment $|P_0P_2|$ is

$$|P_0P_2| = c \sqrt{\sinh^2(\xi_0) \cos^2(\eta_0) + \cosh^2(\xi_0) \sin^2(\eta_0)} d\eta_0 \tag{A9}$$

Because these segments are along the coordinate axes and have to be orthogonal (at small values of da, db , etc.) and utilising Eq. (A2) the increment of the surface area is

$$ds(\eta_0) = |P_0P_1| \times |P_0P_2| = a \cos^2(\eta_0) db + b \sin^2(\eta_0) da \tag{A10}$$

To validate the obtained equation let us consider the well-known equation for the area of an ellipse with the length of semi-axes a and b :

$$S = \pi ab \tag{A11}$$

The increment of this area due to changes of semi-axes is

$$S = \pi (adb + bda) \tag{A12}$$

The same result can be obtained from (A10) by integrating with respect to variable η

$$dS = \int_0^{2\pi} ds d\eta = \int_0^{2\pi} (a \cos^2(\eta) db + b \sin^2(\eta) da) d\eta = \pi (adb + bda) \quad (\text{A13})$$

The main Eq. (A10) can also be validated using other well-known solutions and properties of the elliptic shapes.

References

- [1] R. Brighenti, A. Carpinteri, Surface cracks in fatigued structural components: a review, *Fatigue Fract. Eng. Mater. Struct.* 36 (2013) 1209–1222, <https://doi.org/10.1111/ffe.12100>.
- [2] J. Lebahn, H. Heyer, M. Sander, Numerical stress intensity factor calculation in flawed round bars validated by crack propagation tests, *Eng. Fract. Mech.* 108 (2013) 37–49, <https://doi.org/10.1016/j.engfracmech.2013.04.013>.
- [3] J. Toribio, J.C. Matos, B. González, J. Escuadra, Numerical modelling of cracking path in round bars subjected to cyclic tension and bending, *Int. J. Fatigue* 58 (2014) 20–27, <https://doi.org/10.1016/j.ijfatigue.2013.03.017>.
- [4] A.M.P. de Jesus, A.L.L. da Silva, J.A.F.O. Correia, Fatigue of riveted and bolted joints made of puddle iron – a numerical approach, *J. Constr. Steel Res.* 102 (2014) 164–177, <https://doi.org/10.1016/j.jcsr.2014.06.012>.
- [5] J.A.F.O. Correia, A.M.P. de Jesus, A. Fernández-Canteli, Local unified probabilistic model for fatigue crack initiation and propagation: application to a notched geometry, *Eng. Struct.* 52 (2013) 394–407, <https://doi.org/10.1016/j.engstruct.2013.03.009>.
- [6] A.L.L. Silva, A.M.P. de Jesus, J. Xavier, J.A.F.O. Correia, A.A. Fernandes, Combined analytical-numerical methodologies for the evaluation mixed-mode (I+II) fatigue crack growth rates in structural steels, *Eng. Fract. Mech.* 185 (2017) 124–138, <https://doi.org/10.1016/j.engfracmech.2017.04.016>.
- [7] D. Rozumek, Z. Marciniak, G. Lesiuk, J.A. Correia, A.M.P. de Jesus, Experimental and numerical investigation of mixed mode I+II and I+III fatigue crack growth in S355J0 steel, *Int. J. Fatigue* 113 (2018) 160–170, <https://doi.org/10.1016/j.ijfatigue.2018.04.005>.
- [8] A. Carpinteri, Shape change of surface cracks in round bars under cyclic axial loading, *Int. J. Fatigue* 15 (1993) 21–26, [https://doi.org/10.1016/0142-1123\(93\)90072-X](https://doi.org/10.1016/0142-1123(93)90072-X).
- [9] X.B. Lin, R.A. Smith, Shape growth simulation of surface cracks in tension fatigued round bars, *Int. J. Fatigue* 19 (1997) 461–469, [https://doi.org/10.1016/S0142-1123\(97\)00012-1](https://doi.org/10.1016/S0142-1123(97)00012-1).
- [10] L.A. James, W.J. Mills, Review and synthesis of stress intensity factor solutions applicable to cracks in bolts, *Eng. Fract. Mech.* 30 (1988) 641–654, [https://doi.org/10.1016/0013-7944\(88\)90156-7](https://doi.org/10.1016/0013-7944(88)90156-7).
- [11] C.S. Shin, C.Q. Cai, Experimental and finite element analyses on stress intensity factors of an elliptical surface crack in a circular shaft under tension and bending, *Int. J. Fract.* 129 (2004) 239–264, <https://doi.org/10.1023/B:FRAC.0000047784.23236.7d>.
- [12] M. Heyder, K. Kolk, G. Kuhn, Numerical and experimental investigations of the influence of corner singularities on 3D fatigue crack propagation, *Eng. Fract. Mech.* 72 (2005) 2095–2105, <https://doi.org/10.1016/j.engfracmech.2005.01.006>.
- [13] C.Y. Hou, Simulation of surface crack shape evolution using the finite element technique and considering the crack closure effects, *Int. J. Fatigue* 33 (2011) 719–726, <https://doi.org/10.1016/j.ijfatigue.2010.11.022>.
- [14] P. Hutař, L. Náhlík, Z. Knésl, The effect of a free surface on fatigue crack behaviour, *Int. J. Fatigue* 32 (2010) 1265–1269, <https://doi.org/10.1016/j.ijfatigue.2010.01.009>.
- [15] P. Hutař, L. Náhlík, Z. Knésl, Quantification of the influence of vertex singularities on fatigue crack behavior, *Comput. Mater. Sci.* 45 (2009) 653–657, <https://doi.org/10.1016/j.commatsci.2008.08.009>.
- [16] T. Fett, Stress intensity factors for semi-elliptical surface cracks in a plate under tension based on the Isida's solution, *Int. J. Fract.* 48 (1991) 139–151, <https://doi.org/10.1007/BF00018395>.
- [17] J.C. Newman, I.S. Raju, J. Lewis, G. Sines, Stress intensity factor equations for cracks in three-dimensional finite bodies, *Fract. Mech.* 1 (1983) 238–269.
- [18] V.A. Vainshtok, I.V. Varfolomeyev, Stress intensity factor equations for part-elliptical cracks and their verification, *Eng. Fract. Mech.* 34 (1989) 125–136, [https://doi.org/10.1016/0013-7944\(89\)90246-4](https://doi.org/10.1016/0013-7944(89)90246-4).
- [19] M. Isida, H. Noguchi, Tension of a plate containing an embedded elliptical crack, *Eng. Fract. Mech.* 20 (1984) 387–408, [https://doi.org/10.1016/0013-7944\(84\)90046-8](https://doi.org/10.1016/0013-7944(84)90046-8).
- [20] J. Toribio, N. Álvarez, B. González, J.C. Matos, A critical review of stress intensity factor solutions for surface cracks in round bars subjected to tension loading, *Eng. Fail. Anal.* 16 (2009) 794–809, <https://doi.org/10.1016/j.engfailanal.2008.06.023>.
- [21] S. Strobl, P. Supancic, T. Lube, R. Danzer, Surface crack in tension or in bending—a reassessment of the Newman and Raju formula in respect to fracture toughness measurements in brittle materials, *J. Eur. Ceram. Soc.* 32 (8) (2012) 1491–1501, <https://doi.org/10.1016/j.jeurceramsoc.2012.01.011>.
- [22] S. Kolitsch, H.P. Gänser, R. Pippan, Approximate stress intensity factor solutions for semi-elliptical cracks with large a/W and c/B under tension and bending, *Theor. Appl. Fract. Mech.* 92 (2017) 167–177, <https://doi.org/10.1016/j.tafmec.2017.06.010>.
- [23] Z. He, A. Kotousov, F. Berto, R. Branco, A brief review of three-dimensional effects near crack front, *Phys. Mesomech.* 19 (1) (2016) 6–20, <https://doi.org/10.1134/S1029959916010021>.
- [24] J.A.F.O. Correia, A.M.P. de Jesus, A. Fernández-Canteli, A procedure to derive probabilistic fatigue crack propagation data, *Int. J. Struct. Integrity* 3 (2012) 158–183, <https://doi.org/10.1108/17579861211235183>.
- [25] P.J. Huffman, J. Ferreira, J.A.F.O. Correia, A.M.P. de Jesus, G. Lesiuk, F. Berto, A. Fernandez-Canteli, G. Glinka, Fatigue crack propagation prediction of a pressure vessel mild steel based on a strain energy density model, *Frattura ed Integrita Strutturale* 42 (2017) 170–180, <https://doi.org/10.3221/IGF-ESIS.42.09>.
- [26] J.A.F.O. Correia, P.J. Huffman, A.M.P. de Jesus, S. Cicero, A. Fernández-Canteli, F. Berto, G. Glinka, Unified two-stage fatigue methodology based on a probabilistic damage model applied to structural details, *Theor. Appl. Fract. Mech.* 92 (2017) 252–265, <https://doi.org/10.1016/j.tafmec.2017.09.004>.
- [27] J.A.F.O. Correia, S. Blasón, A. Arcari, M. Calvente, N. Apetre, P.M.G.P. Moreira, A.M.P. de Jesus, A.F. Canteli, Modified CCS fatigue crack growth model for the AA2019-T851 based on plasticity-induced crack closure, *Theor. Appl. Fract. Mech.* 85A (2016) 26–36, <https://doi.org/10.1016/j.tafmec.2016.08.024>.
- [28] M.K. Kassir, G.C. Sih, Three-dimensional crack problems: a new selection of crack solutions in three-dimensional elasticity, *Mechanics of Fracture 2*, Noordhoff-Leyden, The Netherlands, 1975.

Chapter 7

Investigation of Plasticity Induced Crack Closure and 3D Effects on Front Shapes of Fatigue Cracks

Statement of Authorship

Title of Paper	An analytical-based approach for simulating fatigue crack growth in round bars			
Publication Status	<input checked="" type="checkbox"/>	Published	<input type="checkbox"/>	Accepted for Publication
	<input type="checkbox"/>	Submitted for Publication	<input type="checkbox"/>	Unpublished and Unsubmitted work written in manuscript style
Publication Details	Zakavi, B., Kotousov, A., & Branco, R. (2021). An analytical-based approach for simulating fatigue crack growth in round bars, International Journal of Fracture, 1- 12. DOI:10.1007/s10704-021-00558-3.			

Principal Author

Name of Principal Author	Behnam Zakavi		
Contribution to the Paper	Performed analysis, interpreted data, literature review, and wrote manuscript		
Overall percentage (%)	50		
Certification:	This paper reports on original research I conducted during the period of my Higher Degree by Research candidature and is not subject to any obligations or contractual agreements with a third party that would constrain its inclusion in this thesis. I am the primary author of this paper.		
Signature		Date	20 / 08 / 2021

Co-Author Contributions

By signing the Statement of Authorship, each author certifies that:

- i. the candidate's stated contribution to the publication is accurate (as detailed above);
- ii. permission is granted for the candidate to include the publication in the thesis; and
- iii. the sum of all co-author contributions is equal to 100% less the candidate's stated contribution.

Name of Co-Author	Prof. Andrei Kotousov		
Contribution to the Paper	Supervision, and provided major contribution on manuscript writing		
Signature		Date	24/ 08 / 2021

Name of Co-Author	Prof. Ricardo Branco		
Contribution to the Paper	Participated in manuscript review and evaluation		
Signature		Date	23 / 08 / 2021

Name of Co-Author			
Contribution to the Paper			
Signature		Date	



An analytical-based approach for simulating fatigue crack growth in round bars

Behnam Zakavi · Andrei Kotousov · Ricardo Branco 

Received: 7 December 2020 / Accepted: 8 June 2021
© The Author(s), under exclusive licence to Springer Nature B.V. 2021

Abstract This paper presents an analytical-based approach to simulate fatigue growth of surface cracks in round bars subjected to cyclic tension and/or bending. The proposed approach assumes a part-elliptical crack front shape, and it is capable to incorporate plasticity-induced crack closure models. In addition, it is mesh-insensitive, easy to implement, and much faster than the numerical methods which are currently utilised for the same purpose. In the beginning, it is developed, in orthogonal elliptical coordinates, a governing equation describing the crack shape evolution. Then, the governing equation is extended to incorporate plasticity-induced crack closure effects. Further, it is investigated the main parameters affecting fatigue crack growth in round bars, in particular, the initial crack length, the loading conditions and, the material properties. Finally, the outcomes of fatigue crack growth simulations based on the proposed approach are compared with published experimental and theoretical studies. Overall, an excellent agreement can be observed.

Keywords Round bars · Surface cracks · Crack shape evolution · Equivalent thickness concept

1 Introduction

Accurate evaluation of fatigue crack growth in cylindrical metallic components is an important part of safe design of many typical structural components subjected to cyclic loading (Zakavi et al. 2019; Hobbs et al. 2000). In general, fatigue failure of such components is associated with the initiation and propagation of surface defects, which can be introduced by the manufacturing process or originated from irreversible shear slip bands during fatigue loading (Yang et al. 2006; Caspers et al., 1990). The introduction of notches, which is inevitable in engineering design, originates complex stress–strain states nearby the surface and strong tri-dimensional effects, increasing the importance of the fatigue crack propagation stage (Berto et al. 2004; Pook 2013; Zakavi et al. 2021a, b).

Failure process, and in particular, the crack front shape evolution, in cylindrical metallic components subjected to fatigue loading has been studied experimentally or using numerical methods by many researchers (Carpinteri 1992, 1993; Lin and Smith 1997, 1998; Couroneau and Royer 1998). From the previous studies, it was found that the crack front

B. Zakavi · A. Kotousov
School of Mechanical Engineering, The University of
Adelaide, Adelaide, SA 5005, Australia

R. Branco (✉)
Department of Mechanical Engineering, CEMMPRE,
University of Coimbra, Rua Luís Reis Santos,
3030-788 Coimbra, Portugal
e-mail: ricardo.branco@dem.uc.pt

shape evolution is governed by several parameters, among the most significant are the loading conditions, the stress ratio, the material properties, and the initial crack geometry (Shin and Cai 2004; Toribio et al. 2009, 2014; Hou 2008; Branco et al. 2012). This substantial number of parameters makes the problem of fatigue analysis quite challenging, specifically for parametric or sensitivity studies, which require multiple evaluations.

The past investigations have demonstrated that the shapes of surface cracks in circular cross-section components formed by cyclic tension, bending or combined tension-bending can be, in most cases, well approximated by part-elliptical curves (Carpinteri 1992; Lin and Smith 1997; Branco et al. 2012). These findings have enabled the development of several simplified numerical approaches, usually based on the Finite Element Method, which assume a crack front with a semi-elliptical shape during fatigue growth (Carpinteri 1993; Toribio et al. 2014). Based on this useful simplification, the simulated crack fronts and fatigue crack growth predictions were found to be close to the experimental observations.

The main drawbacks of numerical simulations are the issues associated with the mesh optimisation, since the results are mesh-sensitive, as well as the development and implementation of the automatic crack growth subroutines, which are not available in the current commercial software packages, making the process of fatigue analysis laborious and time consuming (Lin and Smith 1997; Branco et al. 2015). Therefore, the development of mesh-independent and efficient procedures, capable of simulating the crack front shape evolution in round bars for various loading conditions and parameters, is of great practical interest.

In the analysis of fatigue phenomena, the effective range of the stress intensity factor is normally considered as a driving force of the crack propagation process. Published results often indicate some discrepancies in the evaluation of the stress intensity factors, specifically for complex 3D geometries and near the free surfaces (James and Mills 1998; Salah and Lovegrove 1981). A possible explanation of these discrepancies can be the limited computer resources used in the early studies, particularly for the analysis of 3D cracked geometries (Kotousov et al. 2018). However, with the increasing of computational power, these differences have been successively eliminated,

except at the so-called “surface layer”, controlled by the 3D corner singularity (He et al. 2015, 2016), where the differences may reach 20–50% (Kotousov et al. 2018). One approach to deal with the surface layer effect is to simply ignore the numerical results in this region and use extrapolation techniques to evaluate the stress intensity factor within the surface layer (Shin and Cai 2004; James and Mills 1998; Salah and Lovegrove 1981).

Another critical point in the analysis of fatigue crack growth is related to crack closure effects, such as roughness, oxide, and plasticity-induced crack closure. The first two closure mechanisms, as it is well-known from the previous studies, tend to be significant near the fatigue threshold regime but, in general, are not particularly significant in the so-called Paris region. In contrast, the plasticity-induced crack closure is usually more profound in this region (Paris region), which is of interest in fatigue analysis. Different analytical and numerical approaches have been developed over the last years to model this phenomenon (Elber 1971; Antunes et al. 2010; Codrington and Kotousov 2009; Yu and Guo 2012; Shen and Guo 2005).

Numerical models to simulate plasticity-induced crack closure, particularly those based on the Finite Element Method, have been developed mostly for plane and 2D geometries (Antunes et al. 2010; Camas et al. 2020; Codrington and Kotousov 2009; Yu and Guo 2012). However, due to the complexity associated with the direct computations and the necessity to introduce several assumptions regarding the crack-opening threshold, the numerical results are not very reliable, always need an independent validation, and have to be used with caution (Garcia-Manrique et al. 2018). In this context, simplified analytical models represent an alternative way to account for the effects of the plasticity-induced crack closure on fatigue crack growth rates and fatigue life of the component.

The application of an analytical crack closure model has several advantages when compared to the numerical approaches (Zakavi et al. 2021a, b). Firstly, it does not require any discretisation of the crack front or even the cracked body. Secondly, it does not need the development of automatic crack growth schemes, which makes the process faster, easier to reproduce, as well as mesh-independent. Last, but not least, the crack front shape evolution can be studied on the basis of two arbitrary points located along the crack front,

eliminating the errors associated with the effects of the surface layer and the corner points (Berto and Lazzarin 2011; Garcia-Manrique et al. 2018; Kotousov et al. 2019; Zakavi et al. 2021a, b).

The present paper aims at developing an analytical-based approach to study the fatigue crack propagation in round bars weakened by surface cracks. This approach assumes a part-elliptical crack front shape during the entire fatigue growth, and it accounts for the plasticity-induced crack closure by incorporating an appropriate analytical model. It can be easily adopted for practical fatigue analysis of engineering components with circular cross-sections (e.g. shafts, cables, wires, bolts, screws, etc.), as it does not require numerical simulations or commercial software, but also for parametric studies. Moreover, it is simpler to implement and significantly faster than the current design methods. Another interesting feature is its mesh-independency, avoiding convergence issues or optimisation tasks. The paper is organised as follows: Sect. 2 introduces the governing equations and the plasticity-induced crack closure model; Sect. 3 is focused on crack shape validation using experimental results; Sect. 4 analyses the effects of crack shape, crack length, loading conditions, propagation rates and stress ratio on fatigue crack growth. The paper ends with some concluding remarks.

2 Fatigue crack propagation model

2.1 Crack shape

This section aims at deriving a governing equation, which describes the evolution of crack front shape during fatigue crack growth. Since the crack fronts have a pre-defined part-elliptical shape, and in order to simplify the analysis, the problem is addressed using orthogonal elliptical coordinates, as shown in Fig. 1. In the beginning, it is developed an inverse relationship between the crack aspect ratio (a/b) and the displacement at an arbitrary location along the crack front, ds , which can be associated with the incremental changes of the semi-axes, da and db (see Fig. 1).

The correlation between the orthogonal elliptical coordinates (ξ, η) and the rectangular coordinate system (x, y) can be established by the following equations (Zakavi et al. 2019):

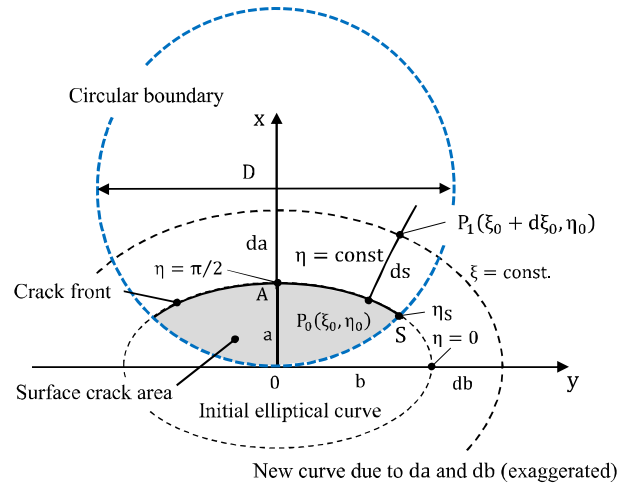


Fig. 1 Elliptical coordinates and crack front change

$$x = c \sinh \xi \sin \eta \tag{1a}$$

$$y = c \cosh \xi \cos \eta \tag{1b}$$

where

$$c = \sqrt{b^2 - a^2} \tag{2}$$

which represents the half focal length. The length of semi-axes, a and b , can be found by setting that $\xi = \xi_0$ and $\eta = \pi/2$ and 0 , respectively, leading to:

$$a = c \sinh \xi_0 \tag{3a}$$

$$b = c \cosh \xi_0 \tag{3b}$$

where ξ_0 is defined by Eq. (4). For surface cracks in round bars, it is expected that $b \geq a$ or $\beta = a/b \leq 1$. Thus, any point P on the ellipse can be identified by its rectangular coordinates (x, y) and elliptical coordinates (ξ, η) where $0 < \eta < 2\pi$.

$$\xi_0 = \operatorname{atanh}\left(\frac{a}{b}\right) \tag{4}$$

If it is considered the change of crack shape due to a small increment dc and $d\xi_0$, then it can be written:

$$da = dc \sinh \xi_0 + d\xi_0 c \cosh \xi_0 \tag{5a}$$

$$db = dc \cosh \xi_0 + d\xi_0 c \sinh \xi_0 \tag{5b}$$

and the increments dc and $d\xi_0$ can be defined by the following equations:

$$dc = db \cosh \xi_0 - da \sinh \xi_0 \tag{6a}$$

$$d\xi_0 = \frac{da \cosh \xi_0 - db \sinh \xi_0}{c} \tag{6b}$$

where the new elliptical curve can be obtained by replacing c and ξ_0 with $c + dc$ and $\xi_0 + d\xi_0$, respectively.

The distance between a point P_0 with coordinates (ξ_0, η_0) located on the initial elliptical curve representing the initial crack front shape and a point P_1 located on the new elliptical curve (see Fig. 1) can be computed as an intersection of the orthogonal segment given by $(\xi_0 + d\xi, \eta_0)$ and the new elliptical curve obtained with increments da and db . Thus, the rectangular coordinates of point $P_1(x_{P1}, y_{P1})$ can be written in the form:

$$\begin{aligned} x_{P1} &= c \sinh(\xi_0 + d\xi) \sin \eta_0 \\ &= (c + dc) \sinh(\xi_0 + d\xi_0) \sin(\eta_0 + d\eta) \end{aligned} \tag{7a}$$

$$\begin{aligned} y_{P1} &= c \cosh(\xi_0 + d\xi) \cos \eta_0 \\ &= (c + dc) \cosh(\xi_0 + d\xi_0) \cos(\eta_0 + d\eta) \end{aligned} \tag{7b}$$

for the elliptical coordinate system on the basis of both the initial crack shape and the new crack shape.

If it is used a Taylor expansion of hyperbolic and trigonometric functions and exclude the variable $d\eta$, the increment $d\xi$ can be defined by Eq. (8)

$$d\xi = \frac{1}{c} \frac{\cosh \xi_0 \sin^2 \eta_0 da + \sinh \xi_0 \cos^2 \eta_0 db}{\cosh^2 \xi_0 \sin^2 \eta_0 + \sinh^2 \xi_0 \cos^2 \eta_0} \tag{8}$$

The value of ds (see Fig. 1), i.e. the length of the segment $|P_0P_1|$, is given by Eq. (9). If $d\xi$ of Eq. (8) is replaced into Eq. (9), it leads to Eq. (10).

$$ds = c \sqrt{\cosh^2 \xi_0 \sin^2 \eta_0 + \sinh^2 \xi_0 \cos^2 \eta_0} d\xi \tag{9}$$

$$ds = \frac{\cosh \xi_0 \sin^2 \eta_0 da + \sinh \xi_0 \cos^2 \eta_0 db}{\sqrt{\cosh^2 \xi_0 \sin^2 \eta_0 + \sinh^2 \xi_0 \cos^2 \eta_0}} \tag{10}$$

Let us define the aspect ratio of the ellipse $\beta = a/b$. After some algebraic manipulations, Eq. (10) yields to Eq. (11).

$$ds = \frac{\tan^2 \eta_0 + \left(\frac{1}{\beta} - \frac{a}{\beta^2} \frac{d\beta}{da}\right) \tanh \xi_0}{\sqrt{\tan^2 \eta_0 + \tanh^2 \xi_0}} \cos \eta_0 da \tag{11}$$

The ratio of the normal distances between the initial and the new curves at the deepest point ($\eta = \pi/2$) and at an arbitrary point ($\eta = \eta_0$), i.e. ds/da , taking into

account Eq. (11) and Eq. (4), can be re-written by Eq. (12).

$$\frac{ds}{da} = \frac{\tan^2 \eta_0 + \left(1 - \frac{a}{\beta} \frac{d\beta}{da}\right)}{\sqrt{\tan^2 \eta_0 + \beta^2}} \cos \eta_0 \tag{12}$$

2.2 Fatigue crack growth

The fatigue crack growth rates can be accounted for using the well-known Paris equation (Paris and Erdogan, 1963):

$$\frac{da}{dN} = C(\Delta K)^m \tag{13}$$

where C and m are material constants determined experimentally for the tested material. Based on this equation, the relative speed at an arbitrary point η normalised by the speed at the deepest point of the crack front $\eta = \pi/2$ (point A) is given by Eq. (14).

$$\bar{V}(\eta) = \left(\frac{\Delta K(\eta)}{\Delta K(\pi/2)}\right)^m = \frac{\tan^2 \eta + \left(1 - \frac{a}{\beta} \frac{d\beta}{da}\right)}{\sqrt{\tan^2 \eta + \beta^2}} \cos \eta \tag{14}$$

From the previous equation, after some algebraic manipulations, the crack shape evolution leads to an ordinary differential equation written in the following form:

$$\frac{\partial \beta}{\partial \delta} = \frac{\beta}{\delta} \left(1 + \tan^2 \eta - \left(\frac{\Delta K(\eta)}{\Delta K(\pi/2)}\right)^m \frac{\sqrt{\tan^2 \eta + \beta^2}}{\cos \eta}\right) \tag{15}$$

where $\delta = a/D$ is the ratio of the crack depth to the diameter of the bar, and $0 < \delta < 1$.

It is clear from Eq. (15) that a stress intensity factor solution for any two arbitrary points can be used in the analysis of crack shape evolution. Most of the stress intensity factor solutions proposed in the past for round bars with surface cracks have been typically obtained for the deepest point, i.e. $\eta = \pi/2$, and the surface point, i.e. $\eta = \eta_S$ (see Fig. 1). Therefore, this work will also be focused on the evaluation of the fatigue crack shape evolution based on these two characteristic points of the crack front. The elliptical coordinates of the surface point (S) can be found as an intersection of the circle describing the outer boundary

of the bar cross-section and the elliptical curve, as follows:

$$\begin{aligned} & \sinh^2 \xi \sin^2 \eta_S + \cosh^2 \xi \cos^2 \eta_S \\ &= \frac{\beta}{\delta \sqrt{1 - \beta^2}} \sinh \xi \sin \eta_S \end{aligned} \tag{16}$$

from which the relationship for two vertex points can be derived, see Eq. (17).

$$\cos \eta_S = \pm \sqrt{1 - \left(\frac{\beta^2 - \sqrt{\beta^4 - 4\delta^2(\beta^2 - 1)}}{2\delta(\beta^2 - 1)} \right)^2} \tag{17}$$

For fatigue life and shape evolution calculations, Eqs. (15) and (16) have to be supplemented with the initial conditions, i.e. $\delta = \delta_0$ and $\beta = \beta_0$, and a suitable stress intensity factor solution reflecting the actual loading conditions, e.g. pure tension, bending or mixed loading. In the case of round bars, the SIF solution is normally represented in the following form:

$$K_I = F_I \left(\beta, \delta, \left| \frac{y}{h} \right| \right) \sigma \sqrt{\pi a} \tag{18}$$

where F_I is the geometric correction factor, σ is the nominal stress, a is the crack depth, and h is the y -coordinate of the surface point S , i.e. the point with $\eta = \eta_S$ (see Fig. 1). So, the ratio $|y/h|$ changes from 0 to 1. Based on Eq. (1), the κ ratio, $\kappa = h/a$, can be defined by:

$$\kappa = \frac{h}{a} = \sqrt{\beta^{-2} - 1} \cosh(\text{atan } \beta) \cos \eta_S \tag{19}$$

where η_S is given in Eq. (17). In the present study it will be considered the closed-form solution provided by Shin et al. (2004), whose geometry correction factor can be written as follows:

$$F_I = \sum_{i=0}^2 \sum_{j=0}^7 \sum_{k=0}^2 M_{ijk} \beta^i \delta^j \left(\left| \frac{y}{h} \right| \right)^k \tag{20}$$

where the coefficients M_{ijk} for the end-free and end-constrained axial tension, and bending can be found in the original paper by the authors (Shin and Cai 2004).

2.3 Plasticity-induced crack closure model

This section deals with a specific analytical model of plasticity-induced crack closure, however, other

models can be easily implemented as well. First introduced by Elber in the early seventies of the past century (Elber 1970, 1971), crack closure concept is often used to explain various aspects of metal fatigue (Antunes et al. 2010; Codrington and Kotousov 2009; Yu and Guo 2012). In accordance with this concept, the stress intensity factor range, ΔK , is replaced by the effective stress intensity factor range, ΔK_{eff} , to reflect the damage accumulation when the crack tip is closed. The effective stress intensity factor range, ΔK_{eff} , is defined by:

$$\Delta K_{\text{eff}} = U \Delta K = U(K_{\text{max}} - K_{\text{min}}) = K_{\text{max}} - K_{\text{op}} \tag{21}$$

where K_{max} and K_{min} are the maximum and minimum values of the stress intensity factor during the fatigue cycle, respectively, and U is the normalised load ratio parameter, which is often utilised to describe the effects of the loading and geometry on crack closure. If crack closure phenomena are considered, the governing equation of crack shape evolution can be rewritten as:

$$\frac{\partial \beta}{\partial \delta} = \frac{\beta}{\delta} \left(1 + \tan^2 \eta - \left(\frac{U_S \Delta K_S}{U_A \Delta K_A} \right)^m \frac{\sqrt{\tan^2 \eta + \beta^2}}{\cos \eta} \right) \tag{22}$$

where index A corresponds to the deepest point ($\eta = \pi/2$), and index S is related to the surface point ($\eta = \eta_S$).

When the calculated crack aspect ratios, $\beta(\delta)$, are compared to the experimental data, it is clear that the Paris equation overestimates the crack growth rate at the free surface. Based on these observations, several researchers have assumed a fixed ratio of the crack closure at the surface point to the deepest point, U_S/U_A . The typical values of U_S/U_A are within the interval 0.8–0.9 and provide a much better correlation with the experimental observations (Newman and Raju 1984).

However, it is clear that the normalised load ratio parameter, U , is not a constant and changes with the geometry and loading conditions. In this paper, a more advanced model based on the equivalent thickness concept is used to account for the crack closure effect (Yu and Guo 2012; Shen and Guo 2005). In this model, the normalised load ratio, U , is represented by the following equation:

$$U(R, \alpha) = \left(\frac{(1 - R^2)^2 (1 + 10.34R^2)}{(1 + 1.67R^{1.61} + \frac{1}{0.15\pi^2\alpha})^{4.6}} \right)^{\frac{1}{3}} \quad (23)$$

The constraint factors for the deepest point (α_A) and the surface point (α_S) are expressed as:

$$\alpha_A = \frac{1 + 0.638g(\lambda)}{1 - 2\nu + 0.54g(\lambda)} \quad (24)$$

$$\alpha_S = 1.181 \quad (25)$$

where $g(x) = x/2 + 2x^2$, $R = K_{\min}/K_{\max}$ is the stress intensity factor ratio, and ν is the Poisson's ratio. The ratio of the plastic zone size to the equivalent thickness is given by:

$$\lambda = \frac{r_p}{t_e} = \frac{\pi}{8t_e} \left(\frac{K_{\max}}{\sigma_f} \right)^2 \quad (26)$$

where σ_f is flow stress of the material, and t_e is the equivalent thickness which for the deepest point is the distance between the intersection points of the circle boundary with the line tangential to the deepest point. It is parallel to the horizontal x-axis and passes through the deepest point:

$$t_e = \sqrt{D a - a^2} \quad (27)$$

where D is the diameter of the bar (see Fig. 1). In the case of a very small plastic zone ahead of the crack front, or when $\lambda \rightarrow 0$, the ratio U_S/U_A becomes:

$$\frac{U_S}{U_A} = \frac{U(R, 1.181)}{U(R, 2.5)} \quad (28)$$

and it can be demonstrated by direct calculations using Eqs. (23)–(27) that this ratio increases with an increase of the R ratio, and varies between 0.8 and 0.9 for $\nu = 0.3$, i.e. it is consistent with previous studies, as highlighted above (Newman and Raju 1984).

3 Experimental validation

The experimental validation of the crack shape evolution has been carried out using data published in the papers by Yang et al. (2006) and by Branco et al. (2012). Briefly, the material utilised was a S45 carbon steel, whose main mechanical properties and fatigue crack growth rates are summarised in Tables 1 and 2, respectively. The specimen geometry, as represented

Table 1 Mechanical properties of S45 steel

Tensile strength, σ_{UTS} (MPa)	Yield strength, σ_{YS} (MPa)	Young's modulus, E (GPa)	Poisson's ratio, ν
775	635	206	0.3

Table 2 Fatigue crack growth rates (da/dN [mm/cycle] and ΔK [MPa \sqrt{m}] of S45 steel

Stress ratio, R	Constant of Paris equation, C	Exponent of Paris equation, m
0.1	1.9037×10^{-9}	3.256

in Fig. 2, was a solid round bar with a diameter of 12 mm and an initial straight edge front crack with a depth of 1 mm.

The tests were conducted in a conventional servo-hydraulic machine, under uniaxial loading conditions, with a stress ratio equal to 0.1, a frequency of 15 Hz and, and a maximum applied force of 25 kN (Yang et al. 2006; Branco et al. 2012). The crack shape was evaluated using a stereomicroscope and the crack fronts were marked on fracture surface by applying overloads at selected instants of the test. A typical example of the appearance of fracture surfaces obtained in the experimental tests is exhibited in Fig. 3a.

As can be seen in Fig. 3a, the crack front shapes marked on the fracture surface are rather symmetrical with regard to a vertical line passing through the centre of the specimen, which agrees with the expected results for round bars subjected to mode-I loading (Carpinteri 1993; Lin and Smith, 1997; Branco et al. 2014). In the case of more complex loading scenarios, e.g. multiaxial loading, the crack front tends to be asymmetrical because the crack growth is governed by mixed-mode loading, causing strong crack front shape changes during the propagation and also higher degrees of out-of-plane propagation (Zhu et al. 2018; Branco et al. 2014).

The comparison between the experimental observations and the theoretical predictions is presented in Fig. 3b for two sets of simulations, i.e. without plasticity-induced crack closure (obtained from Eq. (15)) and with plasticity-induced crack closure

Fig. 2 Specimen geometry used in the cyclic testing program (dimensions in millimetres)

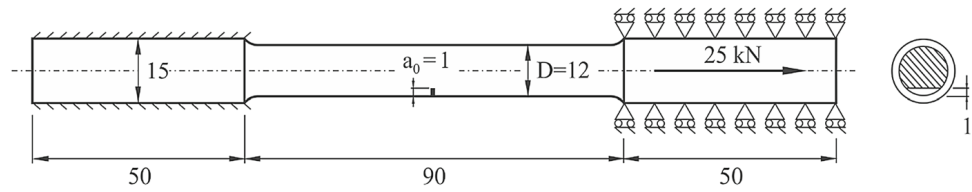
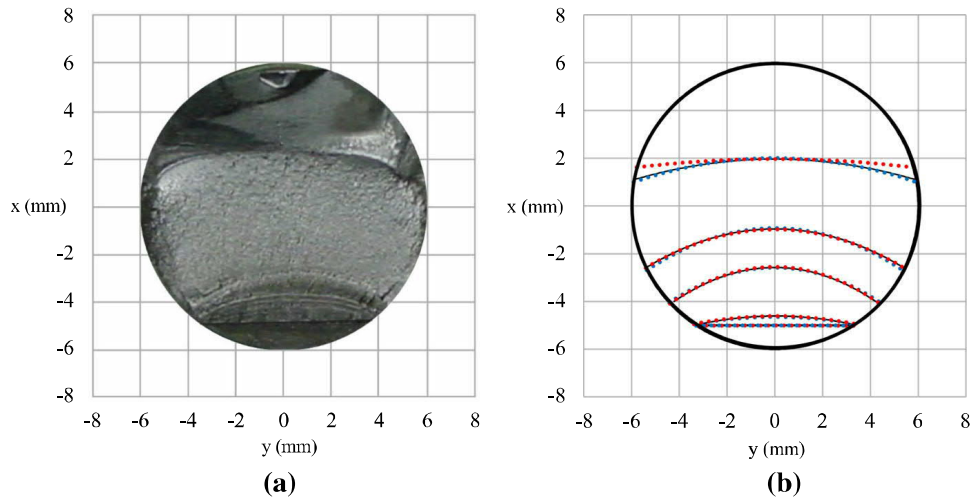


Fig. 3 a The cross section of a round bar with crack front marks; and **b** comparison of theoretical simulations with experimental data (black lines represent experimental data; red lines represent simulations without crack closure; blue lines represent simulations with crack closure)



included through the equivalent thickness model (obtained from Eq. (22)). Overall, the predicted crack fronts in the entire region studied are close to those found in the experiments. A close analysis shows that at the initial stages of fatigue crack growth, there is no or little difference between the experimental data and analytical simulations. However, at later stages, the simulations incorporating the plasticity-induced crack closure effects provide better agreement with the experimental data. This can be explained by the fact that crack closure effects are more pronounced with an increase of the plastic zone size, which becomes larger with the progression of the surface crack subjected to constant amplitude fatigue loading.

4 Analysis and discussion

Figure 4 displays typical examples of the analytical simulations obtained with the proposed approach for different propagation conditions, namely different initial crack lengths, initial crack shapes, exponents of the Paris law, loading types, and crack closure levels. Overall, it can be clearly distinguished significant changes during the propagation which is a good

indication regarding the robustness of the proposed approach.

The sensitiveness of the proposed procedure to the initial crack length can be clearly observed by comparing Fig. 4a, b. In these two simulations, the initial values of the dimensionless crack shape (a_0/b_0) are similar ($a_0/b_0 = 0.5$) and the initial values of the dimensionless crack length (a_0/D) are equal to 0.15 and 0.1, respectively. In fact, the crack front shapes are relatively different, as the crack propagates; however, after some extent, the crack shapes tend to a similar configuration. Previous studies conducted in round bars with surface cracks subjected to constant-amplitude loading have found an identical behaviour (Carpinteri 1992, 1993; Lin and Smith 1997, 1998; Couroneau and Royer 1998).

Regarding the initial crack front shape, its effect on crack front evolution can be distinguished from the analysis of Fig. 4b, c. In both cases, the initial crack length is similar ($a_0/D = 0.1$) while the initial values of the dimensionless crack shapes (a_0/b_0) are equal to 0.5 and 0.25, respectively. It can be seen that the crack fronts at the early stage of propagation are significantly different, but tend to the same shape, as the crack grows. According to the literature, the effect of

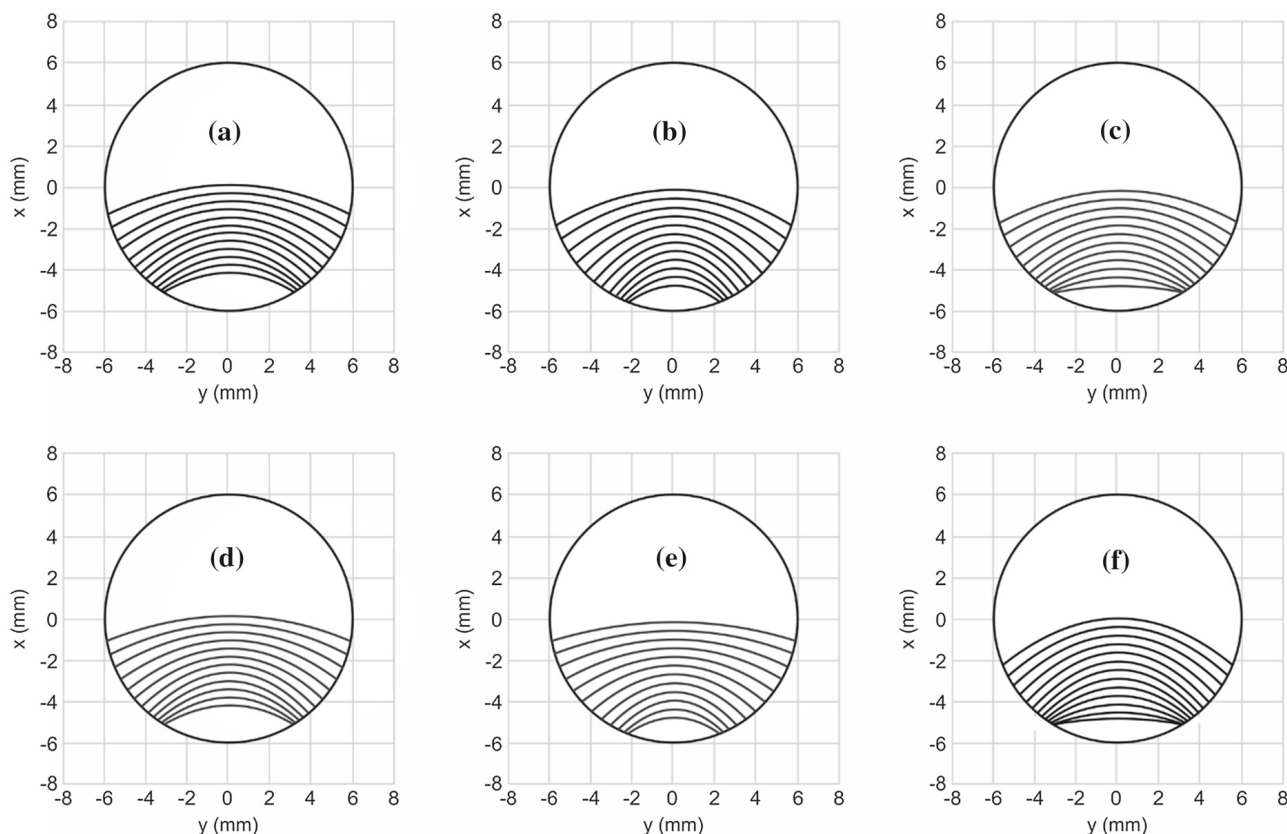


Fig. 4 Analytical simulation of fatigue crack fronts for different propagation conditions: **a** $a_0/b_0 = 0.5$, $a_0/D = 0.15$, $m = 2$, tension; **b** $a_0/b_0 = 0.5$, $a_0/D = 0.1$, $m = 2$, tension; **c** $a_0/b_0 = 0.25$,

$a_0/D = 0.1$, $m = 3$, tension; **d** $a_0/b_0 = 0.5$, $a_0/D = 0.15$, $m = 4$, tension; **e** $a_0/b_0 = 0.5$, $a_0/D = 0.1$, $m = 3$, tension; **f** $a_0/b_0 = 0.25$, $a_0/D = 0.1$, $m = 3$, tension, crack closure

the initial crack shape has an important role at the early stage of crack growth but tends to disappear after some extent (Lin and Smith 1997, 1998; Branco et al. 2012).

Another important variable that affects the crack shape evolution in round bars with surface cracks is the exponent of Paris law (m). Figure 4a, d plot the crack front shape evolution for two values of m , respectively equal to 3 and 4, maintaining fixed the other variables. Although the differences between these two cases are not completely obvious, a close look at the simulations shows a higher crack front curvature for higher values of m , particularly for lower crack lengths. Unlike the initial crack length and the initial crack shape, the m value affects the entire propagation and not only the early stage (Couroneau and Royer 1998; Toribio et al. 2009; Branco et al. 2014).

The loading scenario also has a significant effect on crack shape evolution in round bars weakened by surface cracks. Figure 4b, e compare a simulation

conducted for tension and a simulation conducted for bending, respectively, maintaining fixed the other variables. The analysis of both figures shows a significant effect of this variable on crack front developments. Under tension, the crack fronts tend to be more curved, as the crack extends. On the contrary, under bending, the crack fronts tend to be straighter. Identical conclusions have been reported in previous studies, either based on experimental studies or numerical simulations (Carpinteri 1992, 1993; Lin and Smith 1997, 1998; Couroneau and Royer 1998).

The influence of crack closure mechanisms can be distinguished from the analysis of Fig. 4c, f. Both simulations have been conducted for identical propagation conditions, but the latter case considers the crack closure model introduced in the present paper, while the former discards crack closure phenomena. Not surprisingly, the crack fronts obtained from the model which accounts for crack closure are more curved than those generated discharging the plasticity-

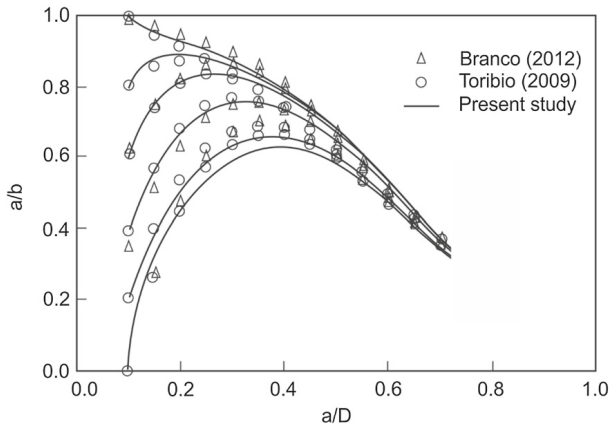


Fig. 5 Evolution of crack paths, in a dimensionless form, for different initial crack front shapes subjected to tension ($a_0/D = 0.1$, $m = 3$, no crack closure)

induced crack closure mechanisms. In fact, crack closure tends to retard the propagation at the free surface, which inevitably leads to crack shapes with higher degree of curvature (Carpinteri et al. 2010).

Despite the previous analysis has identified the typical behaviour of main variables affecting the fatigue crack growth in round bars subjected to tension and bending, a more accurate analysis requires the use of dimensionless parameters (Branco et al. 2015). Figure 5 plots the crack shape evolution in a dimensionless form (full lines) obtained from different initial crack shapes with values of a_0/b_0 varying between 1 and 0. All the other variables were maintained fixed. As it can be seen, at the early stage of growth, the crack shape evolution is strongly governed by the initial value of the dimensionless crack shape.

However, as the crack extends, this effect tends to be less relevant and there is a convergence to the so-called stable crack shape. It is clear from the figure that the time required to reach the stable crack shape depends on the initial crack shape; crack fronts more distant from this equilibrium need more time to attain it and vice-versa. It is also interesting to note that the values obtained with the present approach are quite close to those published in the literature by Branco et al. (2012) and Toribio et al. (2009) for the same propagation conditions. The two above-mentioned studies were conducted using automatic fatigue crack growth approaches. The former study considered no crack shape restraints, while the latter assumed a part-elliptical crack front.

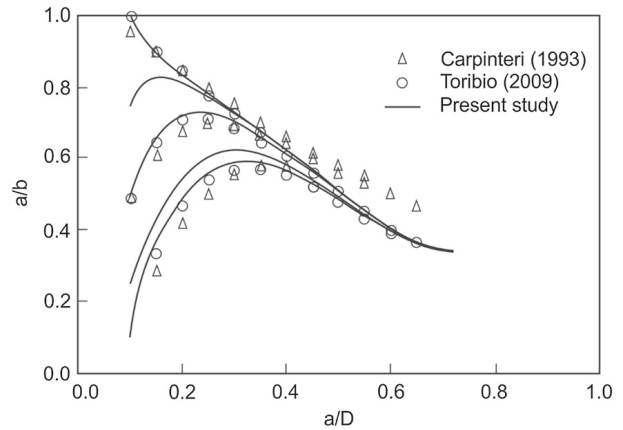


Fig. 6 Evolution of crack paths, in a dimensionless form, for different initial crack front shapes subjected to bending ($a_0/D = 0.1$, $m = 3$, no crack closure)

Regarding bending loads, the comparative analysis plotted in Fig. 6 leads to similar conclusions, i.e. a strong effect of the initial crack shape on the crack trajectories at the early state of propagation; there is also a stable crack shape independent of the initial crack geometry; and the time required to attain the stable configuration depends on the initial distance from the equilibrium. In addition, it can be also concluded that the simulated crack front paths are quite close to those found in the literature for the same propagation conditions, particularly the ones published by Toribio et al. (2009).

As referred to above, the effect of the Paris law exponent acts during the entire propagation. This has a direct effect not only at the early stage of propagation, but also concerning the stable crack paths. Figure 7

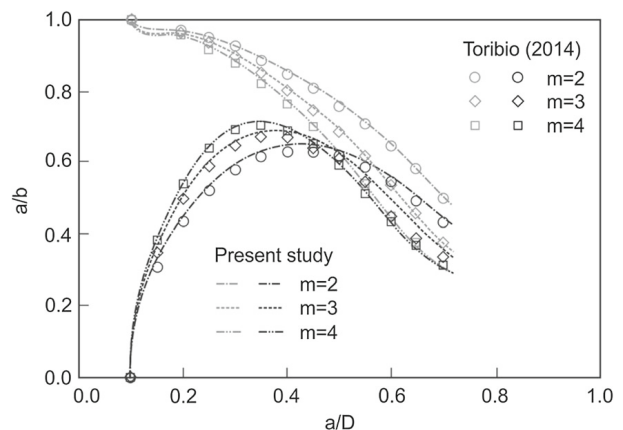


Fig. 7 Evolution of crack paths, in a dimensionless form, for different initial crack front shapes subjected to tension assuming different values of the exponent of Paris law ($a_0/D = 0.1$, $m = 3$, no crack closure)

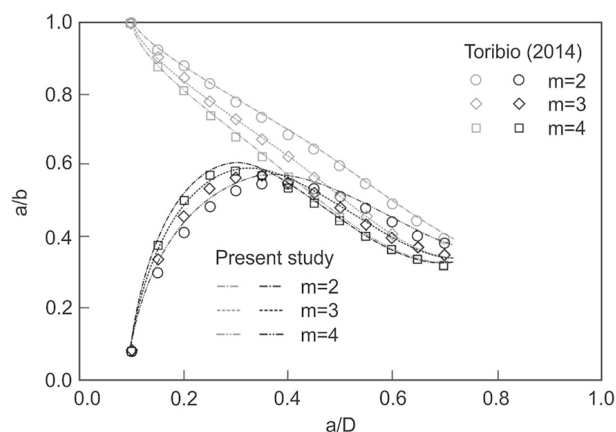


Fig. 8 Evolution of crack paths, in a dimensionless form, for different initial crack front shapes subjected to bending assuming different values of the exponent of Paris law ($a_0/D = 0.1$, $m = 3$, no crack closure)

shows the crack paths simulated for three values of m ($m = 2$, $m = 3$, and $m = 4$) considering two initial crack fronts ($a_0/b_0 = 1$, and $a_0/b_0 = 0$) and tension loads. As can be seen, there are independent trajectories, represented by the dashed lines, throughout the simulations for each value of the Paris law exponent. However, after some propagation, and regardless of the initial crack shape, the trajectories for the same value of m tend to the same stable crack shape. Overall, it can also be seen a strong similarity between the results obtained in the present study and those published by Toribio et al. (2014) for identical propagation conditions.

As far as bending loading is concerned, the effect of the Paris law exponent is exhibited in Fig. 8. The simulations were conducted for two initial crack configurations ($a_0/b_0 = 1$, and $a_0/b_0 = 0.1$) considering three values of m ($m = 2$, $m = 3$, and $m = 4$). Similar to tension, there is an independent trajectory for each value of the Paris law exponent. Nevertheless, for a fixed value of m , independently of the initial crack shape, the crack paths tend to converge to the same crack configuration. It is also clear that this convergence is faster for higher values of m , since the interception of the curves occurs faster. Another interesting outcome is that the results obtained in the present simulations are close to those found in literature (Toribio et al. 2014).

The dimensionless uncracked area parameter (A^*), defined as the ratio of the uncracked area to the cross-sectional area of the round bar, is an alternative parameter that can be used to examine the crack front

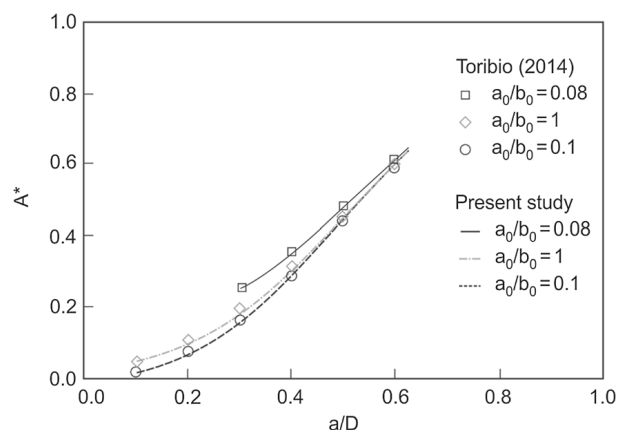


Fig. 9 Evolution of the dimensionless cracked area for different initial crack fronts subjected to tension

shapes computed with the proposed methodology. Figure 9 plots the variation of A^* against the dimensionless crack length (a/D) for two initial crack shapes ($a_0/b_0 = 1$ and $a_0/b_0 = 0.08$) and two initial crack lengths ($a_0/D = 0.1$ and $a_0/D = 0.3$) considering tension loading. As can be seen, this parameter is sensitive to the initial crack shape. At the early stage, the curves are relatively far from each other; however, in a second stage, they tend to overlap. Regarding the values of A^* published in the literature for the tension loading, there is no relevant differences (Toribio et al. 2014). Although it is not represented in the figure, an identical behaviour has been found for bending loading.

Another important analysis is concerned with the accuracy of the stress intensity factor values. Figure 10 compares the value of the geometric correction factor at the free surface of the round bar for tension and bending loads considering different initial crack

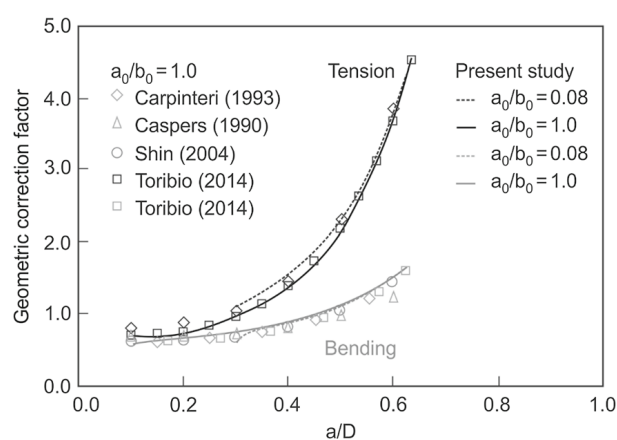


Fig. 10 Evolution of stress intensity factor at the free surface under tension and bending for round bars with surface cracks

shapes ($a_0/b_0 = 1$ and $a_0/b_0 = 0.08$) and different initial crack lengths ($a_0/D = 0.1$ and $a_0/D = 0.3$). As expected, the geometric correction factor increases, as the crack propagates, regardless of the loading type. In addition, the convergence to the same stress intensity factor curve occurs irrespective of the initial crack shape. It is also clear from the figure that convergence is more rapid for bending than for tension.

This behaviour, i.e. the convergence towards similar values, is expected since stress intensity factors are interconnected with the crack shapes. Therefore, if the crack fronts tend to similar shapes, as shown in Fig. 4, the stress intensity factors should have a similar behaviour. Moreover, it can also be inferred from the figure that the stress intensity factor values, at a given crack length, are higher for tension than for bending. This difference tends to increase with the propagation, and it suggests that the risk of failure for tension is higher than for bending (Shin and Cai 2004; Toribio et al. 2014). Regarding the stress intensity factors available in the literature, the results computed here are quite close to those published by different authors, either for tension or bending (Carpers et al., 1990; Carpinteri, 1993; Toribio et al. 2014; Levan and Royer, 1993).

5 Conclusions

The present paper proposed an analytical approach to simulate the crack shape evolution in round bars with surface cracks subjected to tension and/or bending loads. It is mesh-independent avoiding convergence issues or complex implementation procedures. It is also capable to incorporate the effects of plasticity-induced crack closure using various crack closure models. In the current study, the plasticity-induced crack closure model based on the equivalent thickness concept was incorporated. The following main conclusions can be drawn:

1. The fatigue crack growth in round bars subjected to constant-amplitude tension or bending is very sensitive to the following parameters: initial crack length, initial crack shape, exponent of the Paris law, loading scenario, and plasticity-induced crack closure;
2. The comparison between the crack paths obtained with different values of initial crack length, initial crack shape, loading type and exponent of Paris law were quite close to those published in the literature for the same propagation conditions;
3. The analysis of the dimensionless uncracked area has shown a high sensitivity to the initial crack shape, either for tension or bending. The comparison with existing results has demonstrated identical trends to those computed with the proposed approach;
4. The stress intensity factor values for the same dimensionless crack length were higher for tension than for bending, which suggests higher susceptibility to fatigue failure in the former case. This agrees with previous conclusions drawn in the literature.

The excellent coherency between the predicted crack shapes and the results available in literature becomes the proposed analytical approach very attractive for parametric studies of round bars weakened by surface cracks subjected to tension and/or bending. Since this approach does not require any numerical simulation or any advanced commercial software to simulate the crack shape evolution, it can also be easily adopted for practical fatigue analysis, in a rapid and accurate manner.

Acknowledgments This research is sponsored by FEDER funds through the program COMPETE – Programa Operacional Factores de Competitividade – and by national funds through FCT – Fundação para a Ciência e a Tecnologia – under the project UIDB/00285/2020.

References

- Antunes FV, Branco B, Costa JD, Rodrigues DM (2010) Plasticity induced crack closure in middle-crack tension specimen: numerical versus experimental. *Fatigue Fract Eng Mater Struct* 33:673–686
- Berto F, Lazzarin KA (2011) On higher order terms and out-of-plane singular mode. *Mech Mater* 43:332–341
- Berto F, Lazzarin P, Wang CH (2004) Three-dimensional linear elastic distributions of stress and strain energy density ahead of V-shaped notches in plates of arbitrary thickness. *Int J Fract* 127:265–282
- Branco R, Antunes FV, Costa JD, Yang FP, Kuang ZB (2012) Determination of the Paris law constants in round bars from beach marks on fracture surfaces. *Eng Fract Mech* 96:96–106
- Branco R, Costa JD, Antunes FV (2014) Fatigue behaviour and life prediction of lateral notched round bars under bending-torsion loading. *Eng Fract Mech* 119:66–84

- Branco R, Antunes FV, Costa JD (2015) A review on 3D-FE adaptive remeshing techniques for crack growth modelling. *Eng Fract Mech* 141:170–195
- Camas D, Garcia-Manrique J, Perez-Garcia F, Gonzalez-Herrera A (2020) Numerical modelling of three-dimensional fatigue crack closure: Plastic wake simulation. *Int J Fatigue* 131:105344
- Carpinteri A (1992) Elliptical-arc surface cracks in round bars. *Fatigue Fract Eng Mater Struct* 15:1141–1153
- Carpinteri A (1993) Shape change of surface cracks in round bars under cyclic axial loading. *Int J Fatigue* 15:21–26
- Carpinteri A, Brighenti R, Vantadori S (2010) Influence of the cold-drawing process on fatigue crack growth of a V-notched round bar. *Int J Fatigue* 32:1136–1145
- Caspers M, Mattheck C, Munz D (1990) Propagation of surface cracks in notched and unnotched rods. *Surf Crack Growth* 1060:365–389
- Codrington J, Kotousov A (2009) A crack closure model of fatigue crack growth in plates of finite thickness under small-scale yielding conditions. *Mech Mater* 41:165–173
- Couroneau N, Royer J (1998) Simplified model for the fatigue crack growth analysis of surface cracks in round bars under mode I. *Int J Fatigue* 20:711–718
- Elber W (1970) Fatigue crack closure under cyclic tension. *Eng Fract Mech* 2:37–45
- Elber W (1971). The significance of fatigue crack closure. *Damage Tolerance in Aircraft Structures*, ASTM STP 486, America Society for Testing and Materials
- Garcia-Manrique J, Camas D, Parrón-Rubio ME, Gonzalez-Herrera A (2018) Corrections in numerical methodology to evaluate plasticity induced crack closure along the thickness. *Theor Appl Fract Mech* 97:215–223
- He Z, Kotousov A, Berto F (2015) Effect of vertex singularities on stress intensities near plate free surfaces. *Fatigue Fract Eng Mater Struct* 38:860–869
- He Z, Kotousov A, Berto F, Branco R (2016) A brief review of three-dimensional effects near crack front. *Phys Mesomech* 19:6–20
- Hobbs JW, Burguete RL, Heyes PF, Patterson EA (2000) The effect of eccentric loading on the fatigue performance of high-tensile bolts. *Int J Fatigue* 22:531–538
- Hou CY (2008) Simultaneous simulation of closure behavior and shape development of fatigue surface cracks. *Int J Fatigue* 30:1036–1046
- James LA, Mills WJ (1998) Review and synthesis of stress intensity factor solutions applicable to cracks in bolts. *Eng Fract Mech* 30:641–654
- Kotousov A, Zakavi B, Khanna A, Branco R (2018) On the analysis of structures with cracks of elliptical and part-elliptical shapes. *Theor Appl Fract Mech* 98:149–156
- Kotousov A, Khanna A, Branco R, Jesus A, Correia JA (2019) Review of current progress in 3D linear elastic fracture mechanics. *Mech Fatigue Metals Struct Integrity* 7:125–131
- Levan A, Royer J (1993) Part-circular surface cracks in round bars under tension, bending and twisting. *Int J Fract* 61:71–99
- Lin XB, Smith RA (1997) Shape growth simulation of surface cracks in tension fatigued round bars. *Int J Fatigue* 19:461–469
- Lin XB, Smith RA (1998) Fatigue growth simulation for cracks in notched and unnotched round bars. *Int J Mech Sci* 40:405–419
- Newman JC, Raju IS (1984) Prediction of fatigue crack growth patterns and lives in three-dimensional cracked bodies. In: 6th International conference on fracture, December. New Delhi, pp 4–10
- Paris PC, Erdogan F (1963) A critical analysis of crack propagation laws. *J Basic Eng Trans Am Soc Mech Eng Ser D* 85:528–534
- Pook LP (2013) A 50-year retrospective review of three-dimensional effects at cracks and sharp notches. *Fatigue Fract Eng Mater Struct* 36:699–723
- Salah AS, Lovegrove JM (1981) Stress intensity factors for fatigue cracking of round bars. *Int J Fatigue* 3:117–123
- Shen H, Guo W (2005) 3D constraint effect on 3D fatigue crack propagation. *Int J Fatigue* 27:617–623
- Shin CS, Cai CQ (2004) Experimental and finite element analyses on stress intensity factors of elliptical surface crack in a circular shaft under tension and bending. *Int J Fract* 129:239–264
- Toribio J, Matos JC, González B, Escuadra J (2009) Numerical modelling of crack shape evolution for surface flaws in round bars under tensile loading. *Eng Fail Anal* 16:618–630
- Toribio J, Matos JC, González B, Escuadra J (2014) Numerical modelling of cracking path in round bars subjected to cyclic tension and bending. *Int J Fatigue* 58:20–27
- Yang FP, Kuang ZB, Shlyannikov VN (2006) Fatigue crack growth for straight-fronted edge crack in a round bar. *Int J Fatigue* 28:431–437
- Yu P, Guo W (2012) An equivalent thickness conception for prediction of surface fatigue crack growth life and shape evolution. *Eng Fract Mech* 93:65–74
- Zakavi B, Kotousov A, Khanna A, Branco R (2019) A new method for analysis of part-elliptical surface cracks in structures subjected to fatigue loading. *Theor Appl Fract Mech* 103:102258
- Zakavi B, Kotousov A, Branco R (2021a) Overview of three-dimensional linear-elastic fracture mechanics. *Int J Fract.* <https://doi.org/10.1007/s10704-021-00528-9>
- Zakavi B, Kotousov A, Branco R (2021b) The evaluation of front shapes of through-the-thickness fatigue cracks. *Metals* 11:403
- Zhu SP, Yu ZY, Correia J, Jesus A, Berto F (2018) Evaluation and comparison of critical plane criteria for multiaxial fatigue analysis of ductile and brittle materials. *Int J Fat* 112:279–288

Publisher's Note Springer Nature remains neutral with regard to jurisdictional claims in published maps and institutional affiliations.

Statement of Authorship

Title of Paper	The evaluation of front shapes of through-the-thickness fatigue cracks			
Publication Status	<input checked="" type="checkbox"/>	Published	<input type="checkbox"/>	Accepted for Publication
	<input type="checkbox"/>	Submitted for Publication	<input type="checkbox"/>	Unpublished and Unsubmitted work written in manuscript style
Publication Details	Zakavi, B., Kotousov, A., & Branco, R. (2021). The Evaluation of Front Shapes of Through-the-Thickness Fatigue Cracks. Metals (Basel), 11(3), 403–. https://doi.org/10.3390/met11030403			

Principal Author

Name of Principal Author	Behnam Zakavi		
Contribution to the Paper	Performed analysis, interpreted data, literature review, and co-wrote manuscript		
Overall percentage (%)	50		
Certification:	This paper reports on original research I conducted during the period of my Higher Degree by Research candidature and is not subject to any obligations or contractual agreements with a third party that would constrain its inclusion in this thesis. I am the primary author of this paper.		
Signature		Date	19 / 08 / 2021

Co-Author Contributions

By signing the Statement of Authorship, each author certifies that:

- i. the candidate's stated contribution to the publication is accurate (as detailed above);
- ii. permission is granted for the candidate to include the publication in the thesis; and
- iii. the sum of all co-author contributions is equal to 100% less the candidate's stated contribution.

Name of Co-Author	Professor Andrei Kotousov		
Contribution to the Paper	Research supervision, helped in data interpretation, and co-wrote manuscript		
Signature		Date	23 / 08 / 2021

Name of Co-Author	Prof. Ricardo Branco		
Contribution to the Paper	Performed analysis, and co-wrote manuscript		
Signature		Date	20 / 08 / 2021

Name of Co-Author			
Contribution to the Paper			
Signature		Date	

Article

The Evaluation of Front Shapes of Through-the-Thickness Fatigue Cracks

Behnam Zakavi ^{1,*}, Andrei Kotousov ¹  and Ricardo Branco ²

¹ School of Mechanical Engineering, The University of Adelaide, Adelaide, SA 5005, Australia; andrei.kotousov@adelaide.edu.au

² Department of Mechanical Engineering, CEMMPRE, The University of Coimbra, 3030-788 Coimbra, Portugal; ricardo.branco@dem.uc.pt

* Correspondence: behnam.zakavi@adelaide.edu.au; Tel.: +61-88-313-5439

Abstract: Fatigue failure of structural components due to cyclic loading is a major concern for engineers. Although metal fatigue is a relatively old subject, current methods for the evaluation of fatigue crack growth and fatigue lifetime have several limitations. In general, these methods largely disregard the actual shape of the crack front by introducing various simplifications, namely shape constraints. Therefore, more research is required to develop new approaches to correctly understand the underlying mechanisms associated with the fatigue crack growth. This paper presents new tools to evaluate the crack front shape of through-the-thickness cracks propagating in plates under quasi-steady-state conditions. A numerical approach incorporating simplified phenomenological models of plasticity-induced crack closure was developed and validated against experimental results. The predicted crack front shapes and crack closure values were, in general, in agreement with those found in the experimental observations.

Keywords: crack front shape; structural plates; through-the-thickness crack; steady-state loading conditions; small-scale yielding



Citation: Zakavi, B.; Kotousov, A.; Branco, R. The Evaluation of Front Shapes of Through-the-Thickness Fatigue Cracks. *Metals* **2021**, *11*, 403. <https://doi.org/10.3390/met11030403>

Academic Editor: Dariusz Rozumek

Received: 1 February 2021
Accepted: 21 February 2021
Published: 1 March 2021

Publisher's Note: MDPI stays neutral with regard to jurisdictional claims in published maps and institutional affiliations.



Copyright: © 2021 by the authors. Licensee MDPI, Basel, Switzerland. This article is an open access article distributed under the terms and conditions of the Creative Commons Attribution (CC BY) license (<https://creativecommons.org/licenses/by/4.0/>).

1. Introduction

The evaluation of fatigue life and failure conditions of structural components is of permanent and primary interest for engineers. Over the past five decades, significant progress has been made toward the development of more appropriate fatigue crack growth models and life assessment procedures. Significant research effort has been directed to the study of the fatigue crack closure phenomenon, which was first introduced by Elber [1] to explain the experimentally observed features of fatigue crack growth in aluminium alloys. The number of publications grew rapidly since this pioneering study, and continues to grow. It is now commonly accepted that the contributions of various crack closure mechanisms, specifically plasticity-induced crack closure, roughness-induced crack closure, and oxide-induced closure, are significant, and these mechanisms are capable of explaining many fatigue crack growth phenomena, e.g., the influence of thickness on crack growth rates, retardation effects associated with overloads, or higher propagation rates of small cracks in comparison with long cracks [2].

It is well-established that for relatively long cracks propagating in a non-aggressive environment, the plasticity-induced crack closure dominates over the roughness-induced crack and oxide-induced closures. The plasticity-induced crack closure models rely on far fewer assumptions than the two other closure mechanisms. The first theoretical model was developed by Budianski and Hutchinson [3] based on the two-dimensional Dugdale strip-yield model [4]. The theoretical results demonstrated that opening stress intensity factor is surprisingly high, and increases with an increase in the R ratio. All early crack closure models for plate components utilised both plane strain and plane stress simplifications, although real cracks are inherently three-dimensional (3D). To examine the thickness effect

on crack propagation rates, empirical constraint factors were often used, demonstrating a stronger correlation with experimental results. With the advance of numerical methods and the increase in computational power, it became possible to eliminate these simplifications and study more realistic geometries, as well as various 3D effects [5,6].

In 3D problems, the order of the singularity at the intersection of the crack front with the free surface depends on Poisson's ratio and the intersection angle. From energy considerations, it follows that fatigue cracks have to preserve the $1/\sqrt{r}$ singularity. Therefore, the fatigue crack has to intersect the free surface at a critical angle, β_{cr} , which is a function of Poisson's ratio. Several experimental studies have reported that, at least, the Mode I fatigue crack front is shaped to ensure the square root singular behaviour along the entire crack front. However, it seems that the effect of 3D corner singularity is not very significant in the presence of a sufficiently large crack front process zone [7]. This is because the 3D corner singularity effect is a point effect, and is very much localised. Therefore, it might be negated by the plasticity and damage formation near the surface. For example, in an experimental study of steel circular bars subjected to bending and torsion, the experimental intersection angles were found to be very different from the theoretically predicted critical angles [8].

Considerably less effort has been directed toward the study of the effects of the 3D corner singularity and elasto-plastic constraints on plasticity-induced crack closure. Generally, the direct 3D elasto-plastic simulations of fatigue crack growth demand much greater computational resources [9]. These simulations have many issues associated with the validation of the numerical solution and the accuracy of the obtained results. A number of factors affect the accuracy, which are difficult to control: the mesh refinement, the type of finite element, the crack advance scheme (which usually consists of releasing nodes ahead of the crack front), contact conditions, and the local criterion of crack front opening. Branco et al. [10] recently provided an exhaustive review concerning these aspects. The overall conclusion was that the direct numerical approaches are capable of describing the shape evaluation of fatigue cracks. However, the application of these approaches to particular problems can be quite cumbersome. Each problem needs a large effort to calibrate the solution and verify the results. These efforts are usually focused on the reduction in the number of finite elements, the number of simulations required in the analysis, or, eventually, the computation time, which cannot be considered to be of practical relevance [11].

In the present paper, a simplified procedure for the evaluation of the fatigue crack front shapes of through-the-thickness cracks propagating under the cyclic loading conditions is presented. The procedure is based on simplified methods for the evaluation of the plasticity-induced crack closure effect, namely the equivalent-thickness method introduced by Yu and Guo [12,13], as well as the analytical model developed by Kotousov et al. [14,15]. The outcomes of the simulation are compared with available experimental results obtained at the same propagation conditions for validation purposes. The paper is organised as follows: Section 2 addresses the method used to evaluate the crack front shape, as well as the models introduced to evaluate the crack closure along the crack front. Section 3 describes the finite element model developed to calculate the stress intensity factors along the crack front. Section 4 compares the predicted crack front shapes with those obtained experimentally for different materials and propagation conditions. The paper ends with some concluding remarks.

2. Crack Shape Simulation and Crack Closure Models

The main idea behind the evaluation of the steady-state shape of a fatigue crack front proposed in this paper is to select a curve from a parametric family that minimises the deviation of the fatigue driving force along the crack front. In other words, we first specified a possible parametric set of curves in the crack plane (e.g., parabolic, hyperbolic, or elliptical shapes) and then evaluated the local fatigue driving force using a finite element model, along with simplified plasticity-induced crack closure models. In this study, the

local fatigue driving force was defined by the effective stress intensity factor range, ΔK_{eff} , given by the formula:

$$\Delta K_{\text{eff}} = U \cdot \Delta K = U \cdot (K_{\text{max}} - K_{\text{min}}) \quad (1)$$

where U is the normalised load ratio parameter, or normalised effective stress intensity factor, which is often used to describe the effects of loading and geometry on crack closure, and ΔK is the traditional linear-elastic stress intensity factor range [16] defined by the maximum and minimum values of the stress intensity factor experienced for a given load cycle. The load ratio is therefore given by $R = K_{\text{min}}/K_{\text{max}}$. In the case of 3D problems, this normalised load ratio is not a constant, but rather a function of the position along the crack front, $U = U(z)$. Thus, the local crack growth rate is a function of the effective stress intensity factor range, i.e.,

$$\Delta K_{\text{eff}}(z) = K_{\text{max}}(z) - K_{\text{op}}(z) = U(z)\Delta K(z) \quad (2)$$

where $K_{\text{op}}(z)$ is the local opening load stress intensity factor, which corresponds to the minimum load at which the crack faces, at point z , which are fully separated.

A number of sophisticated finite-element (FE) models were developed to evaluate $U(z)$ for different geometries and loading conditions. However, as discussed above, these models have many limitations, and are quite difficult to apply in fatigue calculations. Below, we consider two simplified methods for the evaluation of the normalised load ratio, the equivalent-thickness model introduced by Yu and Guo [13], and the analytical model proposed by Kotousov et al. [14,15], which are addressed in Sections 2.1 and 2.2, respectively. These methods will be further incorporated into the 3D linear elastic finite element simulations to evaluate the shape of the through-the-thickness cracks. This evaluation will be performed via the corner singularity method [17], which is briefly presented in Section 2.3.

2.1. Equivalent-Thickness Model

For through-the-thickness cracked plates, She et al. [17] proposed defining the equivalent thickness based on a numerical analysis of the 3D distribution of the out-of-plane stresses and constraint factor, T_z , which is defined as:

$$T_z = \frac{\sigma_z}{\sigma_x + \sigma_y} \quad (3)$$

where σ_x , σ_y , and σ_z are the normal stresses. This method is illustrated in Figure 1. The equivalent thickness, $2h_{\text{eq}}$, for point P on the crack front is identified as the plate thickness, which leads to the same distribution of T_z at the mid-plane.

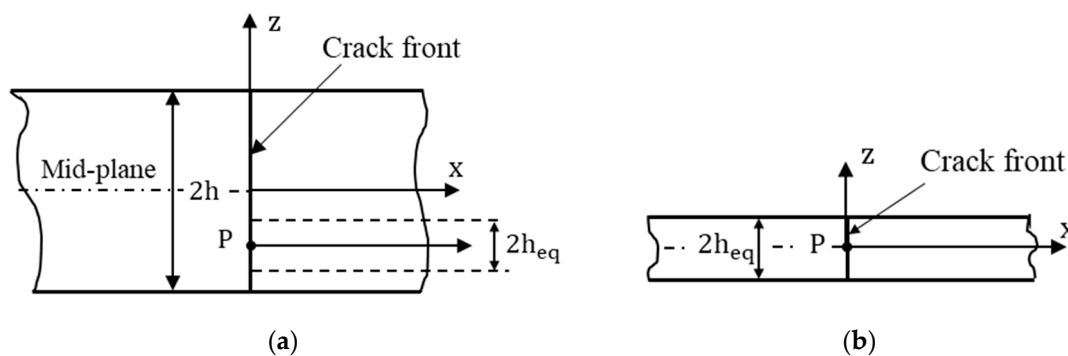


Figure 1. Schematic illustration of the equivalent-thickness method in the through-the-thickness cracks: (a) original straight through-the-thickness cracked geometry; (b) final straight-through-the-thickness cracked geometry with equivalent thickness.

An empirical equation was suggested to evaluate the equivalent-thickness as follows:

$$\frac{h_{eq}}{h} = 1 - \left(\frac{z}{h}\right)^2 \quad (4)$$

where z is the distance from the mid-plane and h is the half-thickness of the plate. The normalised load ratio parameter in this method can be calculated as follows:

$$U = \frac{\sqrt[3]{\kappa}}{1 - R} \quad (5)$$

where κ is a function of the R ratio:

$$\kappa = \frac{(1 - R^2)^2(1 + 10.34R^2)}{\left(1 + 1.67R^{1.61} + \frac{1}{0.15\pi^2\alpha_g}\right)^{4.6}} \quad (6)$$

and α_g is a global constraint factor, α_g , defined by the formula:

$$\alpha_g = \frac{1 + t}{1 - 2\nu + t} \quad (7)$$

where ν is the Poisson's ratio and t is given by:

$$t = 0.2088\sqrt{\frac{r_0}{h_{eq}}} + 1.5046\frac{r_0}{h_{eq}} \quad (8)$$

with:

$$r_0 = \frac{\pi}{16} \left(\frac{K_{max}}{\sigma_0}\right)^2 \quad (9)$$

where σ_0 is the flow stress. These empirical equations were extended to the corner, and surface cracks and were extensively validated using 3D finite element analyses.

2.2. Analytical Model for the Evaluation of Crack Closure

Another method for the evaluation of local plasticity-induced closure is based on a simplified 3D analytical model. In accordance with this model, the parameter U for Mode I loading under small-scale yielding conditions can be approximated from the following expression:

$$U(R, \eta) = a(\eta) + b(\eta)R + c(\eta)R^2 \quad (10)$$

where the fitting functions a , b and c can be written in the form:

$$\begin{aligned} a(\eta) &= 0.446 + 0.266 \cdot e^{-0.41\eta} \\ b(\eta) &= 0.373 + 0.354 \cdot e^{-0.235\eta} \\ c(\eta) &= 0.2 - 0.667 \cdot e^{-0.515\eta} \end{aligned} \quad (11)$$

where $\eta = K_{max}/(h\sqrt{\sigma_f})$ is a dimensionless parameter.

The above equations were obtained within the first-order plate theory based on the Budiansky–Hutchinson crack closure model [3,15]. The results, which correspond to the classical two-dimensional theories (or plane stress state, or plane strain state), can be obtained as limiting cases of very thin and very thick plates, i.e., when $\eta \rightarrow \infty$ or $\eta \rightarrow 0$, respectively. The details of the derivation of these equations can be found in the original paper by Codrington and Kotousov [14].

2.3. Corner Singularity Method

In this study, the evaluation of the steady-state front in the through-the-thickness cracks was carried out using the corner singularity method. First, we approximated the shape of the crack front by a two-parameter elliptical curve, which can be described as:

$$x = b\sqrt{1 - \frac{z^2}{a^2}} \quad -h \leq z \leq h \quad (12)$$

where a and b are the major and minor semi-axes of an ellipse, respectively, as shown in Figure 2.

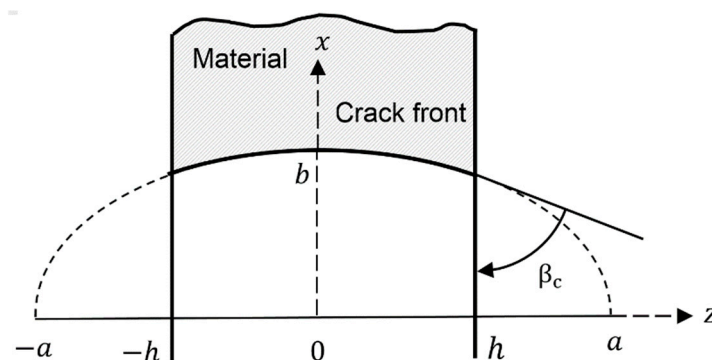


Figure 2. Elliptical-arc crack front shape for geometrical parameters crack propagation.

The crack front tends to intersect the free plate surface at the critical angle, β_c , when the plasticity effects are small. The critical angle is a function of the Poisson's ratio and the type of loading. We found that the critical intersection angle can be approximated by the following formula [18]:

$$\tan \beta_c = \frac{\nu - 2}{\nu} \quad (13)$$

where ν is the Poisson's ratio. Typically, when the size of the plastic zone is greater than 1% of the plate thickness, the stress state near the vertex location is not controlled by the elastic singularity. In these cases, the plasticity effects become more important, and together with the vertex singularity effect, lead to greater critical angles for elastic-plastic materials. To find b , we need to make sure that:

$$\frac{\partial x}{\partial z} \Big|_{z=\pm h} = -\frac{bh}{a\sqrt{a^2 - h^2}} = \frac{\nu}{\nu - 2} \quad (14)$$

where b is defined by:

$$b = \frac{a\nu}{(2 - \nu)} \sqrt{\frac{a^2}{h^2} - 1} \quad (15)$$

Substituting Equation (15) into Equation (12), we obtain:

$$x(z) = \frac{a\nu}{(2 - \nu)} \sqrt{\frac{a^2}{h^2} - 1} \cdot \sqrt{a^2 - z^2} \quad -h \leq z \leq h \quad (16)$$

This equation meets the condition that the crack front intersects with the free surface at the critical angle given by Equation (13), and represents a parametric curve with one single parameter, a . Further, the steady-state condition of the crack propagation requires that the projection of the effective stress intensity factor along the crack propagation direction (x -direction, Figure 1) is constant for all points along the crack front. This condition cannot be satisfied exactly with any multi-parametric equation describing the possible crack front shapes. However, the shape that minimises the difference of the effective stress intensity

factor along the crack front can be considered as the best approximation of the actual fatigue crack front shape.

3. Numerical Approach

This section describes the numerical model developed in this research to determine the stress intensity factor ranges along the crack front. The stress intensity factor ranges, along with the crack closure models described in the previous section, enabled the computation of the local fatigue driving force, which was used to obtain a steady-state crack front shape. The steady-state crack front shape was selected as the one producing the minimum deviation of ΔK_{eff} along the crack front. This evaluation needs to be completed for each curve from the parametric set.

To reduce the computational overhead, we developed a simplified geometry by introducing adequate boundary conditions, capable of describing 3D effects near the crack front. Section 3.1 describes the details of the numerical modelling, and Section 3.2 addresses the boundary conditions considered in this paper. The last section, Section 3.3, is devoted to the validation of the stress intensity factor values obtained with the proposed approach.

3.1. Finite Element Model Description

The typical finite element geometry, developed here to study a through-the-thickness crack in an elastic plate, is shown in Figure 3. As can be seen, the rectangular cross-section geometries were modelled to evaluate the stress and displacement fields near the crack tip. The size of the finite element models is sufficient to avoid the effect of the finite boundaries on the stress state. By taking advantage of the symmetry conditions (i.e., XY symmetry, XZ symmetry, and YZ symmetry), only one-eighth of the crack problem was modelled. The height of the FE models taken was approximately ten times larger than the plate thicknesses. In accordance with the previous studies, this is sufficient to accurately describe the 3D effects near the crack front [19,20].

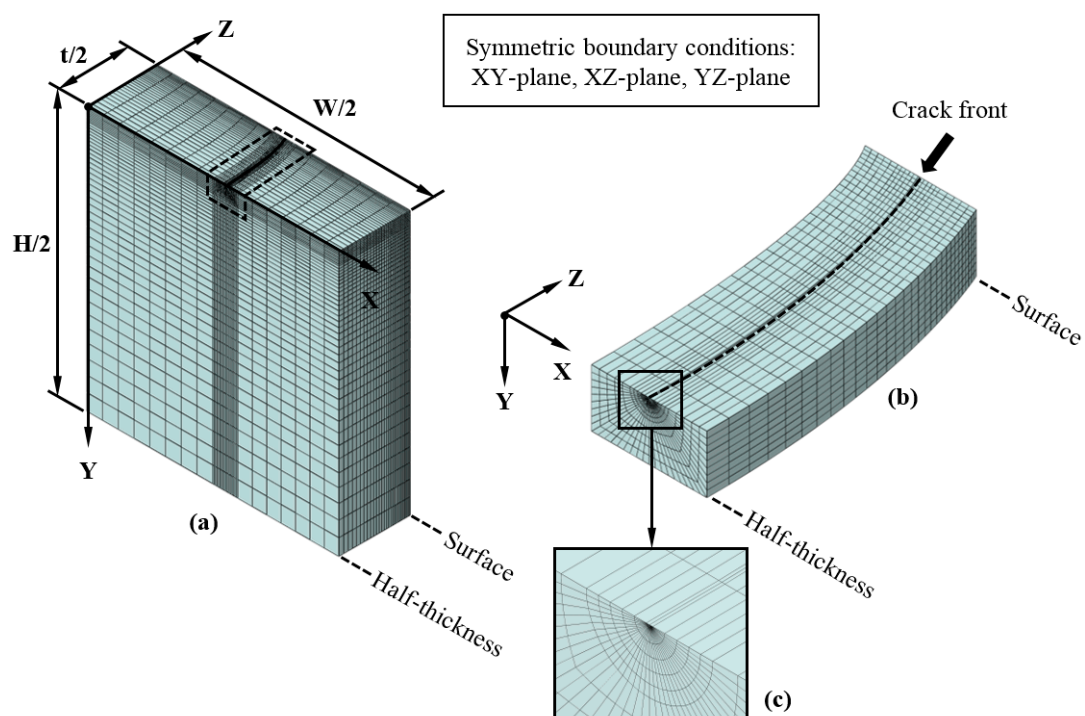


Figure 3. Finite element mesh: (a) assembled model; (b) detail of the crack front; (c) detail of the spider web pattern.

The FE models corresponding to different values of a (Figure 1) were meshed with linear 8-node hexahedral elements of type C3D8R. A reasonably uniform element grid with a structured mesh was considered. A denser mesh, with a spider-web pattern (Figure 3c)

was used near the crack front, where the stress gradients were expected to be maximum (Figure 3b), consisting of 5 concentric rings centred at the crack tip with a radial discretisation of 10° (Figure 3c). Thirty nodes along the plate half-thickness (Figure 3b) were used to define the crack front shape. The specimen was subjected to uniaxial loading applied at the bottom surface (i.e., at the XZ-plane with a Y-coordinate equal to $H/2$). The assembled mode is exhibited in Figure 3a. Further details about the modelling approach can be found in papers published by the present authors [19,21].

The numerical simulations were carried out using Abaqus/CAE 2020 (© Dassault Systèmes, 2019), assuming a homogeneous, isotropic, and linear-elastic behaviour. The mechanical properties inserted into Abaqus/CAE 2020 to perform the numerical simulations were the Young's modulus and the Poisson's ratio of the tested materials (Table 1). The displacement field far from the crack tip was calculated in accordance with the William's solution using MATLAB R2020b, and the obtained results were applied for the boundary conditions. The 3D solutions of the J-integral were used to calculate the stress intensity factor near the crack front. One layer of elements surrounding the crack front was used to calculate the first contour integral. The additional layer of elements was used to compute the subsequent contours. The different contour solutions were approximately coincident after eight contours. The results from averaging contours five through eight was considered. A similar strategy, either in terms of mesh framework or simulation analysis, was carried out for all geometries and crack configurations studied in the present paper.

Table 1. Mechanical properties of the selected materials.

Material	Young's Modulus, E	Poisson's Ratio, ν	Fracture Toughness, K_{IC}	Exponent of Paris Law, m
6082-T6	74 GPa	0.33	20 MPa·m ^{0.5}	3.456
PMMA	3.6 GPa	0.365	1.6 Pa·m ^{0.5}	0.91

3.2. Boundary Conditions

The plane-stress displacements far from the crack tip were calculated in accordance with William's solution [22]:

$$u_x(r, \theta) = \left(\frac{r}{2\pi}\right)^{1/2} \frac{(1 + \nu)}{E} [K_I^\infty f_x^I(\theta)] \quad (17)$$

$$u_y(r, \theta) = \left(\frac{r}{2\pi}\right)^{1/2} \frac{(1 + \nu)}{E} [K_I^\infty f_y^I(\theta)] \quad (18)$$

Being:

$$f_x^I(\theta) = \cos \frac{\theta}{2} \left(k - 1 + 2 \sin^2 \frac{\theta}{2}\right) \quad (19)$$

$$f_y^I(\theta) = \sin \frac{\theta}{2} \left(k + 1 + 2 \cos^2 \frac{\theta}{2}\right) \quad (20)$$

where r is the distance from the crack tip, θ is the angle measured from the symmetry line, K_I^∞ is the remotely applied Mode I stress intensity factor, and k is Kolosov's constant for plane stress and plane strain conditions. The plane stress k value was considered in the boundary conditions, i.e.,

$$k = \frac{3 - \nu}{1 + \nu} \quad (21)$$

where ν is the Poisson's ratio. Bakker [23] showed that a cracked plate under plane stress undergoes a change to plane strain behaviour near the crack tip. He proved that the radial position, where the plane stress to plane strain transition takes place, strongly depends on the position in the thickness direction. The degree of plane strain is essentially zero at distances from the tip greater than five times the thickness, even in the middle plane of the plate [24].

3.3. Validation Study

The numerical results obtained for the maximum stress intensity factor are presented in Figure 4 as a function of the thickness for a Poisson's ratio of 0.3. The classical results for both the plane stress state and the plane strain state are also given in Figure 4. It is evident from Figure 4 that the stress intensity factor changes with the thickness of the plate until the thickness exceeds a critical value. In this particular problem, the results showed that the critical thickness is 25 mm. Once the thickness exceeds the critical dimension, the stress field in the vertex singularity region has a negligible impact on the behavior of the whole structure. The stress intensity factor becomes relatively constant in the sufficiently thick plate, and is equal to the value for plane strain conditions.

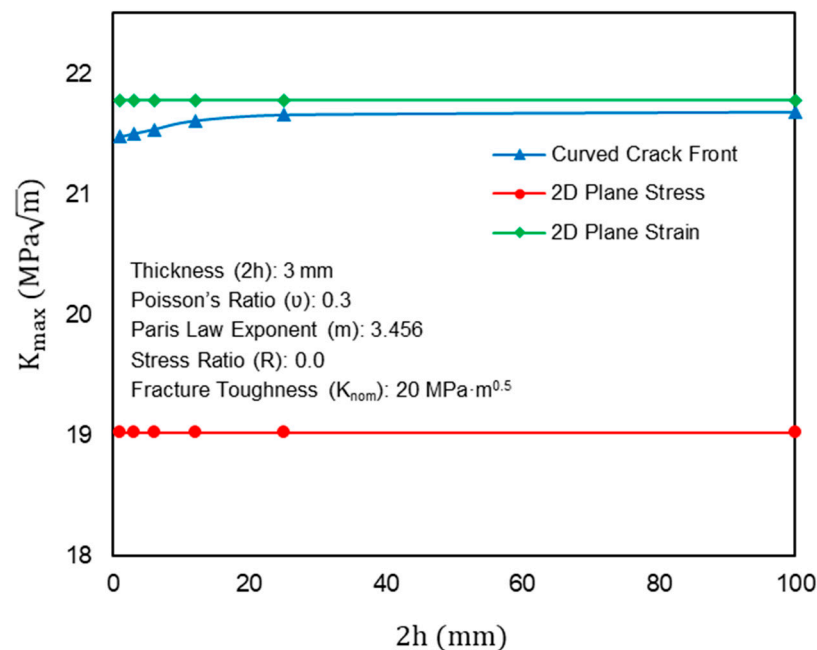


Figure 4. The effect of the thickness on the maximum stress intensity factor.

4. Crack Front Shape Evaluation and Comparison with Experimental Studies

The proposed method for the evaluation of the steady-state crack front shapes was compared against two independent experimental studies. The specimen geometries used in the experimental tests are exhibited in Figure 5, and were made of 6082-T6 aluminium alloy and polymethyl methacrylate (PMMA), separately. The main mechanical properties of both materials are listed in Table 1. The former (Figure 5a) consisted of a standard middle-crack tension specimen with a thickness of 3 mm [11,25]. The tests were conducted under constant-amplitude axial loading using a stress ratio equal to 0.25. Figure 6a shows an example of the typical fracture surfaces obtained in the tests. Fatigue cracks grew over a sufficiently large distance from the initial notch to ensure the quasi-steady-state conditions of propagation. The beach-marking technique was applied to mark the crack front at the fracture surface.

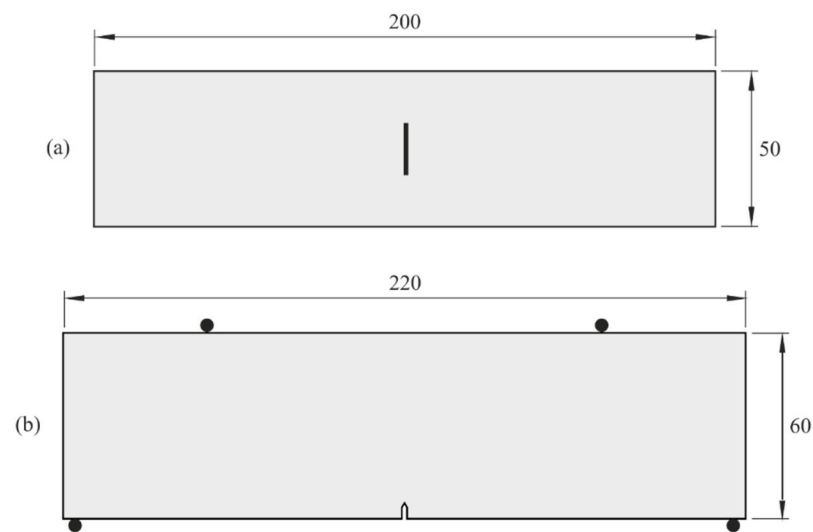


Figure 5. Specimen geometries used in the crack front shape evaluation: (a) 6082-T6 aluminium alloy and (b) polymethyl methacrylate (PMMA). All dimensions are in mm.

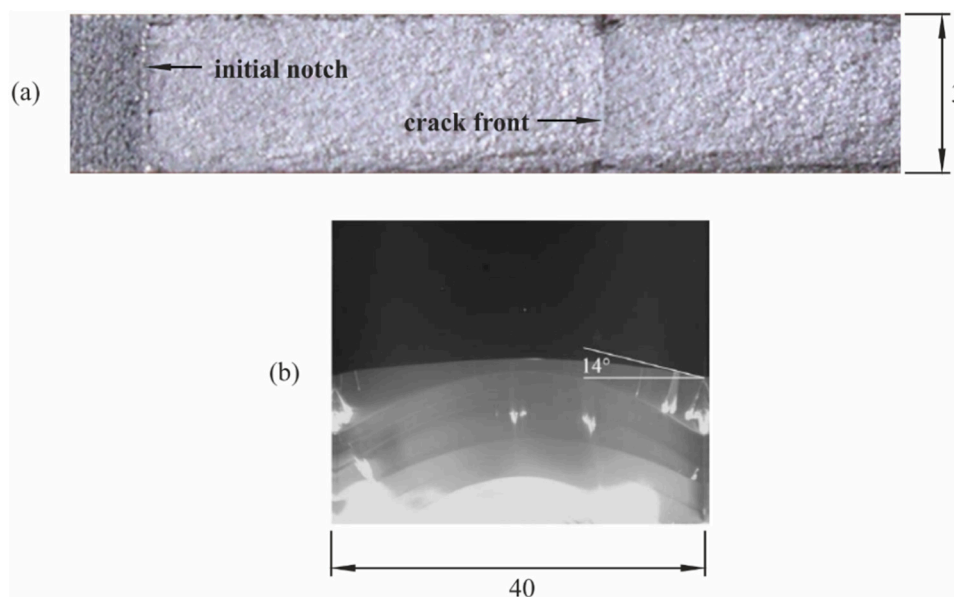


Figure 6. The crack front shapes observed in the experiments for the: (a) 6082-T6 aluminium alloy reprinted with permission from ref. [11], copyright 2021 Elsevier and (b) polymethyl methacrylate reprinted with permission from ref. [26], copyright 2021 Elsevier. Propagation direction is from left to right in case (a) and from bottom to top in case (b). All dimensions are in millimetres.

Regarding the latter (Figure 5b), the specimen geometry was made of polymethyl methacrylate. It had a rectangular cross-section (Figure 5b), with a thickness of 40 mm [26,27], and an initial straight notch at the middle of the specimen. The tests were conducted under four-point bending loading conditions using a stress ratio equal to 0. The crack front shape was evaluated in situ using a high-resolution digital camera. As in the previous case, fatigue cracks propagated over a sufficiently large distance from the initial notch to ensure the quasi-steady state conditions of propagation. An example of the crack front shapes observed in the experiments is exhibited in Figure 6b.

Figure 7a,b displays a comparison of the experimental crack front shapes and those obtained with the proposed methods for the 6082-T6 aluminium alloy and PMMA, respectively. Overall, the results showed that the equivalent-thickness method provides a satisfactory approximation for the fatigue crack propagation under small yielding condi-

tions. Moreover, the experimental results confirmed that the angle at which the crack front intersects the free surface is greater than the proposed empirical equations in the sufficiently plastic materials. We think that the careful combination of the hyperbolic and elliptical functions might provide accurate crack front shape estimation in the presence of residual stresses or large crack closure effects. The good agreement demonstrated in the previous analysis confirmed the possibility of the accurate evaluation of stress intensity factors using the proposed approach in materials controlled by 3D corner singularity effects.

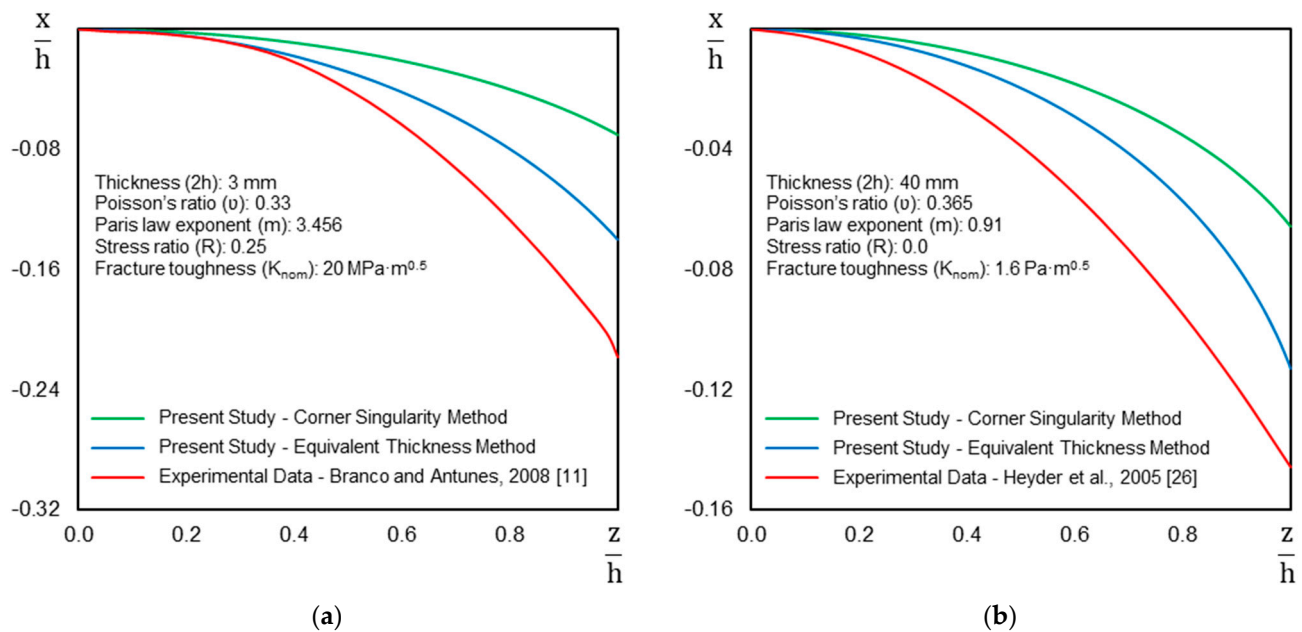


Figure 7. A comparison between the predicted crack shapes and experimental data for the specimens composed of: (a) 6082-T6 aluminium alloy and (b) polymethyl methacrylate.

This methodology can also be applied to conduct parametric studies associated with the main variables affecting the fatigue crack growth of through-the-thickness cracks. A subject that can be analysed with the developed approach is the effect of the stress ratio on crack closure values. Figure 8 plots the ratio of the opening stress intensity factor (K_o) to the maximum stress intensity factor (K_{max}) along the crack front for both materials. As shown, the plane stress curve represents the upper limit, while the plane strain curve represents the lower limit. The values of K_o/K_{max} are between two limiting cases, and decrease with an increase in the stress ratio. In addition, at lower stress ratios, the differences between the maximum and minimum values of K_o/K_{max} are higher for PMMA and tend to be closer for the aluminium alloy.

Figure 9 plots the variation in the K_o/K_{max} ratio at the crack surface obtained from the presented 3D FE simulations against previously published relationships based on experimental tests that incorporated plasticity-induced crack closure. Notably, the results of the presented procedure agree well with the outcomes of the experimental and theoretical studies reported in the literature [1,16,27–29]. The variation between the presented method and published data decreases with an increase in the R ratio, as the size of the reverse plasticity zone (or monotonic plastic zone) becomes smaller in the fatigue crack growth rates. These results provide further support to and validation of the numerical technique outlined in this paper.

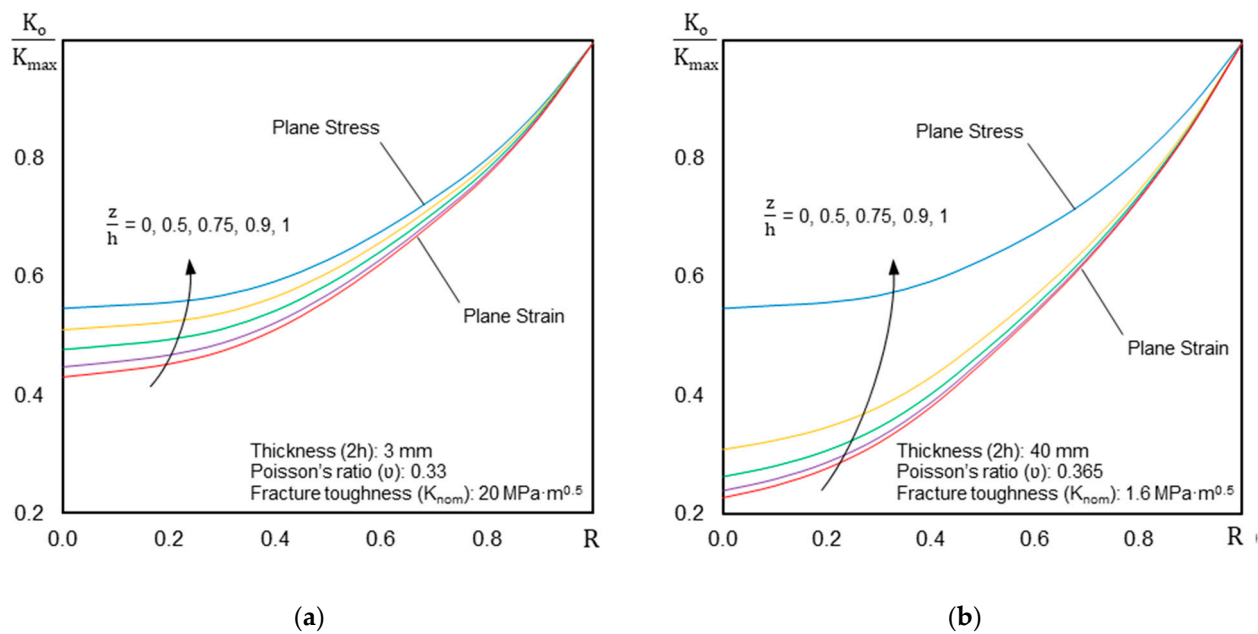


Figure 8. The ratio of the opening stress intensity factor to the maximum stress intensity factor as a function of the R ratio along the crack front: (a) 6082-T6 aluminium alloy; (b) polymethyl methacrylate.

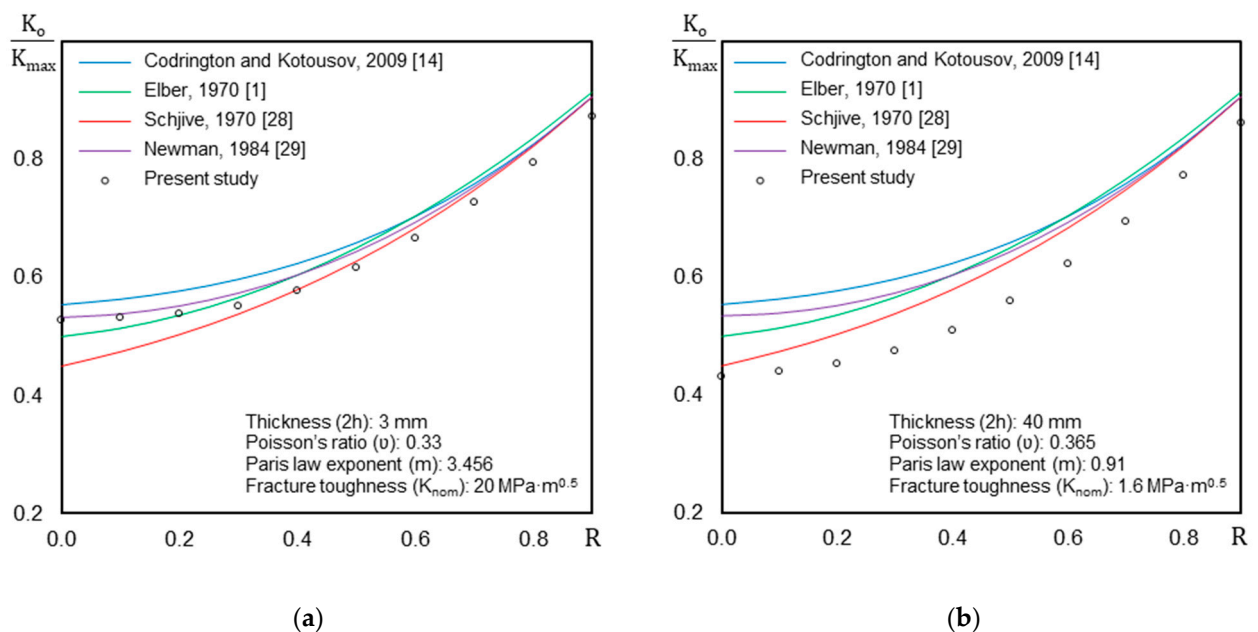


Figure 9. The ratio of the of the opening stress intensity factor to the maximum stress intensity factor as a function of the R ratio along the crack front and past published functions: (a) 6082-T6 aluminium alloy; (b) polymethyl methacrylate.

5. Conclusions

In this paper, new numerical modelling tools capable of simulating the crack shape development of through-the-thickness fatigue cracks in finite plates were presented. The proposed approaches assume a pre-defined crack front shape, and include plasticity-induced crack closure. The methodology was successfully tested for cracked rectangular cross-section geometries when subjected to Mode I loading. The following conclusions can be drawn:

1. The maximum stress intensity factor becomes relatively constant in the sufficiently thick plates and is equal to the value obtained for plane strain state conditions. The

- plane strain fatigue models (2D) may lead to inaccurate predictions when applied to the analysis of fatigue crack growth of thin structural plates;
2. The proposed methodology leads to satisfactory crack front predictions, either for ductile materials or brittle materials. Moreover, it is sensitive to the plate thickness, enabling good results for both thin and thicker geometries. In addition, it is capable of dealing with different stress ratios;
 3. The opening stress intensity factor increases with increasing values of stress ratio, maximum stress intensity factor, and distance from the centre of the crack. Predicted values obtained by the proposed methodology are quite close to those found in the literature for the same propagation conditions.

The comparison with experimental results is encouraging, and demonstrates the validity of the underlying assumptions: (1) the crack front shape intersects the free plate surface at the critical angle; and (2) the local stress intensity factor can be considered as the fatigue crack driving force, which leads to the formation of the crack front shape under high cycling loading. The above assumptions might not be correct in the case of large plastic effects near the crack tip. In this case, the plasticity-induced crack closure, which is significantly different along the crack front, will be the one of the most influential factors affecting the crack front shape.

Future work will be directed to the application of the proposed methodology to more complex problems in terms of geometry, loading scenario, and crack shape configuration. Lastly, the simplicity and speed of calculation of the proposed approach, compared to the current numerical solutions used for the same purpose, make it quite attractive for simulating the fatigue crack growth, in both practical applications and parametric studies.

Author Contributions: Conceptualization, B.Z. and A.K.; methodology, B.Z. and A.K.; software, B.Z.; validation, B.Z. and R.B.; formal analysis, B.Z. and R.B.; investigation, B.Z. and R.B.; data curation, B.Z. and R.B.; writing—original draft preparation, B.Z.; writing—review and editing, B.Z., R.B. and A.K.; visualization, B.Z., A.K. and R.B.; supervision, A.K. All authors have read and agreed to the published version of the manuscript.

Funding: This research was sponsored by FEDER funds through the program COMPETE (Programa Operacional Factores de Competitividade) and by national funds through FCT (Fundação para a Ciência e a Tecnologia) under the project UIDB/00285/202.

Data Availability Statement: The data presented in this study are available from the corresponding author, upon reasonable request. The data are not publicly available due to ethical restrictions.

Conflicts of Interest: The authors declare no conflict of interest.

References

1. Elber, W. Fatigue crack closure under cyclic tension. *Eng. Fract. Mech.* **1970**, *2*, 37–44. [[CrossRef](#)]
2. Vasudeven, A.K.; Sadananda, K.; Louat, N. A review of crack closure, fatigue crack threshold and related phenomena. *Mater. Sci. Eng. A* **1994**, *188*, 1–22. [[CrossRef](#)]
3. Budiansky, B.; Hutchinson, J.W. Analysis of closure in fatigue crack growth. *ASME J. Appl. Mech.* **1978**, *45*, 267–276. [[CrossRef](#)]
4. Dugdale, D.S. Yielding of steel sheets containing slits. *J. Mech. Phys. Solids* **1960**, *8*, 100–104. [[CrossRef](#)]
5. He, Z.; Kotousov, A.; Berto, F.; Branco, R. A brief review of three-dimensional effects near crack front. *Phys. Mesomech.* **2019**, *19*, 6–20. [[CrossRef](#)]
6. Kotousov, A.; Khanna, A.; Branco, R.; Jesus, A.; Correia, J.A. Review of current progress in 3D linear elastic fracture mechanics. In *Mechanical Fatigue of Metals, Structural Integrity*; Springer: Cham, Switzerland, 2019; pp. 125–131. [[CrossRef](#)]
7. Nowell, D.; de Matos, P.F.P. The influence of the Poisson's ratio and corner point singularities in three-dimensional plasticity-induced fatigue crack closure: A numerical study. *Int. J. Fatigue* **2008**, *30*, 1930–1943. [[CrossRef](#)]
8. Lebahn, J.; Heyer, H.; Sander, M. Numerical stress intensity factor calculation in flawed round bars validated by crack propagation tests. *Eng. Fract. Mech.* **2013**, *108*, 37. [[CrossRef](#)]
9. Camas, D.; Garcia-Manrique, J.; Antunes, F.V.; Gonzalez-Herrera, A. Three-dimensional fatigue crack closure numerical modelling: Crack growth scheme. *Theor. Appl. Fract. Mech.* **2020**, *108*, 102623. [[CrossRef](#)]
10. Branco, R.; Antunes, F.V.; Costa, J.D. A review on 3D-FE adaptive remeshing techniques for crack growth modelling. *Eng. Fract. Mech.* **2015**, *141*, 170–195. [[CrossRef](#)]

11. Branco, R.; Antunes, F.V. Finite element modelling and analysis of crack shape evolution in Mode-I fatigue Middle Cracked Tension specimens. *Eng. Fract. Mech.* **2008**, *75*, 3020–3037. [[CrossRef](#)]
12. Guo, W. Three-dimensional analyses of plastic constraint for through-thickness cracked bodies. *Eng. Fract. Mech.* **1999**, *62*, 383–407. [[CrossRef](#)]
13. Yu, P.; Guo, W. An equivalent thickness conception for evaluation of corner and surface fatigue crack closure. *Eng. Fract. Mech.* **2013**, *99*, 202. [[CrossRef](#)]
14. Codrington, J.; Kotousov, A. A crack closure model of fatigue crack growth in plates of finite thickness under small-scale yielding conditions. *Mech. Mater.* **2009**, *41*, 165–173. [[CrossRef](#)]
15. He, Z.; Kotousov, A.; Branco, R. A simplified method for the evaluation of fatigue crack front shapes under mode I loading. *Int. J. Fract.* **2014**, *188*, 203–211. [[CrossRef](#)]
16. Antunes, F.V.; Chegini, A.G.; Correia, L.; Branco, R. Numerical study of contact forces for crack closure analysis. *Int. J. Solids Struct.* **2014**, *51*, 1330–1339. [[CrossRef](#)]
17. She, C.; Zhao, J.; Guo, W. Three-dimensional stress fields near notches and cracks. *Int. J. Fract.* **2008**, *151*, 151–160. [[CrossRef](#)]
18. Pook, L.P. Some implications of corner point singularities. *Eng. Fract. Mech.* **1994**, *48*, 367–378. [[CrossRef](#)]
19. Kotousov, A.; Lazzarin, P.; Berto, F.; Pook, L.P. Three-dimensional stress states at crack tip induced by shear and anti-plane loading. *Eng. Fract. Mech.* **2013**, *108*, 65–74. [[CrossRef](#)]
20. Nakamura, T.; Parks, D.M. Antisymmetrical 3-D stress field near the crack front of a thin elastic plate. *Int. J. Solids Struct.* **1989**, *25*, 1411–1426. [[CrossRef](#)]
21. Kotousov, A. Fracture in plates of finite thickness. *Int. J. Solids Struct.* **2007**, *44*, 8259–8273. [[CrossRef](#)]
22. Williams, M.L. On the stress distribution at the base of a stationary crack. *J. Appl. Mech.* **1957**, *24*, 109–114. [[CrossRef](#)]
23. Bakker, A. Three dimensional constraint effects on stress intensity distributions in plate geometries with through-thickness cracks. *Fatigue Fract. Eng. Mater. Struct.* **1992**, *15*, 1051–1069. [[CrossRef](#)]
24. Levy, N.; Marcal, P.V.; Rice, J.R. Progress in three-dimensional elastic-plastic stress analysis for fracture mechanics. *Nucl. Eng. Des.* **1971**, *17*, 64–75. [[CrossRef](#)]
25. Borrego, L.F. Fatigue Crack Growth under Variable Amplitude Load in an AlMgSi Alloy. Ph.D. Thesis, University of Coimbra, Coimbra, Portugal, 2001.
26. Heyder, M.; Kolk, K.; Kuhn, G. Numerical and experimental investigations of the influence of corner singularities on 3D fatigue crack propagation. *Eng. Fract. Mech.* **2005**, *72*, 2095–2105. [[CrossRef](#)]
27. Heyder, M.; Kuhn, G. 3D fatigue crack propagation: Experimental studies. *Int. J. Fatigue* **2006**, *28*, 627–634. [[CrossRef](#)]
28. Schjive, J. Some formulas for the crack opening stress level. *Eng. Fract. Mech.* **1981**, *14*, 461–465. [[CrossRef](#)]
29. Newman, J.C. A crack opening stress equation for fatigue crack growth. *Int. J. Fatigue* **1984**, *24*, R131–R135. [[CrossRef](#)]

Chapter 8
Conclusions and Future Work

8.1 Summary

Theoretical, numerical, and experimental studies in the fracture and fatigue fields often highlight the significance of 3D stress states and 3D effects. However, the current failure assessment procedures and design codes largely disregard the 3D nature of the stress distribution near stress concentrators and cracks, and the 3D nature of fatigue phenomena as discussed in the Introduction and Literature Review. In addition, these procedures and codes usually utilise simplified crack front shapes (e.g., straight or semi-circular) for evaluations of fatigue life and fracture. All these simplifications and assumptions can have a significant effect on the accuracy of theoretical predictions. At the same time, there is a general expectation in the structural integrity and fracture community that consideration of and accounting for 3D effects will help to improve the accuracy of these theoretical predictions, as well as contribute to our understanding of fracture and fatigue phenomena.

Despite the great progress made over the past two decades, obtaining exact 3D solutions for crack problems is not possible in the near future, except for in very simple cases, e.g., penny-shaped and elliptical cracks in infinite linear-elastic media. Approximate analytical solutions have also been derived over the past fifty years and have largely been focused on through-the-thickness cracks in linear elastic plates. However, these cases represent a small portion of the practically important situations. Numerical techniques (i.e., Finite Element method) can be useful to analyse 3D geometries; however, there is no generally-accepted methodology that can be applied to analyse 3D fatigue phenomena. Therefore, many 3D effects, such as the effect of the crack front shape on fatigue crack growth and fatigue crack closure, or the effect of the 3D vertex singularity on crack front shape evolution remain poorly understood.

The primary objective of this research was to advance knowledge in the areas of 3D Fracture Mechanics, which is a relatively new area in Solid Mechanics. This was achieved by developing the new simplified semi-analytical methods for evaluation of fatigue life in various engineering components with defects (cracks).

The more realistic fatigue crack front shapes, as well as the effects of plasticity-induced crack closure and the 3D corner singularity on front shape evolution were investigated using these methods under steady-state conditions. The theoretical results from the developed methods have been extensively validated against the outcomes of past numerical and experimental studies.

There is no doubt that there are still a large number of significant gaps in our knowledge in relation to the role of 3D effects in Fracture and Fatigue. Therefore, this work can be considered as an initial step towards the development of 3D Fracture Mechanics, which does not rely on various simplifications and assumptions. General recommendations and suggestions for future research directions are briefly outlined below.

8.2 Conclusions

The outcomes of the thesis can be broadly divided into four main categories. The purpose of this section is to provide a brief summary of the major outcomes of this thesis.

1. Understanding the influence of 3D corner singularity on fatigue crack front shapes near a free surface

It has been shown that the critical angle concept is a valid hypothesis if the plastic (or process) zone at the crack tip is much smaller than the size of the region controlled by the 3D vertex singularity. The latter is related to the problem geometry. A new parameter, i.e., the ratio of the 3D vertex singularity characteristic size to the radius of the plastic zone, has been suggested to describe the applicability of the critical angle concept to fatigue problems. Another important observation was the strong effect of the problem geometry changes during fatigue crack propagation and transient loading conditions on the validity of the critical angle concept.

2. Development of simplified methods to describe crack front shapes of through-the-thickness fatigue cracks

A number of analytical and semi-analytical methods based on different hypotheses regarding fatigue crack front shape evolution have been investigated. The accuracy of the developed methods has been evaluated against selected experimental studies. In addition, it has been demonstrated that empirically-introduced crack closure equations allow for a better matching of the theoretical predictions and experimental data.

3. Development of simplified methods to describe the front shape evaluation of surface-breaking fatigue cracks.

A new, effective, analytical method has been developed for the evaluation of fatigue growth of surface flaws in structural components. This theoretical development largely enables avoidance of time-consuming numerical simulations, without compromising the accuracy of the final results. The analytical method and numerical results collapse into a single curve describing the shape evolution of surface defects.

4. Development of simplified analytical models to investigate the effects of plasticity-induced crack closure and 3D effects on front shapes of fatigue cracks

The effect of plasticity-induced crack closure was incorporated into the earlier developed models. A new combined analytical-numerical methodology was developed in order to evaluate crack front shapes for various geometries, including through-the-thickness cracks in plates and surface cracks in round bars under quasi-steady-state loading conditions. It was shown that the fatigue crack growth in such components is very sensitive to the initial crack length and crack shape, the exponent of the Paris law, the loading scenario, and is significantly affected by plasticity-induced crack closure for the higher intensity of the applied loading.

Finally, the outcomes of the thesis are expected to help to improve the accuracy of the theoretical predictions and, as a long-term outcome, reduce the risk of structural failures and decrease the cost of inspections and maintenance procedures.

8.3 Recommendations for Future Work

In the present study, the accuracy of the numerical techniques was validated against limited experimental data, as well as the earlier, published 3D analytical solutions. It is important to compare the crack front shape between both numerical and experimental results for a wider range of the practical geometries in order to provide further support for practical applications of the developed methods. Experimental studies could include the examination of the crack front shape evolution and crack growth rates for different materials, specimen geometry, and loading conditions.

The critical stress intensity factors (or fracture toughness) provide the most important relationships between the critical crack size and the maximum allowable stresses for brittle and quasi-brittle materials. These parameters are currently utilised for assessing the acceptability of flaws in many fatigue and fracture evaluation procedures across many industries and applications. The current industrial standards and failure assessment codes assume that structural failure occurs when the stress intensity factor or a combination of stress intensity factors in modes I, II and III exceed the critical value or fracture toughness. In reality, structural failure does not happen simultaneously across the crack front. Further development of brittle fracture criteria could introduce and incorporate a new parameter for consideration of the most critical locations along the crack front into the assessment procedures. The critical location could be dependent on the applied loading, crack and problem geometries, etc. The incorporation of 3D effects into the brittle fracture initiation criterion is expected to improve the accuracy and applicability of fracture toughness-based criteria.

Appendix A
Asymptotic Analysis of Out-of-plane Strain and Displacement
Fields at Angular Corners

Statement of Authorship

Title of Paper	Asymptotic analysis of out-of-plane strain and displacement fields at angular corners		
Publication Status	<input checked="" type="checkbox"/>	Published	<input type="checkbox"/> Accepted for Publication
	<input type="checkbox"/>	Submitted for Publication	<input type="checkbox"/> Unpublished and Unsubmitted work written in manuscript style
Publication Details	Khanna, A., Kotousov, A., Yakubovich, S., & Zakavi, B. (2019). Asymptotic analysis of out-of-plane strain and displacement fields at angular corners. International Journal of Solids and Structures, 170, 111–122. https://doi.org/10.1016/j.ijsolstr.2019.04.024		

Principal Author

Name of Principal Author	Dr. Aditya Khanna		
Contribution to the Paper	Performed analysis, literature review, interpreted data, and co-wrote manuscript		
Overall percentage (%)	50		
Certification:	This paper reports on original research I conducted during the period of my Higher Degree by Research candidature and is not subject to any obligations or contractual agreements with a third party that would constrain its inclusion in this thesis. I am the primary author of this paper.		
Signature		Date	23 / 08 / 2021

Co-Author Contributions

By signing the Statement of Authorship, each author certifies that:

- i. the candidate's stated contribution to the publication is accurate (as detailed above);
- ii. permission is granted for the candidate to include the publication in the thesis; and
- iii. the sum of all co-author contributions is equal to 100% less the candidate's stated contribution.

Name of Co-Author	Prof. Andrei Kotousov		
Contribution to the Paper	Supervised work development, interpreted data, and co-wrote manuscript		
Signature		Date	09 / 09 / 2021

Name of Co-Author	Assoc. Prof. Semyon Yakubovich		
Contribution to the Paper	Performed analysis, helped to complete, evaluate, and edit the manuscript		
Signature		Date	10 / 09 / 2021

Name of Co-Author	Behnam Zakavi		
Contribution to the Paper	Assisted in FE model creation and analysis		
Signature		Date	09 / 09 / 2021



Asymptotic analysis of out-of-plane strain and displacement fields at angular corners

A. Khanna^a, A. Kotousov^{a,*}, S. Yakubovich^b, B. Zakavi^a

^aSchool of Mechanical Engineering, The University of Adelaide, Adelaide, SA 5005, Australia

^bDepartment of Mathematics, University of Porto, 4099-002 Porto, Portugal



ARTICLE INFO

Article history:

Received 11 October 2018

Revised 22 March 2019

Available online 17 April 2019

Keywords:

Plane problems of elasticity

Sharp corner

Out-of-plane strain

First-order plate theory

Kontorovich–Lebedev transform

3D solution

Stress singularities

ABSTRACT

This paper presents three-dimensional analytical solutions for displacement and strain fields near angular corners in plates subjected to in-plane loading. The approach is based on the first-order plate theory, which represents an elementary extension of the classical plane theory of linear elasticity. Utilising the Kontorovich–Lebedev transform, the asymptotic behaviour of the out-of-plane displacement field near the apex is investigated for both Mode I and Mode II loadings. The analytical solutions obtained in the present work correctly predict several three-dimensional effects, such as the order of stress singularity and the intensity of the coupled (local) out-of-plane singular mode under remote in-plane shear loading as well as the scale effect associated with the plate thickness. The developed solutions are more general than many previous analytical results obtained for crack and notch geometries and, essentially, generalise the classical Williams' solution for angular corners. The analytical predictions compare favourably with three-dimensional finite element modelling and experimental results.

© 2019 Elsevier Ltd. All rights reserved.

1. Introduction

The classical solutions of plane (2D) linear elasticity form the framework of contemporary Linear Elastic Fracture Mechanics and Notch Mechanics, and these are extensively utilised towards the stress analysis and design of plate components (Carpinteri et al., 2008). Analytical, numerical and experimental studies of plane problems of elasticity over the past several decades have indicated that the classical plane stress solutions accurately describe the in-plane stress state in the interior domain of three-dimensional plate-like structures (Rosakis and Ravi-Chandar, 1986; Nakamura and Parks, 1988). However, in the vicinity of free boundaries, interfaces, edges and corner (vertex) points, the stress state is essentially three-dimensional, and the application of plane elasticity solutions may lead to peculiar results. The region of dominance of the three-dimensional (3D) stress state, sometimes referred as the boundary layer (Yang and Freund, 1985), has a characteristic length comparable to the plate thickness (Gregory and Wan, 1988). Although small in comparison with the rest of the structure, the region of 3D stress state dominance is generally the site of failure initiation. Hence, the accurate analysis of the localised three-dimensional stress state is of great practical importance. Experimental evidences collected over the past five decades demonstrate

that the three-dimensional stress states can play an important role in fatigue and fracture phenomena (Aliha and Saghafi, 2013; Pook, 2013). As a result, three-dimensional considerations are being incorporated in advanced analytical and numerical models in an attempt to explain the various experimental observations and tendencies (Kotousov, 2010; He et al., 2016a).

The present work is concerned with the mathematical analysis of the 3D stress state near sharp corners in plates of finite thickness subjected to in-plane loading. A sharp corner geometry represents a classical example where the exact solution of the governing equations of the theory of plane elasticity, i.e. the well-known Williams' solution, leads to peculiar results, predicting infinite or zero out-of-plane displacements at the tip (vertex) of the corner for plane stress and plane strain states, respectively. However, the experimental and numerical studies clearly indicate that the transverse (out-of-plane) displacements as well as the transverse normal strain are finite and depend on the notch opening angle, elastic constants as well as the applied loading (He et al., 2016b). The investigation of the transverse field variables near a tip of a sharp wedge represents a problem of practical interest. For example, the direct experimental measurements of the out-of-plane surface displacements near the sharp wedge can be related to the elastic constants or to the stress field near the tip. This idea was recently presented for the zero notch opening angle (or for a through-the-thickness crack) (He and Kotousov, 2016; He et al., 2016b). In these papers, a new experimental technique was suggested for the

* Corresponding author.

E-mail address: andrei.kotousov@adelaide.edu.au (A. Kotousov).

Nomenclature

(r, ϕ, z)	cylindrical coordinate system with origin at the midpoint of the notch front (Fig. 1)
h	half-thickness of plate (Fig. 1)
2β	wedge angle (Fig. 1)
2α	notch opening angle (Fig. 1)
E, ν	Young's modulus and Poisson's ratio of the plate
κ	characteristic length-scale parameter, $\sim h^{-1}$
$\check{\sigma}_{rr}, \check{\sigma}_{\phi\phi}, \check{\tau}_{r\phi}$	plane stress solution for in-plane stress components
w	out-of-plane displacement function
w_p	plane-stress solution for the out-of-plane displacement function
w_h	decaying solution for the out-of-plane displacement function
u_z	out-of-plane displacement
$\tau_{rz}, \tau_{\phi z}$	out-of-plane shear stress components
λ_1, λ_2	eigenvalues of Williams' plane problem for symmetric and anti-symmetric loadings, respectively
$\varepsilon_1, \varepsilon_2$	exponent values of the in-plane stress components for in-plane symmetric and anti-symmetric loadings, respectively
K_I, K_{II}	remotely-applied Mode I and Mode II stress intensity factors, respectively
A_1, A_2	constants relating the in-plane stress components to the remotely-applied stress intensity factors
λ_0	eigenvalue of the out-of-plane singular mode
K_0	out-of-plane mode (O-mode) stress intensity factor
μ	Kontorovich–Lebedev transform variable
\check{w}_h	Kontorovich–Lebedev transform of the decaying solution, w_h
$K_\nu(z)$	modified Bessel function of second kind
$\Gamma(z)$	gamma function
$\delta(z)$	generalised Dirac delta function
${}_2F_1(a, b; c; z)$	Gauss Hypergeometric function

evaluation of stress intensity factors based on the single measurement of the out-of-plane surface displacement near the tip of a crack.

An exact solution of the problem under consideration is not amenable within the framework of three-dimensional linear elasticity theory (Yoshibash et al., 2004). A compromise between complexity and comprehension can be achieved, for example, with the first order plate theory suggested by Kane and Mindlin (1956). This theory was originally applied to the analysis of high-frequency extensional vibrations in moderately thick plates. It is based on the kinematic assumption that the transverse normal strain is constant across the plate thickness and all stress and strain components are functions of the in-plane coordinates only. Due to this assumption the theory retains the simplicity of a 2D formulation for the analysis of plane problems of elasticity, which are still 3D in nature. The results obtained within this theory normally demonstrate a good agreement with both experimental and numerical results, and are also free from peculiarities associated with the classical 2D singular solutions (Jin and Batra, 1997; Kotousov, 2004; Zappalorto, 2017).

The paper is organised as follows: in the next section, a brief summary of the governing equation is provided. Next, the approach for solving the governing differential equation for a sharp

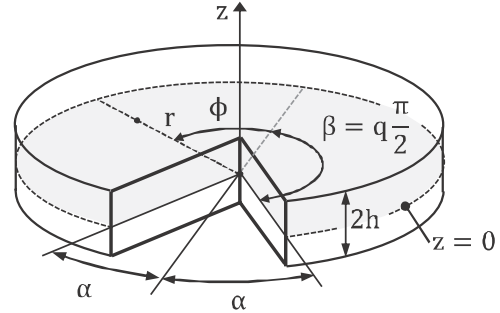


Fig. 1. Plate geometry and coordinate system.

corner (or wedge) subjected to in-plane mixed mode loading is presented. Then, the outcomes of the analytical modelling are compared against previous analytical and numerical results. In the conclusion, the future work and possible applications of the present theoretical results are discussed.

2. Basic equations

Consider a system of cylindrical polar coordinates for a plate of thickness $2h$ with the z axis perpendicular to the faces of the plate as illustrated in Fig. 1. Take the origin of the coordinate system to be located at the mid-plane of the plate at the tip of the sharp wedge. Then, in accordance with the kinematic assumption of the first-order plate theory (Yang and Freund, 1985) and the method suggested by Kotousov et al. (2017), the out-of-plane displacement function, w , which also equals the average out-of-plane normal strain, can be written as

$$\nabla^2 w - \kappa^2 w = \frac{\nu \kappa^2}{E} (\check{\sigma}_{rr} + \check{\sigma}_{\phi\phi}), \quad \kappa^2 = \frac{6(1+\nu)}{h^2}, \quad (1)$$

where ν is Poisson's ratio of the material. The out-of-plane displacements, $u_z(r, \phi, z) = w(r, \phi)z/h$, in this theory vary linearly with the distance from the mid-plane ($z=0$). The governing equations of the first-order plate theory as well as the derivation of Eq. (1) are detailed in a previous publication (Kotousov et al., 2017) and will not be repeated here.

In the last equation, the stress components $\check{\sigma}_{rr}$ and $\check{\sigma}_{\phi\phi}$ are obtained from the solution of the corresponding 2D plane stress problem. For an angular sector with solid angle $2\beta = q\pi \in [\pi, 2\pi]$ (Fig. 1), Williams' (1952) plane stress solution for the leading singular term yields the sum of in-plane normal stresses under mixed-mode loading as

$$\check{\sigma}_{rr} + \check{\sigma}_{\phi\phi} = A_1 r^{\varepsilon_1} \cos \varepsilon_1 \phi + A_2 r^{\varepsilon_2} \sin \varepsilon_2 \phi, \quad (2)$$

where $\varepsilon_i = \lambda_i - 1$ and λ_i are the eigenvalues of the following characteristic equations

$$\sin(\lambda_1 q\pi) + \lambda_1 \sin(q\pi) = 0, \quad \sin(\lambda_2 q\pi) - \lambda_2 \sin(q\pi) = 0. \quad (3)$$

Note that the solution of the characteristic Eq. (3) yields $\lambda_2 > 1$ for $2\beta < 257.4^\circ$, i.e., a non-singular behaviour of the in-plane stress field at the notch-tip under Mode II loading. The constants A_i are related to the notch stress intensity factors, which can be introduced in several ways (Ramesh and Hills, 2016); and one of those definitions which will be utilised in the current study is (Lazzarin and Tovo, 1998)

$$A_1 = \frac{4}{\sqrt{2\pi}} \frac{K_I}{(1+\lambda_1) + \chi_1(1-\lambda_1)}, \quad A_2 = \frac{4}{\sqrt{2\pi}} \frac{K_{II}}{(1-\lambda_2) + \chi_2(1+\lambda_2)}, \quad (4)$$

$$\chi_i = -\frac{\sin[(1 - \lambda_i)\beta]}{\sin[(1 + \lambda_i)\beta]}, \quad i = 1, 2. \quad (5)$$

Since $\check{\sigma}_{rr}$ and $\check{\sigma}_{\phi\phi}$ are obtained from the corresponding two-dimensional plane problem, i.e. $\nabla^2(\check{\sigma}_{rr} + \check{\sigma}_{\phi\phi}) = 0$, the solution of the non-homogenous governing Eq. (1) can be rewritten as

$$w = w_p + w_h, \quad w_p = -\frac{\nu h}{E}(\check{\sigma}_{rr} + \check{\sigma}_{\phi\phi}). \quad (6)$$

In (6), w_p represents the particular solution corresponding to the plane stress solution and w_h corresponds to the solution of the homogeneous modified Helmholtz equation:

$$\nabla^2 w_h - \kappa^2 w_h = 0. \quad (7)$$

For $-0.5 \leq \varepsilon_i < 0$, the particular solution $w_p \propto r^{\varepsilon_i}$ becomes singular at $r=0$. However, based on strain energy considerations, the out-of-plane displacement function, $w(r, \phi)$, must remain finite everywhere, including the notch tip. A corrective solution for the out-of-plane displacement function which satisfies the homogenous governing Eq. (7) and also has the same asymptotic behaviour as w_p at $r \rightarrow 0$ can be constructed using the modified Bessel functions, $K_{\varepsilon_i}(\kappa r)$. The sum of the particular and corrective solutions is well defined at the notch-tip. For $\varepsilon_i \geq 0$, which is the case for solid angle $2\beta < 257.4^\circ$ under Mode II loading, the particular solution $w_p \propto r^{\varepsilon_i}$ remains bounded at the notch-tip, ($r=0$), i.e. a corrective solution utilizing modified Bessel functions is not required. The intermediate solution, w^* , can be written for Mode I and Mode II loading as follows:

$$w^* = -\frac{\nu h}{E} A_1 \left(\frac{2}{\pi} \sin(\varepsilon_1 \pi) \left(\frac{2}{\kappa} \right)^{\varepsilon_1} \Gamma(1 + \varepsilon_1) K_{\varepsilon_1}(\kappa r) + r^{\varepsilon_1} \right) \cos(\varepsilon_1 \phi), \quad (8a)$$

$$w^* = -\frac{\nu h}{E} A_2 \left(\frac{2}{\pi} \sin(\varepsilon_2 \pi) \left(\frac{2}{\kappa} \right)^{\varepsilon_2} \Gamma(1 + \varepsilon_2) K_{\varepsilon_2}(\kappa r) + r^{\varepsilon_2} \right) \sin(\varepsilon_2 \phi), \quad \varepsilon_2 < 0, \quad (8b)$$

$$w^* = -\frac{\nu h}{E} A_2 r^{\varepsilon_2} \sin(\varepsilon_2 \phi), \quad \varepsilon_2 > 0. \quad (8c)$$

The solution for the out-of-plane displacement function corresponding to higher order terms in William's series solution can be obtained in a similar manner, but not discussed here. The transverse (out-of-plane) shear stress must satisfy the traction-free boundary conditions along the wedge faces. In terms of the out-of-plane displacement function, w , these boundary conditions can be written as (Kotousov et al., 2017):

$$\frac{\partial w}{\partial \phi} \Big|_{\phi=\pm\beta} = 0. \quad (9)$$

The intermediate solution, $w^*(r, \phi)$ does not satisfy Eq. (9), except for the special case of a Mode II semi-infinite crack, i.e. $A_1 = 0$, $\beta = \pi$, and $\varepsilon_2 = -0.5$. Hence, a further corrective solution to the homogenous governing Eq. (7) must be obtained and added to the intermediate solution, w^* , such that

$$\frac{\partial w_h}{\partial \phi} \Big|_{\phi=\pm\beta} = -\frac{\partial w^*}{\partial \phi} \Big|_{\phi=\pm\beta}. \quad (10)$$

Taking the power series expansion of the Bessel functions $K_{\varepsilon_i}(\kappa r)$, the boundary condition (10) for the case of Mode I and Mode II loadings can be expressed as

$$\frac{\partial w_h}{\partial \phi} \Big|_{\phi=\pm\beta} = -\frac{\nu h}{E} A_1 \varepsilon_1 \left(\left(\frac{2}{\kappa} \right)^{\varepsilon_1} \Gamma(1 + \varepsilon_1) \left(\sum_{nn=0}^{\infty} \frac{\left(\frac{\kappa r}{2} \right)^{2n - \varepsilon_1}}{n! \Gamma(nn - \varepsilon_1 + 1)} - \sum_{nn=1}^{\infty} \frac{\left(\frac{\kappa r}{2} \right)^{2n + \varepsilon_1}}{n! \Gamma(nn + \varepsilon_1 + 1)} \right) \right) \sin(\varepsilon_1 \beta), \quad (11a)$$

$$\frac{\partial w_h}{\partial \phi} \Big|_{\phi=\pm\beta} = \frac{\nu h}{E} A_2 \varepsilon_2 \left(\left(\frac{2}{\kappa} \right)^{\varepsilon_2} \Gamma(1 + \varepsilon_2) \left(\sum_{n=0}^{\infty} \frac{\left(\frac{\kappa r}{2} \right)^{2n - \varepsilon_2}}{n! \Gamma(n - \varepsilon_2 + 1)} - \sum_{n=1}^{\infty} \frac{\left(\frac{\kappa r}{2} \right)^{2n + \varepsilon_2}}{n! \Gamma(n + \varepsilon_2 + 1)} \right) \right) \cos(\varepsilon_2 \beta), \quad \varepsilon_2 < 0, \quad (11b)$$

$$\frac{\partial w_h}{\partial \phi} \Big|_{\phi=\pm\beta} = \frac{\nu h}{E} A_2 \varepsilon_2 r^{\varepsilon_2} \cos(\varepsilon_2 \beta), \quad \varepsilon_2 > 0. \quad (11c)$$

Next, we develop the method and will derive analytical expressions for w_h , which satisfy the homogeneous modified Helmholtz Eq. (7) as well as boundary conditions (11a)–(11c).

3. The method for the evaluation of out-of-plane displacements

The symmetric and anti-symmetric boundary conditions (11) are of the form

$$\frac{\partial w_h}{\partial \phi} \Big|_{\phi=\pm\beta} = C_1 r^m \sin(\varepsilon_1 \beta), \quad (12a)$$

$$\frac{\partial w_h}{\partial \phi} \Big|_{\phi=\pm\beta} = C_2 r^m \cos(\varepsilon_2 \beta). \quad (12b)$$

The solution to the governing Eq. (7) subject to boundary conditions (12) can be readily obtained in terms of the Kontorovich–Lebedev transform and its inverse, which are defined as follows (Yakubovich, 2003):

$$\tilde{w}_h(\mu, \phi) = \int_0^\infty w_h(\kappa r, \phi) K_{i\mu}(\kappa r) \frac{dr}{r}, \quad (13)$$

$$w_h(\kappa r, \phi) = \frac{2}{\pi^2} \int_0^\infty \tilde{w}_h(\mu, \phi) K_{i\mu}(\kappa r) \mu \sinh(\pi \mu) d\mu. \quad (14)$$

Applying the transform (13) to the governing Eq. (7) and boundary conditions (12a)–(12b) yields

$$\frac{\partial^2 \tilde{w}_h}{\partial \phi^2} - \mu^2 \tilde{w}_h = 0, \quad (15)$$

$$\frac{\partial \tilde{w}_h}{\partial \phi} \Big|_{\phi=\pm\beta} = \frac{C_1 \sin(\varepsilon_1 \beta) \Gamma(m)}{\kappa^m} \int_0^\infty \frac{\cos(\mu t)}{(\cosh t)^m} dt, \quad (16a)$$

$$\frac{\partial \tilde{w}_h}{\partial \phi} \Big|_{\phi=\pm\beta} = \frac{C_2 \cos(\varepsilon_2 \beta) \Gamma(m)}{\kappa^m} \int_0^\infty \frac{\cos(\mu t)}{(\cosh t)^m} dt. \quad (16b)$$

The general solution to the ordinary differential Eq. (15) can be obtained as

$$\tilde{w}_h = c_1(\mu) \cosh(\mu \phi) + c_2(\mu) \sinh(\mu \phi). \quad (17)$$

Along the corner faces,

$$\frac{\partial \tilde{w}_h}{\partial \phi} \Big|_{\phi=\pm\beta} = \mu c_1(\mu) \sinh(\mu \beta) + \mu c_2(\mu) \cosh(\mu \beta), \quad (18)$$

Comparing coefficients in Eq. (18) and (16a)–(16b) yields

$$c_1(\mu) = \frac{C_1 \Gamma(m) \sin(\varepsilon_1 \beta)}{\kappa^m \mu \sinh(\mu \beta)} \int_0^\infty \frac{\cos(\mu t)}{(\cosh t)^m} dt, \quad (19a)$$

$$c_2(\mu) = \frac{C_2 \Gamma(m) \cos(\varepsilon_2 \beta)}{\kappa^m \mu \cosh(\mu \beta)} \int_0^\infty \frac{\cos(\mu t)}{(\cosh t)^m} dt. \quad (19b)$$

For the boundary conditions (11a)–(11c), the functions $c_1(\mu)$ and

$c_2(\mu)$ can be obtained as

$$c_1(\mu) = -\frac{v_h}{E} A_1 \epsilon_1 \left(\frac{2}{\kappa}\right)^{\epsilon_1} \Gamma(1 + \epsilon_1) \frac{\sin(\epsilon_1 \beta)}{\mu \sinh(\mu \beta)} \\ \times \left(\sum_{n=0}^{\infty} \frac{\Gamma(2n - \epsilon_1) \Gamma(2n - \epsilon_1)}{n! \Gamma(n - \epsilon_1 + 1) 2^{2n - \epsilon_1}} - \sum_{n=1}^{\infty} \frac{\Gamma(2n + \epsilon_1) \Gamma(2n + \epsilon_1)}{n! \Gamma(n + \epsilon_1 + 1) 2^{2n + \epsilon_1}} \right) \quad (20a)$$

$$c_2(\mu) = \frac{v_h}{E} A_2 \epsilon_2 \left(\frac{2}{\kappa}\right)^{\epsilon_2} \Gamma(1 + \epsilon_2) \frac{\cos(\epsilon_2 \beta)}{\mu \cosh(\mu \beta)} \\ \times \left(\sum_{n=0}^{\infty} \frac{\Gamma(2n - \epsilon_2) \Gamma(2n - \epsilon_2)}{n! \Gamma(n - \epsilon_2 + 1) 2^{2n - \epsilon_2}} - \sum_{n=1}^{\infty} \frac{\Gamma(2n + \epsilon_2) \Gamma(2n + \epsilon_2)}{n! \Gamma(n + \epsilon_2 + 1) 2^{2n + \epsilon_2}} \right) \quad (20b)$$

$$c_2(\mu) = \frac{v_h}{E} A_2 \epsilon_2 \frac{\Gamma(\epsilon_2)}{\kappa^{\epsilon_2}} \frac{\cos(\epsilon_2 \beta)}{\mu \cosh(\mu \beta)} I(\epsilon_2), \quad \epsilon_2 > 0, \quad (20c)$$

where the integral

$$I(m) = \int_0^{\infty} \frac{\cos(\mu t)}{(\cosh t)^m} dt = \frac{2^{m-2}}{\Gamma(m)} \Gamma\left(\frac{m}{2} - \frac{i\mu}{2}\right) \Gamma\left(\frac{m}{2} + \frac{i\mu}{2}\right), \\ m > 0, \quad (21)$$

and it converges for $m > 0$. The infinite series in Eqs. (20a) and (20b) can be simplified, as shown in Appendix A.

4. Asymptotic results

From the results obtained in previous sections, the solution for the out-of-plane displacement, $w(r, \phi)$ can be written as

$$w(r, \phi) = w^*(r, \phi) + w_h(r, \phi), \quad (22)$$

where the intermediate solution, $w^*(r, \phi)$, is given by Eq. (8a) for Mode I and by Eqs. (8b), (8c) for Mode II loadings, respectively. The corresponding homogenous solutions, $w_h(r, \phi)$ are obtained by applying the inverse transform (14) to Eq. (17), with functions c_1 and c_2 given by Eqs. (20a)–(20c).

Utilising the equality (A4), the solution for $w_h(r, \phi)$ corresponding to Mode I loading can be obtained as

$$w_h(r, \phi) = -\frac{v_h}{E} \frac{A_1 \epsilon_1}{2\pi^2} \left(\frac{2}{\kappa}\right)^{\epsilon_1} \sin(\epsilon_1 \beta) \int_0^{\infty} \Gamma\left(\frac{\epsilon_1 - i\mu}{2}\right) \\ \times \Gamma\left(\frac{\epsilon_1 + i\mu}{2}\right) \frac{\cosh(\mu \phi) \sinh(\pi \mu)}{\sinh(\mu \beta)} K_{i\mu}(\kappa r) d\mu. \quad (23)$$

Similarly, for Mode II loading, the solution for arbitrary notch angle can be obtained as

$$w_h(r, \phi) = \frac{v_h}{E} \frac{A_2 \epsilon_2}{2\pi^2} \left(\frac{2}{\kappa}\right)^{\epsilon_2} \cos(\epsilon_2 \beta) \int_0^{\infty} \Gamma\left(\frac{\epsilon_2 - i\mu}{2}\right) \\ \times \Gamma\left(\frac{\epsilon_2 + i\mu}{2}\right) \frac{\sinh(\mu \phi) \sinh(\pi \mu)}{\cosh(\mu \beta)} K_{i\mu}(\kappa r) d\mu. \quad (24)$$

The above expression is valid for both cases of $\epsilon_2 < 0$ and $\epsilon_2 > 0$.

The integrals in Eqs. (23)–(24) converge absolutely under the condition $|\phi| \leq \beta$, which can be verified by applying the Stirling asymptotic formula for the gamma function at infinity (Erdélyi et al., 1953, Vol. I) and the corresponding behaviour of the modified Bessel function with respect to the index (Erdélyi et al., 1953, Vol. II; Yakubovich and Luchko, 1994). Although these integrals can be evaluated numerically, analytical asymptotic results can be obtained near the notch tip, i.e. $r \rightarrow 0$ and will be presented in the next section.

4.1. Mode I loading

At the notch tip, i.e. $r=0$, the intermediate solution $w^*(r, \phi)$ limits to zero, hence, the out-of-plane displacement function is equal to the homogenous solution, i.e. $w(r=0, \phi) = w_h(r=0, \phi)$. The asymptotic Eq. (C6) derived in Appendix C can be utilised to obtain w_h at the wedge tip as follows:

$$\lim_{r \rightarrow 0} w_h(r, \phi) = \lim_{\mu \rightarrow 0} \mu^2 [c_1(\mu) \cosh(\mu \phi) + c_2(\mu) \sinh(\mu \phi)] \\ = \lim_{\mu \rightarrow 0} \mu^2 c_1(\mu). \quad (25)$$

As expected from the anti-symmetry of Mode II loading, Eq. (25) suggests that the out-of-plane displacement at the notch tip is entirely due to Mode I loading. Substituting Eq. (20a) into Eq. (25) and recalling the equality (A4) yields

$$w(r \rightarrow 0) = -\frac{v_h}{E} \frac{A_1 \epsilon_1}{4\beta} \left(\frac{2}{\kappa}\right)^{\epsilon_1} \sin(\epsilon_1 \beta) \left[\Gamma\left(\frac{\epsilon_1}{2}\right) \right]^2. \quad (26)$$

Note that there is no dependence of the above asymptotic value of the displacement function on the angular position, ϕ . This outcome is in agreement with experimental observations and previous Finite Element modelling results obtained by He et al. (2016a) as well as other researchers.

It is also of interest to obtain asymptotic results for the gradient of the out-of-plane displacement, i.e. $\partial w / \partial r$ at the notch-tip. The asymptotic Eq. (C7) derived in Appendix C for the displacement gradient is only valid if the functions $c_1(\mu) \mu \sinh(\pi \mu)$ and $c_2(\mu) \mu \sinh(\pi \mu)$ are analytic along the imaginary axis. Inspection of Eqs. (20a) and (20b) suggests that this condition is satisfied only for the trivial case of a half-plane, i.e. $\beta = \pi/2$, and for a crack subjected to Mode I loading, i.e. $\beta = 0$, $A_2 = 0$. The latter case is of practical interest to a wide range of problems in fracture mechanics, hence, the asymptotic result for the out-of-plane displacement gradient is presented below. Since $w(r, \phi) = w^*(r, \phi) + w_h(r, \phi)$,

$$\lim_{r \rightarrow 0} \frac{\partial w(r, \phi)}{\partial r} = \lim_{r \rightarrow 0} \frac{\partial w^*(r, \phi)}{\partial r} + \lim_{r \rightarrow 0} \frac{\partial w_h(r, \phi)}{\partial r}. \quad (27)$$

Substituting $\epsilon_1 = -0.5$ and $A_1 = K_I \sqrt{2/\pi}$ in Eq. (8a) and differentiating with respect to r yields

$$\lim_{r \rightarrow 0} \frac{\partial w^*(r, \phi)}{\partial r} = -\frac{v_h K_I}{E} \kappa^{3/2} \frac{1}{\sqrt{2\pi \kappa}} \cos\left(\frac{\phi}{2}\right). \quad (28)$$

Separating the first term, corresponding to $n=0$ from Eq. (20a) and applying Eq. (C7) yields the derivative of the homogenous solution,

$$\lim_{r \rightarrow 0} \frac{\partial w_h(r, \phi)}{\partial r} = \frac{v_h K_I}{E} \kappa^{3/2} \left[\frac{2}{\pi^{3/2}} \int_0^{\infty} \Gamma\left(\frac{1}{4} - \frac{i\mu}{2}\right) \Gamma\left(\frac{1}{4} + \frac{i\mu}{2}\right) \right. \\ \times (K_{i\mu-1}(\kappa r) + K_{i\mu+1}(\kappa r)) \cosh(\mu \phi) d\mu \\ \left. + \left(\sum_{n=1}^{\infty} \frac{\Gamma(n + \frac{3}{4}) \Gamma(n - \frac{1}{4})}{n! \Gamma(n + \frac{3}{2})} - \sum_{n=1}^{\infty} \frac{\Gamma(n + \frac{1}{4}) \Gamma(n - \frac{3}{4})}{n! \Gamma(n + \frac{1}{2})} \right) \cos \phi \right]. \quad (29)$$

4.2. Mode II loading

Although Mode II loading results in zero out-of-plane displacement at the notch tip, it is well known that in-plane shear loading generates a singular transverse shear stress state at the notch tip for non-zero Poisson's ratio (Kotousov and Lew, 2006; Kotousov, 2007). The fracture mode corresponding to the singular transverse shear stress state is referred to as the out-of-plane singular mode or coupled local mode. In Fig. 2a, this singular mode is visualised for a plate containing a through-thickness crack, which represents the limiting case of a V-shaped notch. The characteristic

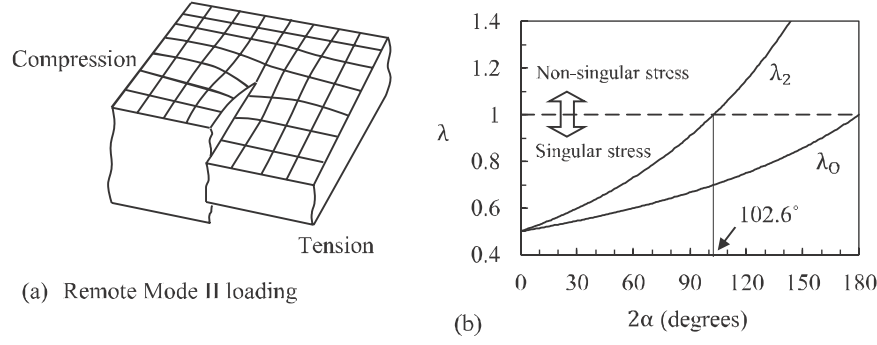


Fig. 2. (a) Exaggerated displacement corresponding to out-of-plane singular mode at a crack tip subjected to remote shear, (b) Eigenvalues of characteristic Eqs. (3) and (30), corresponding to the in-plane and out-of-plane singular modes, respectively.

equation for this coupled mode can be obtained as (Kotousov and Lew, 2006)

$$\cos(\lambda_0\beta) = 0, \tag{30}$$

whose eigenvalue can be easily obtained as $\lambda_0 = \pi/2\beta$. As with the in-plane modes, the out-of-plane mode will produce infinite stresses at the notch-tip for $0.5 \leq \lambda_0 < 1$, corresponding to $\pi < 2\beta \leq 2\pi$. In this instance, the out-of-plane shear stress components, $\tau_{rz}, \tau_{\phi z} \sim r^{\lambda_0-1}$ and the out-of-plane displacement component, $u_z \sim r^{\lambda_0}$ near the notch-tip (Kotousov, 2007). Fig. 2b shows the dependence of the eigenvalues λ_0 and λ_2 upon the wedge angle. The most interesting observation is that for notch opening angles $2\alpha > 102.6^\circ$ (solid angles $2\beta < 257.4^\circ$), when the in-plane stress singularity disappears, the coupled out-of-plane singularity still exists. It means that the presence of singular stress state determines the failure conditions for re-entrant corners regardless of the opening angle. This is contrary to many past studies, which analysed failure at sharp corners loaded in pure mode II using plane theory of elasticity. Although the analysis of the out-of-plane mode has been the subject of several 3D Finite Element studies (see for example, references within Kotousov, 2010), no analytical solutions exist to support and validate these studies.

Under Mode II loading, the asymptotic behaviour of the function $w_h(r, \phi)$ given by Eq. (24) can be obtained by virtue of the representation of this solution in terms of the series of Fox's H-functions (Prudnikov et al. 1986, Vol III). In this paper, we omit the details and simply state the main term of this expansion, which gives the asymptotic behaviour of the solution $w_h(r, \phi)$ when $r \rightarrow 0$. Precisely, we obtain for $2\beta > 257.4^\circ$

$$w_h(r \rightarrow 0, \phi) = \frac{\nu h A_2 \epsilon_2}{E} \left(\frac{2}{\kappa}\right)^{\epsilon_2} \cos(\epsilon_2\beta) \times \left[\frac{\Gamma\left(\frac{\epsilon_2 - \lambda_0}{2}\right)\Gamma\left(\frac{\epsilon_2 + \lambda_0}{2}\right)}{\beta\Gamma(1 + \lambda_0)} \left(\frac{\kappa}{2}\right)^{\lambda_0} r^{\lambda_0} \sin(\lambda_0\phi) + \frac{2}{\epsilon_2} \frac{\Gamma(1 + \epsilon_2)}{\Gamma(1 - \epsilon_2)} \left(\frac{2}{\kappa}\right)^{\epsilon_2} \sec(\epsilon_2\beta) r^{-\epsilon_2} \sin(\epsilon_2\phi) \right], \tag{31}$$

under the following conditions

$$|\phi| \leq \beta, \quad \frac{1}{2} \leq \lambda_0 \leq 1, \quad -1 < \epsilon_2 < 0, \tag{32}$$

$$(2m + 1)\lambda_0 - \epsilon_2 \neq 2n, \quad m, n \in \mathbb{N}_0.$$

Via the same method, we obtain for $2\beta < 257.4^\circ$

$$w_h(r \rightarrow 0, \phi) = \frac{\nu h A_2 \epsilon_2}{E} \left(\frac{2}{\kappa}\right)^{\epsilon_2} \cos(\epsilon_2\beta)$$

$$\times \left[\frac{\Gamma\left(\frac{\epsilon_2 - \lambda_0}{2}\right)\Gamma\left(\frac{\epsilon_2 + \lambda_0}{2}\right)}{\beta\Gamma(1 + \lambda_0)} \left(\frac{\kappa}{2}\right)^{\lambda_0} r^{\lambda_0} \sin(\lambda_0\phi) + \frac{2}{\epsilon_2} \left(\frac{2}{\kappa}\right)^{-\epsilon_2} \sec(\epsilon_2\beta) r^{\epsilon_2} \sin(\epsilon_2\phi) \right], \tag{33}$$

under the following conditions

$$|\phi| < \beta, \quad \epsilon_2 > 0, \tag{34}$$

or

$$|\phi| = \beta, \quad \frac{1}{2} \leq \lambda_0 \leq 1, \quad 0 < \epsilon_2 < \frac{1}{2}, \quad (2m + 1)\lambda_0 - \epsilon_2 \neq 2n, \tag{35}$$

$$m, n \in \mathbb{N}_0.$$

In Fig. 3, the asymptotic solutions given by Eqs. (31) and (33) are compared against the exact solutions given by Eq. (24). The figures are plotted in terms of the following dimensionless variables

$$\bar{w}_h = \frac{w_h E}{\nu h A_2 \epsilon_2} \left(\frac{2}{\kappa}\right)^{-\epsilon_2} \sec(\epsilon_2\beta), \quad \bar{r} = \frac{r}{2h}. \tag{36}$$

The exact solution is obtained by numerically evaluating Eq. (24) and converges to the asymptotic solutions near $r \rightarrow 0$, for both $\epsilon_2 < 0$ (Fig. 3a) and $\epsilon_2 > 0$ (Fig. 3b). The agreement validates the correctness of the obtained asymptotic solutions. The difference between the exact and asymptotic solutions is less than 0.1% for $r/2h < 10^{-3}$.

The asymptotic behaviour of the out-of-plane displacement function $w(r, \phi)$, defined by Eq. (22), can be obtained by adding Eqs. (8b) and (31) for $\epsilon_2 < 0$ and by adding Eqs. (8c) and (33) for $\epsilon_2 > 0$. In both cases, we obtain

$$w(r \rightarrow 0, \phi) = \frac{\nu h A_2 \epsilon_2}{E} \left(\frac{2}{\kappa}\right)^{\epsilon_2} \cos(\epsilon_2\beta) \frac{\Gamma\left(\frac{\epsilon_2 - \lambda_0}{2}\right)\Gamma\left(\frac{\epsilon_2 + \lambda_0}{2}\right)}{\beta\Gamma(1 + \lambda_0)} \times \left(\frac{\kappa}{2}\right)^{\lambda_0} r^{\lambda_0} \sin(\lambda_0\phi). \tag{37}$$

For the trivial case of a semi-infinite crack subjected to Mode II loading, i.e. $\beta = \pi$, it must be remembered that the intermediate solution $w^*(r, \phi)$ given by Eq. (8b) automatically satisfied the boundary condition (9), hence, $w_h(r, \phi) = 0$. Therefore, the asymptotic solution for the special case of a semi-infinite crack cannot be recovered by setting $\beta = \pi$ in Eq. (37). The latter must be found directly from the analysis of Eq. (8b). This will be described later in this paper.

Utilising the kinematic assumption of the first order plate theory, i.e. $u_z = w(z/h)$, together with Hooke's law and the strain-displacement relationship, the transverse shear stress can be

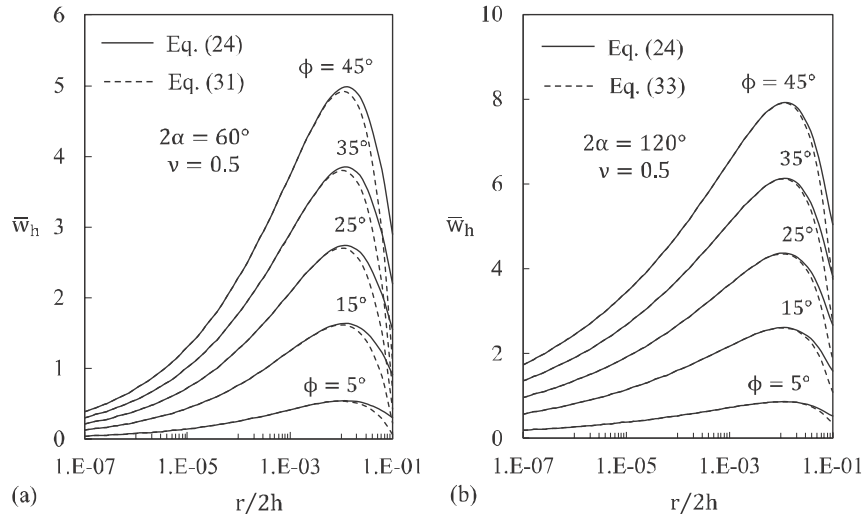


Fig. 3. Comparison of the asymptotic and exact solutions for the dimensionless function $\bar{w}_h(r, \phi)$ for notch opening angles (a) $2\alpha = 60^\circ$ ($\epsilon_2 < 0$), and (b) $2\alpha = 120^\circ$ ($\epsilon_2 > 0$).

defined as

$$\tau_{\phi z}(r, \phi) = \frac{E}{2(1+\nu)} \frac{1}{r} \frac{\partial w}{\partial \phi} \left(\frac{z}{h} \right). \quad (38)$$

We define the out-of-plane mode stress intensity factor corresponding to the singular transverse shear stress state as follows:

$$K_0 = \lim_{\phi=0, r \rightarrow 0} (2\lambda_0) \tau_{\phi z}(r, \phi) (2\pi r)^{1-\lambda_0}, \quad \lambda_0 = \frac{\pi}{2\beta}. \quad (39)$$

For the special case of a semi-infinite crack, i.e. $\beta = \pi$, the above equation yields the well-known definition of the Mode III stress intensity factor. However, there are two main differences between these two singular modes. The out-of-plane singular mode (referred here as O-mode) is a local mode coupled to the remotely applied Mode II, with a symmetric distribution about the mid-plane and a strong dependence on the Poisson's ratio, ν . In contrast, Mode III is an independent failure mode associated with anti-plane loading, and it is independent of the Poisson's ratio. Substituting Eq. (38) into Eq. (39) and utilising the asymptotic solution given by Eq. (37) yields

$$\frac{K_0}{K_{II}} = F(\nu, \beta) \left(\frac{z}{h} \right) h^{(\lambda_2 - \lambda_0)}, \quad (40)$$

where λ_2 and λ_0 are the eigenvalues of the characteristic Eqs. (3) and (30), respectively. The constant F is derived as follows:

$$F(\nu, \beta) = \frac{\nu}{1+\nu} \left(\frac{\sqrt{6(1+\nu)}}{2} \right)^{\lambda_0 - \epsilon_2} \frac{\epsilon_2}{2} \times \left(\frac{A_2}{K_{II}} \right) \cos(\epsilon_2 \beta) \lambda_0^2 (2\pi)^{1-\lambda_0} \frac{\Gamma\left(\frac{\epsilon_2 - \lambda_0}{2}\right) \Gamma\left(\frac{\epsilon_2 + \lambda_0}{2}\right)}{\beta \Gamma(1 + \lambda_0)}, \quad (41)$$

where the constant A_2 is defined by Eq. (4).

Eq. (40) demonstrates a scale effect associated with the plate thickness. As $\lambda_2 - \lambda_0$ is always positive, see Fig. 2b, the intensity of the out-of-plane mode, K_0 grows boundlessly with an increase of the plate thickness. It means that thicker plates weakened by sharp corners and subjected to the same intensity of mode II or mixed mode loading are more susceptible to fracture as the intensity of the out-of-plane mode increases boundlessly. This leads to an interesting conclusion that sufficiently thick plates with sharp angular corners have no strength in shear. The same conclusion was derived based on dimensionless considerations in Kotousov (2010), which was later validated with 3D FE modelling.

5. Semi-infinite crack: comparison against previous solutions

The special case of the semi-infinite through-thickness crack represents an important idealisation relevant to many practical situations, i.e. when the crack length is significantly greater than the plate thickness. It has been previously investigated using both analytical and numerical methods. The purpose of this section is to compare the analytical solution obtained in the present work against the previously-obtained solutions for the out-of-plane displacement near the tip of the semi-infinite crack. Previous analytical solutions by Codrington et al. (2008) for Mode I loading and Kotousov (2007) for Mode II loading will be utilised for comparison, since these studies utilise the same modelling assumptions as the present work, i.e. these were also obtained within the framework of the first order plate theory. The Finite Element modelling results are sourced from He et al. (2016a) for Mode I loading, and He et al. (2016b) for Mode II loading, respectively.

5.1. Mode I loading

In Fig. 4, the obtained solution for the out-of-plane displacement function under Mode I loading is plotted along the line $\phi = 0$ and compared against the solution obtained by Codrington et al. (2008). The solutions obtained using both methods agree well

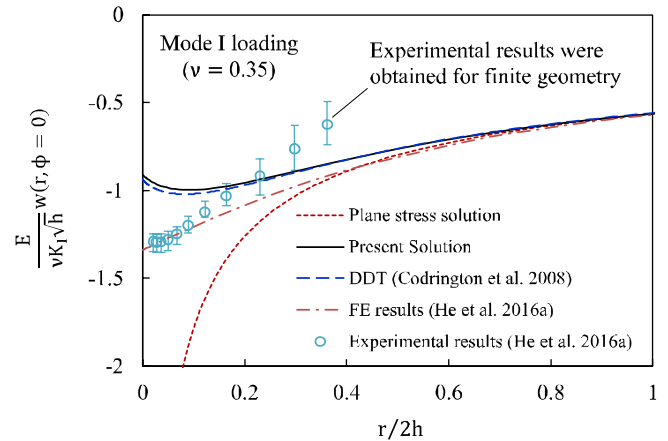


Fig. 4. Dependence of the dimensionless out-of-plane displacement function on the normalised distance from the crack-tip along the line $\phi = 0$ and Mode I loading.

across the entire range of the normalised parameter $r/2h$, with a maximum discrepancy of 3% as $r/2h \rightarrow 0$. The small discrepancy is due to a simplification adopted in the governing Eq. (1), wherein the in-plane stress resultants are approximated by the respective components of the 2D plane stress solution (Kotousov et al., 2017). It is worth pointing out that the analytical solution obtained in the present work possesses two distinct advantages over the previous analytical solution, namely (1) the obtained solution is more general, i.e. applicable for both crack and notch geometries, and (2) the obtained solution can be evaluated more readily, i.e. from a closed-form expression. Nevertheless, the previous solution, which was obtained using the Distributed Dislocation Technique (DDT), is useful in situations where the crack length is comparable to the plate thickness.

The Finite Element simulation results and experimental measurement using Digital Image Correlation from He et al. (2016a) are also superimposed on Fig. 4. The numerical and analytical solutions converge to the plane stress (2D) solution at distances greater than one plate thickness, i.e. $r/2h > 1$. Both solutions predict that the out-of-plane displacement function tends to a constant value as $r \rightarrow 0$, although the predictions differ by $\sim 30\%$ for $\nu = 0.35$. The discrepancy between the analytical and numerical predictions arises due to the underlying kinematical assumption of the first order plate theory regarding the uniformity of the transverse stresses and strains across the plate thickness, and more importantly, due to the effect of the corner (3D) singularity. It is well known that the stress singularity changes its behaviour at the vertex point, where the notch front intersects the free surface. Instead of the classical inverse square root singularity, at this point a new type of singularity appears, the strength of which depends on the Poisson's ratio (Bažant and Estensoro, 1979; Benthem, 1977). This 3D singular effect dominates at distances of approximately 0.1h from the vertex in the radial direction (He et al., 2016b; He et al., 2015; Pook, 2013). The first order plate theory is not capable to capture this 3D effect, which is expected to be largely responsible for the difference between the results, specifically, in the near-surface region. From further analysis it will be demonstrated that beyond this region affected by the 3D corner singularity the agreement is good, see Fig. 9 ahead. The discrepancies between the theoretical and the experimental results far from the crack tip are due to the finite geometry of the test specimen and different boundary conditions than those used in the FE and the present analytical studies.

5.2. Mode II loading

Fig. 5 provides a similar comparison between the present and previous solutions for the case of Mode II loading. In this figure, the obtained solution for the out-of-plane displacement function under Mode II loading is plotted along the line $\phi = \pi/2$. For comparison, the figure also includes the numerical results and experimental measurements obtained by He et al. (2016b). The analytical and numerical solutions are qualitatively similar, i.e. both solutions tend to zero at the crack tip ($r=0$) and converge to the plane stress solution at distances greater than the plate thickness, i.e. $r/2h > 1$. The discrepancy between the analytical and numerical solutions can be attributed to the same factors as discussed previously for the case of Mode I loading.

The solution obtained in the present work can also be utilised to evaluate the strength of the coupled (local) out-of-plane mode for a through-thickness crack subjected to in-plane shear loading. From previously obtained results, the out-of-plane singular mode is described by the conventional inverse square root singularity, same as the in-plane mode II (Kotousov and Lew, 2006). The solution for the out-of-plane displacement function $w(r, \phi)$ for a semi-infinite crack subjected to Mode II loading can be obtained using

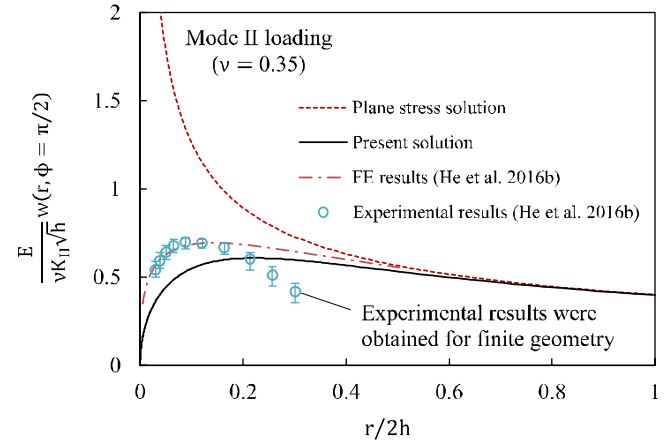


Fig. 5. Dependence of the dimensionless out-of-plane displacement function on the normalised distance from the crack-tip along the line $\phi = \pi/2$ and Mode II loading.

Eq. (8b) and recalling the identity $K_{1/2}(x) = e^{-x}\sqrt{\pi/2x}$.

$$w(r, \phi) = K_{II} \frac{\nu h}{E} \sqrt{\frac{2}{\pi r}} (1 - e^{-\kappa r}) \sin\left(\frac{\phi}{2}\right). \quad (42)$$

Substituting Eq. (42) into Eq. (38) yields the transverse shear stress distribution

$$\tau_{\phi z}(r, \phi) = \frac{\nu K_{II}}{4(1 + \nu)} \frac{h}{r} \sqrt{\frac{2}{\pi r}} (1 - e^{-\kappa r}) \cos\left(\frac{\phi}{2}\right) \left(\frac{z}{h}\right). \quad (43)$$

The out-of-plane mode stress intensity factor can be obtained by substituting $\tau_{\phi z}$ given by Eq. (38) and $\lambda_0 = 0.5$ into Eq. (39) as follows:

$$K_0 = \lim_{\phi=0, r \rightarrow 0} \tau_{\phi z}(r, \phi) (2\pi r)^{1/2} = \nu \left(\frac{3}{2(1 + \nu)}\right)^{1/2} K_{II} \left(\frac{z}{h}\right) \quad (44)$$

In Fig. 6a, the results obtained using Eq. (44) are compared against the analytical results obtained by Kotousov (2007) for a long crack ($h/a = 0.01$, where h is the half-thickness of the plate and a is the half-length of the crack). The analytical results obtained using both methods show good correspondence, with a maximum difference of $\sim 4\%$ for $\nu = 0.5$. As discussed previously, the slight discrepancy is due to a simplification adopted in the governing Eq. (1), wherein the in-plane stress resultants are approximated by the respective components of the 2D plane stress solution (Kotousov et al., 2017). In Fig. 6b, the analytical results are compared against the numerical results obtained by Harding et al. (2010) and Nakamura and Parks (1989). The analytical and numerical results correlate well, and provide the same tendencies, i.e. the intensity of the out-of-plane coupled mode increases monotonically with increasing Poisson's ratio and increasing distance from the mid-plane of the plate. Due to the underlying kinematic assumption of uniform transverse normal strain, the analytical solution obtained within the first order plate theory predicts a linear variation of the out-of-plane mode stress intensity factor along the crack front. Close to the mid-plane of the plate, this linear trend is also observed in the Finite Element modelling results. The evaluation of the stress intensity factor at the vertex point $z/h = 1$, i.e. at the intersection of the crack front and the free surface is quite challenging even using FE models, as evident from the discrepancy in the results obtained by Nakamura and Parks (1989) and Harding et al. (2010). Close to the free surface, i.e. $z/h > 0.9$, the distribution of the out-of-plane mode stress intensity factor is strongly affected by the 3D corner or vertex singularity.

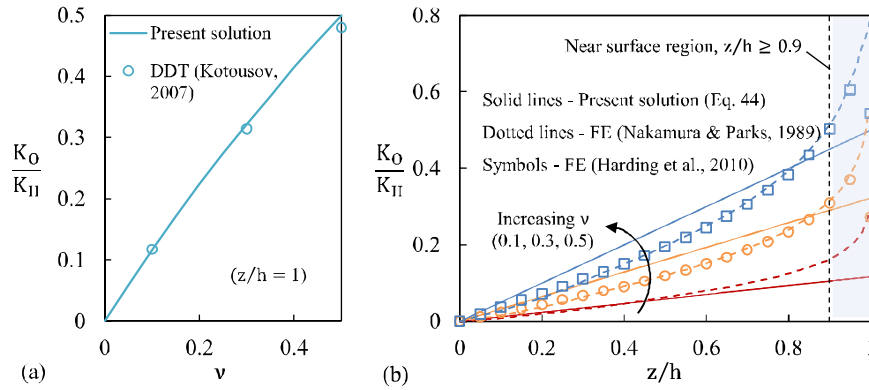


Fig. 6. Dependence of the intensity of the out-of-plane coupled mode, K_0 , on the Poisson's ratio, ν , and the normalised position along the crack front, z/h .

6. Comparison against finite element results for re-entrant corners

In this section, the asymptotic solutions obtained in Section 4 are compared against results obtained using the Finite Element method for both Mode I and Mode II loading for several re-entrant corner angles. The comparative evaluation serves two purposes, namely (1) validation of the analytical approach and asymptotic analysis, and (2) investigation of the capabilities and limitations of the underlying framework of the first order plate theory. For the case of Mode I loading, new finite element modelling results are obtained, whereas for Mode II loading, previously reported results by Harding et al. (2010) are utilised.

6.1. Mode I loading

The Finite Element analysis was conducted using ANSYS Mechanical APDL and the model geometry and mesh details are provided in Fig. 7. The model comprises of a circular sector with radius ten times larger than the plate thickness, which, in accordance with the numerous previous studies, is sufficient to guarantee

that the truncated geometry does not affect the three-dimensional stress and displacement fields near the notch tip front (He et al., 2016a; Nakamura and Parks, 1988). The boundary displacements on the outer radius of the circular sector, which lies outside the region of three dimensional effects, are prescribed in accordance with Williams' series expansion solution for the plane stress state in the vicinity of a sharp notch. The asymptotic solution for the displacement field corresponding to the leading term of the expansion are

$$u_r = \frac{A_1}{8\mu} \frac{r^{\lambda_1}}{\lambda_1} [(\kappa - \lambda_1) \cos(1 - \lambda_1)\phi - \chi_1(1 - \lambda_1) \cos(1 + \lambda_1)\phi], \tag{45a}$$

$$u_\phi = \frac{A_1}{8\mu} \frac{r^{\lambda_1}}{\lambda_1} [-(\kappa + \lambda_1) \sin(1 - \lambda_1)\phi + \chi_1(1 - \lambda_1) \sin(1 + \lambda_1)\phi]. \tag{45b}$$

where r and ϕ are defined in Fig. 7a. The boundary displacement is constant along the plate thickness and can be obtained in Cartesian coordinates for the purposes of the FE model using the

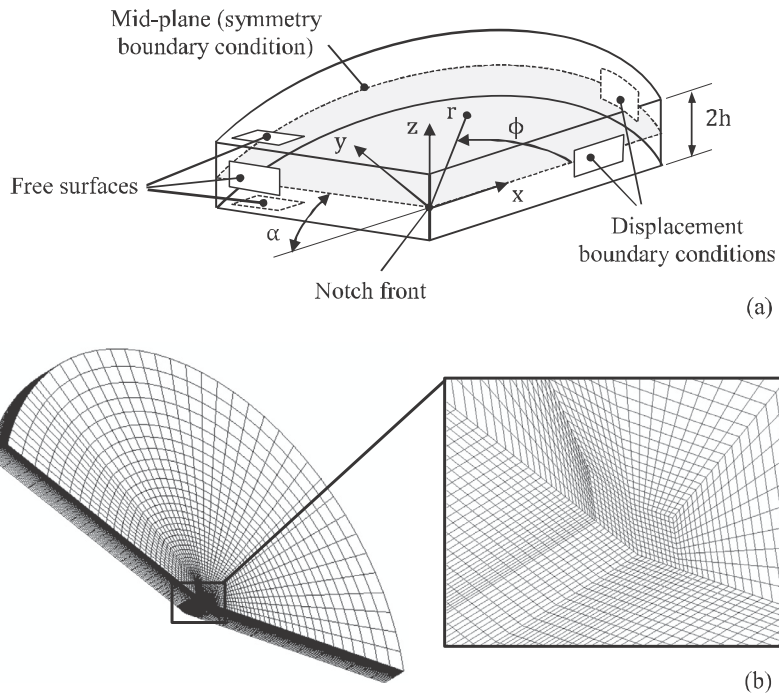


Fig. 7. (a) Finite Element model geometry and boundary conditions (only the region above the mid-plane, i.e., $z \geq 0$, is modelled), (b) Model mesh and detailed view near the sharp corner.

Table 1
Fitting parameters for empirical Eq. (47) based on FE results.

2α	0°	15°	30°	45°	60°	90°	120°	150°	170°
λ_{u1}	0.558	0.532	0.524	0.521	0.536	0.570	0.639	0.771	0.920
C	-0.394	-0.407	-0.412	-0.416	-0.412	-0.379	-0.313	-0.218	-0.145

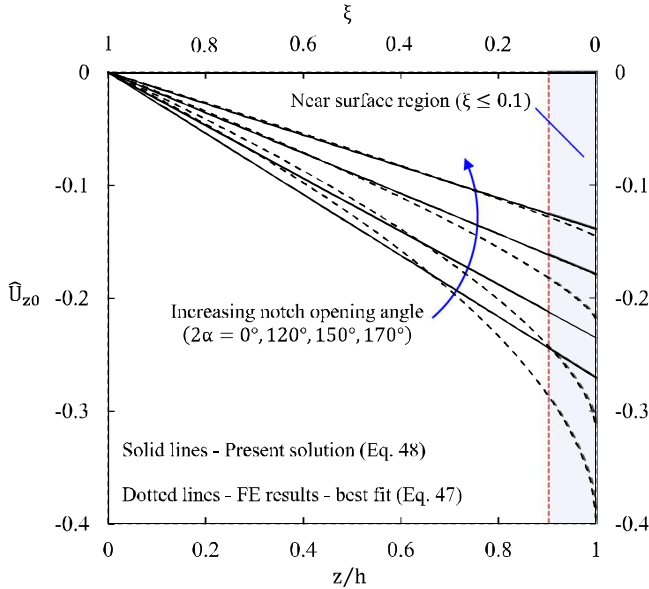


Fig. 8. Variation of the dimensionless notch-tip transverse displacement across the plate thickness at various notch opening angles. The case $2\alpha = 0^\circ$ corresponds to a semi-infinite crack.

transformation

$$u_x = u_r \cos \phi - u_\phi \sin \phi, \quad u_y = u_r \sin \phi + u_\phi \cos \phi. \quad (46)$$

The half thickness of the FE model consists of 30 layers of elements, and the element thickness is gradually decreased from the mid-plane to the free surface in order to accurately capture the behaviour of the stresses and displacements fields near the free surfaces (Fig. 7b). The regions far away from the notch front are modelled with a coarse mesh to reduce the computational time in the FE simulations. The model is meshed with 20 node hexahedral elements. Further details on the numerical approach adopted

in the present work can be found in previous literature (He et al., 2016c; Harding et al., 2010; Berto et al., 2011).

The present numerical simulations as well as experimental and numerical results from He et al. (2016a) demonstrate that the transverse displacement very close to the notch tip is independent of the angular position ϕ , and almost constant along the radial direction in a region around one-tenth of the plate thickness (i.e. $r < 0.1 h$). In this region very near the notch tip, the transverse displacement field was found to be a function of the transverse coordinate only, i.e. $u_z(r < 0.1 h, \phi, z) \approx u_{z0}(z)$. Based on extensive parametric studies, the following best-fit equation for the dimensionless transverse displacement in the very near tip region is obtained

$$\hat{U}_{z0} = \frac{u_{z0}(z)E}{K_I h^{1+\epsilon}} = C(1 - \xi^{\lambda_{u1}}), \quad \xi = 1 - \frac{z}{h}, \quad (47)$$

where ξ is the normalised distance from the free surface in the transverse direction and the constants C and λ_{u1} are functions of the notch opening angle, see Table 1. The constant λ_{u1} represents the strength of the 3D corner singularity.

Recalling the kinematic assumption of the first-order plate theory, i.e. $u_z = w(z/h)$, the analytical expression for the dimensionless transverse displacement at the notch tip can be written as

$$\hat{U}_{z0} = w(r \rightarrow 0) \left(\frac{z}{h} \right) \frac{E}{K_I h^{1+\epsilon}} \quad (48)$$

where the asymptotic value of the displacement function is given by Eq. (26). A comparison of the best fit Eq. (47), which is based on the present FE results, and the analytically obtained Eq. (48) is provided in Fig. 8 for various notch opening angles. Overall, a good qualitative agreement is observed between the analytical solution and FE results, thereby validating the approach developed in this paper. The analytical solution agrees well with the FE results, except close to the free surface of the plate. As discussed previously, the discrepancy is largely attributed to the effect of the corner (or vertex) singularity, which dominates at distances of

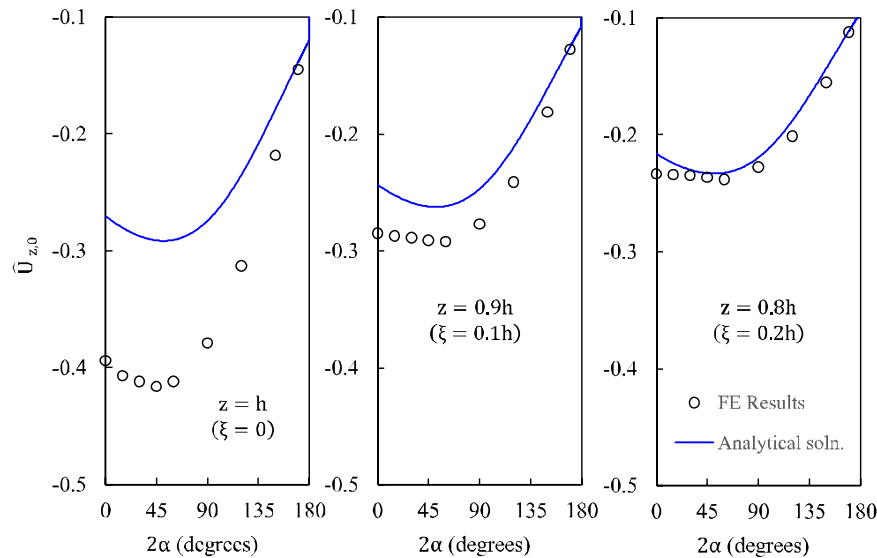


Fig. 9. Comparison of finite element and analytical results for the normalised out-of-plane displacement at three locations along the notch front.

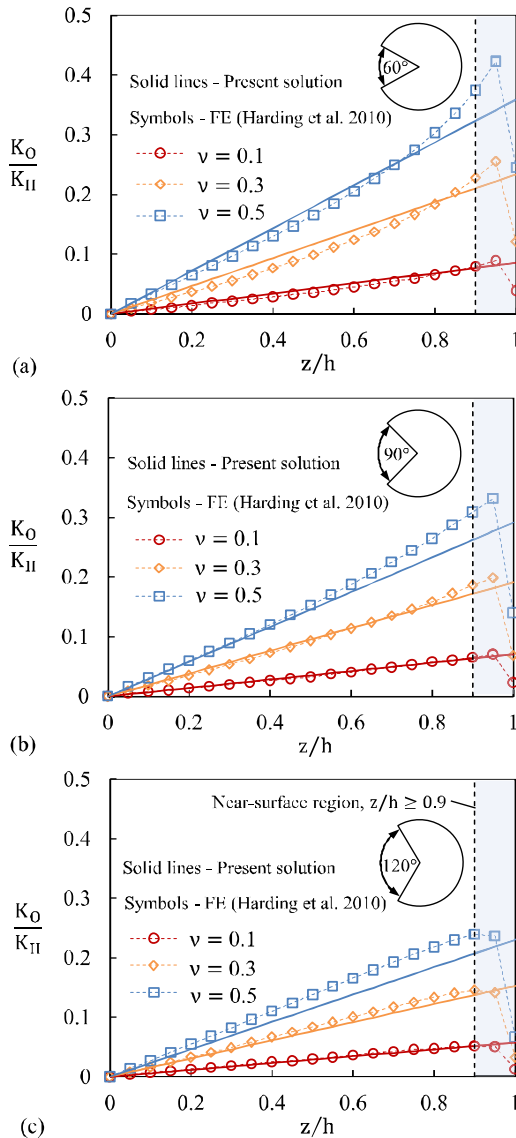


Fig. 10. Variation of the normalised out-of-plane mode stress intensity factor with distance from the mid-plane for various Poisson's ratios, and notch opening angles (a) $2\alpha = 60^\circ$, (b) $2\alpha = 90^\circ$, (c) $2\alpha = 120^\circ$.

approximately 0.1 h from the vertex in the radial direction (He and Kotousov, 2016; He et al., 2015; Pook, 2013).

To further elaborate this point, a comparison of FE results and analytical predictions for the dimensionless transverse displacement \hat{U}_{z0} at different depths from the free surface is presented in Fig. 9. For example, consider $2\alpha = 0^\circ$, which corresponds to the case of a semi-infinite crack. The relative difference between the analytical solution and FE results is about thirty-one percent at the free-surface, where the effect of the corner singularity dominates. At depths of 0.1 h or more from the free surface, the effect of the 3D corner singularity diminishes (He et al., 2016b, 2015; Pook, 2013) and consequently, the agreement between the analytical and FE results improves greatly. It is concluded that the main factor contributing to the discrepancy is the effect of 3D corner singularity, as explained previously.

6.2. Mode II loading

Fig. 10 shows the comparison between the analytical predictions for the out-of-plane mode stress intensity factor, given by Eqs. (40)–(41) and Finite Element modelling results obtained by

Harding et al. (2010). There is a remarkably close agreement between the analytical and numerical results across the wide parametric range of the Poisson's ratio and notch opening angle. This can be explained by an almost linear variation of the out-of-plane mode stress intensity factor across the plate thickness, which supports the basic kinematic assumption of the first order plate theory regarding the linear dependence of the out-of-plane stress and displacement components on the distance from the mid-plane. The most interesting feature of the current analysis is that the analytical solution correctly predicts the existence of the out-of-plane singular stress state for notch opening angles $2\alpha > 102.6^\circ$ despite being based on the plane stress solution for in-plane stress components, see Eqs. (1)–(2).

7. Conclusion

In this paper, the first order plate theory is utilised to analytically obtain the out-of-plane displacements near the tip of an angular corner subjected to in-plane loading. It is important to highlight that the present analysis is currently the only analytical result available to evaluate the out-of-plane displacements, strains and stresses in plane problems of elasticity with stress singularities. Comparison against FE results shows that the obtained analytical solution describes the average out-of-plane displacement across the plate thickness reasonably well at different values of re-entrant corner angles. The analytical results have been obtained only for the leading term of Williams' asymptotic expansion, although there is no difficulties to obtain similar asymptotic results for the higher order terms as well. However, the contribution of the higher order terms of the asymptotic expansion into out-of-plane strain and displacement fields near the corner was found to be small for many practical problems. Therefore, the obtained results can be reasonably extended to finite geometries as well as to arbitrary boundary conditions by taking into account only the singular term in the 2D asymptotic expansion of the stress field and the deformations corresponding to remotely applied stress.

The singular solutions obtained within the theory provide an independent validation of numerous 3D FE studies for sharp corner geometries. In particular, the obtained solutions correctly predict the strength and intensity of the singular stress state corresponding to the coupled modes in the case of shear loading. The theoretical equations also reveal the scale effect of deterministic nature associated with shear loading, which was previously predicted based on dimensionless considerations and demonstrated using FE simulations. In this paper, the scale effect is derived directly from the governing equations rather than attracting various assumptions and hypotheses. It has to be admitted that scaling is one of the most important issues of any theory. The validity of the analytical predictions regarding the scale effect associated with the plate thickness may be a focus of new experimental studies. Another aspect, which is worth to investigate experimentally is the existence of local singular stress states for notch opening angles smaller than 180° in the case of shear loading. The plane theory of linear elasticity predicts the disappearance of stress singularities at the opening angle of 102.6° .

In terms of practical applications, the obtained solutions can potentially provide a new effective method for the characterisation of the notch stress intensity factor from experimental measurements of the out-of-plane displacements near the vertex point. However, as mentioned before, the analytical results disregard the effect of the 3D corner singularity, which can be significant in the close vicinity of the vertex point, or at $r < 0.1 h$. This effect is stronger for small notch opening angles, 2α , as it follows from the comparison with the FEA simulations, see Fig. 9. Therefore, the new method has to utilise the analytical results for the out-of-plane displacement function, $w(r, \phi)$, rather than the asymptotic

results at the vertex point, or $r=0$. In particular, the experimental techniques based on measurements of the surface out-of-plane displacements can largely avoid the necessity of incorporating higher order terms of the near notch tip 2D asymptotic expansion, as demonstrated in our previous studies for through-the-thickness crack geometries (or $\alpha = 0$), see He et al. (2016a, 2016b and 2016c). Finally, the analytical approach developed in this paper is also expected to be useful in other problems in areas of physics and mechanics, which can be reduced to the modified Helmholtz equation (Fowkes and Hood, 1998; Cheng et al., 2006). These include acoustics, electrostatics, and surface tension problems.

Appendix A: Simplification of the infinite series in Eqs. (20a)–(20b)

Using the result (21), the infinite series in Eqs. (20a)–(20b) can be written in the following general form

$$\sum_{n=0}^{\infty} \frac{\Gamma(n - \frac{\epsilon+i\mu}{2})\Gamma(n - \frac{\epsilon-i\mu}{2})}{n!\Gamma(n - \epsilon + 1)} - \sum_{n=1}^{\infty} \frac{\Gamma(n + \frac{\epsilon-i\mu}{2})\Gamma(n + \frac{\epsilon+i\mu}{2})}{n!\Gamma(n + \epsilon + 1)}, \quad \epsilon < 0. \tag{A1}$$

The above series can be rewritten in terms of the Gauss hypergeometric function, employing the reduction formula for the gamma-function $\Gamma(1+z) = z\Gamma(z)$ (Erdélyi et al., 1953, Vol. I), as follows:

$$\begin{aligned} &\sum_{n=0}^{\infty} \frac{\Gamma(n - \frac{\epsilon+i\mu}{2})\Gamma(n - \frac{\epsilon-i\mu}{2})}{n!\Gamma(n - \epsilon + 1)} - \sum_{n=1}^{\infty} \frac{\Gamma(n + \frac{\epsilon-i\mu}{2})\Gamma(n + \frac{\epsilon+i\mu}{2})}{n!\Gamma(n + \epsilon + 1)} \\ &= \frac{\Gamma(-(\epsilon + i\mu)/2)\Gamma(-(\epsilon - i\mu)/2)}{\Gamma(1 - \epsilon)} \\ &\quad \times {}_2F_1\left(-\frac{\epsilon + i\mu}{2}, -\frac{\epsilon - i\mu}{2}; 1 - \epsilon; 1\right) \\ &\quad - \frac{\Gamma((\epsilon - i\mu)/2)\Gamma((\epsilon + i\mu)/2)}{\Gamma(1 + \epsilon)} \\ &\quad \times {}_2F_1\left(\frac{\epsilon - i\mu}{2}, \frac{\epsilon + i\mu}{2}; 1 + \epsilon; 1\right) \\ &\quad + \frac{\Gamma((\epsilon - i\mu)/2)\Gamma((\epsilon + i\mu)/2)}{\Gamma(1 + \epsilon)}, \end{aligned} \tag{A2}$$

The value of the Gauss Hypergeometric function at unity ${}_2F_1(a, b; c; 1)$ can be calculated by the formula

$${}_2F_1(a, b; c; 1) = \frac{\Gamma(c)\Gamma(c - a - b)}{\Gamma(c - a)\Gamma(c - b)}, \quad \text{Re}(c - a - b) > 0. \tag{A3}$$

Therefore, recalling the reduction formula for the gamma-function, Eq. (A2) can be simplified and re-written as follows:

$$\begin{aligned} &\sum_{n=0}^{\infty} \frac{\Gamma(n - \frac{\epsilon+i\mu}{2})\Gamma(n - \frac{\epsilon-i\mu}{2})}{n!\Gamma(n - \epsilon + 1)} - \sum_{n=1}^{\infty} \frac{\Gamma(n + \frac{\epsilon-i\mu}{2})\Gamma(n + \frac{\epsilon+i\mu}{2})}{n!\Gamma(n + \epsilon + 1)} \\ &= \frac{\Gamma(-(\epsilon + i\mu)/2)\Gamma(-(\epsilon - i\mu)/2)}{\Gamma(1 - (\epsilon + i\mu)/2)\Gamma(1 - (\epsilon - i\mu)/2)} \\ &\quad - \frac{\Gamma((\epsilon - i\mu)/2)\Gamma((\epsilon + i\mu)/2)}{\Gamma(1 + (\epsilon - i\mu)/2)\Gamma(1 + (\epsilon + i\mu)/2)} \\ &\quad + \frac{\Gamma((\epsilon - i\mu)/2)\Gamma((\epsilon + i\mu)/2)}{\Gamma(1 + \epsilon)} = \frac{\Gamma((\epsilon - i\mu)/2)\Gamma((\epsilon + i\mu)/2)}{\Gamma(1 + \epsilon)}, \end{aligned} \tag{A4}$$

Appendix B: Asymptotic analysis of $K_\nu(\xi)$ near $\xi = 0$

The modified Bessel function of second kind (Macdonald function) with complex order $\nu = \eta + i\mu$ can be represented by the integral

$$K_\nu(\xi) = \int_0^\infty e^{-\xi \cosh t} \cosh \nu t dt, \quad \xi > 0, \tag{B1}$$

or alternatively,

$$\begin{aligned} \text{Re } K_\nu(\xi) &= \int_0^\infty e^{-\xi \cosh t} \cosh \eta t \cos \mu t dt, \\ \text{Im } K_\nu(\xi) &= \int_0^\infty e^{-\xi \cosh t} \sinh \eta t \sin \mu t dt. \end{aligned} \tag{B2}$$

The improper integrals in (B1)–(B2) are undefined at $\xi = 0$, however

$$\begin{aligned} \lim_{\xi \rightarrow 0} \text{Re } K_\nu(\xi) &= \lim_{t^* \rightarrow \infty} \frac{\eta \sinh \eta t^* \cos \mu t^* + \mu \cosh \eta t^* \sin \mu t^*}{\eta^2 + \mu^2}, \\ \lim_{\xi \rightarrow 0} \text{Im } K_\nu(\xi) &= \lim_{t^* \rightarrow \infty} \frac{\eta \cosh \eta t^* \sin \mu t^* - \mu \sinh \eta t^* \cos \mu t^*}{\eta^2 + \mu^2}, \end{aligned} \tag{B3}$$

Recalling the identities $\sinh x = -i \sin ix$ and $\cosh x = \cos ix$, and the integral representation of the generalised Dirac delta function,

$$\delta(z) = \frac{1}{2\pi} \int_{-\infty}^\infty e^{-izt} dt = \frac{1}{\pi} \int_0^\infty \cos zt dt = \frac{1}{\pi} \lim_{t^* \rightarrow \infty} \frac{\sin zt^*}{z}, \tag{B4}$$

Eq. (B3) can be rewritten after some simplification as

$$\begin{aligned} \lim_{\xi \rightarrow 0} \text{Re } K_\nu(\xi) &= \frac{\pi}{2} [\delta(\mu + i\eta) + \delta(\mu - i\eta)], \\ \lim_{\xi \rightarrow 0} \text{Im } K_\nu(\xi) &= \frac{\pi i}{2} [\delta(\mu + i\eta) - \delta(\mu - i\eta)]. \end{aligned} \tag{B5}$$

Appendix C: Asymptotic analysis of the Kontorovich–Lebedev transform near $r = 0$

The evaluation of the Kontorovich–Lebedev transform and its inverse, which are defined below, is of interest near the origin $r = 0$.

$$\begin{aligned} \tilde{f}(\mu) &= \int_0^\infty f(r) K_{i\mu}(\kappa r) \frac{dr}{r}, \\ f(r) &= \frac{2}{\pi^2} \int_0^\infty \tilde{f}(\mu) K_{i\mu}(\kappa r) \mu \sinh \pi \mu d\mu. \end{aligned} \tag{C1}$$

However, numerical evaluation of the integrals in Eq. (C1) is computationally challenging due to the oscillating behaviour of $K_{i\mu}(\xi)$ as $\xi \rightarrow 0$. For a known solution in the transformed domain, $\tilde{f}(\mu)$, the function $f(r)$ and its derivative at $r \rightarrow 0$ can instead be expressed directly based on the results presented in Appendix B. Letting $\xi = \kappa r$,

$$\begin{aligned} \lim_{r \rightarrow 0} f(r) &= \frac{2}{\pi^2} \int_0^\infty \tilde{f}(\mu) \mu \sinh \pi \mu \left(\lim_{\xi \rightarrow 0} K_{i\mu}(\xi) \right) d\mu, \\ \lim_{r \rightarrow 0} \frac{df(r)}{dr} &= \frac{2\kappa}{\pi^2} \int_0^\infty \tilde{f}(\mu) \mu \sinh \pi \mu \left(\lim_{\xi \rightarrow 0} \frac{dK_{i\mu}(\xi)}{d\xi} \right) d\mu. \end{aligned} \tag{C2}$$

Using the result (B5) and recalling the derivative identity

$$\frac{dK_\nu(\xi)}{d\xi} = -\frac{1}{2} (K_{\nu-1}(\xi) + K_{\nu+1}(\xi)), \tag{C3}$$

Eq. (C2) can be re-written as

$$\begin{aligned} \lim_{r \rightarrow 0} f(r) &= \frac{2}{\pi} \int_0^\infty \tilde{f}(\mu) \mu \sinh \pi \mu \delta(\mu) d\mu, \\ \lim_{r \rightarrow 0} \frac{df(r)}{dr} &= -\frac{\kappa}{\pi} \int_0^\infty \tilde{f}(\mu) \mu \sinh \pi \mu [\delta(\mu + i) + \delta(\mu - i)] d\mu. \end{aligned} \tag{C4}$$

If the function $\tilde{f}(\mu)$ is even and analytic over the entire complex plane, the above integrals can be evaluated using the shifting property of the generalised Dirac delta function

$$\int_0^\infty \tilde{f}(\mu) \mu \sinh \pi \mu \delta(\mu - z_0) d\mu = \frac{1}{2} \lim_{\mu \rightarrow z_0} \tilde{f}(\mu) \mu \sinh \pi \mu. \tag{C5}$$

Using Eq. (C5), the asymptotic values of the function $f(r)$ and its gradient can be obtained as

$$\lim_{r \rightarrow 0} f(r) = \frac{1}{\pi} \lim_{\mu \rightarrow 0} \tilde{f}(\mu) \mu \sinh \pi \mu = \lim_{\mu \rightarrow 0} \mu^2 \tilde{f}(\mu), \quad (C6)$$

$$\lim_{r \rightarrow 0} \frac{df(r)}{dr} = -\frac{\kappa}{\pi} \lim_{\mu \rightarrow 0} \tilde{f}(\mu) \mu \sinh \pi \mu. \quad (C7)$$

References

- Aliha, M.R.M., Saghafi, H., 2013. The effects of thickness and Poisson's ratio on 3D mixed-mode fracture. *Eng. Fract. Mech.* 98, 15–28. doi:10.1016/j.engfracmech.2012.11.003.
- Benthem, J.P., 1977. State of stress at the vertex of a quarter-infinite crack in a half-space. *Int. J. Solids Struct.* 13, 479–492. doi:10.1016/0020-7683(77)90042-7.
- Berto, F., Lazzarin, P., Kotousov, A., 2011. On the Presence of the Out-of-Plane Singular Mode Induced by Plane Loading With $K_{II} = K_I = 0$. *Int. J. Fract.* 119–126. doi:10.1007/s10704-010-9530-5.
- Bažant, Z.P., Estenssoro, L.F., 1979. Surface singularity and crack propagation. *Int. J. Solids Struct.* 15, 405–426. doi:10.1016/0020-7683(79)90062-3.
- Carpinteri, A., Cornetti, P., Sapora, A., Pugno, N., Taylor, D., 2008. A finite fracture mechanics approach to structures with sharp V-notches. *Eng. Fract. Mech.* 75, 1736–1752. doi:10.1016/j.engfracmech.2007.04.010.
- Cheng, H., Huang, J., Leiterman, T., 2006. An adaptive fast solver for the modified Helmholtz equation in two dimensions. *J. Comput. Phys.* 211, 616–637. doi:10.1016/j.jcp.2005.06.006.
- Codrington, J., Kotousov, A., Ho, S.Y., 2008. Out-of-plane stress and displacement for through-the-thickness cracks in plates of finite thickness. *J. Mech. Mater. Struct.* 3, 261–270.
- Erdélyi, A., Magnus, W., Oberhettinger, F., Tricomi, F.G., 1953. *Higher Transcendental Functions, Vols. I and II*. McGraw-Hill, New York, London and Toronto.
- Fowkes, N.D., Hood, M.J., 1998. Surface tension effects in a wedge. *Q. J. Mech. Appl. Math.* 51, 553–562. doi:10.1093/qjmam/51.4.553.
- Gregory, R.D., Wan, F.Y.M., 1988. The interior solution for linear problems of elastic plates. *J. Appl. Mech.* 55, 551–559. doi:10.1115/1.3125829.
- Harding, S., Kotousov, A., Lazzarin, P., Berto, F., 2010. Transverse singular effects in V-shaped notches stressed in mode II. *Int. J. Fract.* 164, 1–14. doi:10.1007/s10704-010-9449-x.
- He, Z., Kotousov, A., 2016. On evaluation of stress intensity factor from in-plane and transverse surface displacements. *Exp. Mech.* 56, 1385–1393. doi:10.1007/s11340-016-0176-8.
- He, Z., Kotousov, A., Berto, F., 2015. Effect of vertex singularities on stress intensities near plate free surfaces. *Fatigue Fract. Eng. Mater. Struct.* 38, 860–869. doi:10.1111/ffe.12294.
- He, Z., Kotousov, A., Fanciulli, A., Berto, F., Nguyen, G., 2016a. On the evaluation of stress intensity factor from displacement field affected by 3D corner singularity. *Int. J. Solids Struct.* 78–79, 131–137. doi:10.1016/j.ijsolstr.2015.09.007.
- He, Z., Kotousov, A., Fanciulli, A., Berto, F., 2016b. An experimental method for evaluating mode II stress intensity factor from near crack tip field. *Int. J. Fract.* 197, 119–126. doi:10.1007/s10704-015-0062-x.
- He, Z., Kotousov, A., Berto, F., Branco, R., 2016c. A brief review of recent three-dimensional studies of brittle fracture. *Phys. Mesomech.* 19, 6–20. doi:10.1134/S1029959916010021.
- Jin, Z.H., Batra, R.C., 1997. A crack at the interface between a Kane-Mindlin plate and a rigid substrate. *Eng. Fract. Mech.* 57 (4), 343–354. doi:10.1016/S0013-7944(97)00036-2.
- Kane, T.R., Mindlin, R.D., 1956. High frequency extensional vibrations of plates. *J. Appl. Mech.* 23, 277–283.
- Kotousov, A., 2004. An application of the Kane and Mindlin theory to crack problems in plates of arbitrary thickness. *Meccanica* 39, 495–509. doi:10.1007/s11012-004-5735-x.
- Kotousov, A., Lew, T.L., 2006. Stress singularities resulting from various boundary conditions in angular corners of plates of arbitrary thickness in extension. *Int. J. Solids Struct.* 43, 5100–5109. doi:10.1016/j.ijsolstr.2005.06.037.
- Kotousov, A., 2007. Fracture in plates of finite thickness. *Int. J. Solids Struct.* 44, 8259–8273. doi:10.1016/j.ijsolstr.2007.06.011.
- Kotousov, A., 2010. Effect of plate thickness on stress state at sharp notches and the strength paradox of thick plates. *Int. J. Solids Struct.* 47, 1916–1923. doi:10.1016/j.ijsolstr.2010.03.029.
- Kotousov, A., Bun, S., Khanna, A., 2017. A new analytical method for the evaluation of transverse displacements and stresses in plane problems of elasticity. *Int. J. Solids Struct.* 118–119, 89–96. doi:10.1016/j.ijsolstr.2017.04.020.
- Lazzarin, P., Tovo, R., 1998. A notch intensity factor approach to the stress analysis of welds. *Fatigue Fract. Eng. Mater. Struct.* 21, 1089–1103. doi:10.1046/j.1460-2695.1998.00097.x.
- Nakamura, T., Parks, D.M., 1988. Three-dimensional stress field near the crack front of a thin elastic plate. *J. Appl. Mech.* 55, 805–813. doi:10.1115/1.3173725.
- Nakamura, T., Parks, D.M., 1989. Antisymmetric 3-D field near the crack front of a thin plate. *Int. J. Solids Struct.* 25, 1411–1426. doi:10.1016/0020-7683(89)90109-1.
- Pook, L.P., 2013. A 50-year retrospective review of three-dimensional effects at cracks and sharp notches. *Fatigue Fract. Eng. Mater. Struct.* 36, 699–723. doi:10.1111/ffe.12074.
- Prudnikov, A.P., Brychkov, Yu.A., Marichev, O.I., 1986. *Integrals and series. Elementary Functions, I. Gordon and Breach, New York Integrals and Series: Vol. 2: Special Functions, Gordon and Breach, New York (1986); Vol. 3: More Special Functions, Gordon and Breach, New York (1990).*
- Ramesh, R., Hills, D.A., 2016. Sharp notch roots subject to in-plane and anti-plane loading: an alternative normalisation of the eigenfields & their application to example problems. *Theor. Appl. Fract. Mech.* 86, 301–308. doi:10.1016/j.tafmec.2016.08.005.
- Rosakis, A., Ravi-Chandar, K., 1986. On crack-tip stress state: an experimental evaluation of three-dimensional effects. *Int. J. Solids Struct.* 22, 121–134. doi:10.1016/0020-7683(86)90002-8.
- Williams, M.L., 1952. Stress singularities resulting from various boundary conditions in angular corners of plate in extension. *J. Appl. Mech.* 19, 526–534.
- Yakubovich, S., 2003. On the Kontorovich-Lebedev transformation. *J. Integral Equ. Appl.* 15, 95–112. doi:10.1216/jiea/1181074947.
- Yakubovich, S., Luchko, Yu., 1994. *The hypergeometric approach to integral transforms and convolutions. Mathematics and its Applications*, 287. Kluwer Academic Publishers Group, Dordrecht.
- Yang, W., Freund, L.B., 1985. Transverse shear effects for through-cracks in an elastic plate. *Int. J. Solids Struct.* 21, 977–994. doi:10.1016/0020-7683(85)90111-8.
- Yoshibash, Z., Bussiba, A., Gilad, I., 2004. Failure criteria for brittle elastic materials. *Int. J. Fract.* 125, 307–333. doi:10.1023/B:FRAC.0000022244.31825.3b.
- Zappalorto, M., 2017. On the stress state in rectilinear anisotropic thick plates with blunt cracks. *Fatigue Fract. Eng. Mater. Struct.* 40, 103–119. doi:10.1111/ffe.12479.